PALACKÝ UNIVERSITY IN OLOMOUC

Faculty of Science

Department of Analytical Chemistry

COMBINATION OF IONIZATION TECHNIQUES AND ION MOBILITY-MASS SPECTROMETRY IN THE ANALYSIS OF NEW PSYCHOACTIVE SUBSTANCES

DOCTORAL THESIS

Autor: Marianna Nytka, M.Sc.
Field of study: Analytical Chemistry
Supervisor: Prof. RNDr. Karel Lemr, Ph.D.

Olomouc 2024

I hereby declare that I have written the dissertation thesis myself under the supervision of Prof. RNDr. Kaler Lemr, PhD. All used information and literary sources are indicated in the references.

I agree that this work will be accessible in the Department of Analytical Chemistry library, Faculty of Science, Palacký University in Olomouc.

In Olomouc ....

                                                                                    signature

Acknowledgment

BIBLIOGRAPHIC INFORMATION

Author's First and Last Name, title :	Marianna Nytka, M.Sc.
Title:	Combination of ionization techniques and ion mobility – mass spectrometry in the analysis of new psychoactive substances
Type of Thesis:	Doctoral
Department:	Department of Analytical Chemistry
Supervisor:	prof. RNDr. Karel Lemr, Ph.D.
The Year of Submission:	2024
Keywords:	Ambient ionization, ion mobility, mass spectrometry, new psychoactive substances
Number of Pages:	106
Number of Appendecies:	2
Language:	English

SUMMARY

This dissertation thesis is devoted to the application of different ionization techniques and ion mobility-mass spectrometry in the analysis of new psychoactive substances. The main goal of this work is to investigate ionization and ion mobility, developing a new modification of desorption nanoelectrospray and a new approach to cyclic ion mobility of new psychoactive substances (NPS). The knowledge was used to develop new methods for identifying and distinguishing abused drugs.

The theoretical part is focused on ambient ionization mass spectrometry, particularly spray-based liquid extraction techniques, and on ion mobility-mass spectrometry (IM-MS). It also covered the application of ambient ionization in analyses of new psychoactive substances and coupling ambient ionization to IM-MS.

The first part of the research covers enhancing ionization efficiency of desorption nanoelectrospray by implementing pressure regulation at the inlet of the mass spectrometer. The influence of the transfer capillary length, pressure drop, and the heating capillary temperature was tested by analyzing NPS. It was confirmed that the pressure regulation between the mass spectrometer's atmospheric and evacuated region and the heated capillary temperature is crucial to maximize sensitivity. The applicability of the modified inlet was tested by analyzing the trace amount of synthetic cathinone on a wallet surface and paracetamol tablets.

The second part of the research focuses on analyzing isomeric mixtures of NPS by cyclic ion mobility-mass spectrometry. Two approaches to determine their isomeric ratios were proposed. The separation of lithium adducts in multipass experiments was compared with the simple procedure based on multiple linear regression applied to characteristic arrival time distribution (ATD) profiles of isomers and their mixture. Direct infusion and flow injection analysis with electrospray, and desorption electrospray for solid samples were employed. Both approaches, lithiated molecules separation and ATD profiles of protonated molecules or ion fragments, provided comparable results. While adducts need to be sufficiently separated, the ATD profile approach can be used for overlapping signals.

BIBLIOGRAFICKÁ IDENTIFIKACE

Jméno a Příjmení Autora, Titul :   Marianna Nytka, M.Sc.

Název Práce: Kombinace ionizačních technik a spojení iontové mobility s hmotnostní spektrometrií v analýze nových psychoaktivních látek

Typ Práce: Disertační

Pracoviště: Katedra analytické chemie

Vedoucí práce: prof. RNDr. Karel Lemr, Ph.D.

Rok odevzdání práce: 2024

Klíčová slova: Ambientní ionizace, iontová mobilita, hmotnostní spektrometrie, nové psychoaktivní látky

Počet stran::   106

Počet příloh: 2

Jazyk: Angličtina

SOUHRN

Hlavním cílem této práce je výzkum ionizace a iontové mobility, který zahrnoval především vývoj citlivější modifikace desorpčního nanoelektrospreje a nový přístup k cyklické iontové mobilitě nových psychoaktivních látek (NPS). Poznatky byly využity k vývoji nových postupů pro identifikaci a rozlišení zneužívaných drog.

Teoretická část je zaměřena na hmotnostní spektrometrii s ionizací ambientními technikami, zejména technikou kapalinové extrakce na bázi sprejování, a na hmotnostní spektrometrii ve spojení s iontovou mobilitou (IM-MS). Dále pojednává o ambientních technikách využitých při analýze nových psychoaktivních látek a jejich spojení s IM-MS.

První část výzkumu zahrnuje zvýšení intenzity signálu pro desorpční ionizaci nanoelektrosprejem zavedením regulace tlaku na vstupu hmotnostního spektrometru. Na analýze NPS byl testován vliv délky vstupní vyhřívané kapiláry, snížení tlaku a teploty vyhřívané kapiláry. Bylo potvrzeno, že pro dosažení maximální citlivosti je rozhodující regulace tlaku mezi atmosférickou a vakuovou částí hmotnostního spektrometru a teplota vyhřívané kapiláry. Použitelnost upraveného vstupu do hmotnostních spektrometru byla testována na detekci stopového množství syntetického katinonu na povrchu peněženky a na analýze tablet neopioidní analgetika a antipyretika.

Druhá část výzkumu byla zaměřena na analýzu izomerních směsí NPS pomocí cyklické iontové mobility-hmotnostní spektrometrie. Byly navrženy dva přístupy ke stanovení jejich izomerních poměrů. Separace aduktů lithia ve víceprůchodových experimentech byla porovnána s jednoduchým postupem založeným na mnohonásobné lineární regresi aplikované na profily charakteristické distribuce doby příchodu (ATD) izomerů a jejich směsi. Byla použita přímá infuze a průtoková injekční analýza s elektrosprejem a rovněž desorpční elektrosprej pro pevné vzorky. Oba přístupy, separace lithiovaných molekul a ATD profily protonovaných molekul nebo iontových fragmentů, poskytly srovnatelné výsledky. Zatímco adukty je třeba dostatečně separovat, pro překrývající se signály lze využít ATD profily charakteristické pro jednotlivé izomery

Table of Contents

1 INTRODUCTION

The production of new psychoactive substances often consists of the variation of functional group position or, more generally, the production of isomers. It increases the requirements for analyses when developing rapid, selective, sensitive methods, which are essential to detect and separate an increasing number of NPS. Ambient ionization coupled with ion mobility-mass spectrometry (IM-MS) represents a promising tool for solving this analytical task. This coupling provides a fast (millisecond timescale) gas-phase separation with minimal sample pretreatment. So far, the application of this method is limited in the analysis of NPS.

This doctoral thesis focuses on enhancing ion transport in desorption nanoelectrospray by pressure regulation at the mass spectrometry inlet. A mixture of new psychoactive substances was used to evaluate the influence of pressure regulation, the temperature of the heated capillary, and its length. The applicability of desorption nanoelectrospray was proven by analyzing traces of abused drugs or a non-opioid analgesic and antipyretic agent.

Cyclic ion mobility-mass spectrometry was used to discriminate NPS isomers and determine their ratios. The high resolving power of multipass experiments could not resolve isomeric protonated molecules. Nevertheless, the characteristic ATD profiles were obtained by direct infusion or flow injection analysis with electrospray and desorption electrospray ionization. Characteristic ATD profiles of protonated molecules provided comparable results to the separation of lithium adducts, which opens new possibilities for the differentiation of isomers of small organic molecules.

2 THEORETICAL PART

2.1 Ambient Ionization Mass Spectrometry

Since 2004, when Cooks et al. [1] presented desorption electrospray ionization-mass spectrometry (DESI-MS), and 2005, when Laramee and Cody [2] presented direct analysis in real time (DART), the rise of ambient techniques began. In ambient ionization mass spectrometry (AIMS), samples are ionized under ambient conditions with minimal or no sample preparation [3]. AIMS sources have compatibility with multiple mass spectrometers and allow rapid, in-situ [4] and in vivo analysis [5]. Most AIMS sources can be classified based on their desorption process (see Fig. 1) into three groups [6]:

a) Liquid extraction – mainly utilizes the ESI mechanism;

b) Plasma desorption (thermal) – based on the same principles as atmospheric pressure chemical ionization (APCI), where the ions are produced using a corona discharge;

c) Laser ablation/desorption (laser-based) techniques - the analyte's desorption is performed by irradiation with high power lasers.
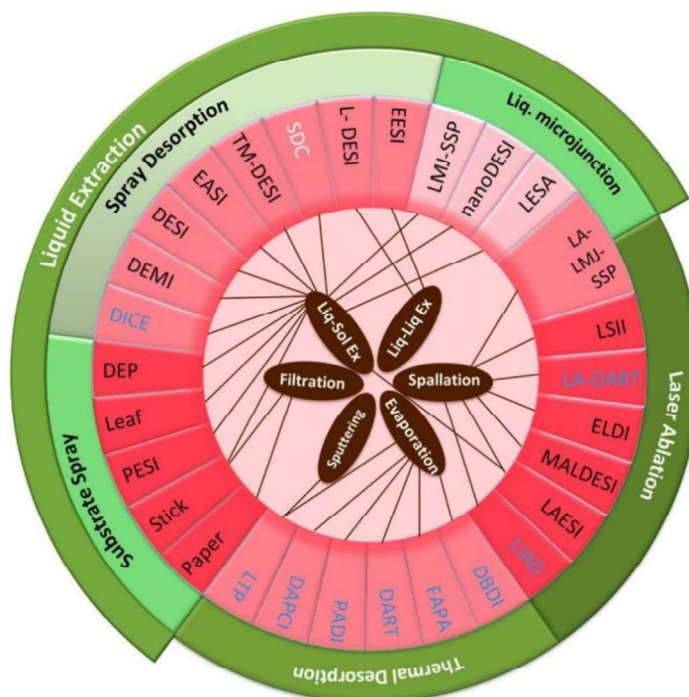

Figure 1 Scheme of the major classes of ambient ionization techniques. Adopted and reprinted from [6]. Copyright © 2013 American Chemical Society

The liquid extraction techniques can be divided by the sample processing into three groups: spray desorption, substrate spray (e.g., paper spray (PS), probe electrospray ionization (PESI), etc.), and liquid microjunction (e.g., liquid microjunction-surface sampling probe (LMJ-SSP), liquid extraction surface analysis (LESA), nano-DESI) [6].

The next subchapter will be dedicated only to spray desorption techniques.

2.1.2 Spray-Based Ambient Ionization Mass Spectrometry

Part of this section was published in a first-author publication [7] and adapted and reprinted with permission from the journal:

Nytka, M, Borovcová, L, Fryčák, P, Barták, P, Lemr, K. Signal enhancement in desorption nanoelectrospray ionization by custom-made inlet with pressure regulation. J Mass Spectrom. 2020;55:e4642.https://doi.org/10.1002/jms.4642 Copyright 2020 John Wiley & Sons, Ltd.
License number 5730170914154.

Author's Contribution. Marianna Nytka – investigation, formal analysis, visualization, and writing the original draft.

Spray-based ambient techniques use the charged droplets produced from the solvent spray to desorb or extract analyte from the sample surface. During this process, desorbed analytes undergo an electrospray-like ionization mechanism by ion evaporation or charge residues [8,9]. Desorbed analytes are ionized and sent to a mass spectrometer for analysis [6].

The most used spray-based AIMS technique is desorption electrospray ionization-mass spectrometry (DESI-MS). In DESI, the desorption and ionization is accomplished by a droplet pick–up mechanism [10] (Fig. 2). The surface is sprayed with the charged solvent droplets generated with the assistance of the nebulizing gas, providing the thin wet film on the sample's surface. This process is followed by solid-liquid microextraction and production of the secondary droplets drawn towards the mass spectrometer inlet by an electric field potential. Nitrogen is typically used as a nebulizing gas. Nevertheless, a recent report shows the benefits of using helium as a nebulizing gas [11]. In this study, an increase in signal intensities of 5 times for myoglobin and more than 20-fold for protonated

hydrocortisone was observed using helium instead of nitrogen. The increase in signal intensities could result from more than double the volumetric flow for helium (2 L/min) than for nitrogen (1 L/min) at 120 psi supply pressures. The desorption footprint was evaluated on the width of the desorption band on the microscope slide containing the Rhodamin 6G. The desorption profile decreased from ~ 500 μm with nitrogen to ~200 μm with helium. This might be explained by a more focused droplet beam that is more efficient in producing and less scattering of the secondary droplets that are released from the sample surface [11]. DESI-MS requires minimal sample preparation and no matrix deposition compared with MALDI [8].
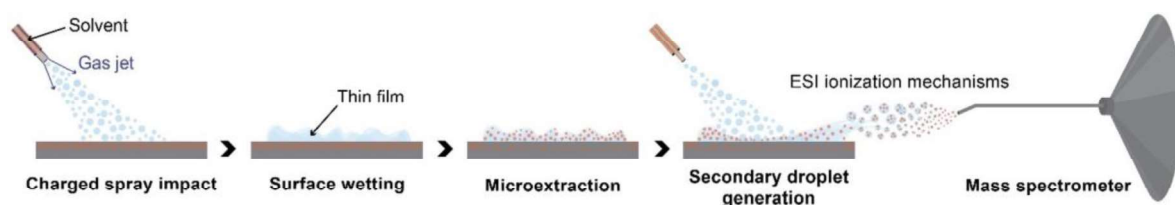
Figure 2 The droplet pick-up mechanism scheme in DESI. Adapted and reprinted with permission from [12]. Copyright © 2023 American Chemical Society.

Reproducibility in DESI experiments depends on the geometry, the pressure of the nebulizing gas, the composition and flow rate of the spraying liquid, and the surface's properties from which the analyte is desorbed [10,13]. DESI has a myriad of qualitative and quantitative applications, such as the detection of inks [14,15], polymers [16–18], explosives, chemical warfare [19,20], cancer biomarkers [21–23], and proteins [24]. Moreover, reactive DESI allows the detection of less polar compounds. That can be accomplished by adding additives to the solvent to increase ionization efficiency. For instance, the formation of the chloride complexes of bromophycolides via adding 100 μM ammonium chloride into the spraying solvent improved the sensitivity of the analysis of algal tissue. The limit of detection (LOD) (S/N ≥ 3) improved for chloride complexes of bromophycolides A, B, and E to 8 pmol/mm^2, 8 pmol/mm^2, and 10 pmol/mm^2 compared to LOD for deprotonated analytes (85 pmol/mm^2, 146 pmol/mm^2, and 66 pmol/mm^2) [25]. Chemical derivatization can be used to enhance the sensitivity of the detection of nonpolar compounds. For example, adding 50 ppm of betaine aldehyde into the spraying solvent

(ACN/H$_2$O (1:1, v/v) can form hemiacetal salt by reacting with the alcohol group of cholesterol using nucleophilic addition. This method was used to detect cholesterol in human serum and in rat brain tissue [26]. Another example of chemical derivatization is the production of oxime by a reaction between hydroxylamine from the spray solvent and steroids in urine[26]. Reactive DESI-MS was also used in the study of degradation processes [28]. Apart from the analysis of solid samples, DESI can also analyze liquid samples. The basic setup of liquid DESI-MS is shown in Fig. 3. The sample is delivered through the flat-ended capillary with constant flow by a syringe pump. Selective non-covalent adduct protein probing (SNAPP) was used to evaluate the effect of the ionization process on protein structure. 18-Crown-6 molecule was used to non-covalently bind to protonated side chains of lysine and arginine or to the N-terminus [27]. Miao and Chen [28] showed the application of the liquid DESI-MS on biological fluids such as raw urine, determining the content of methamphetamine with the limit of detection 200 ng/mL.
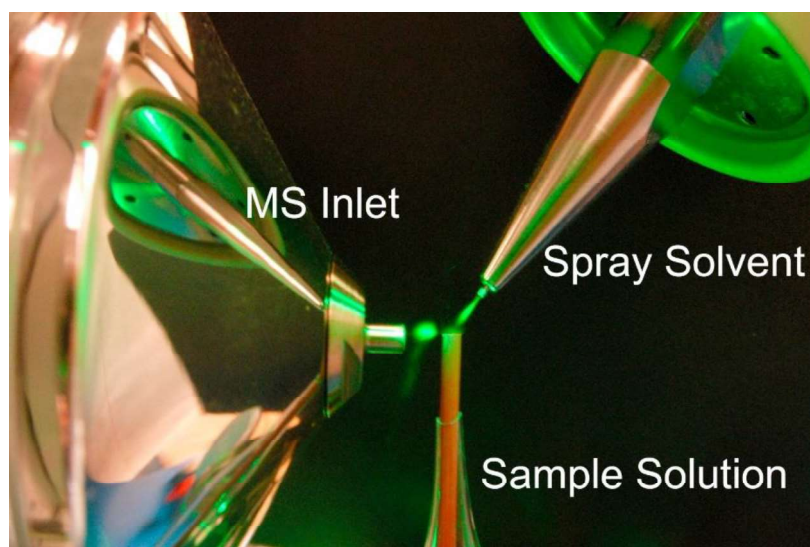
Figure 3 Liquid DESI source setup, where the green laser with green color pointed to the droplet cloud. Reprinted from [27] with permission from Elsevier.

Another modification of the DESI source is the transmission mode desorption electrospray ionization (TM-DESI). The sample is deposited onto a sampling mesh, with a spray angle of 0°, to transmit the spray solvent through the sample. This source setup eliminates the influence of geometry [29].

One of the advantages of some spray-based AIMS is the simplicity of the source design. Easy ambient sonic spray ionization (EASI) (first reported in 2006 under the name "desorption sonic-spray ionization.") uses sonic spray ionization (SSI) [30]. The simple design of the source could lead to its usage by minimally trained people. Ion formation occurs due to an imbalanced distribution of charges. Usually, the analytes are present as $[M+H]^+$ as well as $[M+ Na^+/K^+]$ or $[M-H]^-$ ions. The solvent flow, assisted with supersonic nebulizing gas flow, hits the sample's surface to desorb analytes. Unlike DESI, EASI does not use voltage [30]. EASI could be coupled with thin-layer chromatography (TLC) (Fig. 4) for drug analysis as well as analysis of vegetable oils [32] or high-performance TLC for the analysis of biodiesel [31]. Also, EASI was coupled with membrane introduction mass spectrometry (EASI-MIMS) for analysis of solution constituents [32].
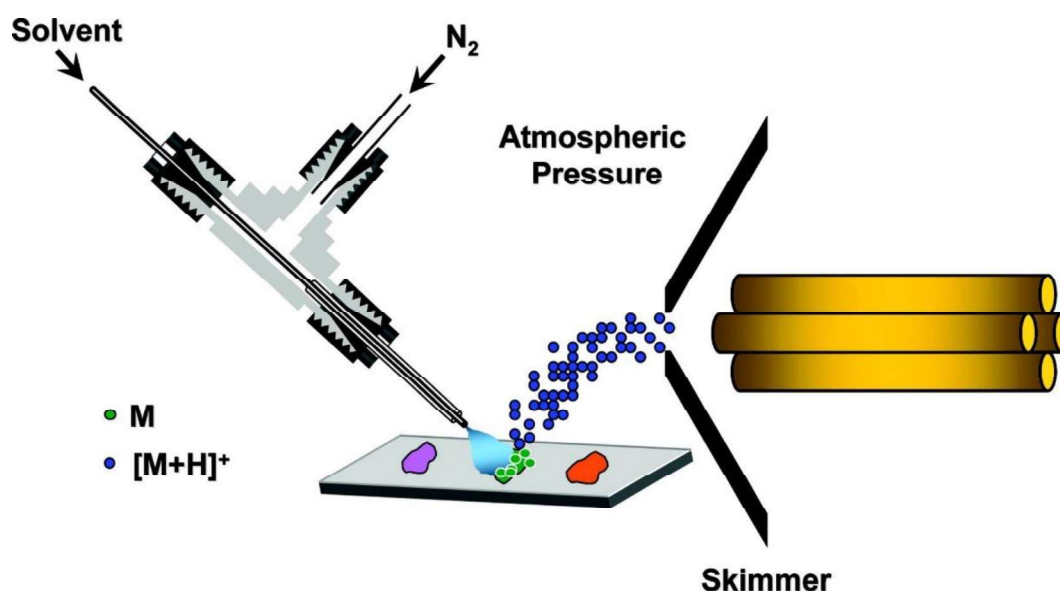
Figure 4 Scheme of coupling EASI with TLC plate. Reprinted with permission from [33]. Copyright © 2008 American Chemical Society

Since EASI uses the sonic nebulizing gas flow, the self-pumping via the Venturi effect is applied. The high-speed fluid coming through the narrow part of the capillary causes a drop in pressure and self-pumping. Therefore, the pumping system is not needed and costs are decreased [34,35]. V-EASI can be used for liquid samples as well as for solid samples. Thus, this method was used in determining the methanol in biofuels by forming the methyl esters of nicotinic acid [36] and for the study of the self-assembly of

nucleobases [37]. The simplicity of the V-EASI source allows the bipolar analysis of myoglobin, cytochrome C, and redox active inorganic substances by only switching the polarity of ion optics and mass analyzer without applying the spray voltage [38].

After two years of introduction of DESI, Cooks et al. [39] presented the new ambient technique extractive electrospray ionization (EESI). This technique is based on liquid-liquid extraction, where two capillaries are being used. One of the capillaries delivers the analyte solution, the flow of which is assisted by the nebulizing gas, and another capillary is used to generate the charged microdroplets from the solvent. Similar to EESI, secondary electrospray ionization (SESI) uses the ESI-based ionization setup to ionize analytes in the gas phase. In SESI, the water-cooled electrospray system uses two LC pumps. The first pump is used to deliver liquid to the electrospray needle, and the second LC pump – introduces the volatile sample solution [40]. SESI is much softer than ESI. This was proven by providing lower internal energies for benzylamine thermometer ions than the ESI source [41]. This technique is commonly used in breath analysis [42].

Another modification of the DESI source, desorption nanoelectrospray (nanoDESI, Fig. 5), was reported in 2007 by Ranc et al. [43]. It should not be confused with coincidently abbreviated nanospray desorption electrospray (nano-DESI), which was introduced a few years later and is more related to liquid extraction surface analysis (LESA) than to desorption electrospray (DESI). Nano-DESI uses two capillaries without the assistance of the nebulizing gas to create a liquid microjunction, the principle of the technique differs from DESI and nanoDESI. [44,45].
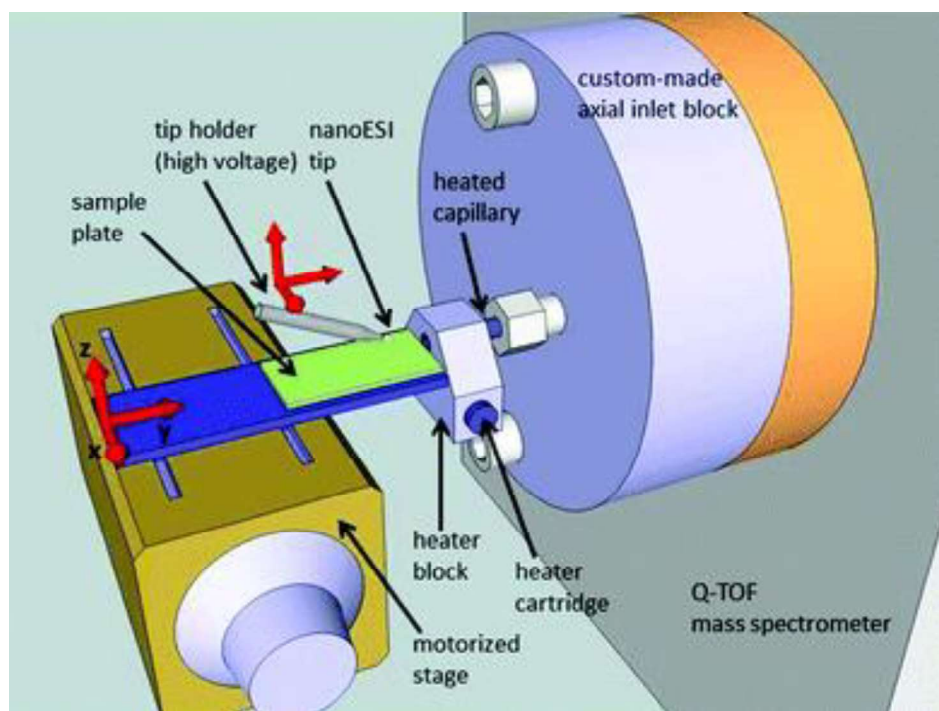
Figure 5 Scheme of nanoDESI. Reprinted with permission from [46]. © The Royal Society of Chemistry 2016

Compared with DESI, nanoDESI generates a lower flow rate of spraying liquid and smaller primary charged droplets. Instead of an electrospray tip (tens of micrometers ID), it uses a nanoelectrospray tip (~2 μm ID) without the assistance of nebulizing gas. Both techniques are suitable for direct surface analysis, are tolerant to sample contamination by salt, and produce ions with similar internal energy. For nanoDESI, the signal-to-noise ratio did not deteriorate substantially for samples containing up to 2.5 mol/L NaCl [47]. In the first application of nanoDESI, the chiral analysis of ephedrine in an untreated drop of the commercial pharmaceutical deposited on the surface was demonstrated using this ion source and the Cooks kinetic method. This method is based on forming trimeric clusters of the analyte with a chiral selector (usually optically pure reference substance) and a metal ion. Two fragmentation pathways can occur, one with the loss of the selector and the second with the loss of the analyte. The ratio of fragment intensities depends on the relative stability of the complexes formed by the different enantiomers [43]. The applicability of nanoDESI was shown further, for example, by chiral analysis of pharmaceuticals in whole blood [48] or analysis of anthocyanins in a drop of red wine [49]. Considering imaging applications, the low flow rate of spraying liquid decreases sample washing off, which can be advantageous for lateral resolution and enables repeat scans of

the same surface area. Promising good resolution of dye squares (60 μm × 60 μm) has been achieved by Hartmanová L. et al. [46]. Although technical development has improved the robustness of nanoDESI [47] and a modification of the inlet has allowed its implementation on a Q-TOF mass spectrometer (Fig. 5) [46], the sensitivity of the measurements can still be an issue. Due to the small surface area sampled, only a tiny amount of analyte is available for desorption and ionization.

2.1.3 Application of Ambient Ionization Mass Spectrometry to New Psychoactive Substances

New psychoactive substances (NPS) are a broad group of the different classes of abused drugs (e.g., synthetic cathinones, synthetic cannabinoids, fentanyl analogs, piperazines, etc.). They are substitutes for known narcotics such as cannabis, cocaine, or LSD. NPS are made in order to avoid detection by analytical methods or to create psychoactive substances that are not yet regulated [50]. There has been a significant increase in the number of NPS first reported to EU Early Warning throughout the 17 years, as can be seen in Fig. 6. Over the last 15 years, 1184 NPS were identified worldwide, 41 of which were first reported in Europe in 2022 [51,52]. The potency of some synthetic analogs can be much higher than the drugs they replace. Consequently, new NPS production increases the demand for fast, sophisticated, selective, and sensitive analytical methods. Typical methods for NPS analysis are color and microcrystalline tests [53], infrared and Raman spectroscopy [54], chromatography, mass spectrometry, and other techniques [55–58].

Cathinones ● **Cannabinoids** ● **Opioids** ● **Benzodiazepines**
Aminoindanes ● **Arylalkylamines** ● **Arylcyclohexylamines** ● **Other substances**
Phenethylamines ● **Piperazines** ● **Piperidines & pyrrolidines** ● **Tryptamines**
Plants and extracts

EMCDDA (data) | Highcharts (chart tool)
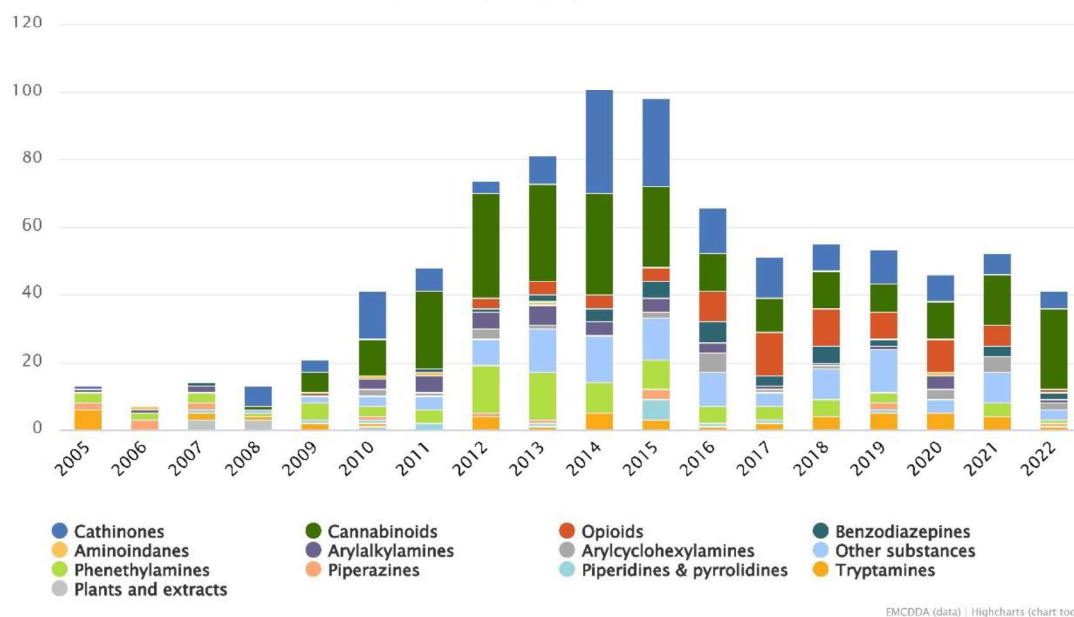
Figure 6 Number of NPS reported to the EU Early Warning system for the first time from 2005-2022 [51].

AIMS techniques usually do not require extensive sample preparation, are minimally destructive, and directly ionize the analytes for mass spectrometry. There are not many reports dedicated to the analysis of NPS using ambient ionization techniques. Nevertheless, DESI-MS has found its applications in detecting the mixture of drugs of abuse in the presence of interfering matrices such as topical sprays and hand lotions from fabric samples [59].

The surface material is one of the critical parameters in DESI. Various studies of the surface showed that a semi-porous PTFE plate is a vital surface material for detecting 4-MMC, providing a LOD and limit of quantitation (LOQ) of 2.3 $\mu g/mm^2$ and 14.3 ng/mm^2, respectively [60], and screening piperazine analogs with LOD in the range of 0.02-2.80 $\mu g/mm^2$ [61]. Silica and polylactide-based functionalized with oxidized carbon nanoparticles surfaces were shown to be the most effective in detecting synthetic cannabinoids by microextraction using packed sorbent (MEPS)-DESI-HRMS in oral fluid [62]. The surface is also essential in paper spray ionization (PS). The cellulosic paper has a hydrophilic nature that promotes the elution of low-polar compounds and improves their ionization. At the same time, it can compromise the ionization of polar compounds [63]. The analysis of the synthetic cathinones, N-benzyl-substituted phenethylamines, and synthetic cannabinoids was performed by rubbing the samples against the PS paper [64].

This method has been used in the detection of fentanyl analogs in urine samples at the lowest concentration of 0.5 ng/mL [65].

Similarly to PS, fiber spray ionization-mass spectrometry (FSI-MS) was used to identify the synthetic cathinones, opioids, and phenethylamines. Analytes were deposited onto the capillary polypropylene hollow fiber or, in the case of the urine analysis, fiber was dipped into the solution. FSI-MS showed better sensitivity by having five times higher ion intensity for ethylone from the tablet than PS ionization [66].

Aside from liquid extraction techniques, plasma ionization AIMS such as DART have been used to detect illicit drug trace levels (LOD = 0.025 µg/100 cm^2) [67]. Since herbal products can be doped with synthetic cannabinoids, their targeted analysis was performed by DART-MS to reveal the presence of synthetic cannabinoids [68–70]. One of the advantages of DART is that the solid sample can be analyzed directly by placing the sample directly in front of MS inlet, as shown in Fig. 7.
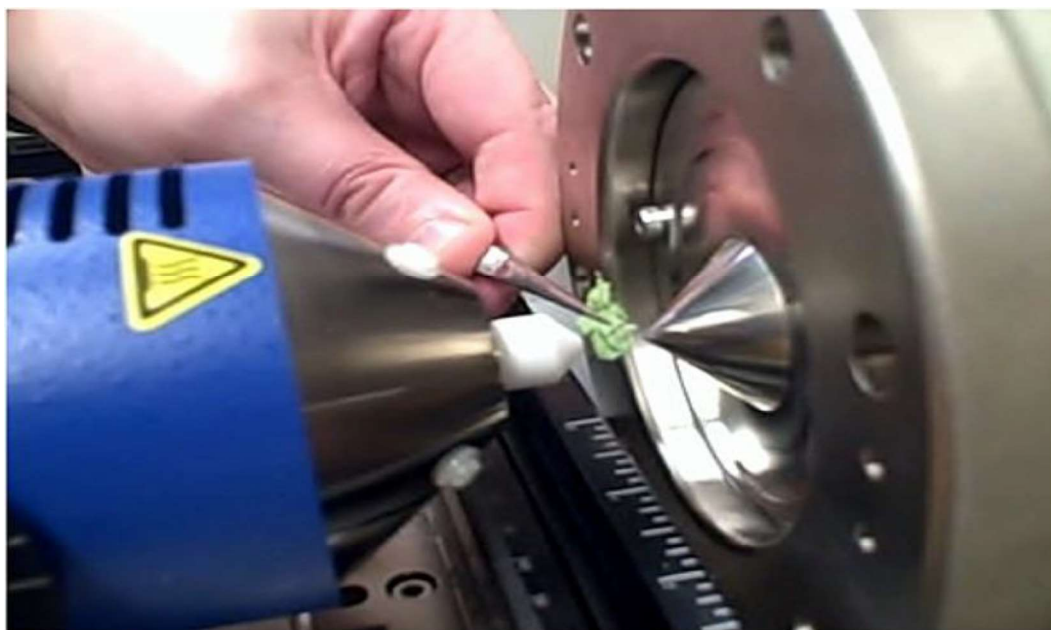
Figure 7 Analysis of the doped plant by DART-MS [68]. Copyright © 2012 John Wiley & Sons, Ltd.

Apart from their analysis in plant samples, synthetic cannabinoids were detected in human blood by DART-MS/MS. The blood was spiked with abused drugs with further sonication and centrifuged. The supernatant was then subjected to DART-MS/MS analysis. The LOD for 22 synthetic cannabinoids was between 0.01 and 1 ng/mL [71].

Standards of synthetic cathinones alone and in a mixture were detected and differentiated by DART-MS using in-source collision-induced dissociation (CID). This fragmentation method allowed to obtain different fragmentation spectra for isobaric and isomeric analytes [72]. Aside from DART, the Atmospheric Pressure Solids Analysis Probe (ASAP) usually uses the glass capillary for sample introduction, where, due to the heated desolvation stream of nitrogen, analytes are thermally desorbed and ionized by corona discharge [73]. ASAP enables the analysis of solid and liquid samples. The capillary is dipped into the analyte solution or rubbed against the solid sample. There are few reports of the identification of NPS by ASAP-MS. The 11 NPS, including synthetic cannabinoids and synthetic cathinones, were identified by ASAP-MS and MS/MS analysis [74]. Medical swabs were used for the sample collection instead of glass capillary, allowing the screening of synthetic cannabinoids, cathinones, and tryptamines with a LOD of 1 μg for cathinones and 12 μg for cannabinoids and tryptamines [75].

Mentioned reports show the applicability of AIMS in the detection of NPS despite their limitations, such as low reproducibility, low ionization efficiency in comparison to ESI, ion suppression due to the matrix effect, poor selectivity, and inability to differentiate the isomers or isobars [76]. Coupling AIMS techniques with ion mobility mass spectrometry could help to increase the selectivity and discriminate isomeric or isobaric compounds.

2.2. Ion Mobility – Mass Spectrometry

Ion mobility (IM) is a powerful tool for separating ions in drift gas ("buffer gas") under the electric field. The electric field accelerates ions through the inert gas, producing collisions of ions with the buffer gas. Those collisions produce friction force. If collisions are frequent enough, electric force and friction force cancel each other, and the stationary state can be achieved, providing a constant average speed (drift velocity, V_d). Therefore, drift velocity is proportional to the electric field (E), and ion mobility (K) (Eq.1). The mobility, K, can be determined by the time (t_d) that ions spend inside a mobility cell of fixed length (L) (Eq.2) [77,78].

$$v_d = KE \qquad (1)$$

$$K = \frac{V_d}{E} = \frac{L}{t_d \cdot E} \qquad (2)$$

The mobility K depends on the mass and charge of the ions and their shape. Therefore, small ions have higher drift velocities than larger, less mobile ions. Reduced mobility is calculated under the standard conditions (electric field is 1 V/cm, buffer gas temperature is 273.15 K, pressure is 760 Torr). Reduced mobility can be calculated for the different IM-MS platforms operating in different conditions by Eq.3 [79,80].

$$K_0 = \frac{L \cdot p \cdot 273.15}{t_d \cdot E \cdot 760 \cdot T} \qquad (3)$$

The mobility of an ion is related to its collision cross-section (CCS). The term "collision cross-section" is used and accepted widely by the IMS community. The number of collisions is not as important as knowing the momentum transfer during the collision between the ion and the buffer gas. The term "cross-section" covers the idea that the molecule is a sphere and depends on its surface area. The atoms and molecules consist of nuclei, electrons, and void, which does not make them a hard sphere. When the two particles collide, their electron densities influence each other. Therefore, IM measurements determine the integral of the collision cross-section on the collision energy distribution [77]. Momentum transfer collision integral (Ω or CCS) describes the collisions of ions with the buffer gas and ion conformations in a mobility cell and can be calculated by the fundamental low-field mobility equation (Mason-Schamp) (Eq.4) [81],

$$\Omega = \frac{\frac{3}{16} \cdot \left(\frac{2 \cdot \pi}{\mu \cdot k_b \cdot T}\right)^{1/2} \cdot z \cdot e}{N_0 \cdot K_0} \tag{4}$$

where e is charge of the electron; $z \cdot e$ - ion charge; N_0 - buffer gas density; μ - reduced mass; k_b – Boltzann's constant; T- absolute temperature in drift region.

There are three ways to characterize ions in ion mobility spectrometry (IMS): drift time (t_d), reduced mobility (K_0), and CCS (Ω). The drift time depends on the instrument and its conditions. Consequently, most databases for IM-MS measurements contain CCS values [82]. The CCS values for different IMS platforms may differ up to 2% [83]. Ion mobility-mass spectrometry (IM-MS) is used to separate conformational isomers or complex mixtures of isobars or isomers. IM-MS separates the charge states of ions (e.g., proteins) or filters the spectra by extracting the targeted analytes' signals [77].

Computational methods are important tools in understanding experimental data and can be used to calculate CCS values. Molecular modeling generates the model structures of the analyte and then matches them experimentally. Different theoretical computational approaches are used to predict the 3D structures of analytes, such as molecular mechanics, molecular dynamics, docking, semi-empirical, density functional theory, or ab initio calculations [84]. Born-Oppenheimer Molecular Dynamics (BOMD) theory assumes that the electronic waveform is at its ground state. BOMD provides time-resolved trajectories by calculating nuclei motions and all valence-electron interactions [85]. The workflow of calculating CCS values via BOMD and density function theory (DFT) is shown in Fig. 8. Briefly, the initial structures of molecules should be generated, and BOMD trajectories for each conformer/protomer should be run. The proton's initial position is not constrained, so it can change its position due to nuclear and valence-electron motion. Then, the snapshots of each trajectory are gradient-optimized, with further removal of duplicates and high-energy ions. The remaining ions are subjected to density functional theory calculations with further calculation of CCS values using MobCal$_{MPI}$ [85–87].
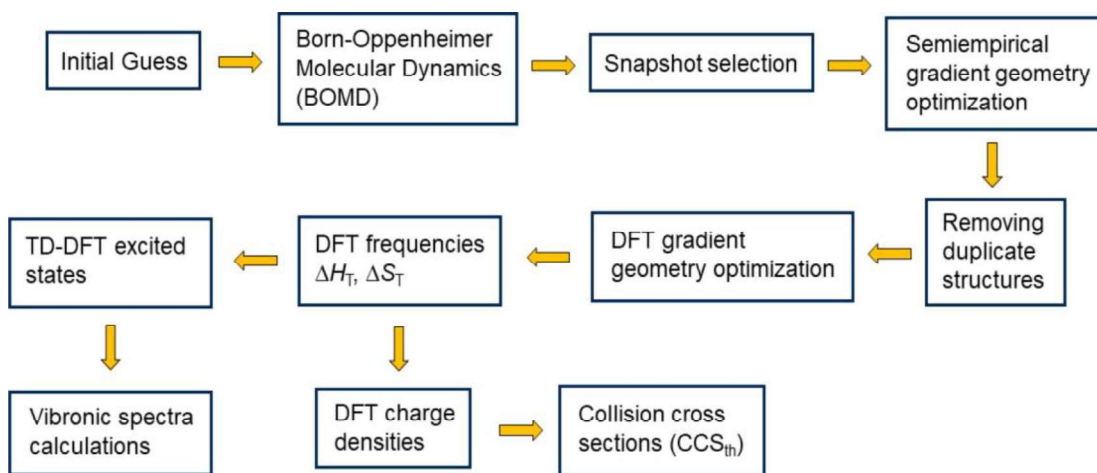
Figure 8 Scheme of procedure for theoretical calculations of CCS by BOMD and density function calculations. Reprinted with permission from [87]. Copyright © 2024 American Society for Mass Spectrometry.

There are several methods for theoretical calculations of CCS values. One of those is projection approximation (PA). This is the simplest, fastest method but lacks accuracy [88]. This method takes atoms of molecules as hard spheres with a radius. The sample has various orientations on which a rotation matrix (buffer gas) can be randomly applied. Then Monte Carlo integration method can be used to determine the projection area at each orientation. It also takes into account the buffer gas radius. CCS is determined from the averaged area of the ion's projection across many random orientations. This method ignores the scattering process and long-range interactions between buffer gas and ion [84,89].

Nevertheless, the modified PA-based algorithms have better accuracy than the PA method alone. This can be seen in the work of Bleiholder et al. where the modified PA-based method showed a good correlation (<2%) with the trajectory method (TM) [89]. The PA-based algorithm - the projected superposition approximation (PSA) method reproduces the CCS calculation with an error of 10% [90]. A local collision probability approximation (LCPA) method combines the calculations of the PA method as well as TM. It is based on replacing the scattering trajectory with the collision probability function using the same potential of interaction between the ion and the buffer gas [91].

Another method of theoretical CCS determination is the exact hard sphere scattering (EHSS) method. This method neglects the interactions of buffer gas and the ion and uses only the scattering and hard-sphere collisions [92]. The EHSS-based method of Scattering on Electron Density Isosurfaces (SEDI) uses the defined surface shape and

defined total electronic density value [93,94]. The diffuse hard sphere scattering model (DHSS) is based on the prediction of how atoms would collide with the buffer gas if they vibrate and rotate [95].

The trajectory method (TM) is considered to be a more complex, most accurate method for CCS prediction [84,88]. This method models the momentum transfer using the scattering process, long-range interactions between the buffer gas and the ion, and their collisions. This method uses the ion-induced dipole term with Lennard-Jones (L-J) interaction potential to predict the CCS values [96]. TM-based method Callidoscope uses both helium and nitrogen as buffer gas options. Ewing S. A. et al. compared CCS values calculated from a Collidoscope and IMoS. CCS values from Collidoscope are within 4 % of CCS calculated with IMoS software for ions with masses ~18 Da to ~800 kDa [97].

Different software based on the theoretical calculations mentioned above are shown in Table 1 [84].

Table 1. Summary of the most common CCS software. Reprinted and adapted with permission from [84].

Software	Method	Buffer gas	Reference
MobCal	PA	He	[92,98]
	EHSS	He	
	TM	He	
MobCal[a]	TM-L-J-scaled	He, N_2	[96,99,100]
WebPSA	PSA	He, N_2	[89]
Sigma	PA	He	[101]
IMPACT	PA	He	[102]
CCSCal	PA	He	[103]
-	LCPA	He, N_2	[91]
-	SEDI	He	[94]
Collidoscope	TM	He, N_2	[97]
HPCCS	TM	He, N_2	[104]
MobCal-MPI	TM	He, N_2	[105,106]
IMoS	PA	He, N_2	[107]
	EHSS/DHSS	He, N_2	[95]
	TM/DTM	He, N_2	[108]

Machine learning and deep learning are the alternative approaches to the theoretical calculations of CCS. Machine learning uses the training data set with known experimental CCS values, a set of molecular descriptors, a prediction algorithm, and a validation data set [109]. Different prediction algorithms [110] are used in machine learning, such as support vector regression [111–113], artificial neural networks, or partial least squares regression

[114]. CCS prediction using machine learning methods based on regression models is faster (less than 10 min on an office laptop) than MOBCAL (15 h, requiring high performance computing facility) [114]. Deep learning is a part of machine learning that uses large data sets and neural networks to make CCS predictions. Meier F. et al. used deep learning to predict over 1 million CCS values of peptides [115]. Another example of deep learning is AlphaPeptDeep software [116]. It can predict the retention times, intensities in mass spectra, and CCS values. This software can process peptides and peptides with post-translational modifications [116]. Other software that uses neural networks are DeepCCS [117] and DarkChem [118]. Both software have an average error of ~ 2.5% for predicting CCS values.

Several IMS platforms are available on the market, as seen in Fig. 9. Those ion mobility spectrometers can be divided into three categories: a) time-dispersive (drift tube IMS (DTIMS), traveling wave IMS (TWIMS)), b) space or spatially dispersive (high-field asymmetric IMS (FAIMS), differential mobility analyzer (DMA), c) ion trapping and selective release (trapped IMS (TIMS)) [119].

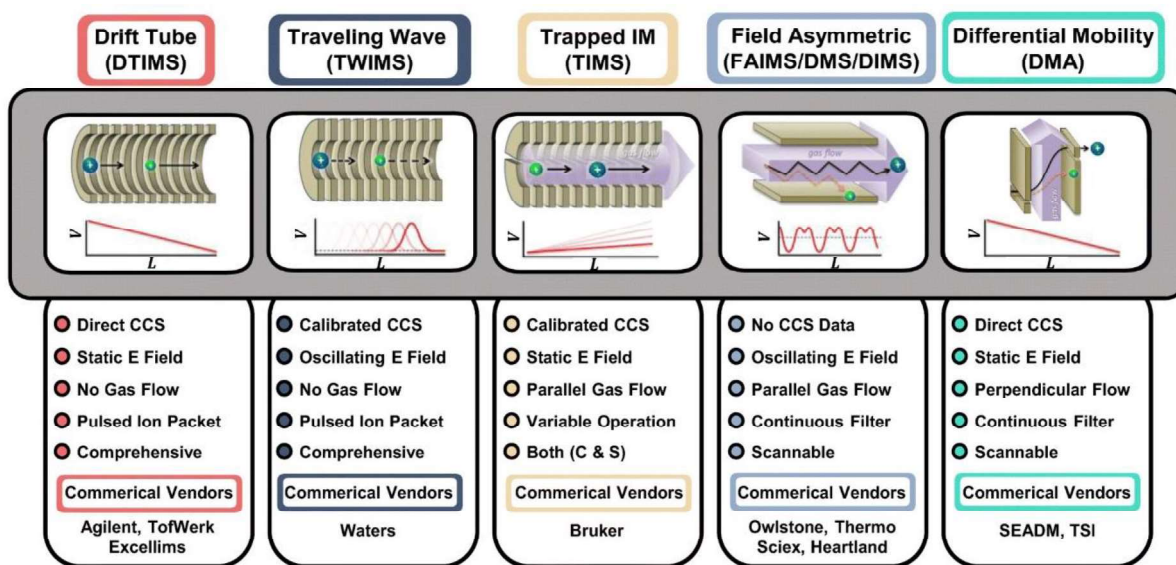
Figure 9 Different IMS instrumental platforms. Reprinted and adapted from [120]. Copyright © 2019 © American Society for Mass Spectrometry 2019

DTIMS enables the direct measurement of the CCS without the need for calibration. All accessible CCS databases use CCS determined by DTIMS [96,121,122]. The drift tube utilizes a uniform electric field through the drift region. There is no flow of

the buffer gas in the IM cell. Thus, ions move by applying the weak, uniform electric field. This enables the measurement of K, which can be used to calculate CCS values using Eq.3 [123]. There are two methods for CCS measurements in DTIMS: single-field (calibrant dependent) and stepped-field (calibrant independent). The stepped-field is the only calibrant-independent method that uses the multiple drift voltages that allow direct measurement of CCS from Eq.4. CCS values are estimated from the linear regression between the arrival time and inversed drift voltage. Therefore, stepped-field is the "golden method" of determination of CCS in DTIMS. The single-field method uses the single drift voltage and calibrants with known CCS values. The linear calibration curve between the CCS values and arrival time allows calculation of the experimental CCS [109,124–126]. The usage of the different calibrants for single-field methods can affect the CCS values. For example, after the IM calibration with homogeneously substituted fluorinated triazatriphosphorines, caffeine ([M+H]$^+$, m/z 195) had a CCS value of 139.6 Å^2 [127]. Calibration based on singly charged poly-DL-alanine (n=2-21) and drug compounds provided the CCS value for caffeine 135.2 Å^2 [128,129]. Stepped-field DTIM was also used for CCS determination of caffeine, which resulted in 145.4 Å^2 [128,130]. All of this affects the deviation of CCS experimental values from TWIMS platform, which uses the CCS values from the various databases of DTIMS.

TWIMS was first introduced by Waters Corp. in 2006 [131]. Similarly to DTIMS, there is no specific buffer gas flow in the drift region. IM cell consists of stacked ring electrodes on which the oscillation electric field is applied, which propels ions like on waves with the assistance of RF confinement to focus ion packets. Unlike the DTIMS, the TWIMS instruments need to use CCS calibration [132–134]. Constant wave height enables the use of low voltages, which can be beneficial for designing long path length platforms. One such platform is Structures for Lossless Ion Manipulations (SLIM), which has over 1.1 km path length with resolving power up to 2000 with multipass devices. The RF voltage and DC "guard" are applied for efficient ion transmission, allowing ions to pass the same path repeatedly [135,136].

Another IMS platform that uses the TWIM technology is cyclic TWIM. It consists of a closed-looped separator with a 98 cm path length that allows multipass separation (Fig. 10).
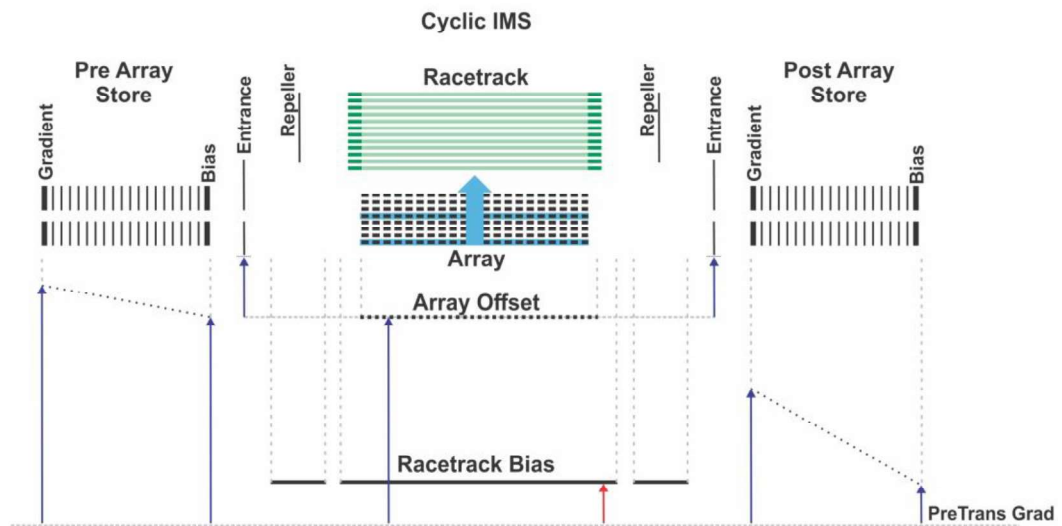
Figure 10 The scheme of the potential energy diagram of cyclic TWIMS system featuring the acceleration of ions on the T-Wave array sidewise into the cIM cell. (Screenshot from the Quarts Cyclic Sequence page, Masslynx).

Ions arrive at the entrance/exit multifunction array of pin electrodes (T-Wave array). As this T-Wave array can be programmable, it can accelerate ions sidewise by a traveling wave to the cyclic separator region. Aside from the cyclic drift cell, the instrument has two chambers, pre-array store (before cyclic ion mobility (cIM) but after the trap region and post-array (after the cIM) but before the transfer region), as can be seen in Fig. 10. Pre-array store and post-array are located in the same chamber as the cyclic ion mobility. They are used to transport the ions on and from the T-Wave array. Also, they can store the ions from the mobility experiments ("slices of ions") from the T-wave array [137]. This technology gives a unique possibility to perform IMS^n experiments. Ions are separated in multipass experiments. Higher resolving power (R) (up to ~750) can be achieved by increasing the number of passes (time that ions spend inside the mobility cell), which correlates with path length ($R \sim R_1 \cdot$ (number of passes)$^{0.5} \propto R \sim L^{0.5}$) [137]. The part of the ions can be isolated according to the arrival time and ejected to the pre-array store. The remaining part of ions, which are still in the mobility cell, can be removed by being ejected to TOF without triggering the data acquisition. Upon the reinjection from the pre-array store to the T-Wave array, potential can be applied to increase kinetic energy and, as a consequence, to induce the collision activation of ions. Therefore, the fragments can enter the T-Wave array for separation. These steps can be repeated, leading to IMS^n experiments [137–139].

Another advantage of cTWIM involving ion manipulation is the "top (or tip) and tail" function. This was applied by Kovac et al. [140] to the isomeric Tau phosphopeptides (Fig. 11). The sequence consists of injecting ions into the T-Wave array and their multipass separation. Then, the part of the arrival time distribution (ATD) can be selected. To perform such an experiment, "trimming" the part of the interest should be done by ejection of the tip. This step consists of "cutting" (sending the part of the ions to the detector without the data acquisition) before the peak of interest. The next step is to isolate the major peak part (s) and ejection of the tail (send everything behind the peak of interest to the detector without triggering data acquisition). In the end, only the peak of interest will be present on the ATD profile, which can be sent to multipass separation experiments (Fig. 11). This function can be beneficial allowing the separation of the desired conformer from the complex mixture [140].
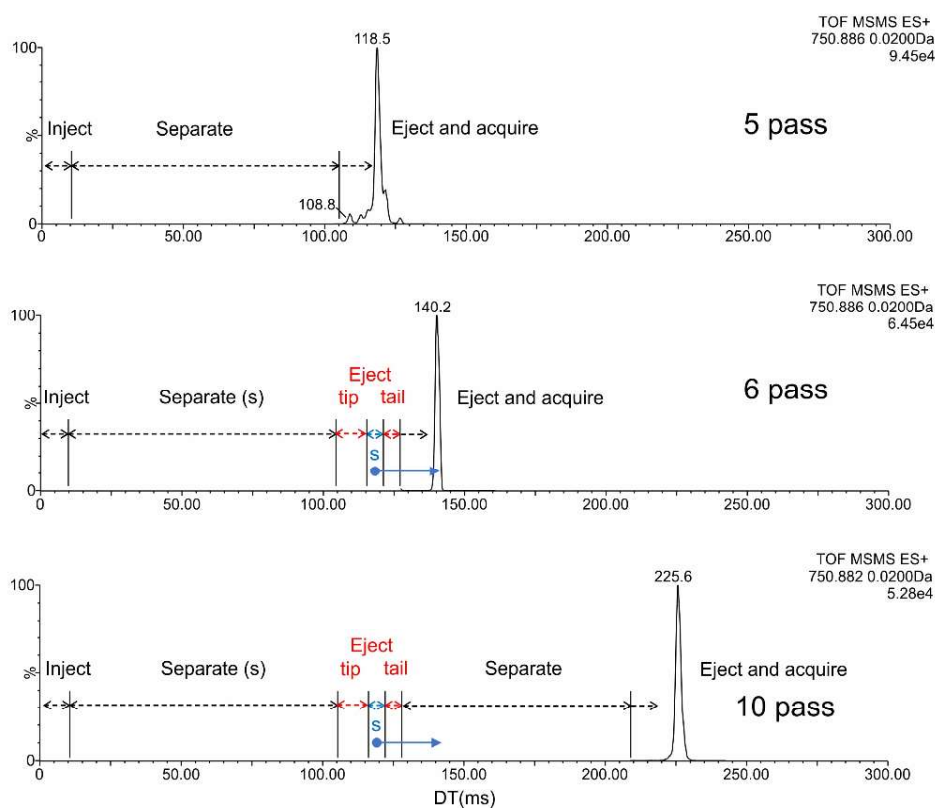
Figure 11 "Tip and tail multipass separation" of Tau phosphopeptides. Reprinted and adapted from [140]. Copyright © 2023 American Society for Mass Spectrometry.

Trapped ion mobility spectrometry (TIMS) uses the stationary electric field to accelerate ions against buffer gas flow (unlike DTIMS and TWIMS). The TIMS analyzer consists of a set of electrodes forming three regions: entrance funnel, TIMS mobility

tunnel, and exit funnel. The field strength decreases toward the ejection of ions from the mobility region. TIMS can only analyze each ion as it is being ejected, making it a highly selective technique. TIMS has high resolving power (~ 300). TIMS, as well as TWIMS, requires CCS calibration [120,141,142].

Field asymmetric waveform ion mobility (FAIMS), along with differential mobility spectrometry (DMS) and differential ion mobility spectrometry (DIMS), use the oscillating electric field in parallel buffer gas flow [120,143,144]. These IMS platforms are used as filters in the same way as quadrupoles. They do not pulse the ions into the mobility region. Due to the asymmetric waveform, FAIMS/DMS/DIMS cannot be used to directly measure CCS values. Nevertheless, they acquire continuous mobility data for selected analyte without the loss in the duty cycle and increase the signal-to-noise ratio for analytes by working as a filter [143,145].

Differential mobility analyzers (DMA) utilize the constant electric field in the same way as DTIMS. They are able to directly measure the mobility and CCS values without the need for calibration. DMA is used for the analysis of macromolecules and has very small applications for small molecules [146]. Nevertheless, recent studies show the separation of small molecules [147,148].

2.3 Coupling Ambient Ionization to Ion Mobility - Mass Spectrometry

Ambient ionization mass spectrometry allows rapid analysis of samples with minimal sample preparation or the use of a matrix. One of the disadvantages, as with other ionization sources, is that these methods cannot separate isomeric or isobaric species [149]. Therefore, coupling AIMS with ion mobility could increase its selectivity and applicability due to the ability to differentiate isomers [150].

The DESI source was first coupled to IMS/Q-TOF by Weston et al. [112] to analyze pharmaceutical drug formulations directly. Their work showed the limit of detection to the nanomole range with increased selectivity for the drugs. Desorption electrospray mass spectrometry imaging coupled with IMS can show the spatial distribution of the analyte on the sample surface, e.g., the analysis of edible nuts with CCS identification for lipids [151], or detection of fluoropezil in rat brain [152]. Another work is devoted to the analysis of tryptic peptides by DESI-IM-MS, which helped to improve the signal-to-noise ratio and distinguish charge-states and isobaric peptides [153].

Nanospray desorption electrospray can be coupled with various types of IMS, such as FAIMS, DTIMS, TWIMS, and TIMS platforms, to analyze proteins in complex biological samples [154–157]. Here, nano-DESI was modified with pneumatically-assisted transmission of ionized molecules towards the FAIMS and orifice of the mass spectrometer. This coupling successfully reduced isobaric interferences and enhanced the image contrast of protein ions but had poor protein sequence coverage [157]. Coupling nano-DESI with DTIMS allowed direct analysis of mobility (K) and, therefore, CCS values and provided an isomer-selective ion image [154]. Due to the low resolving power of DTIMS, nano-DESI was coupled with TIMS, which allowed the lipid isomers and isobars to be resolved [156].

PS-DTIM-MS and leaf-spray (LS)–DTIM-MS are used to rapidly separate constitutional pesticide isomers and determine CCS [126]. Moreover, PS-cTWIM-MS allowed the fast analysis of biomarkers for the diagnosis of Parkinson's disease [158].

Analysis of abused drugs can be performed by hyphenation of DART-MS with differential mobility spectrometry [159] while ASAP-IM-MS found application in the analysis of lubricants[160], and polymers[161,162].

All these applications show that merging ambient ionization with IM-MS offers advantages in improving the signal intensity and providing ion-selective drift time data. On the other hand, many of the AIMS techniques have not been coupled with IM-MS so far.

3 AIMS OF THE DISSERTATION THESIS

The thesis aimed to investigate ionization by developing the new modification of desorption nanoelectrospray ionization and to find new approach to cyclic ion mobility of new psychoactive substances. Different ionization techniques (ESI, nano-DESI, and DESI) and cyclic traveling wave ion mobility were used.

This dissertation thesis can be divided into the following tasks:

1. To develop the modification of desorption nanoelectrospray to improve ion transmission to increase the applicability of the ionization source;

2. To develop a simple procedure of isomeric ratio determination using characteristic ATD profiles of individual isomers.

The results could be found in articles published in [7] and [163].

4 EXPERIMENTAL PART

4.1 Signal Enhancement of Desorption Nanoelectrospray Ionization by Pressure Regulation at the Mass Spectrometer Inlet

This work was published in a first-author publication [7] and adapted and reprinted with permission from the journal:

Author's Contribution. Marianna Nytka – investigation, formal analysis, visualization, and writing the original draft.

Chemicals and samples preparation

3-fluoromethcathinone (3-FMC) and 3-methymethcathinone (3-MMC) were purchased from Cayman Pharma (Neratovice, Czech Republic); cathinone, buphedrone, methedrone, methylone, butylone, naphyrone were purchased from the Lipomed AG (Arlesheim, Switzerland), see Fig.12 for the structures. Methanol (LC-MS grade), formic acid ($\geq$98%), and hexamethyldisilazane ($\geq$99%) were purchased from Sigma-Aldrich (Prague, Czech Republic), and pyridine (p.a.) was purchased from Penta (Czech Republic). Milli-Q system (Millipore, Mollsheim, France) was used for water purification. Paracetamol (Paralen®, Zentiva-Sanofi Company, Czech Republic) was bought from a local pharmacy. Stock solutions were prepared with a concentration of 1 mg/mL in methanol/ water (1:1, v/v) and stored in a fridge. The working solution of a mixture was prepared by diluting the stock solutions to a final concentration of 1 µg/mL. NanoDESI analysis was performed using a mixture of methanol/water (75/25, v/v) as a spraying solvent.
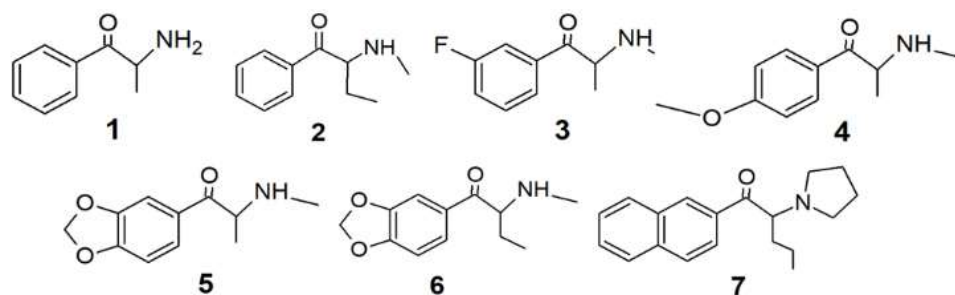
Figure 12 Structures of NPS (*m/z* of protonated molecules): (1) cathinone (*m/z* 150); (2) buphedrone (*m/z* 178); (3) 3-FMC (3-fluoromethcathinone; *m/z* 182); (4) methedrone *(m/z* 194); (5) methylone (*m/z* 208); (6) butylone *(m/z* 222); (7) naphyrone (*m/z* 282). Reprinted and adapted from [7]. Copyright 2020 John Wiley & Sons, Ltd

Microscope slide treatment and sample deposition

The silanization procedure was performed and optimized at the Department of Analytical Chemistry, Palacký University Olomouc. It is based on immersing the microscope slides into the hexamethyldisilazane/ pyridine (50/50, v/v) in a closed vessel for 2 h at 120 °C with subsequent washing with water and ultrasonication for 1 min in water. The mixture of analytes was deposited (total volume 56 µl in five layers) onto silanized slides by SunCollect MALDI spotter (SunChrom, Friedrichsdorf, Germany) to generate homogeneous layers. The final concentration of each analyte on the surface was 0.5 ng/mm^2 (surface area of 1.89 x 0.6 cm). Paracetamol or traces of NPS were fixed onto microscope slides by a double-sided tape. In the nanoelectrospray setup, the spraying tip pointed toward the inlet of the heated transfer capillary. The nanoelectrospray setup was evaluated using 1µg/mL of the NPS in methanol/water/formic acid (75/25/2, v/v/v)).

Instruments

Analysis of NPS was performed on Xevo TQD triple quadrupole mass spectrometer (Waters, Manchester, UK) with modified custom-made inlet (Fig. 13).
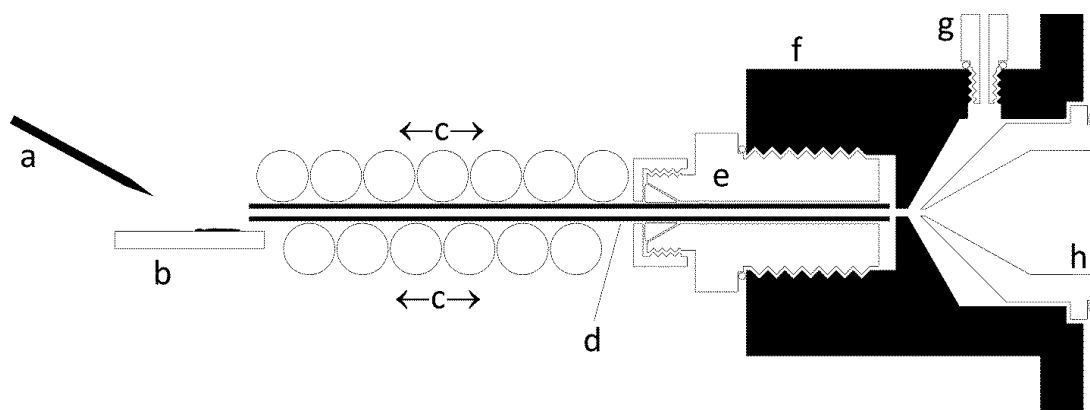
Figure 13 Scheme of custom-made MS inlet: a - nanoelectrospray tip; b - sample on support; c - threads of a heating rope; d - stainless steel inlet capillary; e - Swagelok SS-100-1-OR tube fitting, sealing the heated capillary (d) by a ferrule; sealed to the inlet block by an O-ring; f - inlet block; g - reduced pressure port hose adapter, sealed to the inlet block by an O-ring; h - sample cone (native part of the mass spectrometer, fitted in its original location and held by the inlet block (f), sealed to the instrument by an O-ring). Reprinted and adapted from [7]. Copyright 2020 John Wiley & Sons, Ltd

Data were collected in positive ionization mode six times (1 min acquisition each). The nanoDESI consists of an inlet block, heated capillary, and original sample cone. The inlet block is equipped with a port for an auxiliary pump connection. It allowed pumping of the inner compartment of the MS inlet in comparison with designs connecting a pump to a refluence tube [164] or a source chamber [165] in front of the inlet. Pressure drop (difference between atmospheric pressure and pressure in the inlet) was measured by a manometer and regulated by a needle valve, both mounted between a port (g) and the auxiliary pump. The capillary was heated by a heating rope connected to the Regbox heater driver (Jakar Electronics, Karvina, Czech Republic). As in the DESI source [1], the gas flow outlet and the interlock for the ESI source were blocked. Desorption nanoelectrospray consisted of a nanoelectrospray tip (2 ± 1 μm I.D., PicoTips emitter, New Objective, Woburn, USA) and a sample stage, both manually movable in the $x - y - z$ axes.

Proper geometry was set to obtain the best spectra quality:

- nanospray tip - target plate: vertical distance ~ 2 mm;
- angle ~ 30°;
- nanospray tip - the center of sample spot: horizontal distance ~ 2 mm;
- microscope slide - heated capillary: vertical distance ~ 1 mm, angle ~ 0°;
- center of sample spot - heated capillary: horizontal distance ~ 2 mm.

Source parameters were tuned in positive ionization mode and set as follows: capillary voltage 2.2 kV, TQD source temperature 100 °C, temperature of the heated capillary 100°C, 180 °C, 200 °C, 220 °C, pressure drop from 0.08 (closed needle valve) to 0.8 bar. MassLynx 4.1 software (Waters Corp., Wilmslow, UK) was used for instrument operation and data acquisition. Data were collected in six replicates (1 min acquisition each) and processed by OriginPro 2020 (OriginLab, Northampton, USA).

4.2 Cyclic Ion Mobility-Mass Spectrometry of New Psychoactive Substances

This work was published as a first-author publication [163] and with the permission adapted and reprinted from:

Nytka M., Wan J., Tureček F., Lemr K. Cyclic ion mobility of isomeric new psychoactive substances employing characteristic arrival time distribution profiles and adduct separation. J. Am. Soc. Mass Spectrom. 2024; https://doi.org/10.1021/jasms.4c00127

ACS open access

Author's Contribution. Marianna Nytka – investigation, formal analysis, visualization, and writing the original draft.

Chemicals and samples' preparation

Standards of hydrochlorides of 3-fluoromethcathinone and 3-methymethcathinone were purchased from Cayman Pharma (Neratovice, Czech Republic), 4-fluoromethcathinone, 1,3-benzodioxolylbutanamine, methedrone, buphedrone were provided from the Lipomed AG (Arlesheim, Switzerland) and used as-is (see Fig.14 for structures). LC-MS grade methanol and water were provided by Fisher Chemical (Fisher Scientific, United Kingdom). Sodium nitrate (p.a.) was provided by Penta (Ing. P.Švec, Czech Republic). Lithium chloride (≥99.0 %, BioXtra), sodium hydroxide (p.a.) and formic acid (≥98%), N-ethylaniline, acetaminophen, caffeine, sulfaguanidine, and alprenolol were provided by Sigma Aldrich (Prague, Czech Republic). The mixture of N-ethylaniline, acetaminophen, caffeine, sulfaguanidine, and alprenolol will be called a "small molecule mixture" in the further text.

Stock and working solutions of individual analytes were prepared at concentrations of 1 mg/mL and 100 ng/mL, respectively, in methanol/water (1/1, v/v). Isomeric mixtures with a total concentration of 100 ng/mL (methanol/ water, 1/1 v/v) were analyzed: a) 3-MMC and buphedrone (*m/z* 178.13); b) 3-FMC and 4-FMC (*m/z* 182.11); c) BDB and methedrone (*m/z* 194.13). They were prepared in isomeric ratios: 5%, 10%, 25%, 40%, 50%, 60%, 75%, 90%, 95%. Six data acquisitions were performed for each solution. The model samples for FIA-cIM-MS analysis were prepared in the range from 5% to 45% in six replicates, one data acquisition for each replica was performed.

CCS calibrants (small molecules mixture) were prepared with the working concentration of 2 µg each/mL (acetonitrile/water (1/1) with 0.1 % of formic acid).

Figure 14 Structures of investigated cathinones and phenethylamine (BDB) [163]. ACS open access

Instrument

Cyclic ion mobility- mass spectrometry

The analyses were conducted on SELECT SERIES Cyclic IMS Q-TOF (Waters Corp., Wilmslow, UK). Samples were directly infused into a normal flow ESI source at the flow rate of 5 µL/min and measured in positive ionization mode. 0.5 mmol/L sodium formate in propan-2-ol/water (90/10, v/v) was used for mass calibration (*m/z* 50-1200). The instrument was operated under two sets of settings, default and labile (Table 2). The precursor ion was selected in quadrupole resolution with highmass 15, lowmass 4.9 for protonated ions, and highmass 10, lowmass 2 for the adduct ions. Ion mobility parameters for single and multipass experiments are shown in Tables 3 and 4.

Table 2 Instrument settings

Settings	Default	Labile*
Capillary Voltage (kV)	2	1
Cone Voltage (kV)	10	
Source Temperature (°C)	100	
Desolvation Temperature (°C)	250	

Cone Gas Flow (L/h)	30	
Desolvation Gas Flow (L/h)	600	
CE Trap (V)	6	2
CE Transfer (V)	4	1
StepWave Body Gradient (V)	20	10
Ion Guide TW Pusle Height (V)	0.4	0.2
Trap Entrance (V)	2	1
Trap Bias (V)	2	1.5
Trap DC (V)	-4	-4
Post Trap Gradient (V)	3	1.5
Post Trap Bias (V)	35	16
StepWave RF (V)	200	100
Ion Guide RF (V)	300	
Drift Cell RF (V)	300	200
Transfer RF (V)	200	
Transfer RF Gain	5	
Helium Flow Rate (L/h)	120	
Nitrogen Flow Rate (L/h)	40	
TW Static Height (V)	15	13
Wave Amplitude (V) (Eject and acquire)	15	10
TOF push per bin	1	

    * used for BDB and methedrone only

Table 3 c-IMS Parameters for single pass separation for all isomeric pairs and CCS calibrant [163]. ACS open access

Traveling wave parameters		Sequence			
		Parameter	Inject	Separate	Eject and Acquire
Cyclic TW Velocity (m/s)	375	Time (ms)	10	2	Automatic

Array TW Velocity (m/s)	375	Pre Array Gradient (V)	85	85	85
TW static height (V)	15	Pre Array Bias (V)	70	70	70
TW start height (V)	15	Array Entrance (V)	10	30	50
TW limit height (V)	35	Wave Height (V)	2	0	15
TW ramping rate (V/ms)	2.5	Array Offset (V)	45	70	45
		Array Mode	Forward	Sideways	Forward Eject
		Array Exit (V)	50	30	2
		Post Array Gradient (V)	35	35	35
		Post Array Bias (V)	10	10	10

The separation time for CCS calibrants for 2 pass separation experiments is shown in Table 7.

Table 4. Separation time in multipass experiment [163]. ACS open access

Precursor ion	Number of passes	Separation time (ms)
3-MMC/Buphedrone		
[M+H]$^+$ (m/z 178.13)	5*	32
	7	46.5 (DI, DESI) 47 (FIA)
[M+Na]$^+$ (m/z 200.11)	5	40
	10	85
[M+Li]$^+$ (m/z 184.13)	5	40
	10	82
3-FMC/4-FMC		
[M+H]$^+$	5	30

(*m/z* 182.10)	10	65.65 (DI) 65.95 (FIA, DESI)
[M+Na]+ (*m/z* 204.08)	10	80
[M+Li]+ (*m/z* 188.10)	25	204.9

Flow injection analysis

FIA-cIM-MS analyses were performed on the Waters ACQUITY UPLC I-Class system fitted with the PEEK tubing (1/16"x0.13 mm) to bypass the column. It was coupled with the SELECTED SERIES Cyclic IMS (Waters Corp., Wilmslow, UK) and operated in positive ionization mode. The instrument settings (default (Table 2)) and the ion mobility (Tables 3 and 4) were the same as for direct infusion. The precursor ion was isolated in quadrupole and then fragmented in the trap cell with CE 28 V for BDB and methedrone (*m/z* 194.11). Methanol/water (1/1, v/v) was selected as a carrying liquid with a flow rate of 0.1 mL/min. Injection volume was 5.0 µL for 3-MMC and buphedrone *(m/z* 178.13); 3-FMC and 4-FMC (*m/z* 182.11) pairs. Samples were measured in six replicates, and one data acquisition was made for each replicate. The injection volume for BDB and methedrone was 10.0 µL.

Desorption electrospray

The mixtures of isomeric pairs with the same ratios as for the ESI-cIM-MS experiments (see the Chemicals and samples´ preparation) were deposited onto the Omni Slide Hydrophobic Arrays (Prosolia, Waters Corporation, Wilmslow, UK). The amount on the spot was 3.54 ng/mm^2 and was calculated by the mass of the analyte on the spot divided by the area of the spot. Analysis was performed on Select Series Cyclic IMS equipped with a 2D-DESI ionization source (Prosolia, Waters Corporation, Wilmslow, UK). The original sprayer was replaced with a DESI XS sprayer (Waters Corporation, Wilmslow, UK). Methanol/water (80/20, v/v) was used as a spraying solvent at 2.0 µL/min. The capillary voltage was held at 0.75 kV; the nebulizing pressure was 0.076 MPa; source temperature was set to 150 °C; the cone voltage to 10 V. The ion mobility settings were kept as in Tables 2 and 3.

DESI sprayer geometry was set as follows:

- the spray impact angle was 75°;
- spray nozzle to the inlet tube orifice was 4 mm;
- distance between the inlet tube orifice and the surface ~0.5 mm;
- spray nozzle to the surface distance was 2 mm.

Born-Oppenheimer molecular dynamics (BOMD) trajectory calculations

Prediction of structures' geometries and theoretical calculations of CCS values was performed by Prof. Tureček's team at the University of Washington in Seattle, USA. (Details see in [163] and in Chapter 2.2)

Briefly, ion structures were obtained by applying Born-Oppenheimer molecular dynamics (BOMD) trajectory calculations of several initial conformers, tautomers, and protonation isomers. That was followed by gradient geometry optimization with density functional theory. No other protonation isomers than those displayed in Fig. 27 were found as local low-energy minima in the gas phase. The lithium adducts showed multiple conformers for keto and enol tautomers that were local energy minima. The lowest-energy structures for each Li-ion tautomer are shown in Fig. 33. Collision cross sections (CCS) in nitrogen were calculated using the modified ion trajectory method (MobCal$_{MPI}$) [105,106,166] using the MK charge densities. The reported CCS and standard deviations are obtained from averaging data from ten trajectory runs. The cartesian coorditanes of the M06-2X/6-31+G(d.p) optimized geometry of ions **1a$^+$**, **2a$^+$**, **1b$^+$**, **2b$^+$**, **3a$^+$**, **4a$^+$**, **3b$^+$**, **4b$^+$** shown in tables A1-A8, respectevly.

Table 5 Relative energies of protonated molecules [163]. ACS open access

Ion	Relative Gibbs Energy[a,b]		
	B3LYP[c]	M06-2X	M06-2X[d]
	6-31 +G(d,p)	6-31 +G(d,p)	def2qzvpp
(3-MMC-keto+H)$^+$ (**1a$^+$**)	0.0	0.0	0.0
(Buphedrone-keto+H)$^+$ (**2a$^+$**)	16	15	14
(3-MMC-enol+H)$^+$ (**1b$^+$**)	45	33	31
(Buphedrone-enol+H)$^+$ (**2b$^+$**)	62	50	47

[a]In kJ mol^{-1}. [b]Including zero-point energies, enthalpies, and entropies and referring to 310 K. [c]Fully optimized with GD3-BJ empirical dispersion corrections. [d]Single-point energy calculations on M06-2X/6-31+G(d,p) optimized geometries.

Table 6 Relative energies of $[M+Li]^+$ ions [163]. ACS open access

Ion	Relative Gibbs Energy[a,b]		
	B3LYP[c]	M06-2X	M06-2X[d]
	6-31 +G(d,p)	6-31 +G(d,p)	def2qzvpp
(3-MMC-keto+Li)$^+$ (**3a$^+$**)	0.0	0.0	0.0
(Buphedrone-keto+Li)$^+$ (**4a$^+$**)	17	15	16
(3-MMC-enol+Li)$^+$ (**3b$^+$**)	82	78	75
(Buphedrone-enol+Li)$^+$ (**4b$^+$**)	101	95	93

[a]In kJ mol^{-1}. [b]Including zero-point energies, enthalpies, and entropies and referring to 310 K. [c]Fully optimized with GD3-BJ empirical dispersion corrections. [d]Single-point energy calculations on M06-2X/6-31+G(d,p) optimized geometries.

Data were acquired and processed using Masslynx v.4.2 (Software Change Note 1016, Waters Corp., Wilmslow, UK), a modified version of Driftscope v.2.9 (Waters Corp., Wilmslow, UK), and processed in OriginPro 2020 (OriginLab, Northampton, USA).

Cyclic-TWIM CCS calibration for multipass separation

The mixture of small molecules (Table 7) was directly infused into the ESI source using default settings. The flow rate was set to 5µL/min. Each *m/z* of the calibrant was isolated in quadrupole and sent to one pass (98 cm) and two passes (196cm) separation in the cTWIM cell. The data was peak detected with Drifscope 2.9 software. CCS calibration was performed according to the procedure of McCullagh et al. [167]. Arrival time is the value that includes injection time (time needed for ions to arrive on the T-Wave array), drift time (time that ions spend inside the mobility cell), and dead time (time the ions exit the mobility cell to reach the detector).

We used the calibrant's arrival times at the peak's apex. The arrival time in bin number was converted to a millisecond scale. This was performed by multiplying the bin number by the number of TOF pushes per bin and the V mode pusher period for a specific mass range (*m/z* 50-1200, 0.066). The result of multiplication was added ADC start delay (Eq.5).

$$t_{ms} = t_{bin} \times Pusher\ Period \times TOF\ pushes\ per\ bin + ADC\ start\ delay \qquad (5)$$

ADC start delay includes the injection time and separation time.

The calibration drift times (cycle time) were calculated by subtracting the arrival time for 1 pass (t_{a1p}) from two passes arrival time (t_{a2p}) (Eq.6).

$$t_d = t_{a\,2p} - t_{a\,1p} \qquad (6)$$

The time ion exiting the cyclic cell to reach the detector (dead time) (t_0) was calculated by subtracting the cycle time from 1 pass data (Eq.7).

$$t_0 = t_{a\,1p} - t_d \qquad (7)$$

For the analytes, CCS values were calculated using respective drift times ($t_{d\,analyte}$) (Eq.8)

$$t_{d\,analyte} = \frac{t_{a\,analyte}\ - \overline{t_0}}{n} \qquad (8)$$

Where $t_{a\,analyte}$ is the arrival time of analytes, $\overline{t_0}$ - the dead time (average value from 6 measurements), and n - the number of passes.

Excel file provided by Waters Corp. (e.g. the one from © Johanna Hofmann, Kevin Pagel, Fritz-Haber-Institute of the Max-Planck-Institute, Berlin) was used to evaluate CCS values. A calibration curve was constructed by plotting ln(CCS', Å^2) vs. ln(t_d') (Fig.15). CCS' is the collision cross section corrected for ion charge and reduced mass of ion and drift gas (nitrogen). t_d′ is a corrected drift time for *m/z* dependent flight time (depends on Enhanced Duty Cycle (ECD) delay coefficient, 1.50 ms for our experiments, Eq.9) [168,169].

$$t_d' = t_{d\,analyte} - 0.001 * \text{EDC delay coefficient} * \sqrt{m/z_{analyte}} \qquad (9)$$

Table 7 Ions Used for CCS Calibration [163]. ACS open access

Name of the Compound	m/z	z	MW (Da)	DTCCS$_{N2}$ (Å^2)	Ref.	Separation Time* (ms)
N-ethylaniline	122.12	1	121.18	124.50	[96]	6
Acetaminophen	152.07	1	151.17	130.40	[96]	8
Caffeine	195.10	1	194.19	136.90	[129]	10
Suflaguanidine	215.06	1	214.05	148.40	[122]	10
Alprenolol	250.20	1	249.34	157.50	[96]	12

* 2 pass separation experiments
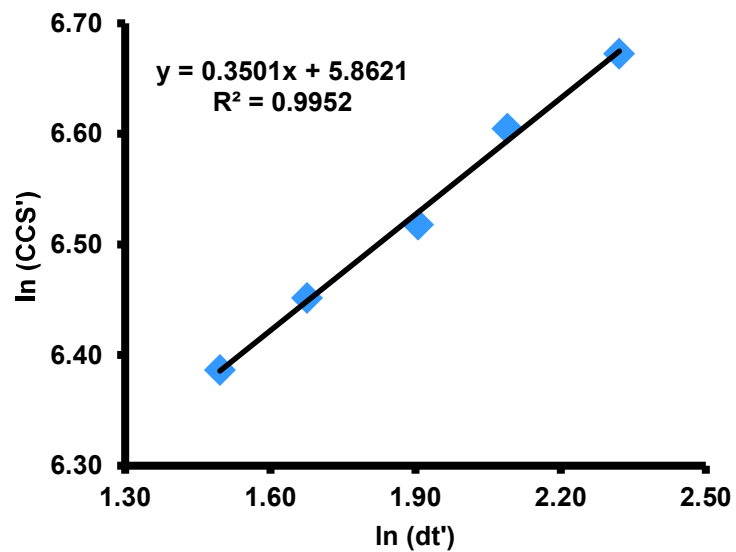
Figure 15 Calibration plot for protonated molecules.

Similar to Fig. 15, a calibration curve was constructed for lithiated molecules $(\ln(CCS') = 0.3617 \times \ln(t_d) + 5.842, R^2 = 0.9953)$.

5 RESULTS AND DISCUSSION

5.1 Signal Enhancement of Desorption Nanoelectrospray Ionization by Pressure Regulation at the Mass Spectrometer Inlet

This work was published in a first-author publication [7] and adapted and reprinted with permission from the journal:

Nytka, M, Borovcová, L, Fryčák, P, Barták, P, Lemr, K. Signal enhancement in desorption nanoelectrospray ionization by custom-made inlet with pressure regulation. J Mass Spectrom. 2020;55:e4642. https://doi.org/10.1002/jms.4642 Copyright 2020 John Wiley & Sons, Ltd.
Licence number 5730170914154.

Author's Contribution. Marianna Nytka −investigation, formal analysis, visualization, and writing the original draft.

The new custom-made mass spectrometer inlet was designed and constructed considering three parameters: length of the heated capillary, its temperature, and pressure regulation at the MS inlet (the first vacuum stage). All three parameters can control the desolvation of ions, affect ion transmission, and increase the intensity of the ion signal. Their influence was evaluated for synthetic cathinones (Fig. 12) as nanoDESI might be useful for their detection, e.g., in seized street samples. Four different lengths (Fig. 16) of the heated capillary were tested (46, 61, 76, and 99 mm) at 200 °C. Although the effect of the capillary length was insignificant, slightly better ion signal intensities were observed using the shortest one selected for the following experiments.

Figure 16 Tested ion transfer capillaries for nanoDESI with different lengths.
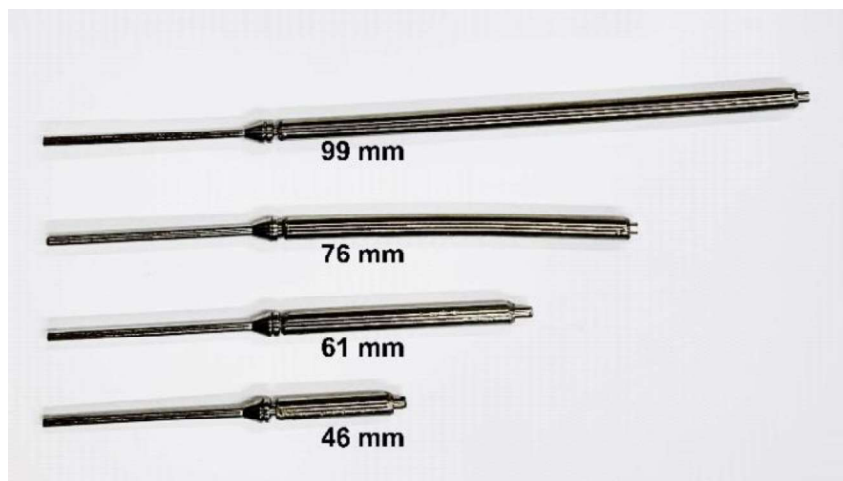
5.1.1 Influence of the Pressure Drop

The regulation of pressure drop at the MS inlet significantly influenced the signal intensity. Auxiliary pumping generated a pressure drop at the MS inlet in the 0.20–0.80 bar range. At reference condition (the lowest pressure drop 0.08 bar, which means the highest pressure in the inlet), the needle valve connecting the auxiliary pump with the MS inlet was closed, and the pressure reduction was generated only by the vacuum system of the mass spectrometer. Since pressure drop represents the difference between atmospheric pressure and pressure in the evacuated inlet compartment, its higher value means lower pressure in the inlet and, thus, higher vacuum suction. In the tested range, the ion signal intensity of all NPS grew between 0.08 and 0.20 bar, reached a maximum, and then gradually decreased (Fig. 17). The effect is similar to that observed for the extracting gas flow rate in DESI equipped with the transport tube [170]. The signal improvement was compound dependent.The change from 0.08 to 0.20 bar caused the increase of signal intensity less than two-fold for naphyrone but almost one order for buphedrone and more than one order for cathinone and 3-FMC.

Further, nanoDESI experiments were performed at a pressure drop of 0.40 bar, giving slightly lower signal intensities than 0.20 bar. Nevertheless, the dependencies are flatter at around 0.40 bar (Fig. 17), and variation of signal intensity is less sensitive to pressure drop changes. Generally, the pressure at the mass spectrometer inlet is determined by the power of the vacuum system of a particular mass spectrometer, and the influence of auxiliary pumping can vary. Its optimum setting can be instrument dependent. Nonetheless, it is evident that vacuum suction is important for nanoDESI efficiency.

Hence, neither nebulizing gas nor auxiliary gas is used, pressure drop regulation is the only available experimental parameter driving drag force in the source. Pressure regulation increased the drag force occurring due to vacuum suction. The force influenced the transport of charged droplets and ions from the sampling area (atmospheric pressure) to the first evacuated region of the mass spectrometer.

The effect of pressure regulation was also evaluated in the nanoelectrospray setup. The nanoelectrospray tip was turned towards the heated capillary inlet. Although such source geometry may not be optimal, a higher pressure drop might help to overcome this drawback. A signal intensity increased substantially between 0.08 and 0.20 bar, and the effect was less compound dependent than for nanoDESI (see Fig. 17 and 18). Vacuum suction enables the collection of more charged droplets/ions created by nanoelectrospray and generates a gas flow that can assist in ion evaporation from the charged droplets. As the effect of pressure drop regulation on signal intensity differs for the analyzed compounds using nanoDESI (Fig. 17), we could speculate that the pressure regulation does not influence just the transport of ions but might also affect the process of desorption. Nevertheless, the desorption is dependent on various experimental conditions and properties of analytes (e.g., the composition of spraying liquid, as well as surface activity and polarity of analytes), and all of them can influence the resulting ion signal intensity in a mass spectrum.
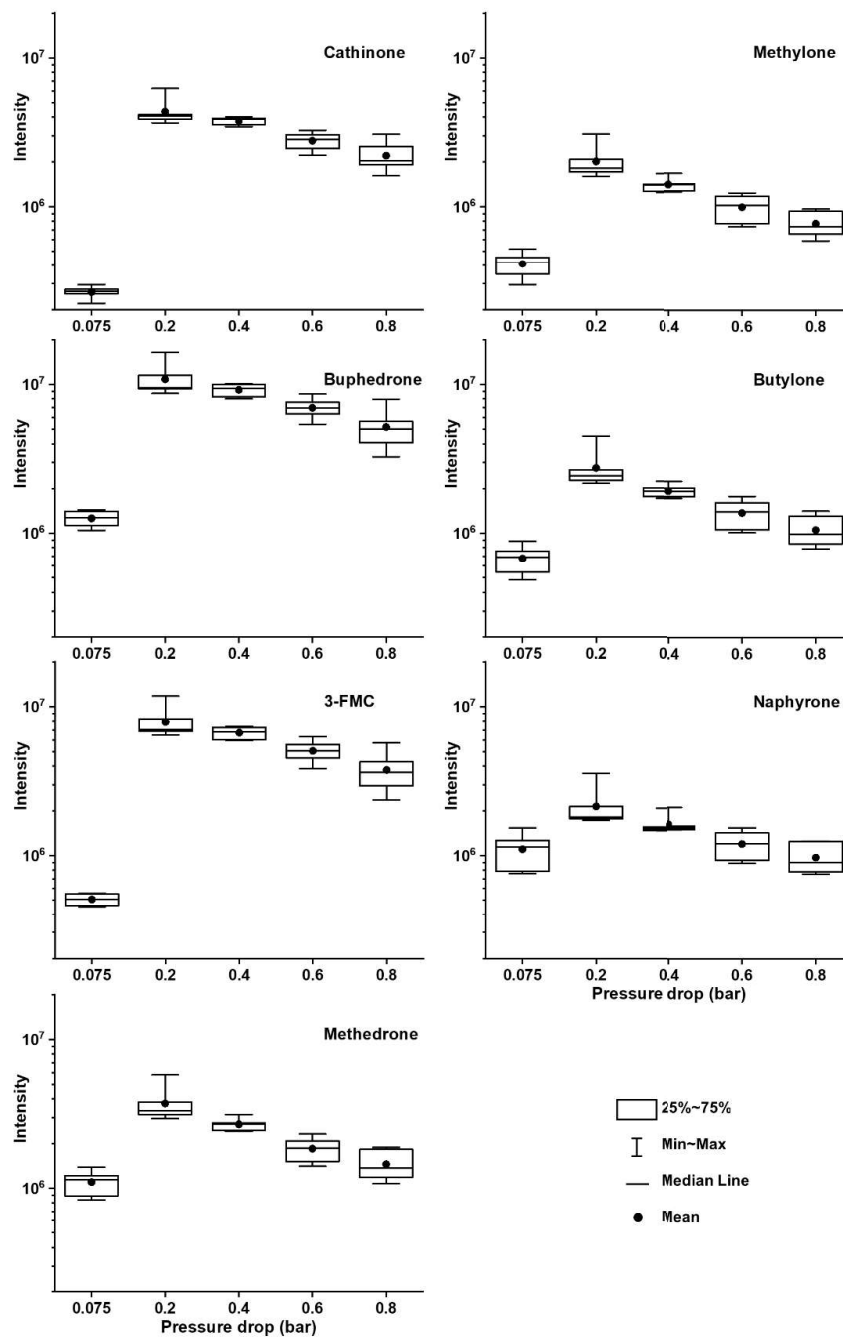
Figure 17 Influence of pressure drop on the $[M+H]^+$ ion signal intensity of cathinones ionized by desorption nanoelectrospray (nanoDESI). The temperature of the heated capillary (46 mm) was set to 200 °C. A mixture of the standards was deposited on a silanized microscope slide [7]. Copyright 2020 John Wiley & Sons, Ltd
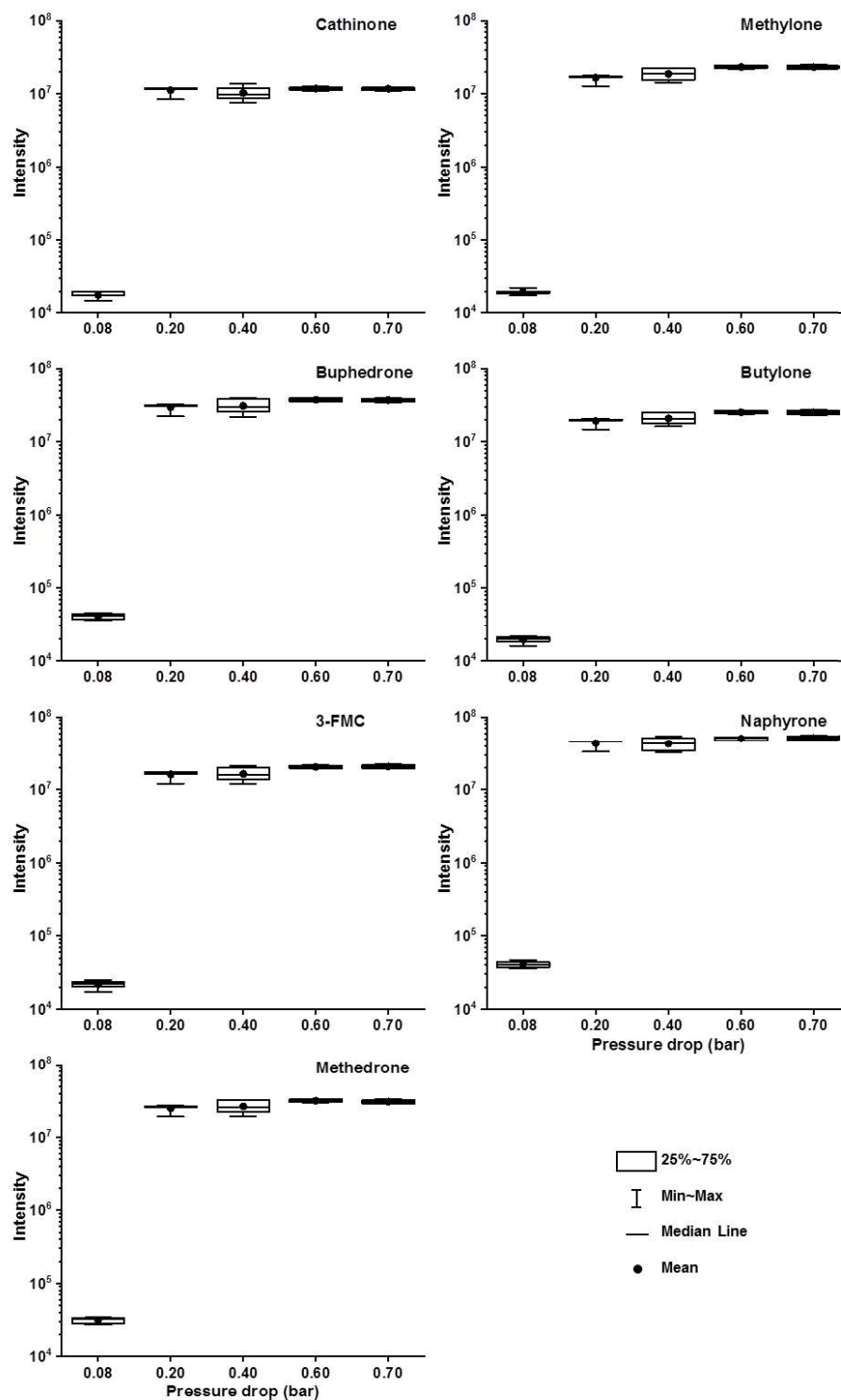
Figure 18 Influence of pressure drop on the [M+H]$^+$ ion signal intensity of cathinones ionized by nanoelectrospray. A spraying capillary was filled with the solution of a mixture of standards and directed toward the heated capillary inlet. The temperature of the heated capillary (46 mm) was set at 200 °C. The maximum pressure drop of 0.7 bar

was achievable for the nanoelectrospray setup [7]. Copyright 2020 John Wiley & Sons, Ltd

5.1.2 Influence of the Temperature of the Heated Capillary

Finally, the heated capillary's temperature was also considered as an important experimental parameter. The profile of change of signal intensity shown in Fig. 19 is typical for five studied analytes (cathinone, methedrone, methylone, butylone, and naphyrone).
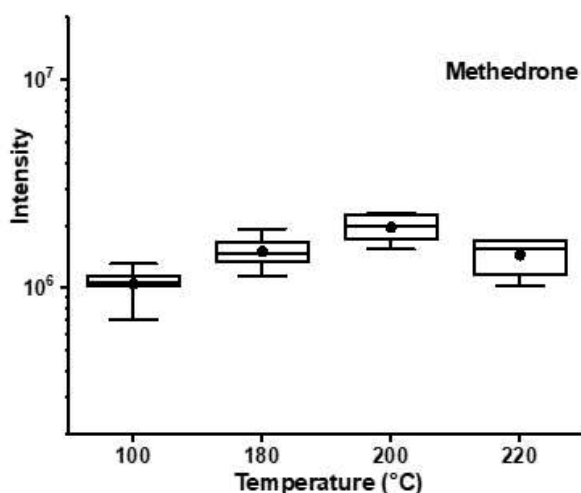
Figure 19 Influence of the heated capillary temperature on the $[M+H]^+$ ion signal intensity of the methedrone [7]. Copyright 2020 John Wiley & Sons, Ltd

For buphedrone and 3-FMC, the signal intensities were comparable between 100 °C and 200 °C (the differences were not statistically significant). A decrease in signal intensity was observed at 220 °C for all compounds. At lower temperatures, the droplets/ions can be less effectively desolvated. Higher temperature of the heated capillary can cause too fast solvent evaporation from the nearby sample surface, which can worsen its wetting. This wetting forms a thin liquid layer that is considered to be important for desorption and ionization in DESI [140], but less effective desorption and ionization may also be observed in nanoDESI. Although the temperature did not show such a strong effect as pressure regulation, its proper setting may be beneficial to the quality of mass spectra. The substantial effect of pressure regulation is also evident when the mass spectra of the analyzed mixture at 0.08 and 0.40 bar are compared (Fig.20).
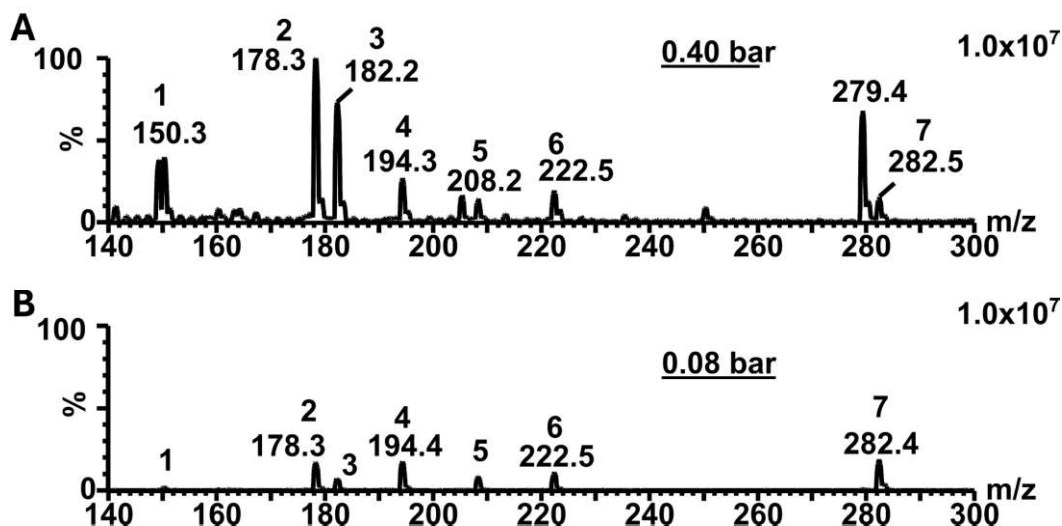
Figure 20 Desorption nanoelectrospray (nanoDESI) mass spectra of NPS (A) with the auxiliary pumping pressure drop 0.40 bar and (B) without the auxiliary pumping (B) pressure drop 0.08 bar. Both spectra are normalized to the highest ion signal intensity of 1.0×10^7 . The temperature of the heated capillary was set to 200 °C. The mixture of standards was deposited on a silanized microscope slide. Numbers indicated at each mass spectra correspond to $[M+H]^+$ of (1) cathinone, *m/z* 150 ;(2) buphedrone, *m/z* 178; (3) 3-FMC *m/z* 182; (4) methedrone, *m/z* 194; (5) methylone *m/z* 208; (6) butylone *m/z* 222; (7) naphyrone, *m/z* 282 [7]. Copyright 2020 John Wiley & Sons, Ltd

The signal intensities of all analytes are higher at 0.40 bar. Their increase is significant, especially for cathinone (1), buphedrone (2), and 3-FMC (3). No interfering signals were observed for a blank (see Fig. 21A).

Figure 21 NanoDESI mass spectra of different blanks without auxiliary pumping (pressure drop of 0.08 bar) and with auxiliary pumping (pressure drop of 0.40 bar): (A) Silanized microscope slide (a blank corresponding to a mixture of cathinones, Figure 20); (B) Double-sided tape on a microscope slide (a blank corresponding to methedrone (m/z 194), Figure 23); (C) Double-sided tape on a microscope slide (a blank corresponding to paracetamol (m/z 152), Figure 24). The spectra are normalized to the highest ion signal intensity in Figures 20, 23, and 24, respectively. The temperature of the heated capillary was set at 200 °C [7]. Copyright 2020 John Wiley & Sons, Ltd

5.1.3 Analysis of Model Samples

The effect of pressure regulation was proven in the analysis of "real-world samples," where detecting traces of NPS on personal items can represent a relevant

example. Tiny amounts (less than 0.3 mg) of the abused drugs were deposited on the wallet. "Unknown powder" was then collected from the surface using double-sided tape on a microscope slide and subjected to analysis by nanoDESI (Fig. 22).
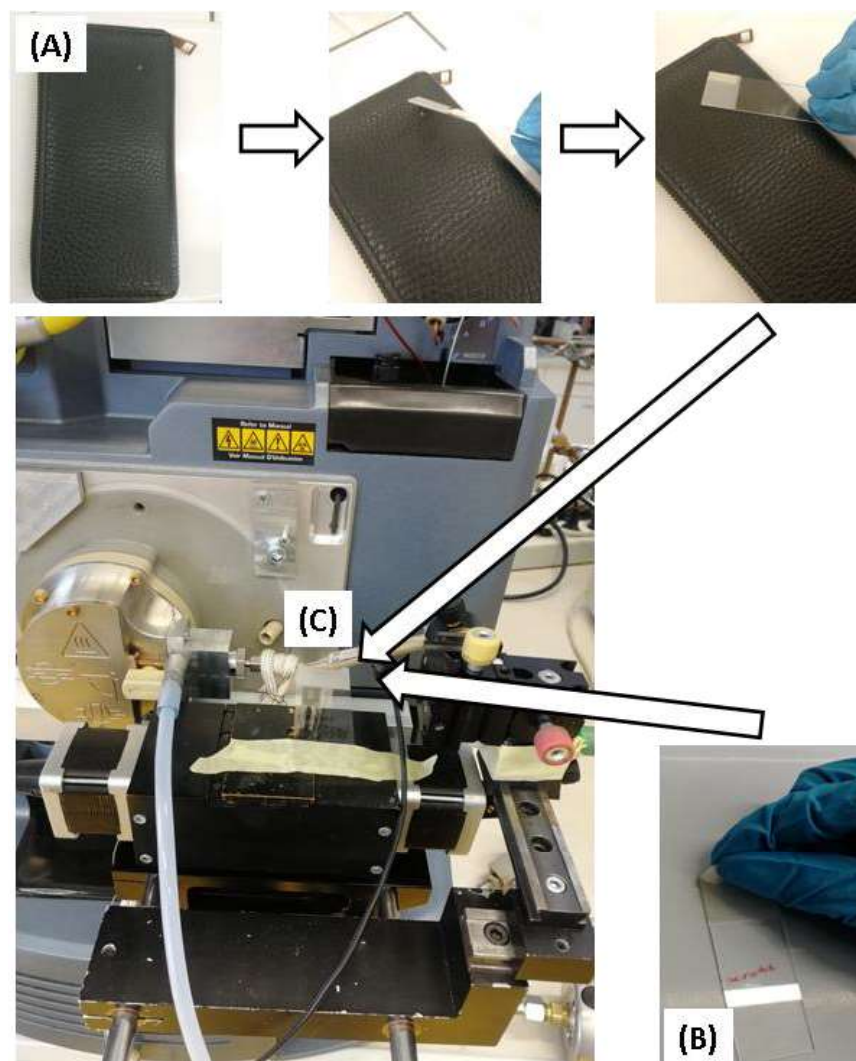
Figure 22 Direct sampling of solid materials. (A), sampling from the surface using a double-sided tape on a microscope slide. (B), a broken pill rubbed against a double-sided tape on a microscope slide. (C), microscope slide placed on the stage of desorption nanoelectrospray [7]. Copyright 2020 John Wiley & Sons, Ltd

Desorption and ionization were performed directly from the tape surface. The acquired spectra confirmed the significant influence of reduced pressure regulation (Fig. 23). Although the surface for sample deposition was different (tape vs. silanized glass), detection of the abused drugs was also significantly improved in this "real sample"

analysis. No interfering signals were observed for a double-sided tape blank (see Fig. 21B,C).
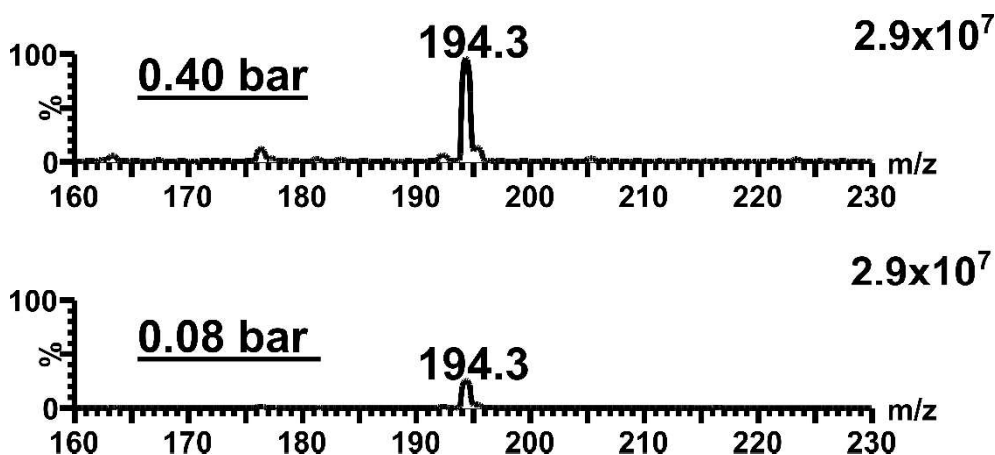
Figure 23 Desorption nanoelectrospray (nanoDESI) mass spectra of the trace amount of methedrone on double-sided tape recorded at a pressure drop of 0.40 (A) and 0.08 bar (B), respectively. A solid sample was collected from the wallet. Both spectra are normalized to the highest ion signal intensity of 2.9×10^7. The temperature of the heated capillary was set at 200 °C [7]. Copyright 2020 John Wiley & Sons, Ltd

Another possible application can be the analysis of pills. A paracetamol pill broken in two pieces was rubbed against double-sided tape on a microscope slide, leaving traces of the drug that were directly analyzed (Fig. 22). Significant signal intensity improvement was observed when applying pressure drop of 0.40 bar (Fig.24). The same results were obtained for the powdered paracetamol, proving that different forms of samples can be collected and successfully analyzed. Evidently, the proposed approach can be applied to analyses of different analytes deposited in different ways on silanized glass, double-sided tape, or other surfaces that can be tested in the future.
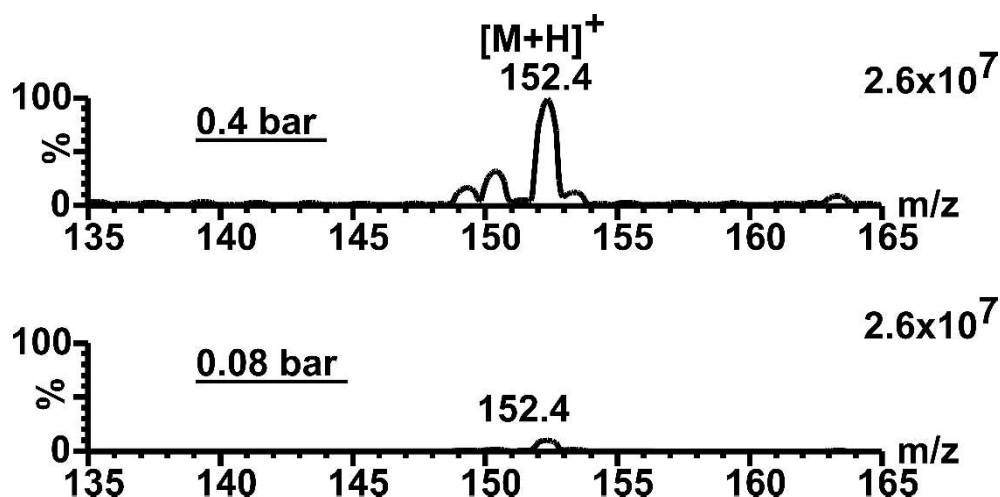
Figure 24 Desorption nanoelectrospray (nanoDESI) mass spectra of paracetamol traces on double-sided tape recorded at a pressure drop of (A) 0.40 bar and (B) 0.08 bar. Both spectra are normalized to the highest ion signal intensity of 2.6×10^7. The temperature of the heated capillary was set at 200 °C [7]. Copyright 2020 John Wiley & Sons, Ltd

5.1.4 Conclusion

Because nanoDESI with its lateral resolution in tens of micrometers samples small surface area, only a tiny amount of analyte is desorbed, and the measurement sensitivity can be an issue. The yield of ions was significantly improved by properly regulated pressure reduction in the MS inlet. The pressure reduction drives the flow of gas (air) generated by suction to the inlet and, consequently, the drag force acting on charged droplets and ions in the source. Regulation of the pressure drop was recognized to have a crucial influence on signal intensity. Both the pressure drop and temperature of the heated capillary were tuned to achieve maximum sensitivity. The change in signal intensity for some of the compounds was more than one order of magnitude higher. The tested custom-made inlet permits the setting of these experimental parameters and supports the applicability of nanoDESI. One order of magnitude higher response was achieved for some of the analyzed new psychoactive substances, which may be critical in the analysis of traces of unknown samples. The development of a new ion source and the described effects of studied experimental parameters can encourage applications of nanoDESI in general. The impact of the reduced pressure regulation can differ for different mass spectrometers due to the different power of vacuum systems. Nevertheless, it was confirmed that pressure drop between the atmospheric and evacuated region of a mass spectrometer strongly

influences the efficiency of nanoDESI. It should be considered if this ion source is attached to any other mass spectrometer.

5.2 Cyclic Ion Mobility-Mass Spectrometry of New Psychoactive Substances

This work was published as a first-author publication [163] and with the permission adapted and reprinted from:

Nytka M., Wan J., Tureček F., Lemr K. Cyclic ion mobility of isomeric new psychoactive substances employing characteristic arrival time distribution profiles and adduct separation. J. Am. Soc. Mass Spectrom. 2024; https://doi.org/10.1021/jasms.4c00127

ACS open access

Author's Contribution. Marianna Nytka – investigation, formal analysis, visualization, and writing the original draft.

New psychoactive substances (Fig. 14 (structures)) were easily protonated by electrospray but were not well separated by ion mobility even at higher resolving power. Nevertheless, the arrival time distribution (ATD) profiles were characteristic of the individual isomers (see, e.g., Fig. 26). This agrees with the previous observations using the linear and cyclic mobility cell for isomeric oligosaccharides [171] and oligonucleotides [172]. Mass spectra of standards were inspected on the presence of sodium and potassium adducts. Only sodium adducts were present at low intensity (Fig. 25). Therefore, due to the low adduct formation Na^+, Li^+, K^+, $Ag^{+,}$ and Cs^+ salts were alternatively added to the analyzed solutions to support adduct formation and to allow their ion mobility analysis. The results showed sufficient intensities for high-resolution cTWIM experiments for solely Na^+ and Li^+ adduct ions.
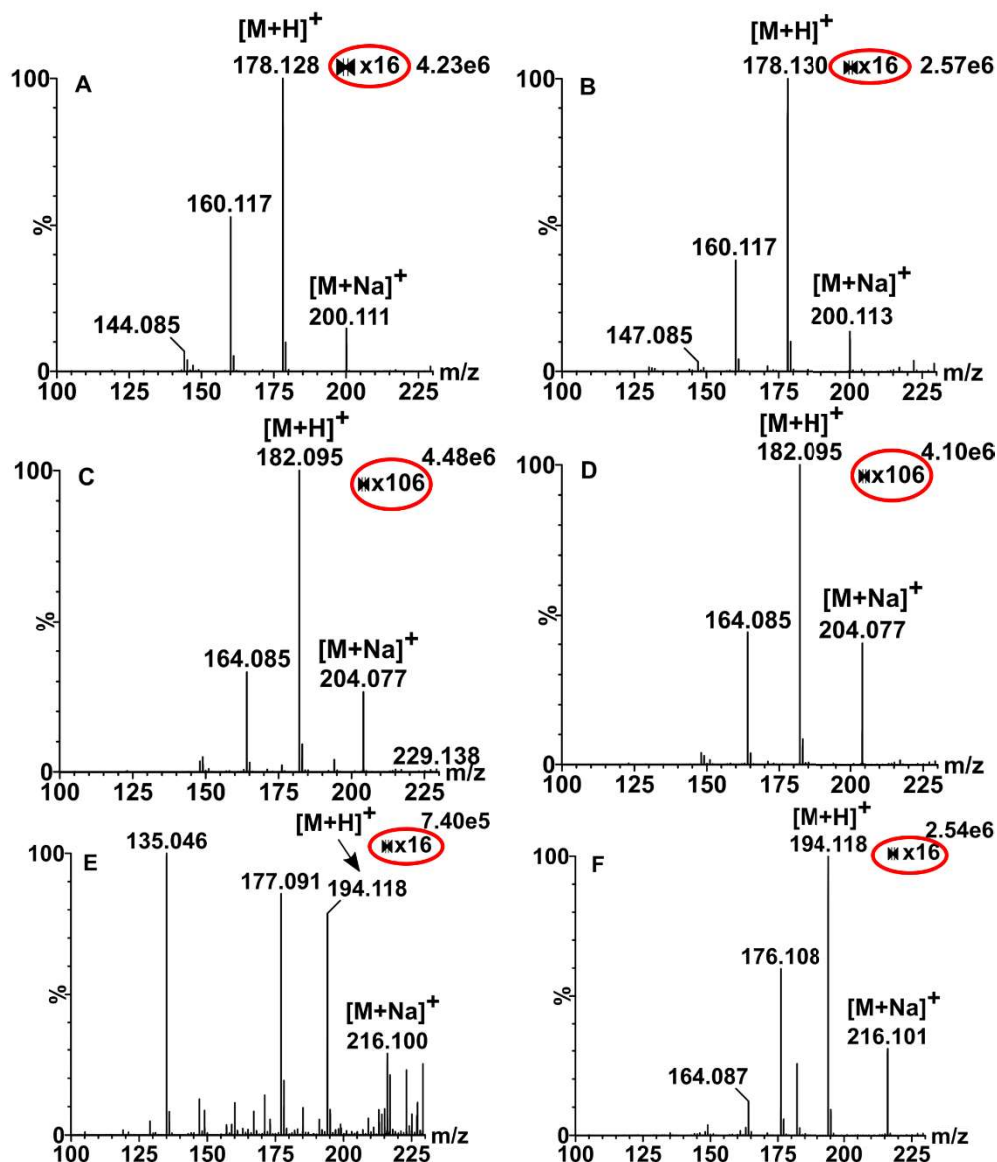
Figure 25. +ESI-mass spectra: A) 3-MMC; B) buphedrone; C) 3-FMC; D) 4-FMC; E) BDB; F) methedrone. Compared to the protonated molecules, the sodium adducts show signal intensities lower by more than one- (A, B, E, F) and two- (C, D) orders of magnitude (see zoom ranges marked in red). Sodium salt was not added in this experiment [163]. ACS open access

5.2.1 Protonated Molecules vs Li-Adducts

The pairs 3-MMC and buphedrone or 3-FMC and 4-FMC were directly infused into the electrospray. Both pairs underwent the single pass (98 cm) separation. It enabled the recognition of the individual isomers for 3-MMC and buphedrone ([M+H]$^+$, *m/z* 178.13), but it was insufficient for the mixture (Fig. 26A).
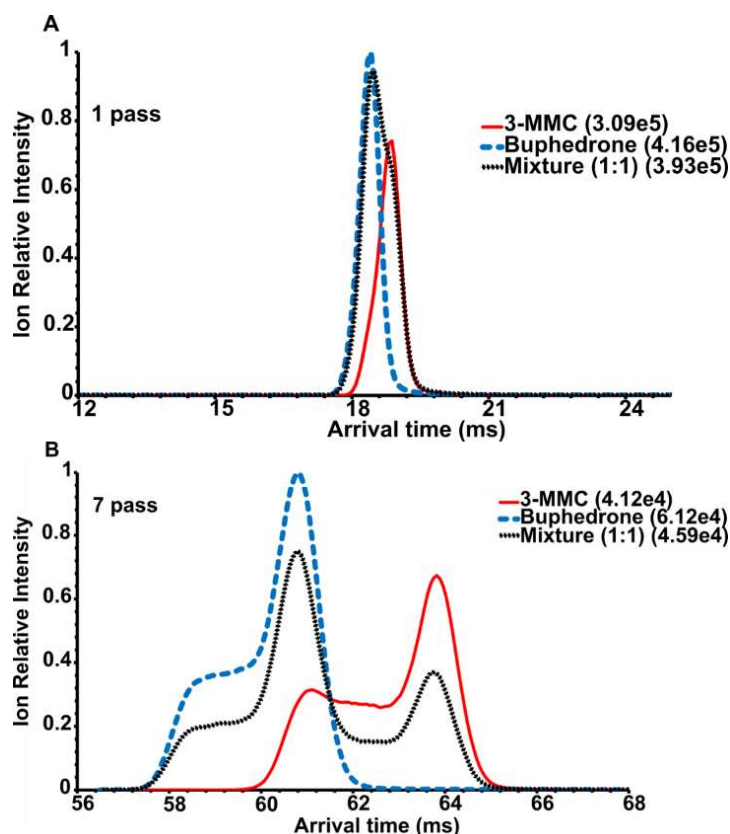
Figure 26 Extracted ATD profiles ([M+H]$^+$, *m/z* 178.13) of 3-MMC, buphedrone and their mixture (50 : 50): (A) 1 pass, (B) 7 pass experiment. The highest absolute intensity for each mobilogram is given in brackets [163]. ACS open access

As mentioned in Chapter 2.2, the increasing number of passes increases resolving power. Seven pass (686 cm) separation experiments for 3-MMC and buphedrone showed that we could recognize the major forms in a mixture, but complete separation was not achieved (Fig. 26B). This was consistent with the expected CCS for the keto and enol isomers of protonated 3-MMS (ions **1a**$^+$ and **1b**$^+$) and buphedrone (ions **2a**$^+$ and **2b**$^+$) that were in the narrow range of 139-141 Å^2 (Fig. 27). The narrow range was also observed for experimental CCS values.
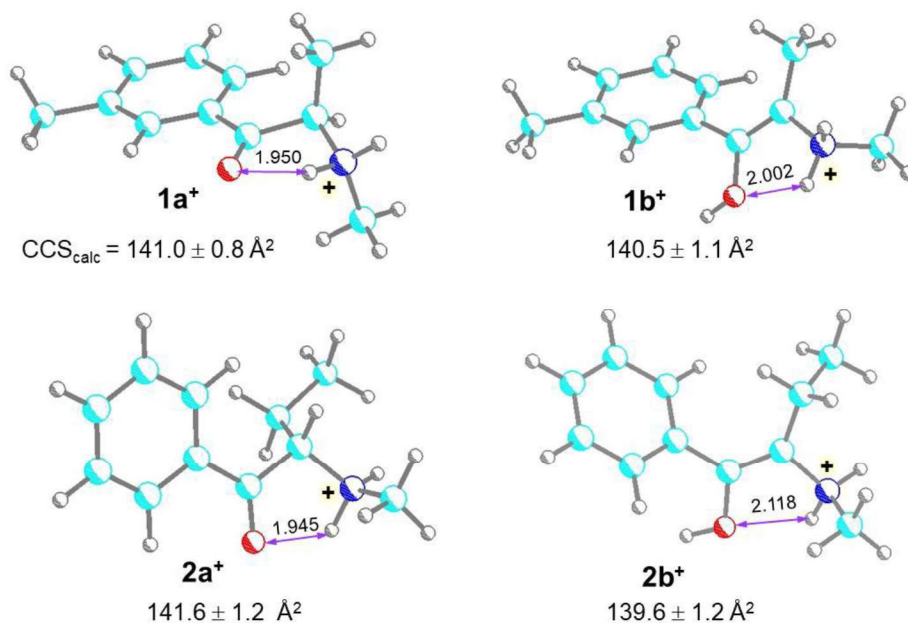
Figure 27 M06-2X/6-31+G(d,p) optimized structures of 3-MMC and buphedrone ions with calculated CCS in nitrogen. Atom color coding is as follows: cyan = C, blue = N, red = O, gray = H. Hydrogen bonds are shown with purple double-headed arrows with distances in Ångstroms [163]. ACS open access
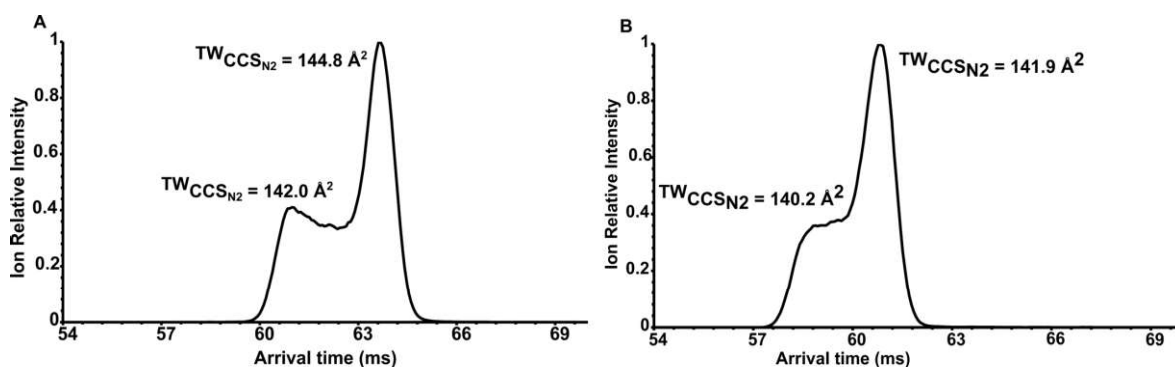
Figure 28 Extracted ATD profiles ([M+H]+, *m/z* 178.13) of 3-MMC (A) and buphedrone (B) in 7 pass separation.

The experimental CCS values were averaged from six data acquisitions. The cycle time and dead time were calculated from one pass and seven pass data of analytes. CCS values in 1 pass fwere 145 Å^2, and 142.1 Å^2 for 3-MMC and buphedrone, respectively. CCS values in 7 pass experiments (see Fig. 28) were 142.0 Å^2 (enol-form) and 144.8 Å^2 (keto-form) for 3-MMC, and for buphedrone they were 140.2 Å^2 (enol-form) and 141.9 Å^2

(keto-form). The difference between the experimental and calculated CCS was < 3% for 3-MMC and <1% for buphedrone. These results are consistent with measurements under the same conditions taken four years ago in 2020. The standards underwent the five pass separation. The experimental CCS for 3-MMC were 141.8 Å^2 and 144.8 Å^2, and for buphedrone were 139.5 Å^2 and 141.8 Å^2. These results show good reproducibility of CCS determination over multiple years.

The previously reported $^{DT}CCS_{N2}$ value for buphedrone was 141.2 Å^2 [127]. That correlates well with the cTWIM measurements and the calculated CCS for the keto ($2a^+$) form. There are no current research articles that would show CCS values for 3-MMC. Only one report of the CCS values of 3-MMC with linear TWIM measurements was found in the diploma thesis of Ondruchová Jana. In her work, the CCS were 144.9 Å^2 and 142.7 Å^2 for 3-MMC and buphedrone, respectively [173]. Those values correspond to the dominant keto ($1a^+$ and $2a^+$) form. CCS values from linear TWIM for 3-MMC correlate well with the cTWIM results. The higher error between theoretical and calculated CCS values for multipass experiments could be explained by the inconsistencies of CCS of calibrants presented in databases, sometimes ranging up to 10 Å^2 for different compounds (see Chapter 2.2).

It was estimated that the CCS-based resolving power R_{CCS} of about 104 was required to achieve the two-peak resolution $R_{p-p} = 1.23$ (ca. 90 % separation, defined for two Gaussian peaks of equal abundance) [174]. For buphedrone, the single pass experiment gave $R_{1,CCS} \approx 45$ (both keto- and enol-form contributed to peak width). After the multi-pass experiment with seven passes (L = 686 cm), we were able to separate the major isomeric forms of 3-MMC and buphedrone (experimental $R_{7,CCS} \approx 126$). The signals of both isomers were clearly detected in the mobilograms of their mixtures (Fig. 26B). While it can be sufficient for the detection of individual isomers, simple integration of mobility peaks was not possible even at higher resolving power, as the isomers' ATD profiles became broader. The less abundant enol isomer of 3-MMC still significantly overlapped with buphedrone (Fig. 26B).

The higher number of passes (higher resolving power) did not improve the separation. It just broadened the ATD profiles of isomers. Similarly, ion mobility peaks of isomeric protonated molecules interfered, e.g., for cathinones and peptides separated by trapped ion mobility [175] and cyclic TWIMS [140], respectively. Peak broadening at higher resolving power can compromise the separation of isomers. This is more significant for more complex ATD profiles of the individual isomers. It can be a general issue when

separating isomers existing in different conformer (protomer) states. However, the broadening effect can be suppressed by separating adducts of isomeric molecules with alkali metal cations. Separation of adducts has been described, e.g., for fentanyl [176], glycan [177], and flavonoid [178] isomers. On the other hand, if the broadening effect is characteristic of individual isomers, it can be advantageous. Both approaches are demonstrated in the following examples.

Multiple linear regression (MLR) was performed on ATD profiles of protonated 3-MMC and buphedrone (1 pass separation, Fig. 29 and 7 pass separation experiment, Fig. 30(A)) to determine the isomeric ratio. The isomeric ratio was a_1:a_2, where $y = a_0 + a_{1x1} + a_{2x2}$.

Averaged intensities of the overall extracted ATD profiles of the individual isomers (six data acquisitions) and the intensity of the ATD profile of the mixture (six data acquisitions individually) represented the input data, independent (x_1,x_2) and dependent (y) variables, respectively. Compared to the previous fitting procedure using Gaussian functions [171], the new data processing was more accessible to implement because MLR is the common part of routinely used software, such as OriginPro. As shown in Fig. 30(A), the relationship between the determined and given content of 3-MMC showed good linearity.
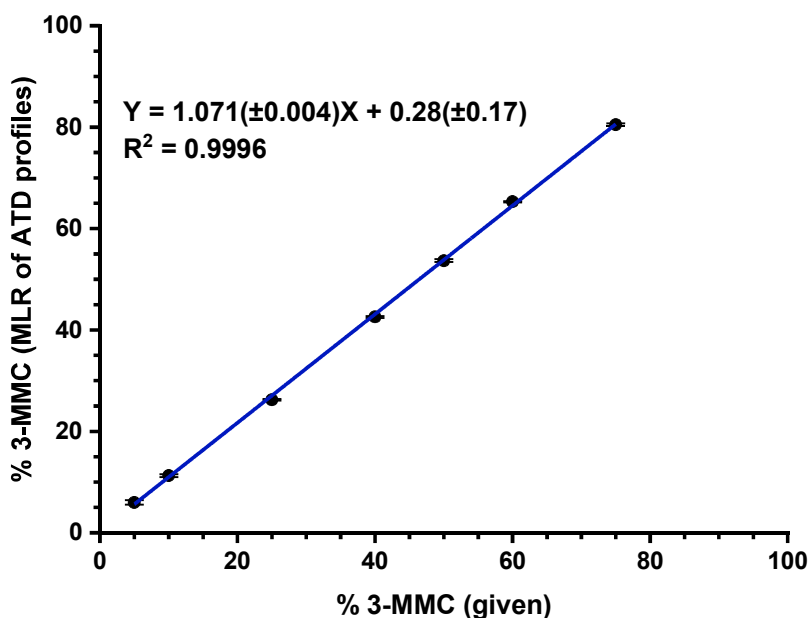
Figure 29. Determination of 3-MMC in the mixture with buphedrone. Multiple linear regression (MLR) applied to ATD profiles of protonated molecules, single pass

64

separation. Standard deviations of slope and intercept are given in brackets. Each point was measured in six data acquisitions. The range of the relationship was limited to 5 % - 75 % of 3-MMC because the analysis of the mixtures 95: 5 and 90: 10 failed. The determined ratios were 100 : 0 and 99.4: 0.6, respectively, and all values for these two mixtures were evaluated as outliers from the linear relationship [163]. ACS open access
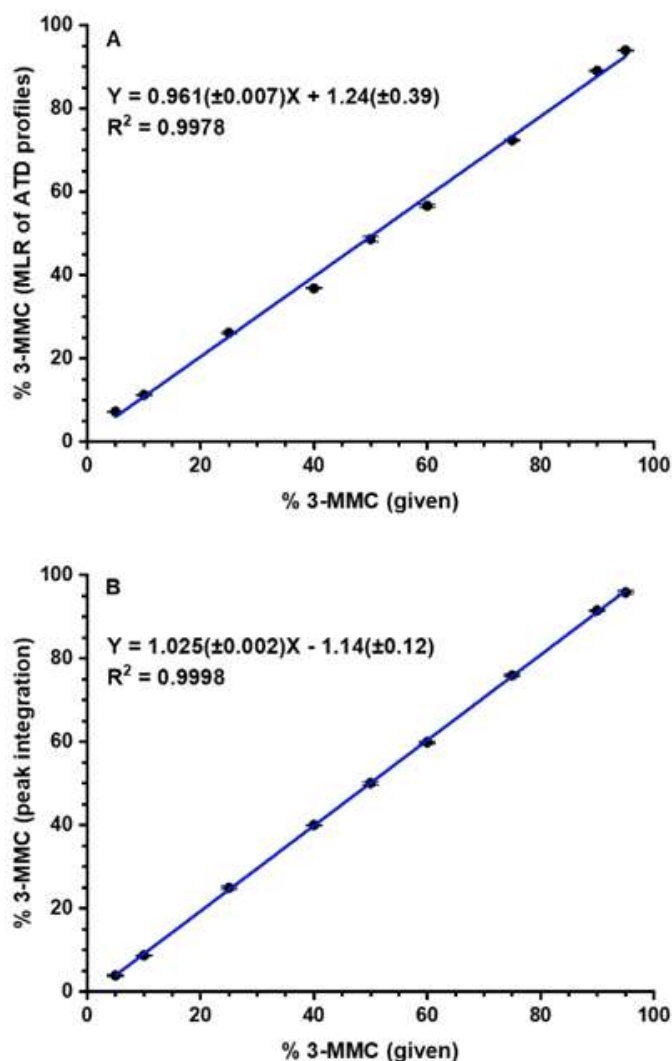
Figure 30 Determination of 3-MMC in the mixture with buphedrone: (A) Multiple linear regression (MLR) applied to ATD profiles of protonated molecules, seven pass separation; (B) Ion mobility of lithiated molecules, ten pass separation. Standard deviations of slope and intercept are shown in brackets. Each point was measured in six data acquisitions [163]. ACS open access

This proves that the proposed procedure is useful in defining the isomeric ratio using the ATD profiles and MLR. Notably, the linear calibration curve was obtained in single-pass experiments but in a limited range (5%-75% of 3-MMC, see Fig. 29) due to insufficient detection of buphedrone in excess of 3-MMC in a mixture (95:5 and 90:10). The higher resolving power helped to overcome this issue (Fg. 30(A)).

For MLR application, we evaluated stability of ATD profiles. Good intra-day repeatability of mobilograms of the isomers was observed. Inter-day measurements showed the shift in arrival time and/or relative intensities of the conformers (protomers), which led to a change in the shape of the mobilograms (Fig. 31).
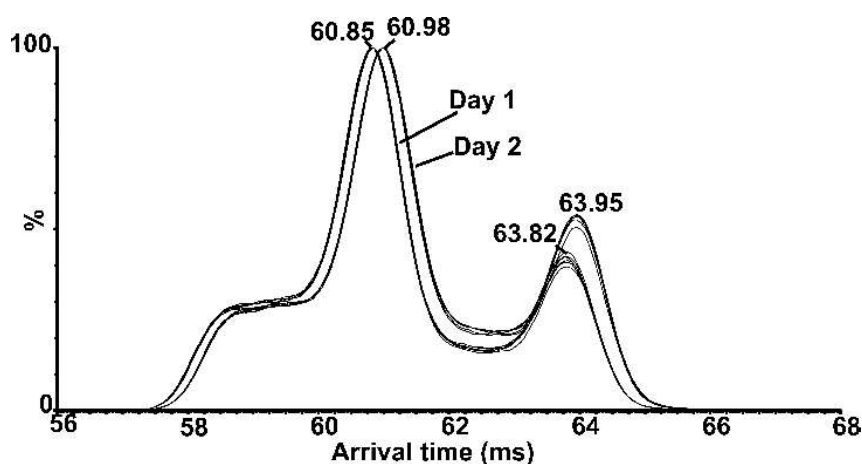
Figure 31 Extracted ATD profiles ([M+H]$^+$, *m/z* 178.13) of the mixture of 3-MMC and buphedrone (50 : 50) on two different days, 7 pass experiment [163]. ACS open access

This shift might be due to the drift or collision gas pressure variation for the same instrumental setting. To minimize such variation, we recommend waiting two hours to stabilize the gas pressure after switching from standby to run mode. If necessary, the shift in the arrival time was compensated by peak alignment.

Sodium and lithium adducts of 3-MMC and buphedrone were separated in 10 pass experiments (980 cm). Lithium adducts showed more than one order higher signal intensity than sodium adducts (see Fig. 32). Therefore, [M+Li]$^+$ ions were selected for isomeric ratio determination. Baseline separation allowed direct integration of the peaks (Fig. 32) and provided good linearity for the dependence between the determined and given 3-MMC content (Fig. 30(B)). The adduct ion formation can affect the conformation of ions in the gas phase due to the coordination at different positions [179,180]. The conformers for

[M+Li]$^+$ (Fig. 32(B)) were not observed compared to protonated molecules. This result was consistent with the calculations of structures and CCS (Fig. 27 and 34, Tables 5 and 6). The differences in theoretical CCS for keto (ions **1a**$^+$ and **2a**$^+$) and enol (ions **1b**$^+$ and **2b**$^+$) isomers of protonated molecules of 3-MMC and buphedrone were 0.4 % and 0.6 %, respectively. For both **1**$^+$ and **2**$^+$, the enol isomers had higher Gibbs energies than the keto forms (Table 5) and thus could contribute as minor components to the signal at *m/z* 178.13 in mobilograms, as manifested by peaks broadening (Fig. 26(B)). For lithiated isomers (Fig. 33), the keto forms (ions **3a**$^+$ and **4a**$^+$) differed by 1.5 % in CCS. Enol isomers of the Li$^+$ adducts (ions **3b**$^+$ and **4b**$^+$) showed much higher energies than the keto-tautomers (Table 6) and were unlikely to significantly contribute to the signal at *m/z* 184.13 in mobilograms. This was consistent with the well separated symmetrical peaks of Li$^+$ adducts in ATD (Fig. 32(B)). The experimental CCS values for [M+Li]$^+$ of 3-MMC were 154.0 Å^2 (1 pass separation) and 153.3 Å^2 (10 pass), and for buphedrone 151.2 Å^2 (1 pass) and 150.4 Å^2 (10 pass). Those results fit well with the theoretically calculated ones (see Fig. 32; difference < 2 %). The relationships in Fig. 30 showed that the separation of lithium adducts gave lower standard deviations of intercept and slope and a slightly higher coefficient of determination than the MLR approach. Nevertheless, both approaches are comparable and useful for the determination of isomeric ratios in mixtures.
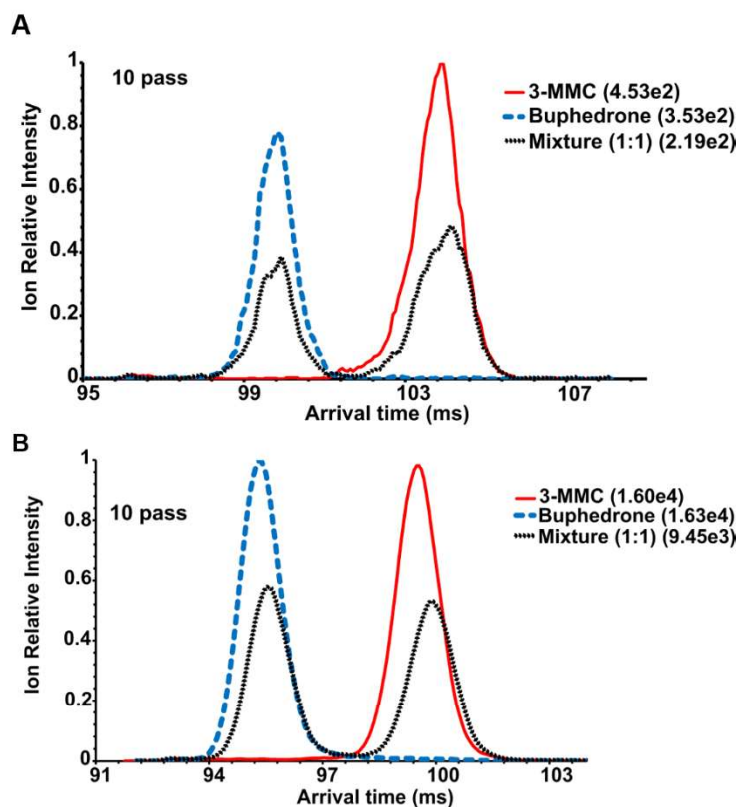
Figure 32. Extracted ATD profiles of 3-MMC, buphedrone and their mixture (50 : 50), ten pass experiment of A) [M+Na]$^+$, *m/z* 200.10 and B) [M+Li]$^+$, *m/z* 184.13. The highest absolute intensity for each mobilogram is given in brackets [163]. ACS open access.

3a$^+$
CCS$_{calc}$ = 151.0 ± 1.2 Å^2

3b$^+$
CCS$_{calc}$ = 151.7 ± 1.4 Å^2

4a$^+$
CCS$_{calc}$ 148.7 = ± 1.3 Å^2

4b$^+$
CCS$_{calc}$ = 152.0 ± 1.4 Å^2
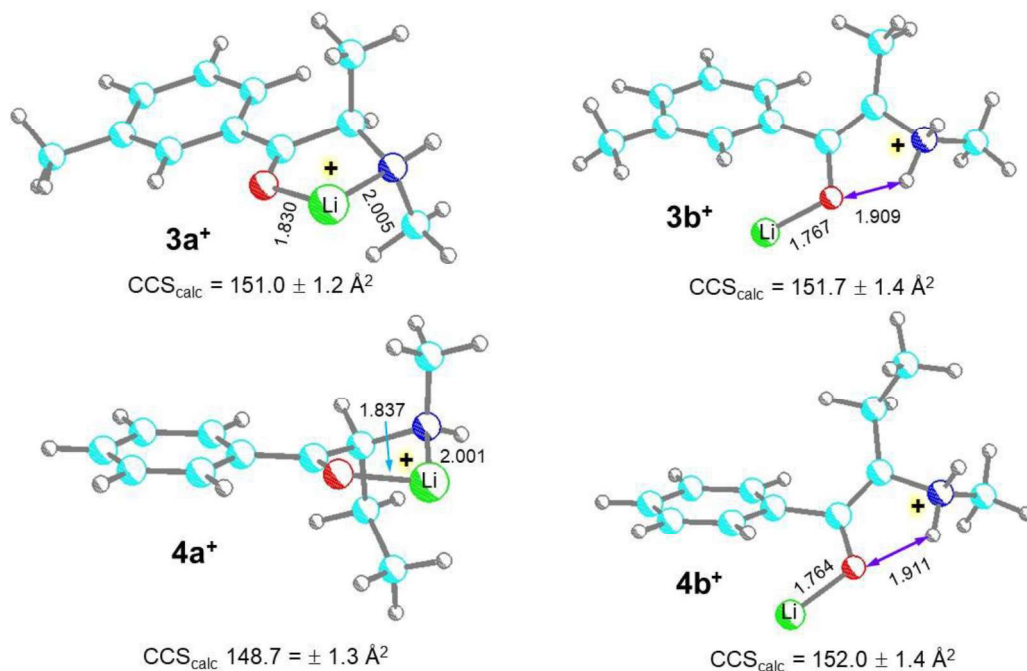
Figure 33. M06-2X/6-31+G(d,p) optimized structures of 3-MMC and buphedrone [M+Li]$^+$ ions with calculated CCS in nitrogen. Atom color coding is as follows: cyan = C,

blue = N, red = O, gray = H. Hydrogen bonds are shown with ochre double-headed arrows. All bond lengths are in Ångstrøms [163]. ACS open access.

Protonated molecules of 3-FMC and 4-FMC produced symmetrical and highly overlapping mobility peaks that hindered the determination of the isomeric ratio by multiple linear regression in single pass separation (Fig. 34A). Ten pass (980 cm) separation provided partial separation of the isomers in a mixture and produced the characteristic mobilogram profiles for individual isomers, as shown in Fig. 34B.
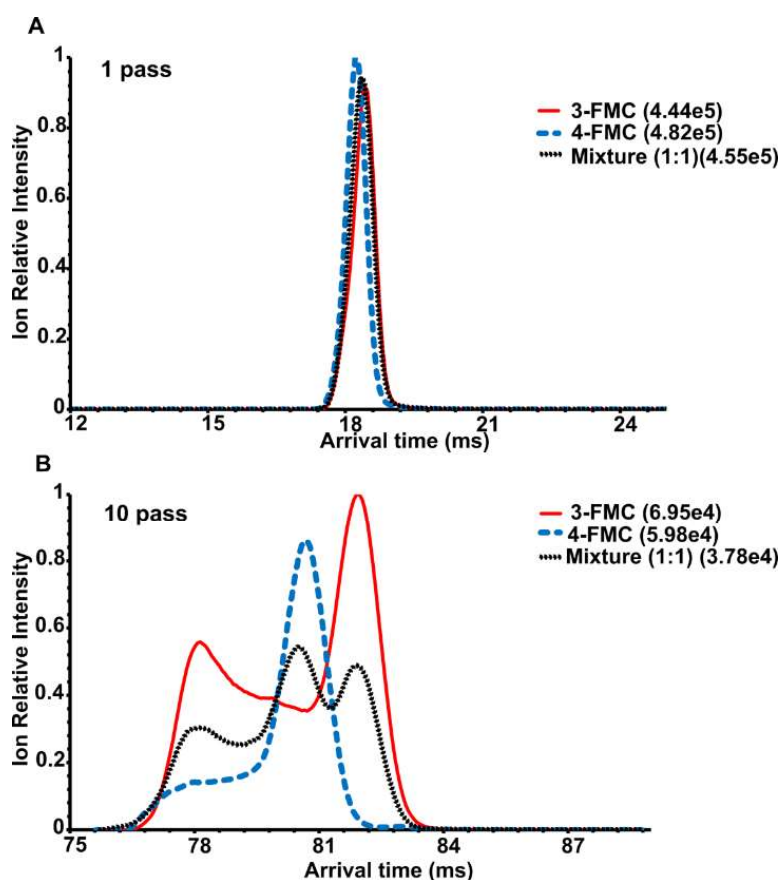
Figure 34 Extracted ATD profiles ($[M+H]^+$, *m/z* 182.10) of 3-FMC, 4-FMC, and their mixture (50 : 50): (A) 1 pass, (B) 10 pass experiment. The highest absolute intensity for each mobilogram is given in the brackets [163]. ACS open access.

The high resolving power enabled MLR to produce the linear dependence of determined and given 3-FMC content in a mixture (Fig. 35A). These results highlight the advantage of cyclic TWIMS over the linear cell.
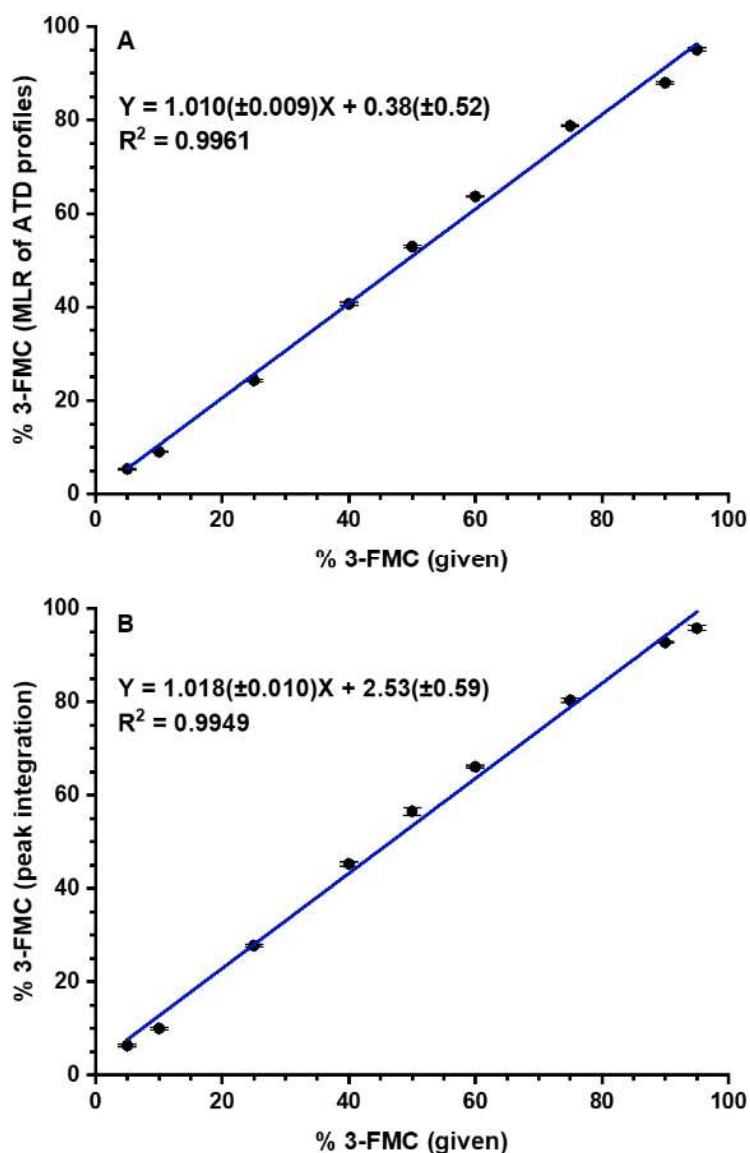
Figure 35 Determination of 3-FMC in the mixture with 4-FMC: (A) Multiple linear regression (MLR) applied to ATD profiles of protonated molecules, ten pass separation; (B) Ion mobility of lithiated molecules, 25 pass separation. Standard deviations of slope and intercept are shown in brackets. Each point was measured in six data acquisitions [163]. ACS open access.

It was observed that 3-FMC and 4-FMC did not efficiently form the sodium adducts (Fig. 36A). $[M+Li]^+$ were generated with sufficient intensity, enabling partial separation in 25 pass experiments (2450 cm) shown in Fig. 36B. It allowed the peak integration. The relationship between the determined and given content of 3-FMC in a

mixture of protonated and lithiated molecules produced comparable standard deviations of slope, intercept, and coefficient of determination (Fig. 35). MLR of ATD profiles gave similar results to the separation of adducts and may be more advantageous when adduct formation or separation is insufficient, as in the case of sodium adducts.
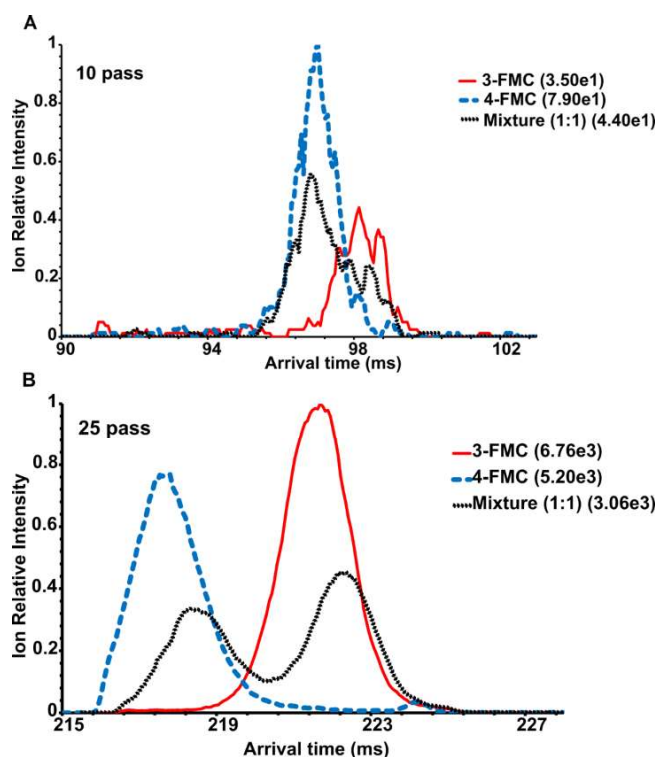
Figure 36 Extracted ATD profiles of 3-FMC, 4-FMC, and their mixture (50 : 50): (A) [M+Na]$^+$, *m/z* 204.08; 10 passes; (B) [M+Li*]$^+$, *m/z* 188.11; 25 passes. The highest absolute intensity for each mobilogram is given in brackets [163]. ACS open access.

5.2.2 Flow Injection Analysis of Isomers using Ion Mobility-Mass Spectrometry of Fragment Ions

BDB and methedrone showed a significant difference in the intensities of protonated molecules. BDB and methedrone belong to phenylamines and synthetic cathinones, respectively. Both isomers produce symmetrical and completely overlapped ATD profiles (Fig. 37 (A),(B)). Signal intensities at the peak maxima in a single pass and three pass separation showed the two order difference using the default instrument settings. Settings for labile analytes (Table 2) were used to decrease the fragmentation of protonated BDB and increase its intensity. Nevertheless, the three pass experiment did not improve the separation of the isomers and led to a decrease in the intensity of BDB (Fig. 37C,D).

Even at these conditions, both isomers produced symmetric and overlapped peaks with a significant difference in intensity, which hindered the use of the ATD profiles.
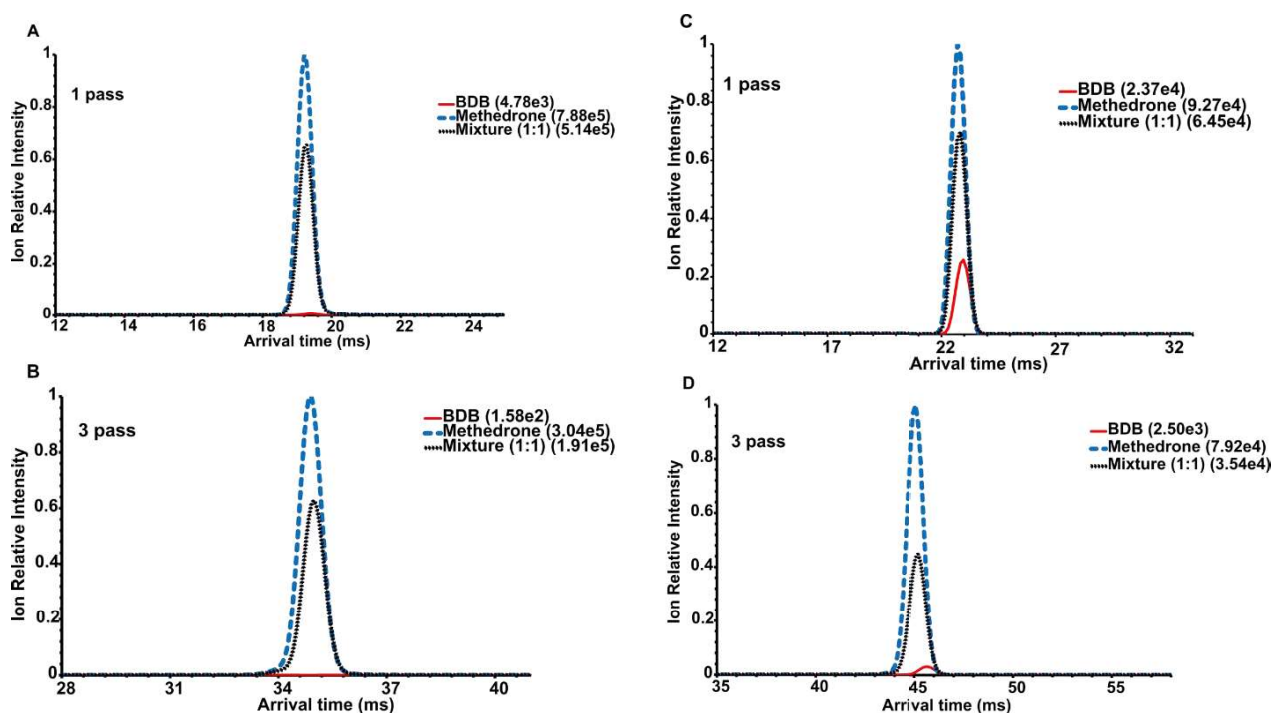
Figure 37. Extracted ATD profiles ([M+H]$^+$, *m/z* 194.13) of BDB, methedrone, and their mixture (50: 50): (A) default setting, 1 pass; (B) default setting, 3 passes; (C) setting for labile compounds (here BDB), 1 pass; (D) setting for labile compounds (here BDB), 3 passes. The highest absolute intensity for each mobilogram is given in the brackets [163]. ACS open access.

Furthermore, we proposed another approach using the ATD profiles of the fragments. The experiments were performed by flow injection analysis, allowing faster data acquisition. The precursor ion *m/z* 194.11 ([M+H]$^+$) was isolated in the quadrupole and fragmented in the trap cell (before the cIM cell). BDB and methedrone produced product ions at *m/z* 135.04, and methedrone also fragmented to *m/z* 135.08 (Fig. 38).
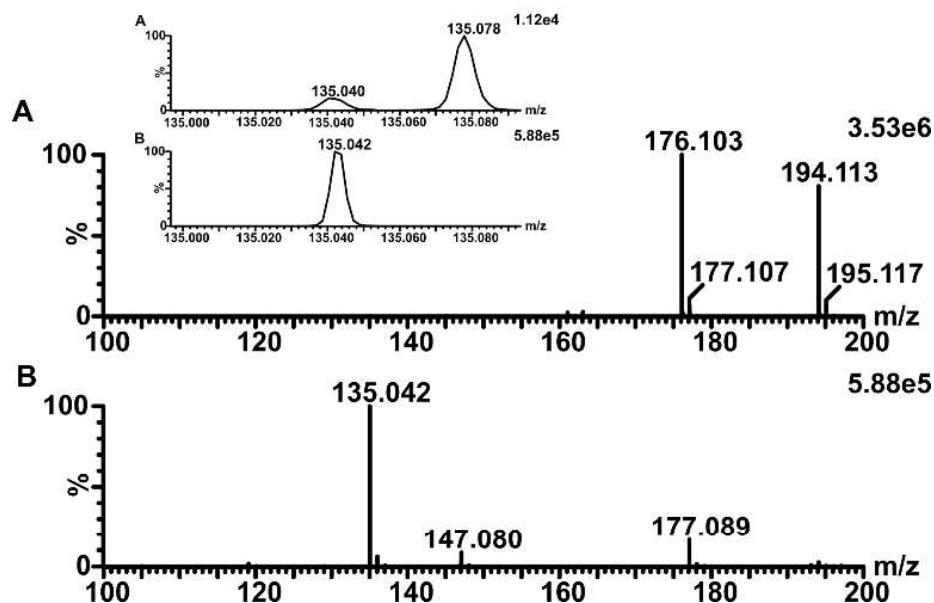
Figure 38 +ESI mass spectra after 1 pass separation: (A) methedrone; (B) BDB. The inset shows the zoomed detail of the signal of the fragment ions (*m/z* 135) [163]. ACS open access.
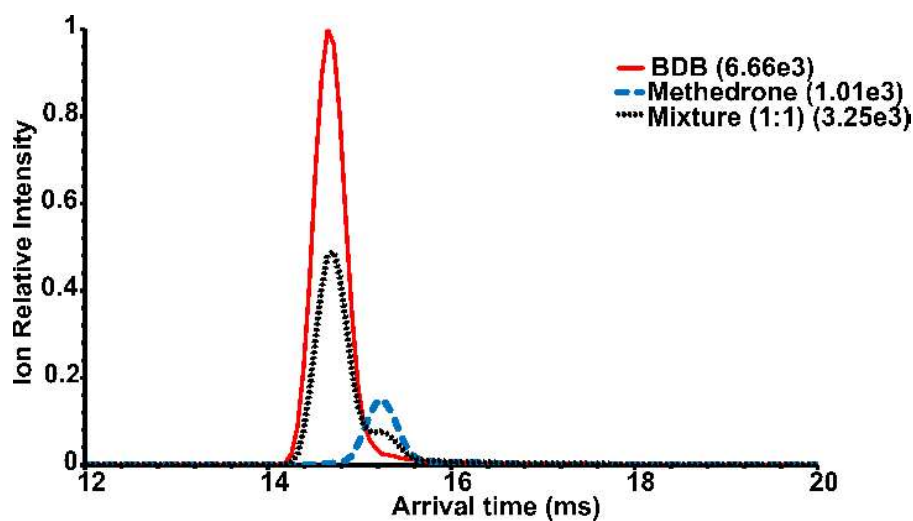
Figure 39 Extracted ATD profiles of fragment ions (*m/z* 135.04-135.08) of BDB, methedrone, and their mixture (50:50) in single pass separation. The highest absolute intensity for each mobilogram is given in brackets [163]. ACS open access.

Both fragments (*m/z* 135.04 and *m/z* 135.08) were included in the extracted ATD profiles (Fig. 39). The mobilograms were characteristic for each isomer and partially separated, which allowed the use of the MLR approach. The linear dependence between the determined and given BDB content in the mixture produced a lower coefficient of

determination and higher standard deviations for slope and intercept compared to the other two isomeric pairs (Fig. 40). This might be due to the more complex experiment requiring the generation and separation of the fragmented ions. The determined contents for 90% and 95% of BDB in a mixture were not significantly different. Nevertheless, the determination of isomeric ratios and separation of isomers were still possible, although with lower accuracy in a higher content of BDB.
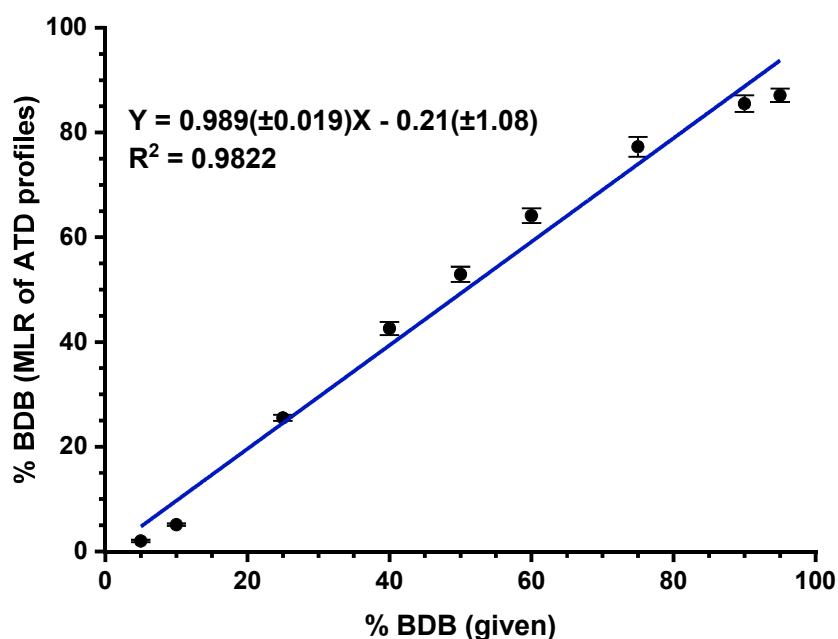
Figure 40 Determination of BDB in the mixture with methedrone. Multiple linear regression (MLR) applied to ATD profiles of fragment ions (*m/z* 135.04-135.08), single pass separation. Standard deviations of slope and intercept are shown in brackets. Each point was measured in six data acquisitions [163]. ACS open access.

5.2.3 Desorption Electrospray Ionization of Isomers

Similarly to the direct infusion and flow injection analysis, all three pairs were ionized by DESI, providing the characteristic ATD profiles with lower intensities (Fig. 41). The shapes of the ATD profiles are similar to the ESI source for 3-FMC and 4-FMC (Fig. 34(B) and 41(B)). In contrast, due to the different ionization mechanisms, the ATD profiles for 3-MMC and buphedrone are significantly different (Fig. 26(B) and 41(A)). Therefore,

it is impossible to use ATD profiles of individual isomers produced by ESI to evaluate the samples measured by the DESI source.
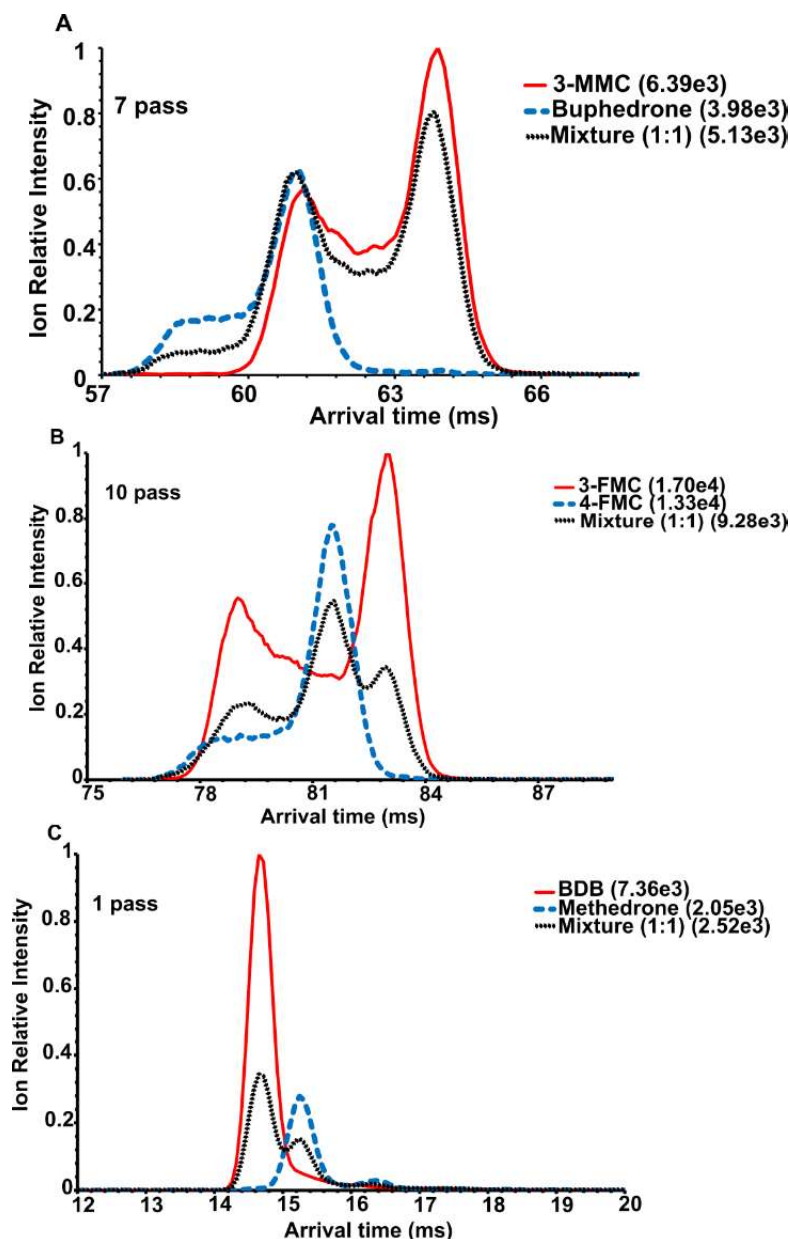
Figure 41. Extracted ATD profiles of individual isomers and their mixtures (50 : 50) desorbed and ionized by DESI: (A) 3-MMC and buphedrone ([M+H]$^+$, m/z 178.13), 7 passes; (B) 3-FMC and 4-FMC ([M+H]$^+$, m/z 182.10), 10 passes; (C) fragment ions *(m/z 135.04-135.08)* of BDB, methedrone, 1 pass. The highest absolute intensity for each mobilogram is given in brackets [163]. ACS open access.

The analytes were pipetted onto the hydrophobic spot and left to dry on air. It formed the heterogeneous layer that explained higher data variability (error bars Fig. 42)

compared to ESI. Linear dependence between the determined and given content of 3-MMC in a mixture (Fig. 42(A)) showed a lower coefficient of determination and higher standard deviations for slope and intercept in contrast to the other two pairs. Despite that, the increase in the 3-MMC content was visible. For other two pairs, higher coefficients of determination, lower standard devitions of slopes and intercepts as well as narrower error bars were achieved. DESI-cIM-MS proved the applicability of the ATD profile-based method on solid samples.
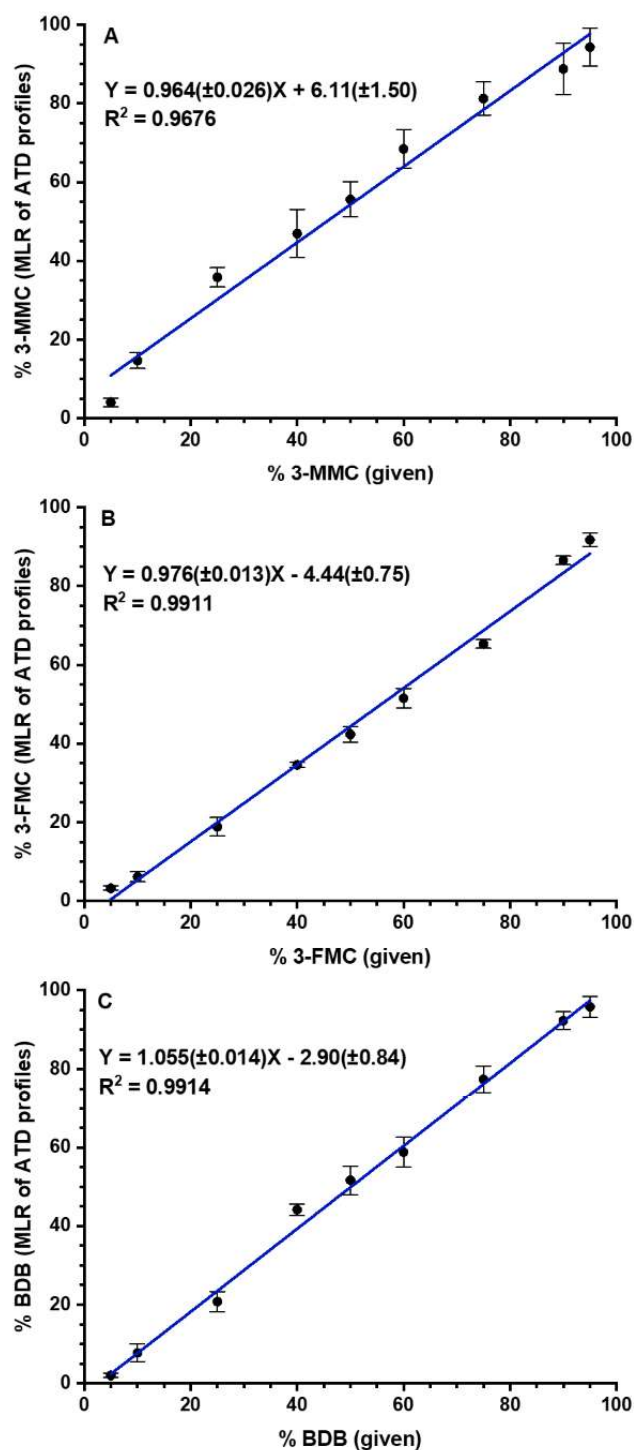
Figure 42. Determination of isomeric ratios using DESI and multiple linear regression (MLR) applied to ATD profiles: (A) 3-MMC in the mixture with buphedrone, ([M+H]$^+$, *m/z* 178.13, 7 passes); (B) 3-FMC in the mixture with 4-FMC ([M+H]$^+$, *m/z* 182.10, 10 passes); (C) BDB in the mixture with methedrone (fragment ions at *m/z* 135.04-135.08, 1 pass). Standard deviations of slope and intercept are shown in brackets. Each point was measured in six data acquisitions [163]. ACS open access.

5.2.4 Analysis of the Model Samples

Flow injection analysis was used to analyze two isomeric pairs of synthetic cathinones (four analytes) in a mixture. Calibration was prepared in a range of 5% to 45%. Six replicates of calibration and sample solutions were injected (5 µL) into the flow of methanol-water (50:50, v/v). FIA with autosampler allowed rapid and automatic data, decreasing the acquisition time to 3 hours for 96 injections with the time of the analysis 1.5 min when compared to direct infusion (more than one week). Linear correlation for 3-MMC/buphedrone and 3-FMC/4-FMC showed good linearity with the coefficient of determination 0.9974 and 0.9988, respectively (Fig. 43). In model samples containing two pairs of isomers in a mixture with 10% of 3-MMC and 3-FMC, the determined content of 3-MMC was 9.3% with a standard deviation of 0.37, and for 3-FMC, it was 11.0 %, and 0.42. The obtained results showed a good accuracy of this method.
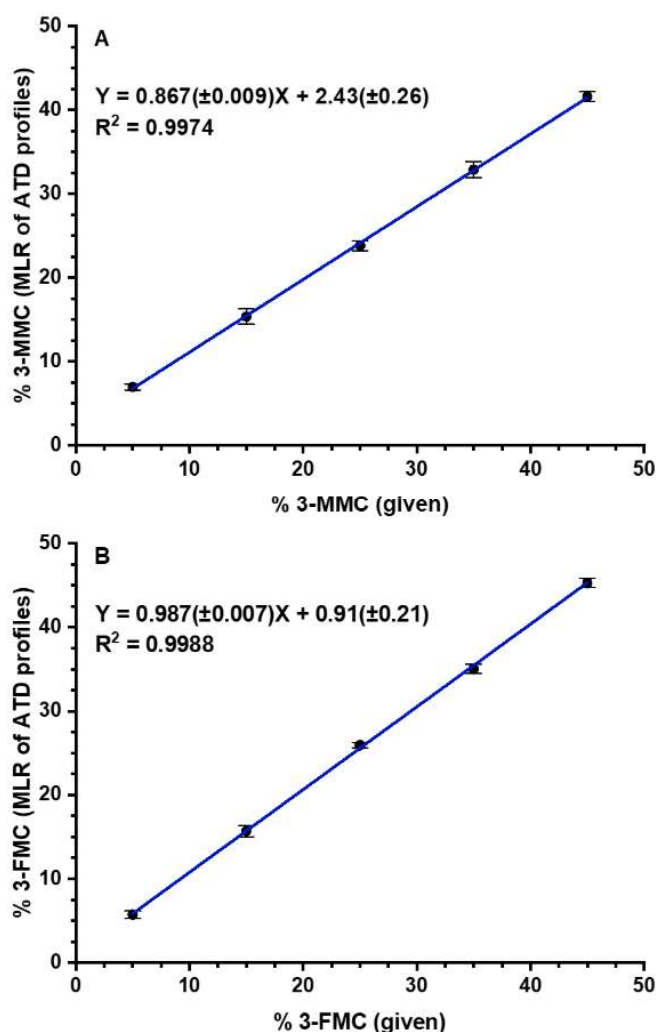
Figure 43. Calibration curve for FIA of two isomeric pairs mixture: (A) 3-MMC in the mixture with buphedrone, seven pass separation; (B) 3-FMC in the mixture with 4-FMC, ten pass separation. Multiple linear regression (MLR) was applied to ATD profiles of protonated molecules. Standard deviations of slope and intercept are shown in brackets. Each point was measured in six replicates [163]. ACS open access.

5.2.5 Conclusion

Two approaches based on the separation of lithium adducts and on multiple linear regression using the characteristic ATD profiles of individual isomers and ATD profiles from the isomeric mixtures were shown to be efficient in distinguishing and quantifying NPS isomers. The formation of lithium adducts by adding its salt to the sample solution showed the best results for these applications. The higher resolving power of cyclic

TWIMS in multipass experiments improved the separation of Li-ion adducts, whereas the mobility peaks of protonated molecules were broadened and still overlapped due to the presence of tautomers associated with individual ion structures. Similar behavior was observed, e.g., for peptides [140] and oligonucleotides [171]. In the previous report, ATD profiles were fitted by Gaussian functions, and a single ATD function was generated for each isomer. These ATD functions allowed determining isomeric ratios of oligosaccharides by ESI linear TWIMS [171]. Here, the fitting was replaced by multiple linear regression, which noticeably simplified the analysis. Direct infusion experiments confirmed that both approaches, the separation of lithiated molecules and the use of ATD profiles characteristic to isomers, are comparable.

The isomeric pair of BDB/methedrone showed significant differences in the intensities of $[M+H]^+$ ions and completely overlapping mobility peaks. In this case, the ATD profiles of the fragment ions allowed us to achieve a successful analysis, proving that the proposed approach is not limited to only protonated molecules. These analyses were performed by FIA as an alternative to direct infusion. Obviously, this approach is feasible for liquid samples. In the case of solid samples, desorption electrospray was utilized. DESI-cIM-MS provided characteristic ATD profiles of isomers, although they differed to some extent from those obtained by electrospray. This could be attributed to the different ionization mechanisms, electrospraying of solutions vs. desorption, and ionization from solid samples. Finally, the rapid analysis of a mixture containing two isomeric pairs was demonstrated. FIA combined with an autosampler enabled automatic data acquisition, speeding up the analysis.

The mean mobility values were recently used to identify cathinones, while isomeric ratios have not been determined [175]. We confirmed the excellent repeatability of the ATD profiles and included the entire ATD profiles analyzing isomeric mixtures. Although the higher resolving power of cyclic TWIMS may not allow for the complete separation of isomers, it may help to generate more distinct ATD profiles of isomers.

The ATD profile-based approach can generally be used to analyze isomeric molecules by ion mobility. While the integration of peaks requires a good separation, the described approach is applicable even for overlapping signals.

6 CONCLUSION AND OUTLOOK

Coupling different ionization techniques with IM-MS has excellent potential for detecting and separating isomers in mixtures. Nevertheless, some AIMS have never been hyphened with ion mobility; some are only at the beginning of this fruitful collaboration.

NanoDESI, with the improved custom-made inlet, showed great applicability in detecting the NPS on the silanized glass surface. The increased ionization efficiency of nanoDESI should encourage new applications. Nevertheless, a few modifications can still be made, starting with automating spraying solvent delivery by possibly connecting it to a nanoLC pump, which will allow high-resolution MS imaging measurements as well as coaupling it with cTWIM.

Ion mobility faces a new revolution with the production of high-resolving power IMS systems (cyclic TWIM, SLIM, TIMS), which has opened the possibility for new applications. cTWIM can reveal the hidden conformers/protomers, which cannot be seen in linear TWIM or lower resolving power instruments.

A new, simple approach for isomeric ratio determination in mixtures was performed by multiple linear regression of characteristic ATD profiles that overlapped in a mixture for protonated ions (generally for any overlapped ions). This method also showed excellent results by using the characteristic ATDs of fragment ions. Coupling the DESI source with cTWIMS demostrated the application of our approach on solid samples. Therefore, it might also be used in the future for quantitative imaging experiments. The different profiles of ATDs produced by ESI and DESI experiments could lead to more fundamental experiments based on the effect of desorption in DESI on ATD profiles in cTWIM and how different parameters of ion optics can influence the results.

7 LIST OF ABBREVIATIONS

3-FMC	3-fluoromethcathinone
3-MMC	3-methylmethcathinone
4-FMC	4-fluoromethcathinone
4-MMC	4-methylmethcathinone
ACN	Acetonitrile
ADC	Analog-to-digital converter
AIMS	Ambient ionization mass spectrometry
AM-251	1-(2,4-Dichlorophenyl)-5-(4-iodophenyl)-4-methyl-N-1-piperidinyl-1H-pyrazole-3-carboxamide
APCI	Atmospheric Pressure chemical ionization
APPI	Atmospheric Pressure Photoionization
ASAP	Atmospheric Solid Analysis Probe
ATD	Arrival Time Distribution
BDB	1,3-benzodioxolylbutanamine
BOMD	Born-Oppenheimer Molecular Dynamics
CCS	Collison Cross-Section
CE	Collision Energy
CID	Collission-Induced Dissociation
cIM	Cyclic Ion Mobility
cTWIM	Cyclic Travel Wave Ion Mobility
DART	Direct Analysis in Real Time
DC	Direct Current
DESI	Desorption Electrospray Ionization
DHSS	Diffuse Exact Hard Sphere Scattering
DMA	Differential Mobility Analyzer
DTF	Density Function Theory
DTIMS	Drift Tube Ion Mobility Spectrometry
EASI	Easy Ambient Sonic Spray Ionization
EASI-MIMS	Easy Ambient Sonic Spray Ionization-Membrane Introduction Mass Spectrometry
EESI	Extractive Electrospray Ionization
EHSS	Exact Hard Sphere Scattering

EI	Electron Impact Ionization
ESI	Electrospray Ionization
EU	European Union
FAIMS	High-Field Asymmetric Ion Mobility Spectrometry
FIA	Flow Injection Analysis
FSI	Fiber Spray Ionization
HRMS	High Resolution Mass Spectrometry
ID	Internal Diametr
IM	Ion Mobility
IMS	Ion Mobility Spectrometry (Separation)
JWH-015	(2-methyl-1-propyl-1H-indol-3-yl)(naphthalen-1-yl)methanone
LCPA	Local Collision Probability Approximation
LESA	Liquid Extraction Surface Analysis
L-J	Lennard-Jones
LMJ-SSP	Liquid Microjunction-Surface Sampling Probe
LOD	Limit of Detection
LOQ	Limit of Quantitation
LSD	Lysergic Acid Diethylamide
MALDI	Matrix-Assisted Desorption Ionization
MEPS	Microextraction by Packed Sorbent
MK	Merz, Singh, Kollman
MLR	Multiple Linear Regression
MW	Molecular Weight
nanoDESI	Desorption Nanoelectrospray Ionization
nano-DESI	Nanospray Desorption Electrospray Iionization
NPS	New Psychoactive Substances
PA	Projection Approximation
PEEK	Polyetheretherketone
PESI	Probe Electrospray Ionization
PS	Paper Spray
PSA	Projection Superposition Approximation
PTFE	Polytetrafluoroethylene
Q-TOF	Quadrupol-Time of Flight

RF	Radio Friquency
S/N	Signal-to-Noise
SEDI	Scattering on Electron Density Isosurfaces
SESI	Secondary Electrospray Ionization
SLIM	Structures for Lossless Ion Manipulations
SNAPP	Selective Non-Covalent Adduct Protein Probing
SRIG	Stacked Ring Ion Guide
SSI	Sonic Spray Ionization
TIMS	Trapped Ion Mobility Spectrometry
TLC	Thin Liquid Chromatography
TM	Trajectory Method
TM-DESI	Transmission Mode Desorption Electrospray Ionization
TQD	Triple Quadrupole
T-Wave	Quadrupol-Time of Flight
TWIMS	Travel Wave Ion Mobility Spectrometry
V-EASI	Venturi- Easy Ambient Sonic Spray Ionization

REFERENCES

[1]   Z. Takáts, J.M. Wiseman, B. Gologan, R.G. Cooks, Mass Spectrometry Sampling Under Ambient Conditions with Desorption Electrospray Ionization, Science (1979) 306 (2004) 471–473. https://doi.org/10.1126/science.1104404.

[2]   R.B. Cody, J.A. Laramée, H.D. Durst, Versatile new ion source for the analysis of materials in open air under ambient conditions, Anal Chem 77 (2005) 2297–2302. https://doi.org/10.1021/ac050162j.

[3]   C.L. Feider, A. Krieger, R.J. Dehoog, L.S. Eberlin, Ambient Ionization Mass Spectrometry: Recent Developments and Applications, Anal Chem 91 (2019) 4266–4290. https://doi.org/10.1021/acs.analchem.9b00807.

[4]   K.I. Kocurek, R.L. Griffiths, H.J. Cooper, Ambient ionisation mass spectrometry for in situ analysis of intact proteins, Journal of Mass Spectrometry 53 (2018) 565–578. https://doi.org/10.1002/jms.4087.

[5]   J. Balog, S. Kumar, J. Alexander, O. Golf, J. Huang, T. Wiggins, N. Abbassi-Ghadi, A. Enyedi, S. Kacska, J. Kinross, G.B. Hanna, J.K. Nicholson, Z. Takats, In Vivo Endoscopic Tissue Identification by Rapid Evaporative Ionization Mass Spectrometry (REIMS), Angewandte Chemie 127 (2015) 11211–11214. https://doi.org/10.1002/ange.201502770.

[6]   A.R. Venter, K.A. Douglass, J.T. Shelley, G. Hasman, E. Honarvar, Mechanisms of real-time, proximal sample processing during ambient ionization mass spectrometry, Anal Chem 86 (2014) 233–249. https://doi.org/10.1021/ac4038569.

[7]   M. Nytka, L. Borovcová, P. Fryčák, P. Barták, K. Lemr, Signal enhancement in desorption nanoelectrospray ionization by custom-made inlet with pressure regulation, Journal of Mass Spectrometry 55 (2020). https://doi.org/10.1002/jms.4642.

[8]   Z. Takáts, J.M. Wiseman, R.G. Cooks, Ambient mass spectrometry using desorption electrospray ionization (DESI): Instrumentation, mechanisms and applications in forensics, chemistry, and biology, Journal of Mass Spectrometry 40 (2005) 1261–1275. https://doi.org/10.1002/jms.922.

[9]   J.B. Fenn, Ion Formation from Charged Droplets: Roles of Geometry, Energy, and Time, J Am Soc Mass Spectrom 4 (1993) 524–535.

[10]   A. Venter, P.E. Sojka, R.G. Cooks, Droplet dynamics and ionization mechanisms in desorption electrospray ionization mass spectrometry, Anal Chem 78 (2006) 8549–8555. https://doi.org/10.1021/ac0615807.

[11]   R. Javanshad, R. Panth, T.L. Maser, A.R. Venter, Helium assisted desorption and spray ionization, Int J Mass Spectrom 479 (2022). https://doi.org/10.1016/j.ijms.2022.116891.

[12]   N.M. Morato, R.G. Cooks, Desorption Electrospray Ionization Mass Spectrometry: 20 Years, Acc Chem Res 56 (2023) 2526–2536. https://doi.org/10.1021/acs.accounts.3c00382.

[13] M. Volný, A. Venter, S.A. Smith, M. Pazzi, R.G. Cooks, Surface effects and electrochemical cell capacitance in desorption electrospray ionization, Analyst 133 (2008) 525–531. https://doi.org/10.1039/b717693g.

[14] D.R. Ifa, L.M. Gumaelius, L.S. Eberlin, N.E. Manicke, R.G. Cooks, Forensic analysis of inks by imaging desorption electrospray ionization (DESI) mass spectrometry, Analyst 132 (2007) 461–467. https://doi.org/10.1039/b700236j.

[15] A. Khatami, S.S. Prova, A.K. Bagga, M. Yan Chi Ting, G. Brar, D.R. Ifa, Detection and imaging of thermochromic ink compounds in erasable pens using desorption electrospray ionization mass spectrometry, Rapid Communications in Mass Spectrometry 31 (2017) 983–990. https://doi.org/10.1002/rcm.7867.

[16] M. Friia, V. Legros, J. Tortajada, W. Buchmann, Desorption electrospray ionization - Orbitrap mass spectrometry of synthetic polymers and copolymers, Journal of Mass Spectrometry 47 (2012) 1023–1033. https://doi.org/10.1002/jms.3057.

[17] J.A. Amalian, T. Mondal, E. Konishcheva, G. Cavallo, B.E. Petit, J.F. Lutz, L. Charles, Desorption Electrospray Ionization (DESI) of Digital Polymers: Direct Tandem Mass Spectrometry Decoding and Imaging from Materials Surfaces, Adv Mater Technol 6 (2021). https://doi.org/10.1002/admt.202001088.

[18] M.F. Mirabelli, A. Chramow, E.C. Cabral, D.R. Ifa, Analysis of sexual assault evidence by desorption electrospray ionization mass spectrometry, Journal of Mass Spectrometry 48 (2013) 774–778. https://doi.org/10.1002/jms.3205.

[19] I. Cotte-Rodríguez, R.G. Cooks, Non-proximate detection of explosives and chemical warfare agent simulants by desorption electrospray ionization mass spectrometry, Chemical Communications (2006) 2968–2970. https://doi.org/10.1039/b606020j.

[20] F. Bianchi, A. Gregori, G. Braun, C. Crescenzi, M. Careri, Micro-solid-phase extraction coupled to desorption electrospray ionization-high-resolution mass spectrometry for the analysis of explosives in soil, Anal Bioanal Chem 407 (2015) 931–938. https://doi.org/10.1007/s00216-014-8208-7.

[21] A.M. Porcari, J. Zhang, K.Y. Garza, R.M. Rodrigues-Peres, J.Q. Lin, J.H. Young, R. Tibshirani, C. Nagi, G.R. Paiva, S.A. Carter, L.O. Sarian, M.N. Eberlin, L.S. Eberlin, Multicenter Study Using Desorption-Electrospray-Ionization-Mass-Spectrometry Imaging for Breast-Cancer Diagnosis, Anal Chem 90 (2018) 11324–11332. https://doi.org/10.1021/acs.analchem.8b01961.

[22] S. Banerjee, R.N. Zare, R.J. Tibshirani, C.A. Kunder, R. Nolley, R. Fan, J.D. Brooks, G.A. Sonn, Diagnosis of prostate cancer by desorption electrospray ionization mass spectrometric imaging of small metabolites and lipids, Proc Natl Acad Sci U S A 114 (2017) 3334–3339. https://doi.org/10.1073/pnas.1700677114.

[23]   K. Margulis, A.S. Chiou, S.Z. Aasi, R.J. Tibshirani, J.Y. Tang, R.N. Zare, Distinguishing malignant from benign microscopic skin lesions using desorption electrospray ionization mass spectrometry imaging, Proc Natl Acad Sci U S A 115 (2018) 6347–6352. https://doi.org/10.1073/pnas.1803733115.

[24]   K.A. Douglass, A.R. Venter, Protein analysis by desorption electrospray ionization mass spectrometry and related methods, Journal of Mass Spectrometry 48 (2013) 553–560. https://doi.org/10.1002/jms.3206.

[25]   L. Nyadong, E.G. Hohenstein, A. Galhena, A.L. Lane, J. Kubanek, C.D. Sherrill, F.M. Fernández, Reactive desorption electrospray ionization mass spectrometry (DESI-MS) of natural products of a marine alga, Anal Bioanal Chem 394 (2009) 245–254. https://doi.org/10.1007/s00216-009-2674-3.

[26]   G. Huang, H. Chen, X. Zhang, R.G. Cooks, Z. Ouyang, Rapid screening of anabolic steroids in urine by reactive desorption electrospray ionization, Anal Chem 79 (2007) 8327–8332. https://doi.org/10.1021/ac0711079.

[27]   B.N. Moore, O. Hamdy, R.R. Julian, Protein structure evolution in liquid DESI as revealed by selective noncovalent adduct protein probing, Int J Mass Spectrom 330–332 (2012) 220–225. https://doi.org/10.1016/j.ijms.2012.08.013.

[28]   Z. Miao, H. Chen, Direct Analysis of Liquid Samples by Desorption Electrospray Ionization-Mass Spectrometry (DESI-MS), J Am Soc Mass Spectrom 20 (2009) 10–19. https://doi.org/10.1016/j.jasms.2008.09.023.

[29]   J.E. Chipuk, J.S. Brodbelt, Transmission Mode Desorption Electrospray Ionization, J Am Soc Mass Spectrom 19 (2008) 1612–1620. https://doi.org/10.1016/j.jasms.2008.07.002.

[30]   R. Haddad, R. Sparrapan, M.N. Eberlin, Desorption sonic spray ionization for (high) voltage-free ambient mass spectrometry, Rapid Communications in Mass Spectrometry 20 (2006) 2901–2905. https://doi.org/10.1002/rcm.2680.

[31]   L.S. Eberlin, P. V. Abdelnur, A. Passero, G.F. De Sa, R.J. Daroda, V. De Souza, M.N. Eberlin, Analysis of biodiesel and biodiesel-petrodiesel blends by high performance thin layer chromatography combined with easy ambient sonic-spray ionization mass spectrometry, Analyst 134 (2009) 1652–1657. https://doi.org/10.1039/b817847j.

[32]   R. Haddad, R. Sparrapan, T. Kotiaho, M.N. Eberlin, Easy ambient sonic-spray ionization-membrane interface mass spectrometry for direct analysis of solution constituents, Anal Chem 80 (2008) 898–903. https://doi.org/10.1021/ac701960q.

[33]   R. Haddad, H.M.S. Milagre, R.R. Catharino, M.N. Eberlin, Easy ambient sonic-spray ionization mass spectrometry combined with thin-layer chromatography, Anal Chem 80 (2008) 2744–2750. https://doi.org/10.1021/ac702216q.

[34] V.G. Santos, T. Regiani, F.F.G. Dias, W. Romão, J.L.P. Jara, C.F. Klitzke, F. Coelho, M.N. Eberlin, Venturi easy ambient sonic-spray ionization, Anal Chem 83 (2011) 1375–1380. https://doi.org/10.1021/ac102765z.

[35] N. V. Schwab, A.M. Porcari, M.B. Coelho, E.M. Schmidt, J.L. Jara, J. V. Visentainer, M.N. Eberlin, Easy dual-mode ambient mass spectrometry with Venturi self-pumping, canned air, disposable parts and voltage-free sonic-spray ionization, Analyst 137 (2012) 2537–2540. https://doi.org/10.1039/c2an16312h.

[36] D.U. Tega, H. Nascimento, J.L. Jara, J.M. Santos, M.N. Eberlin, A Rapid and Versatile Method to Determine Methanol in Biofuels and Gasoline by Ambient Mass Spectrometry using a V-EASI Source, Energy and Fuels 34 (2020) 4595–4602. https://doi.org/10.1021/acs.energyfuels.9b02827.

[37] N. Na, R. Shi, Z. Long, X. Lu, F. Jiang, J. Ouyang, Real-time analysis of self-assembled nucleobases by Venturi easy ambient sonic-spray ionization mass spectrometry, Talanta 128 (2014) 366–372. https://doi.org/10.1016/j.talanta.2014.04.080.

[38] M.M. Antonakis, A. Tsirigotaki, K. Kanaki, C.J. Milios, S.A. Pergantis, Bipolar mass spectrometry of labile coordination complexes, redox active inorganic compounds, and proteins using a glass nebulizer for sonic-spray ionization, J Am Soc Mass Spectrom 24 (2013) 1250–1259. https://doi.org/10.1007/s13361-013-0668-z.

[39] H. Chen, A. Venter, R.G. Cooks, Extractive electrospray ionization for direct analysis of undiluted urine, milk and other complex mixtures without sample preparation, Chemical Communications (2006) 2042–2044. https://doi.org/10.1039/b602614a.

[40] C. Wu, W.F. Siems, H.H. Hill, Secondary electrospray ionization ion mobility spectrometry/mass spectrometry of illicit drugs, Anal Chem 72 (2000) 396–403. https://doi.org/10.1021/ac9907235.

[41] J. Kaeslin, C. Wüthrich, S. Giannoukos, R. Zenobi, How Soft Is Secondary Electrospray Ionization?, J Am Soc Mass Spectrom 33 (2022) 1967–1974. https://doi.org/10.1021/jasms.2c00201.

[42] C. Wüthrich, S. Giannoukos, Advances in secondary electrospray ionization for breath analysis and volatilomics, Int J Mass Spectrom 498 (2024). https://doi.org/10.1016/j.ijms.2024.117213.

[43] Ranc Václav, Havlicek Vladimír, Bednar Petr, Lemr Karel, Desorption electrospray: A modern tool for organic surface analysis., Chem. Listy 101 (2007) 524–529.

[44] P.J. Roach, J. Laskin, A. Laskin, Nanospray desorption electrospray ionization: An ambient method for liquid-extraction surface sampling in mass spectrometry, Analyst 135 (2010) 2233–2236. https://doi.org/10.1039/c0an00312c.

[45]   S.R. Ellis, S.H. Brown, M. In Het Panhuis, S.J. Blanksby, T.W. Mitchell, Surface analysis of lipids by mass spectrometry: More than just imaging, Prog Lipid Res 52 (2013) 329–353. https://doi.org/10.1016/j.plipres.2013.04.005.

[46]   L. Hartmanová, I. Lorencová, M. Volný, P. Fryčák, V. Havlíček, H. Chmelíčková, T. Ingr, K. Lemr, Lateral resolution of desorption nanoelectrospray: A nanospray tip without nebulizing gas as a source of primary charged droplets, Analyst 141 (2016) 2150–2154. https://doi.org/10.1039/c5an02665b.

[47]   L. Hartmanová, P. Fryčák, M. Soural, F. Tureček, V. Havlíček, K. Lemr, Ion internal energy, salt tolerance and a new technical improvement of desorption nanoelectrospray, Journal of Mass Spectrometry 49 (2014) 750–754. https://doi.org/10.1002/jms.3383.

[48]   V. Ranc, V. Havlíček, P. Bednar, K. Lemr, Nano-Desorption Electrospray and Kinetic Method in Chiral Analysis of Drugs in Whole Human Blood Samples, European Journal of Mass Spectrometry 14 (2008) 411–417. https://doi.org/10.1255/ejms.978.

[49]   L. Hartmanova, V. Ranc, B. Papouskova, P. Bednar, V. Havlicek, K. Lemr, Fast profiling of anthocyanins in wine by desorption nano-electrospray ionization mass spectrometry, J Chromatogr A 1217 (2010) 4223–4228. https://doi.org/10.1016/j.chroma.2010.03.018.

[50]   United Nations Office on Drugs and Crime, The Synthetic Drug Phenomenon, World Drug Report 2023, 2023. https://doi.org/https://doi.org/10.18356/9789210028233c022.

[51]   European Monitoring Centre for Drugs and Drug Addiction, European Drug Report 2023: Trends and Developments (single PDF version), European Drug Report 2023: Trends and Developments (2023). https://www.emcdda.europa.eu/publications/european-drug-report/2023_en (accessed April 19, 2024).

[52]   United Nations: Office on Drugs and Crime, World Drug Report 2023, Executive Summary, United Nations Publication, Vienna, Australia (2023).

[53]   E. Cuypers, A.J. Bonneure, J. Tytgat, The use of presumptive color tests for new psychoactive substances, Drug Test Anal 8 (2016) 137–141. https://doi.org/10.1002/dta.1847.

[54]   H. Muhamadali, A. Watt, Y. Xu, M. Chisanga, A. Subaihi, C. Jones, D.I. Ellis, O.B. Sutcliffe, R. Goodacre, Rapid detection and quantification of novel psychoactive substances (NPS) using Raman spectroscopy and surface-enhanced Raman scattering, Front Chem 7 (2019). https://doi.org/10.3389/fchem.2019.00412.

[55]   E. G. de Campos, A.J. Krotulski, B. S. De Martinis, J.L. Costa, Identification of synthetic cathinones in seized materials: A review of analytical strategies applied in forensic chemistry, WIREs Forensic Science 4 (2022). https://doi.org/10.1002/wfs2.1455.

[56]   V. Bolcato, C. Carelli, A. Radogna, F. Freni, M. Moretti, L. Morini, New synthetic cathinones and phenylethylamine derivatives analysis in hair: A review, Molecules 26 (2021). https://doi.org/10.3390/molecules26206143.

[57] D. Florou, V.A. Boumba, Hair analysis for New Psychoactive Substances (NPS): Still far from becoming the tool to study NPS spread in the community?, Toxicol Rep 8 (2021) 1699–1720. https://doi.org/10.1016/j.toxrep.2021.09.003.

[58] F.A. Esteve-Turrillas, S. Armenta, M. de la Guardia, Sample preparation strategies for the determination of psychoactive substances in biological fluids, J Chromatogr A 1633 (2020). https://doi.org/10.1016/j.chroma.2020.461615.

[59] N. Talaty, C.C. Mulligan, D.R. Justes, A.U. Jackson, R.J. Noll, R.G. Cooks, Fabric analysis by ambient mass spectrometry for explosives and drugs, Analyst 133 (2008) 1532–1540. https://doi.org/10.1039/b807934j.

[60] N. Stojanovska, M. Tahtouh, T. Kelly, A. Beavis, S. Fu, Presumptive analysis of 4-methylmethcathinone (mephedrone) using Desorption Electrospray Ionisation - Mass Spectrometry (DESI-MS), Australian Journal of Forensic Sciences 46 (2014) 411–423. https://doi.org/10.1080/00450618.2013.879206.

[61] N. Stojanovska, T. Kelly, M. Tahtouh, A. Beavis, S. Fu, Analysis of amphetamine-type substances and piperazine analogues using desorption electrospray ionisation mass spectrometry, Rapid Communications in Mass Spectrometry 28 (2014) 731–740. https://doi.org/10.1002/rcm.6832.

[62] F. Bianchi, S. Agazzi, N. Riboni, N. Erdal, M. Hakkarainen, L.L. Ilag, L. Anzillotti, R. Andreoli, F. Marezza, F. Moroni, R. Cecchi, M. Careri, Novel sample-substrates for the determination of new psychoactive substances in oral fluid by desorption electrospray ionization-high resolution mass spectrometry, Talanta 202 (2019) 136–144. https://doi.org/10.1016/j.talanta.2019.04.057.

[63] W.T. Alsaggaf, The Chemistry of Paper in Paper Spray Ionization Mass Spectrometry, Int J Chem 12 (2019) 16. https://doi.org/10.5539/ijc.v12n1p16.

[64] M.C.C. Diniz, F. de Moura, Y. Machado, J. Coelho Neto, E. Piccin, A simple, quick and non-destructive approach for sampling drugs of abuse in tablets and blotter for qualitative analysis by paper spray mass spectrometry, Analytical Methods 15 (2023) 6259–6265. https://doi.org/10.1039/d3ay01393f.

[65] J.H. Kennedy, J. Palaty, C.G. Gill, J.M. Wiseman, Rapid analysis of fentanyls and other novel psychoactive substances in substance use disorder patient urine using paper spray mass spectrometry, Rapid Communications in Mass Spectrometry 32 (2018) 1280–1286. https://doi.org/10.1002/rcm.8164.

[66] J.F.A. Filho, N.A. dos Santos, K.B. Borges, V. Lacerda, F.S. Pelição, W. Romão, Fiber spray ionization mass spectrometry in forensic chemistry: A screening of drugs of abuse and direct determination of cocaine in urine, Rapid Communications in Mass Spectrometry 34 (2020). https://doi.org/10.1002/rcm.8747.

[67] A.H. Grange, G.W. Sovocool, Detection of illicit drugs on surfaces using direct analysis in real time (DART) time-of-flight mass spectrometry, Rapid Communications in Mass Spectrometry 25 (2011) 1271–1281. https://doi.org/10.1002/rcm.5009.

[68] R.A. Musah, M.A. Domin, M.A. Walling, J.R.E. Shepard, Rapid identification of synthetic cannabinoids in herbal samples via direct analysis in real time mass spectrometry, Rapid Communications in Mass Spectrometry 26 (2012) 1109–1114. https://doi.org/10.1002/rcm.6205.

[69] M.A. Marino, B. Voyer, R.B. Cody, A.J. Dane, M. Veltri, L. Huang, Rapid Identification of Synthetic Cannabinoids in Herbal Incenses with DART-MS and NMR, J Forensic Sci 61 (2016) 82–91. https://doi.org/10.1111/1556-4029.12932.

[70] L. Habala, J. Valentová, I. Pechová, M. Fuknová, F. Devínsky, DART - LTQ ORBITRAP as an expedient tool for the identification of synthetic cannabinoids, Leg Med 20 (2016) 27–31. https://doi.org/10.1016/j.legalmed.2016.03.006.

[71] J. Ji, J. Wang, Y. Zhang, Rapid screening of 23 synthetic cannabinoids in blood by direct analysis in real time - Tandem mass spectrometry, Int J Mass Spectrom 469 (2021). https://doi.org/10.1016/j.ijms.2021.116667.

[72] A.D. Lesiak, R.A. Musah, R.B. Cody, M.A. Domin, A.J. Dane, J.R.E. Shepard, Direct analysis in real time mass spectrometry (DART-MS) of "bath salt" cathinone drug mixtures, Analyst 138 (2013) 3424–3432. https://doi.org/10.1039/c3an00360d.

[73] C.N. McEwen, R.G. McKay, B.S. Larsen, Analysis of solids, liquids, and biological tissues using solids probe introduction at atmospheric pressure on commercial LC/MS instruments, Anal Chem 77 (2005) 7826–7831. https://doi.org/10.1021/ac051470k.

[74] E. Jagerdeo, A. Wriston, Rapid analysis of forensic-related samples using two ambient ionization techniques coupled to high-resolution mass spectrometers, Rapid Communications in Mass Spectrometry 31 (2017) 782–790. https://doi.org/10.1002/rcm.7844.

[75] D. Fabregat-Safont, D. Felis-Brittes, M. Mata-Pesquera, J. V. Sancho, F. Hernández, M. Ibáñez, Direct and Fast Screening of New Psychoactive Substances Using Medical Swabs and Atmospheric Solids Analysis Probe Triple Quadrupole with Data-Dependent Acquisition, J Am Soc Mass Spectrom 31 (2020) 1610–1614. https://doi.org/10.1021/jasms.0c00112.

[76] T.H. Kuo, E.P. Dutkiewicz, J. Pei, C.C. Hsu, Ambient Ionization Mass Spectrometry Today and Tomorrow: Embracing Challenges and Opportunities, Anal Chem 92 (2020) 2353–2363. https://doi.org/10.1021/acs.analchem.9b05454.

[77] A.E. Ashcroft, F. Sobott, V. Gabelica, New Developments in Mass Spectrometry No. 11 Ion Mobility-Mass Spectrometry: Fundamentals and Applications Edited 1.1 What is Ion

Mobility Spectrometry? 1.1.1 Spectrometry Ion Mobility-Mass Spectrometry: an Overview, 2022. www.rsc.org.

[78] L.A. Viehland, E.A. Mason, Gaseous Ion Mobility in Electric Fields of Arbitrary Strength*, Ann Phys (N Y) 91 (1975) 499–533.

[79] C.L. Crawford, B.C. Hauck, J.A. Tufariello, C.S. Harden, V. McHugh, W.F. Siems, H.H. Hill, Accurate and reproducible ion mobility measurements for chemical standard evaluation, Talanta 101 (2012) 161–170. https://doi.org/10.1016/j.talanta.2012.09.003.

[80] W. Vautz, B. Bödeker, J.I. Baumbach, S. Bader, M. Westhoff, T. Perl, An implementable approach to obtain reproducible reduced ion mobility, International Journal for Ion Mobility Spectrometry 12 (2009) 47–57. https://doi.org/10.1007/s12127-009-0018-9.

[81] W.F. Siems, L.A. Viehland, H.H. Hill, Improved momentum-transfer theory for ion mobility. 1. Derivation of the fundamental equation, Anal Chem 84 (2012) 9782–9791. https://doi.org/10.1021/ac301779s.

[82] V. Gabelica, E. Marklund, Fundamentals of ion mobility spectrometry, Curr Opin Chem Biol 42 (2018) 51–59. https://doi.org/10.1016/j.cbpa.2017.10.022.

[83] V. Gabelica, A.A. Shvartsburg, C. Afonso, P. Barran, J.L.P. Benesch, C. Bleiholder, M.T. Bowers, A. Bilbao, M.F. Bush, J.L. Campbell, I.D.G. Campuzano, T. Causon, B.H. Clowers, C.S. Creaser, E. De Pauw, J. Far, F. Fernandez-Lima, J.C. Fjeldsted, K. Giles, M. Groessl, C.J. Hogan, S. Hann, H.I. Kim, R.T. Kurulugama, J.C. May, J.A. McLean, K. Pagel, K. Richardson, M.E. Ridgeway, F. Rosu, F. Sobott, K. Thalassinos, S.J. Valentine, T. Wyttenbach, Recommendations for reporting ion mobility Mass Spectrometry measurements, Mass Spectrom Rev 38 (2019) 291–320. https://doi.org/10.1002/mas.21585.

[84] M.M. Zimnicka, Structural studies of supramolecular complexes and assemblies by ion mobility mass spectrometry, Mass Spectrom Rev (2023). https://doi.org/10.1002/mas.21851.

[85] Y. Liu, F. Tureček, Photodissociative Cross-Linking of Diazirine-Tagged Peptides with DNA Dinucleotides in the Gas Phase, J Am Soc Mass Spectrom 30 (2019) 1992–2006. https://doi.org/10.1007/s13361-019-02189-4.

[86] J. Wan, B. Brož, Y. Liu, S.R. Huang, A. Marek, F. Tureček, Resolution of Identity in Gas-Phase Dissociations of Mono- and Diprotonated DNA Trinucleotide Codons by 15N-Labeling and Computational Structure Analysis, J Am Soc Mass Spectrom 33 (2022) 1936–1950. https://doi.org/10.1021/jasms.2c00194.

[87] J. Wan, M. Nytka, H. Qian, K. Vu, K. Lemr, F. Tureček, Nitrile Imines as Peptide and Oligonucleotide Photo-Cross-Linkers in Gas-Phase Ions, J Am Soc Mass Spectrom 35 (2024) 344–356. https://doi.org/10.1021/jasms.3c00379.

[88] D.H. Ross, H. Bhotika, X. Zheng, R.D. Smith, K.E. Burnum-Johnson, A. Bilbao, Computational tools and algorithms for ion mobility spectrometry-mass spectrometry, Proteomics (2024). https://doi.org/10.1002/pmic.202200436.

[89] C. Bleiholder, T. Wyttenbach, M.T. Bowers, A novel projection approximation algorithm for the fast and accurate computation of molecular collision cross sections (I). Method, Int J Mass Spectrom 308 (2011) 1–10. https://doi.org/10.1016/j.ijms.2011.06.014.

[90] C. Bleiholder, S. Contreras, T.D. Do, M.T. Bowers, A novel projection approximation algorithm for the fast and accurate computation of molecular collision cross sections (II). Model parameterization and definition of empirical shape factors for proteins, Int J Mass Spectrom 345–347 (2013) 89–96. https://doi.org/10.1016/j.ijms.2012.08.027.

[91] C. Bleiholder, A local collision probability approximation for predicting momentum transfer cross sections, Analyst 140 (2015) 6804–6813. https://doi.org/10.1039/c5an00712g.

[92] A.A. Shvartsburg, M.F. Jarrold, An exact hard-spheres scattering model for the mobilities of polyatomic ions, Chem Phys Lett 261 (1996) 86–91.

[93] A.A. Shvartsburg, B. Liu, M.F. Jarrold, K.-M. Ho, Modeling ionic mobilities by scattering on electronic density isosurfaces: Application to silicon cluster anions, J Chem Phys 112 (2000) 4517–4526. https://doi.org/10.1063/1.481042.

[94] Y. Alexeev, D.G. Fedorov, A.A. Shvartsburg, Effective ion mobility calculations for macromolecules by scattering on electron clouds, Journal of Physical Chemistry A 118 (2014) 6763–6772. https://doi.org/10.1021/jp505012c.

[95] C. Larriba-Andaluz, J. Fernández-García, M.A. Ewing, C.J. Hogan, D.E. Clemmer, Gas molecule scattering & ion mobility measurements for organic macro-ions in He versus N2 environments, Physical Chemistry Chemical Physics 17 (2015) 15019–15029. https://doi.org/10.1039/c5cp01017a.

[96] I. Campuzano, M.F. Bush, C. V. Robinson, C. Beaumont, K. Richardson, H. Kim, H.I. Kim, Structural characterization of drug-like compounds by ion mobility mass spectrometry: Comparison of theoretical and experimentally derived nitrogen collision cross sections, Anal Chem 84 (2012) 1026–1033. https://doi.org/10.1021/ac202625t.

[97] S.A. Ewing, M.T. Donor, J.W. Wilson, J.S. Prell, Collidoscope: An Improved Tool for Computing Collisional Cross-Sections with the Trajectory Method, J Am Soc Mass Spectrom 28 (2017) 587–596. https://doi.org/10.1007/s13361-017-1594-2.

[98] M.F. Mesleh, J.M. Hunter, A.A. Shvartsburg, G.C. Schatz, M.F. Jarrold, Structural Information from Ion Mobility Measurements: Effects of the Long-Range Potential, 1996. https://pubs.acs.org/sharingguidelines.

[99] C.K. Siu, Y. Guo, I.S. Saminathan, A.C. Hopkinson, K.W.M. Siu, Optimization of parameters used in algorithms of ion-mobility calculation for conformational analyses, Journal of Physical Chemistry B 114 (2010) 1204–1212. https://doi.org/10.1021/jp910858z.

[100] H. Kim, H.I. Kim, P. V. Johnson, L.W. Beegle, J.L. Beauchamp, W.A. Goddard, I. Kanik, Experimental and theoretical investigation into the correlation between mass and ion mobility for choline and other ammonium cations in N2, Anal Chem 80 (2008) 1928–1936. https://doi.org/10.1021/ac701888e.

[101] G. Von Helden, M.-T. Hsu, N. Gotts, M.T. Bowers, Carbon Cluster Cations with up to 84 Atoms: Structures, Formation Mechanism, and Reactivity, 1993. https://pubs.acs.org/sharingguidelines.

[102] E.G. Marklund, M.T. Degiacomi, C. V Robinson, A.J. Baldwin, J.L.P. Benesch, Collision cross sections for structural proteomics, Structure 23 (2015) 791–799.

[103] J.P. Williams, J.A. Lough, I. Campuzano, K. Richardson, P.J. Sadler, Use of ion mobility mass spectrometry and a collision cross-section algorithm to study an organometallic ruthenium anticancer complex and its adducts with a DNA oligonucleotide, Rapid Communications in Mass Spectrometry 23 (2009) 3563–3569. https://doi.org/10.1002/rcm.4285.

[104] L. Zanotto, G. Heerdt, P.C.T. Souza, G. Araujo, M.S. Skaf, High performance collision cross section calculation-HPCCS, J Comput Chem 39 (2018) 1675–1681. https://doi.org/10.1002/jcc.25199.

[105] A. Haack, C. Ieritano, W.S. Hopkins, MobCal-MPI 2.0: an accurate and parallelized package for calculating field-dependent collision cross sections and ion mobilities, Analyst 148 (2023) 3257–3273. https://doi.org/10.1039/d3an00545c.

[106] C. Ieritano, J. Crouse, J.L. Campbell, W.S. Hopkins, A parallelized molecular collision cross section package with optimized accuracy and efficiency, Analyst 144 (2019) 1660–1670. https://doi.org/10.1039/c8an02150c.

[107] C. Larriba, C.J. Hogan, Free molecular collision cross section calculation methods for nanoparticles and complex ions with energy accommodation, J Comput Phys 251 (2013) 344–363. https://doi.org/10.1016/j.jcp.2013.05.038.

[108] V. Shrivastav, M. Nahin, C.J. Hogan, C. Larriba-Andaluz, Benchmark Comparison for a Multi-Processing Ion Mobility Calculator in the Free Molecular Regime, J Am Soc Mass Spectrom 28 (2017) 1540–1551. https://doi.org/10.1007/s13361-017-1661-8.

[109] Z. Zhou, J. Tu, Z.J. Zhu, Advancing the large-scale CCS database for metabolomics and lipidomics at the machine-learning era, Curr Opin Chem Biol 42 (2018) 34–41. https://doi.org/10.1016/j.cbpa.2017.10.033.

[110] K.Y. Kartowikromo, O.E. Olajide, A.M. Hamid, Collision cross section measurement and prediction methods in omics, Journal of Mass Spectrometry 58 (2023). https://doi.org/10.1002/jms.4973.

[111] D.H. Ross, R.P. Seguin, A.M. Krinsky, L. Xu, High-Throughput Measurement and Machine Learning-Based Prediction of Collision Cross Sections for Drugs and Drug Metabolites, J Am Soc Mass Spectrom 33 (2022) 1061–1072. https://doi.org/10.1021/jasms.2c00111.

[112] Z. Zhou, X. Shen, J. Tu, Z.J. Zhu, Large-scale prediction of collision cross-section values for metabolites in ion mobility-mass spectrometry, Anal Chem 88 (2016) 11084–11091. https://doi.org/10.1021/acs.analchem.6b03091.

[113] Z. Zhou, X. Xiong, Z.J. Zhu, MetCCS predictor: A web server for predicting collision cross-section values of metabolites in ion mobility-mass spectrometry based metabolomics, in: Bioinformatics, Oxford University Press, 2017: pp. 2235–2237. https://doi.org/10.1093/bioinformatics/btx140.

[114] G.B. Gonzales, G. Smagghe, S. Coelus, D. Adriaenssens, K. De Winter, T. Desmet, K. Raes, J. Van Camp, Collision cross section prediction of deprotonated phenolics in a travelling-wave ion mobility spectrometer using molecular descriptors and chemometrics, Anal Chim Acta 924 (2016) 68–76. https://doi.org/10.1016/j.aca.2016.04.020.

[115] F. Meier, N.D. Köhler, A.D. Brunner, J.M.H. Wanka, E. Voytik, M.T. Strauss, F.J. Theis, M. Mann, Deep learning the collisional cross sections of the peptide universe from a million experimental values, Nat Commun 12 (2021). https://doi.org/10.1038/s41467-021-21352-8.

[116] W.F. Zeng, X.X. Zhou, S. Willems, C. Ammar, M. Wahle, I. Bludau, E. Voytik, M.T. Strauss, M. Mann, AlphaPeptDeep: a modular deep learning framework to predict peptide properties for proteomics, Nat Commun 13 (2022). https://doi.org/10.1038/s41467-022-34904-3.

[117] P.-L. Plante, É. Francovic-Fontaine, J.C. May, J.A. Mclean, E.S. Baker, F. Laviolette, M. Marchand, J. Corbeil, Predicting Ion Mobility Collision Cross-Sections Using a Deep Neural Network: DeepCCS HHS Public Access, Anal Chem 91 (2019) 5191–5199. https://doi.org/10.1021/acs.anal-chem.8b05821.

[118] S.M. Colby, J.R. Nuñez, N.O. Hodas, C.D. Corley, R.R. Renslow, Deep Learning to Generate in Silico Chemical Property Libraries and Candidate Molecules for Small Molecule Identification in Complex Samples, Anal Chem 92 (2020) 1720–1729. https://doi.org/10.1021/acs.analchem.9b02348.

[119] J.C. May, J.A. McLean, Ion mobility-mass spectrometry: Time-dispersive instrumentation, Anal Chem 87 (2015) 1422–1436. https://doi.org/10.1021/ac504720m.

[120] J.N. Dodds, E.S. Baker, Ion Mobility Spectrometry: Fundamental Concepts, Instrumentation, Applications, and the Road Ahead, J Am Soc Mass Spectrom 30 (2019) 2185–2195. https://doi.org/10.1007/s13361-019-02288-2.

[121] E.S. Baker, C. Hoang, W. Uritboonthai, H.M. Heyman, B. Pratt, M. MacCoss, B. MacLean, R. Plumb, A. Aisporna, G. Siuzdak, METLIN-CCS: an ion mobility spectrometry collision

cross section database, Nat Methods 20 (2023) 1836–1837. https://doi.org/10.1038/s41592-023-02078-5.

[122] J.A. Picache, B.S. Rose, A. Balinski, K.L. Leaptrot, S.D. Sherrod, J.C. May, J.A. McLean, Collision cross section compendium to annotate and predict multi-omic compound identities, Chem Sci 10 (2019) 983–993. https://doi.org/10.1039/c8sc04396e.

[123] S.M. Stow, T.J. Causon, X. Zheng, R.T. Kurulugama, T. Mairinger, J.C. May, E.E. Rennie, E.S. Baker, R.D. Smith, J.A. McLean, S. Hann, J.C. Fjeldsted, An Interlaboratory Evaluation of Drift Tube Ion Mobility-Mass Spectrometry Collision Cross Section Measurements, Anal Chem 89 (2017) 9048–9055. https://doi.org/10.1021/acs.analchem.7b01729.

[124] L. Belova, A. Celma, G. Van Haesendonck, F. Lemière, J.V. Sancho, A. Covaci, A.L.N. van Nuijs, L. Bijlsma, Revealing the differences in collision cross section values of small organic molecules acquired by different instrumental designs and prediction models, Anal Chim Acta 1229 (2022). https://doi.org/10.1016/j.aca.2022.340361.

[125] S.M. Stow, T.J. Causon, X. Zheng, R.T. Kurulugama, T. Mairinger, J.C. May, E.E. Rennie, E.S. Baker, R.D. Smith, J.A. McLean, S. Hann, J.C. Fjeldsted, An Interlaboratory Evaluation of Drift Tube Ion Mobility-Mass Spectrometry Collision Cross Section Measurements, Anal Chem 89 (2017) 9048–9055. https://doi.org/10.1021/acs.analchem.7b01729.

[126] O.E. Olajide, B. Donkor, A.M. Hamid, Systematic Optimization of Ambient Ionization Ion Mobility Mass Spectrometry for Rapid Separation of Isomers, J Am Soc Mass Spectrom 33 (2022) 160–171. https://doi.org/10.1021/jasms.1c00311.

[127] R. Lian, F. Zhang, Y. Zhang, Z. Wu, H. Ye, C. Ni, X. Lv, Y. Guo, Ion mobility derived collision cross section as an additional measure to support the rapid analysis of abused drugs and toxic compounds using electrospray ion mobility time-of-flight mass spectrometry, Analytical Methods 10 (2018) 749–756. https://doi.org/10.1039/c7ay02808c.

[128] D.H. Ross, J.H. Cho, L. Xu, Breaking down Structural Diversity for Comprehensive Prediction of Ion-Neutral Collision Cross Sections, Anal Chem 92 (2020) 4548–4557. https://doi.org/10.1021/acs.analchem.9b05772.

[129] K.M. Hines, D.H. Ross, K.L. Davidson, M.F. Bush, L. Xu, Large-Scale Structural Characterization of Drug and Drug-Like Compounds by High-Throughput Ion Mobility-Mass Spectrometry, Anal Chem 89 (2017) 9023–9030. https://doi.org/10.1021/acs.analchem.7b01709.

[130] X. Zheng, N.A. Aly, Y. Zhou, K.T. Dupuis, A. Bilbao, V.L. Paurus, D.J. Orton, R. Wilson, S.H. Payne, R.D. Smith, E.S. Baker, A structural examination and collision cross section database for over 500 metabolites and xenobiotics using drift tube ion mobility spectrometry, Chem Sci 8 (2017) 7724–7736. https://doi.org/10.1039/c7sc03464d.

[131] S.D. Pringle, K. Giles, J.L. Wildgoose, J.P. Williams, S.E. Slade, K. Thalassinos, R.H. Bateman, M.T. Bowers, J.H. Scrivens, An investigation of the mobility separation of some peptide and protein ions using a new hybrid quadrupole/travelling wave IMS/oa-ToF instrument, Int J Mass Spectrom 261 (2007) 1–12. https://doi.org/10.1016/j.ijms.2006.07.021.

[132] A.A. Shvartsburg, R.D. Smith, Fundamentals of traveling wave ion mobility spectrometry, Anal Chem 80 (2008) 9689–9699. https://doi.org/10.1021/ac8016295.

[133] K. Giles, J.P. Williams, I. Campuzano, Enhancements in travelling wave ion mobility resolution, in: Rapid Communications in Mass Spectrometry, 2011: pp. 1559–1566. https://doi.org/10.1002/rcm.5013.

[134] A.T. Kirk, C.R. Raddatz, S. Zimmermann, Separation of isotopologues in ultra-high-resolution ion mobility spectrometry, Anal Chem 89 (2017) 1509–1515. https://doi.org/10.1021/acs.analchem.6b03300.

[135] Y.M. Ibrahim, A.M. Hamid, L. Deng, S.V.B. Garimella, I.K. Webb, E.S. Baker, R.D. Smith, New frontiers for mass spectrometry based upon structures for lossless ion manipulations, Analyst 142 (2017) 1010–1021. https://doi.org/10.1039/c7an00031f.

[136] L. Deng, I.K. Webb, S.V.B. Garimella, A.M. Hamid, X. Zheng, R. V. Norheim, S.A. Prost, G.A. Anderson, J.A. Sandoval, E.S. Baker, Y.M. Ibrahim, R.D. Smith, Serpentine Ultralong Path with Extended Routing (SUPER) High Resolution Traveling Wave Ion Mobility-MS using Structures for Lossless Ion Manipulations, Anal Chem 89 (2017) 4628–4634. https://doi.org/10.1021/acs.analchem.7b00185.

[137] K. Giles, J. Ujma, J. Wildgoose, S. Pringle, K. Richardson, D. Langridge, M. Green, A Cyclic Ion Mobility-Mass Spectrometry System, Anal Chem 91 (2019) 8564–8573. https://doi.org/10.1021/acs.analchem.9b01838.

[138] S. Ollivier, L. Tarquis, M. Fanuel, A. Li, J. Durand, E. Laville, G. Potocki-Veronese, D. Ropartz, H. Rogniaux, Anomeric Retention of Carbohydrates in Multistage Cyclic Ion Mobility (IMS n): De Novo Structural Elucidation of Enzymatically Produced Mannosides, Anal Chem 93 (2021). https://doi.org/10.1021/acs.analchem.1c00673.

[139] C. Eldrid, A. Ben-Younis, J. Ujma, H. Britt, T. Cragnolini, S. Kalfas, D. Cooper-Shepherd, N. Tomczyk, K. Giles, M. Morris, R. Akter, D. Raleigh, K. Thalassinos, Cyclic Ion Mobility-Collision Activation Experiments Elucidate Protein Behavior in the Gas Phase, J Am Soc Mass Spectrom 32 (2021) 1545–1552. https://doi.org/10.1021/jasms.1c00018.

[140] A. Kováč, P. Majerová, M. Nytka, M.Z. Cechová, P. Bednář, R. Hájek, D.A. Cooper-Shepherd, A. Muck, K. Lemr, Separation of Isomeric Tau Phosphopeptides from Alzheimer's Disease Brain by Cyclic Ion Mobility Mass Spectrometry, J Am Soc Mass Spectrom (2023). https://doi.org/10.1021/jasms.2c00289.

[141] M.E. Ridgeway, M. Lubeck, J. Jordens, M. Mann, M.A. Park, Trapped ion mobility spectrometry: A short review, Int J Mass Spectrom 425 (2018) 22–35. https://doi.org/10.1016/j.ijms.2018.01.006.

[142] M.E. Ridgeway, J.A. Silveira, J.E. Meier, M.A. Park, Microheterogeneity within conformational states of ubiquitin revealed by high resolution trapped ion mobility spectrometry, Analyst 140 (2015) 6964–6972. https://doi.org/10.1039/c5an00841g.

[143] H.J. Cooper, To What Extent is FAIMS Beneficial in the Analysis of Proteins?, J Am Soc Mass Spectrom 27 (2016) 566–577. https://doi.org/10.1007/s13361-015-1326-4.

[144] B.M. Kolakowski, Z. Mester, Review of applications of high-field asymmetric waveform ion mobility spectrometry (FAIMS) and differential mobility spectrometry (DMS), Analyst 132 (2007) 842–864. https://doi.org/10.1039/b706039d.

[145] P. Hatsis, J.T. Kapron, A review on the application of high-field asymmetric waveform ion mobility spectrometry (FAIMS) in drug discovery, Rapid Communications in Mass Spectrometry 22 (2008) 735–738. https://doi.org/10.1002/rcm.3416.

[146] L.F. Pease, J.T. Elliott, D.H. Tsai, M.R. Zachariah, M.J. Tarlov, Determination of protein aggregation with differential mobility analysis: Application to IgG antibody, Biotechnol Bioeng 101 (2008) 1214–1222. https://doi.org/10.1002/bit.22017.

[147] A. Skyttä, J. Gao, R. Cai, M. Ehn, L.R. Ahonen, T. Kurten, Z. Wang, M.P. Rissanen, J. Kangasluoma, Isomer-Resolved Mobility-Mass Analysis of α-Pinene Ozonolysis Products, Journal of Physical Chemistry A 126 (2022) 5040–5049. https://doi.org/10.1021/acs.jpca.2c03366.

[148] A. Bianco, I. Neefjes, D. Alfaouri, H. Vehkamäki, T. Kurtén, L. Ahonen, M. Passananti, J. Kangasluoma, Separation of isomers using a differential mobility analyser (DMA): Comparison of experimental vs modelled ion mobility, Talanta 243 (2022). https://doi.org/10.1016/j.talanta.2022.123339.

[149] L. Shi, A. Habib, L. Bi, H. Hong, R. Begum, L. Wen, Ambient Ionization Mass Spectrometry: Application and Prospective, Crit Rev Anal Chem (2022). https://doi.org/10.1080/10408347.2022.2124840.

[150] W. Jiang, N.A. Chung, J.C. May, J.A. McLean, R.A.S. Robinson, Ion Mobility-Mass Spectrometry, in: Encyclopedia of Analytical Chemistry, John Wiley & Sons, Ltd, 2019: pp. 1–34. https://doi.org/10.1002/9780470027318.a9292.pub2.

[151] J. Hou, Z. Zhang, L. Zhang, W. Wu, Y. Huang, Z. Jia, L. Zhou, L. Gao, H. Long, M. Lei, W. Wu, D. an Guo, Spatial lipidomics of eight edible nuts by desorption electrospray ionization with ion mobility mass spectrometry imaging, Food Chem 371 (2022). https://doi.org/10.1016/j.foodchem.2021.130893.

[152] R. Guo, L. Zhou, X. Chen, Desorption electrospray ionization (DESI) source coupling ion mobility mass spectrometry for imaging fluoropezil (DC20) distribution in rat brain, (n.d.). https://doi.org/10.1007/s00216-021-03563-6/Published.

[153] G. Kaur-Atwal, D.J. Weston, P.S. Green, S. Crosland, P.L.R. Bonner, C.S. Creaser, Analysis of tryptic peptides using desorption electrospray ionisation combined with ion mobility spectrometry/mass spectrometry, Rapid Communications in Mass Spectrometry 21 (2007) 1131–1138. https://doi.org/10.1002/rcm.2941.

[154] D. Unsihuay, R. Yin, D.M. Sanchez, M. Yang, Y. Li, X. Sun, S.K. Dey, J. Laskin, High-resolution imaging and identification of biomolecules using Nano-DESI coupled to ion mobility spectrometry, Anal Chim Acta 1186 (2021). https://doi.org/10.1016/j.aca.2021.339085.

[155] O.J. Hale, J.W. Hughes, H.J. Cooper, Simultaneous spatial, conformational, and mass analysis of intact proteins and protein assemblies by nano-DESI travelling wave ion mobility mass spectrometry imaging, Int J Mass Spectrom 468 (2021). https://doi.org/10.1016/j.ijms.2021.116656.

[156] L.X. Jiang, E. Hernly, H. Hu, R.T. Hilger, H. Neuweger, M. Yang, J. Laskin, Nanospray Desorption Electrospray Ionization (Nano-DESI) Mass Spectrometry Imaging with High Ion Mobility Resolution, J Am Soc Mass Spectrom 34 (2023) 1798–1804. https://doi.org/10.1021/jasms.3c00199.

[157] C.L. Chen, T.H. Kuo, H.H. Chung, P. Huang, L.E. Lin, C.C. Hsu, Remodeling nanoDESI Platform with Ion Mobility Spectrometry to Expand Protein Coverage in Cancerous Tissue, J Am Soc Mass Spectrom 32 (2021) 653–660. https://doi.org/10.1021/jasms.0c00354.

[158] D. Sarkar, E. Sinclair, S.H. Lim, C. Walton-Doyle, K. Jafri, J. Milne, J.P.C. Vissers, K. Richardson, D.K. Trivedi, M. Silverdale, P. Barran, Paper Spray Ionization Ion Mobility Mass Spectrometry of Sebum Classifies Biomarker Classes for the Diagnosis of Parkinson's Disease, JACS Au 2 (2022) 2013–2022. https://doi.org/10.1021/jacsau.2c00300.

[159] I. Ayodeji, T. Vazquez, R. Bailey, T. Evans-Nguyen, Rapid pre-filtering of amphetamine and derivatives by direct analysis in real time (DART)-differential mobility spectrometry (DMS), Analytical Methods 9 (2017) 5044–5051. https://doi.org/10.1039/c7ay00892a.

[160] C. Barrère, M. Hubert-Roux, C. Afonso, A. Racaud, Rapid analysis of lubricants by atmospheric solid analysis probe-ion mobility mass spectrometry, Journal of Mass Spectrometry 49 (2014) 709–715. https://doi.org/10.1002/jms.3404.

[161] E. Cossoul, M. Hubert-Roux, M. Sebban, F. Churlaud, H. Oulyadi, C. Afonso, Evaluation of atmospheric solid analysis probe ionization coupled to ion mobility mass spectrometry for characterization of poly(ether ether ketone) polymers, Anal Chim Acta 856 (2015) 46–53. https://doi.org/10.1016/j.aca.2014.12.013.

[162] A.L. Mendes Siqueira, M. Beaumesnil, M. Hubert-Roux, C. Loutelier-Bourhis, C. Afonso, Y. Bai, M. Courtiade, A. Racaud, Atmospheric Solid Analysis Probe Coupled to Ion Mobility Spectrometry-Mass Spectrometry, a Fast and Simple Method for Polyalphaolefin Characterization, J Am Soc Mass Spectrom 29 (2018) 1678–1687. https://doi.org/10.1007/s13361-018-1991-1.

[163] M. Nytka, J. Wan, F. Tureček, K. Lemr, Cyclic ion mobility of isomeric new psychoactive substances employing characteristic arrival time distribution profiles and adduct separation, J Am Soc Mass Spectrom (2024).

[164] J. He, F. Tang, Z. Luo, Y. Chen, J. Xu, R. Zhang, X. Wang, Z. Abliz, Air flow assisted ionization for remote sampling of ambient mass spectrometry and its application, Rapid Communications in Mass Spectrometry 25 (2011) 843–850. https://doi.org/10.1002/rcm.4920.

[165] S. Garimella, W. Xu, G. Huang, J.D. Harper, R.G. Cooks, Z. Ouyang, Gas-flow assisted ion transfer for mass spectrometry, Journal of Mass Spectrometry 47 (2012) 201–207. https://doi.org/10.1002/jms.2955.

[166] C. Ieritano, W.S. Hopkins, Assessing collision cross section calculations using MobCal-MPI with a variety of commonly used computational methods, Mater Today Commun 27 (2021). https://doi.org/10.1016/j.mtcomm.2021.102226.

[167] M. McCullagh, S. Goscinny, M. Palmer, J. Ujma, Investigations into pesticide charge site isomers using conventional IM and cIM systems, Talanta 234 (2021). https://doi.org/10.1016/j.talanta.2021.122604.

[168] M.F. Bush, Z. Hall, K. Giles, J. Hoyes, C. V. Robinson, B.T. Ruotolo, Collision cross sections of proteins and their complexes: A calibration framework and database for gas-phase structural biology, Anal Chem 82 (2010) 9557–9565. https://doi.org/10.1021/ac1022953.

[169] B.T. Ruotolo, J.L.P. Benesch, A.M. Sandercock, S.J. Hyung, C. V. Robinson, Ion mobility-mass spectrometry analysis of large protein complexes, Nat Protoc 3 (2008) 1139–1152. https://doi.org/10.1038/nprot.2008.78.

[170] Z. Luo, J. He, Y. Chen, J. He, T. Gong, F. Tang, X. Wang, R. Zhang, L. Huang, L. Zhang, H. Lv, S. Ma, Z. Fu, X. Chen, S. Yu, Z. Abliz, Air flow-assisted ionization imaging mass spectrometry method for easy whole-body molecular imaging under ambient conditions, Anal Chem 85 (2013) 2977–2982. https://doi.org/10.1021/ac400009s.

[171] L. Borovcová, M. Hermannová, V. Pauk, M. Šimek, V. Havlíček, K. Lemr, Simple area determination of strongly overlapping ion mobility peaks, Anal Chim Acta 981 (2017) 71–79. https://doi.org/10.1016/j.aca.2017.05.003.

[172] J. Wan, M. Nytka, H. Qian, K. Lemr, F. Tureček, Do d(GCGAAGC) Cations Retain the Hairpin Structure in the Gas Phase? A Cyclic Ion Mobility Mass Spectrometry and Density

Functional Theory Computational Study, J Am Soc Mass Spectrom 34 (2023) 2323–2340. https://doi.org/10.1021/jasms.3c00228.

[173] Ondruchová Jana, Účinný Srážkovy Průřez Při Identifikaci Drog Spojením Iontové Mobility s Hmotnostní Spectrometrií, Univerzita Palackého v Olomouci, 2016.

[174] J.N. Dodds, J.C. May, J.A. McLean, Correlating Resolving Power, Resolution, and Collision Cross Section: Unifying Cross-Platform Assessment of Separation Efficiency in Ion Mobility Spectrometry, Anal Chem 89 (2017) 12176–12184. https://doi.org/10.1021/acs.analchem.7b02827.

[175] H.A. Majeed, T.S. Bos, R.L.C. Voeten, R.F. Kranenburg, A.C. van Asten, G.W. Somsen, I. Kohler, Trapped ion mobility mass spectrometry of new psychoactive substances: Isomer-specific identification of ring-substituted cathinones, Anal Chim Acta 1264 (2023). https://doi.org/10.1016/j.aca.2023.341276.

[176] R. Aderorho, C.D. Chouinard, Improved separation of fentanyl isomers using metal cation adducts and high-resolution ion mobility-mass spectrometry, Drug Test Anal 16 (2024) 369–379. https://doi.org/10.1002/dta.3550.

[177] X. Zheng, X. Zhang, N.S. Schocker, R.S. Renslow, D.J. Orton, J. Khamsi, R.A. Ashmus, I.C. Almeida, K. Tang, C.E. Costello, R.D. Smith, K. Michael, E.S. Baker, Enhancing glycan isomer separations with metal ions and positive and negative polarity ion mobility spectrometry-mass spectrometry analyses, Anal Bioanal Chem 409 (2017) 467–476. https://doi.org/10.1007/s00216-016-9866-4.

[178] C.R. de Bruin, M. Hennebelle, J.P. Vincken, W.J.C. de Bruijn, Separation of flavonoid isomers by cyclic ion mobility mass spectrometry, Anal Chim Acta 1244 (2023). https://doi.org/10.1016/j.aca.2022.340774.

[179] A.L. Rister, T.L. Martin, E.D. Dodds, Application of Group I Metal Adduction to the Separation of Steroids by Traveling Wave Ion Mobility Spectrometry, J Am Soc Mass Spectrom 30 (2019) 248–255. https://doi.org/10.1007/s13361-018-2085-9.

[180] D. Hadavi, E. de Lange, J. Jordens, Y. Mengerink, F. Cuyckens, M. Honing, Adduct ion formation as a tool for the molecular structure assessment of ten isomers in traveling wave and trapped ion mobility spectrometry, in: Rapid Communications in Mass Spectrometry, John Wiley and Sons Ltd, 2019: pp. 49–59. https://doi.org/10.1002/rcm.8419.

CURRICULUM VITAE

Name: Marianna Nytka

Year and place of birth: 1994, Uzhhorod, Ukraine

E-mail: mariannanytka@gmail.com,

marianna.nytka@upol.cz

Education

2011-2015   B.Sc. studies, Analytical Chemistry, Chemistry Faculty, Uzhhorod National University, Ukraine. Thesis: Studies of superionic materials and heat-resistant alloys as active substances of ISE

2015-2017   M.Sc. study, Analytical Chemistry, Chemical Faculty, Uzhhorod National University, Ukraine. Thesis: Comparative characteristics of solid-state and plastificated potentiometric sensors

2017-now   Ph.D study, Analytical Chemistry, Faculty of Science, Palacky University in Olomouc, Czech Republic. Topic: Combination of ionization techniques and ion mobility-mass spectrometry in the analysis of new psychoactive substances

Internship

2019   Research stay, Department of Chemistry and Biochemistry, University of Texas at Arlington, TX, USA, 6 months (supervisor: prof. Kevin Schug).

Awards

2017-2021   Fisher Scholarship for foreigner students

2021   1st place in the section "Chemistry-Doctoral students"-Dean's Award.

Projects

2018	IGA UP: Efficient processing of samples with complex matrices, team member
2019	IGA UP: Innovative methods of analyzing samples with complex matrices, team member
2019	Support of Academic mobility at Palacky University Olomouc CZ.02.2.69/0.0/0.0/16_027/0008482 (mobility n.36)
2020	IGA_PrF_2020_030: Modern trends in the analysis of samples with complex matrices, team member
2020-2022	OA ITI – ARTECA Advanced physico-chemical methods in research and protection of cultural and art heritage CZ.0.2.1.01/0.0/0.0/17_048/0007378, team member
2020-2022	TAČR TL04000476: The effect of disinfectants on historical surfaces among visiting historical institutions during emergency epidemiological measures (SPP 663103131), team member
2021	IGA_PrF_2021_021: New trends in the analysis of complex samples, team member
2022	IGA_PrF_2022_023: Modern methods of processing complex samples, team member
2023-now	GAČR (23-07254S): "Shape of mobility peaks as a tool for discrimination of isomers by ion mobility-mass spectrometry"; team member
2023	IGA_PrF_2023_027: Application of

instrumental methods in the analysis of substances in complex matrices, team member

2024　　　　　IGA_PrF_2024_026: Modern methods of analysis for complex samples

Pedagogical activities

2020　　　　　Teaching of Laboratory Documentation in English language (ACH/LADA), 1 semester

2021　　　　　Teaching of Laboratory Documentation in English language (ACH/LADA), 1 semester

2022　　　　　Teaching of Laboratory Documentation in English language (ACH/LADA), 1 semester

2023　　　　　Teaching of Practicals in Analytical Chemistry (Czech language), 1 semester

2023　　　　　Teaching of English for Chemists 2 (ACH/CHA2), 4 hours, taken and correction of exam

2023　　　　　Teaching of Technical English, 4 hours

2024　　　　　Teaching of Practicals in Analytical Chemistry (Czech language), 1 semester

International/Czech conferences and summer schools

The 43rd International Symposium on Capillary Chromatography & The 16th GCxGC Symposium – May 12th- 17th, 2019 Fort Worth, Texas USA Poster, "Mass spectrometry of new psychoactive substances using desorption nanoelectrospray with improved custom-made inlet" Nytka M., Borovcova L., Barták P., Fryčák P., Lemr K.

Prague Meeting on Historical Perspectives of Mass Spectrometry, October 13-14, 2021 Prague, Czech Republic. Poster "Multipass Separation of Synthetic Cathinones by Cyclic Ion Mobility: Collision Cross Section Determination" Nytka M., Palmer M., Muck A., Lemr K.

Advances in Chromatography and Electrophoresis& Chiranal 2022- June 13th-16th ,2022 Olomouc, Czech Republic. Oral presentation "Cyclic ion mobility-mass spectrometry of isomeric cathinones" Nytka M., Palmer M., Muck A., Lemr K.

"Advanced Mass Spectrometry Applied To Cultural Heritage "Bordeaux Summer School and The 10th International MaSC MeetingMass Spectrometry and Chromatography in Cultural Heritage", Bordeaux, France, September 26-30, 2022

Czech Mass Spectrometry Conference 2023, Brno, June 19 – 21, 2023. Oral presentation: "Multiple linear regression of mobilograms of isomeric new synthetic drugs analyzed by cyclic ion mobility", Nytka M., Lemr K

SELECT SERIES on Tour: In-Person Meeting, Bellinzona, Switzerland, May 15th 2024. Oral presentation: "Cyclic Ion Mobility of Peptides – from Alzheimer's Disease Brain to Photochemical Crosslinking", Nytka M.

72nd ASMS Conference on Mass Spectrometry and Allied Topics, Anaheim Convention Center, Anaheim, California, USA, June 2-6, 2024. Poster: "Flow injection analysis of new psychoactive substances using cyclic ion mobility mass spectrometry", Nytka M., Tureček F., Lemr K.

Advances in Chromatography and Electrophoresis & Chiranal 2024- June 17th-20th ,2024 Olomouc, Czech Republic. Poster: "Desorption Electrospray Ionization Coupled to Cyclic Ion Mobility in Analysis of New Psychoactive Substances". Nytka M., Wan J., Tureček F., Lemr K.

Publications

Nytka M, Borovcová L, Fryčák P, Barták P, Lemr K. Signal enhancement in desorption nanoelectrospray ionization by custom-made inlet with pressure regulation. J

Mass Spectrom. 2020 Oct;55(10):e4642. doi: 10.1002/jms.4642.

Liu.Y,Liu Y, <u>Nytka M</u>, Huang S.R, Lemr K, Turecek F. Probing d- and l-Adrenaline Binding to β2-Adrenoreceptor Peptide Motifs by Gas-Phase Photodissociation Cross-Linking and Ion Mobility Mass Spectrometry. J. Am. Soc. for Mass Spectrom. 2021, 32 (4), 1041-1052 doi: 10.1021/jasms.1c00019

Kováč A., Majerová P., <u>Nytka M</u>., Zajacová Cechová M., Bednář P., Hájek R., Cooper-Shepherd Dale A., Muck A., and Lemr K. Separation of Isomeric Tau Phosphopeptides from Alzheimer's Disease Brain by Cyclic Ion Mobility Mass Spectrometry. , J. Am. Soc. Mass Spectrom. 2023, 34, 3, 394–400. doi: 10.1021/jasms.2c00289

Wan J., <u>Nytka M.,</u> Qian H., Lemr K and Tureček F. Do d(GCGAAGC) Cations Retain the Hairpin Structure in the Gas Phase? A Cyclic Ion Mobility Mass Spectrometry and Density Functional Theory Computational Study. J. Am. Soc. Mass Spectrom. 2023, 34 (10), 2323-2340. doi: 10.1021/jasms.3c00228

Wan J., <u>Nytka M</u>., Qian H., Vu K., Lemr K., Tureček F. Nitrile Imines as Peptide and Oligonucleotide Photo-Cross-Linkers in Gas Phase Ions. J. Am. Soc. Mass Spectrom. 2024, 35, 2. doi: 10.1021/jasms.3c00379.

Nytka M., Wan J., Tureček F., Lemr K. Cyclic ion mobility of isomeric new psychoactive substances employing characteristic arrival time distribution profiles and adduct separation. J. Am. Soc. Mass Spectrom. 2024, DOI: 10.1021/jasms.4c00127

Other activities:
Member of Czech Society of Mass Spectrometry (2023-now)
Consultation of bachelor thesis: Matěj Rousek.
Consultation of master thesis: Dominik Halman
Reviewer of 1 publication for Monastshefte für Chemie (Impact Factor: 1.8).
Contract research for TEVA Czech Industries.

APPENDICES

Appendix A

Table A1. Cartesian coordinates of the M06-2X/6-31+G(d,p) optimized geometry of ion **1a**[+]. Standard orientation:

Center Number	Atomic Number	Atomic Type	Coordinates (Angstroms)		
			X	Y	Z
1	6	0	-0.501145	0.061142	-0.015535
2	6	0	-1.562269	-0.833726	0.195504
3	6	0	-2.881550	-0.432502	0.010587
4	6	0	-3.117899	0.890256	-0.394399
5	6	0	-2.073833	1.786672	-0.609083
6	6	0	-0.758130	1.378214	-0.419782
7	6	0	-4.031150	-1.378208	0.236217
8	6	0	0.863021	-0.438400	0.197665
9	8	0	1.134348	-1.600760	0.454351
10	6	0	2.053068	0.549016	0.164201
11	6	0	2.142100	1.332861	1.471739
12	7	0	3.269771	-0.319504	0.003934
13	6	0	3.574366	-0.702462	-1.409840
14	1	0	-1.333336	-1.848168	0.508867
15	1	0	-4.142532	1.220754	-0.544454
16	1	0	-2.286827	2.801942	-0.925264
17	1	0	0.044152	2.088604	-0.596209
18	1	0	-3.679260	-2.367099	0.534718
19	1	0	-4.693889	-1.000620	1.019984
20	1	0	-4.626232	-1.487732	-0.674721
21	1	0	2.991885	2.020939	1.463936
22	1	0	1.232780	1.920061	1.611105
23	1	0	2.231371	0.651357	2.323475
24	1	0	3.037359	-1.183940	0.527560
25	1	0	4.423773	-1.384243	-1.414700

26	1	0	2.695773	-1.200577	-1.818892
27	1	0	3.805771	0.198908	-1.975978
28	1	0	2.013378	1.211489	-0.703475
29	1	0	4.083164	0.123760	0.438051

Rotational constants (GHZ):   1.6424647   0.4222286   0.3800671

Table A2. Cartesian coordinates of the M06-2X/6-31+G(d,p) optimized geometry of ion **2a$^+$**. Standard orientation:

Center Number	Atomic Number	Atomic Type	Coordinates (Angstroms)		
			X	Y	Z
1	6	0	-1.134810	-0.265645	-0.072742
2	6	0	-2.174918	-1.032772	-0.619104
3	6	0	-3.494052	-0.650621	-0.417263
4	6	0	-3.781136	0.493641	0.329968
5	6	0	-2.751043	1.259588	0.877812
6	6	0	-1.428373	0.883440	0.677537
7	6	0	0.244168	-0.716307	-0.310503
8	8	0	0.529802	-1.758671	-0.877914
9	6	0	1.427272	0.178888	0.118155
10	7	0	2.622367	-0.731204	0.114022
11	6	0	1.636311	1.329306	-0.874599
12	6	0	2.748803	2.293991	-0.463951
13	6	0	2.817437	-1.506791	1.377657
14	1	0	-1.928549	-1.917924	-1.196309
15	1	0	-4.299729	-1.240777	-0.839873
16	1	0	-4.813046	0.790236	0.487363
17	1	0	-2.980731	2.145156	1.459934
18	1	0	-0.640165	1.489972	1.114875
19	1	0	1.311476	0.554648	1.138821
20	1	0	2.428793	-1.403246	-0.651439
21	1	0	0.687843	1.868300	-0.951640
22	1	0	1.824643	0.903533	-1.868619
23	1	0	3.740811	1.827358	-0.442499

24	1	0	2.555279	2.725188	0.522458
25	1	0	2.814633	3.114896	-1.180113
26	1	0	3.011583	-0.808767	2.191120
27	1	0	1.907523	-2.075882	1.566799
28	1	0	3.659668	-2.185263	1.248326
29	1	0	3.467034	-0.199945	-0.111832

Rotational constants (GHZ):   1.3708135   0.4695843   0.4019368

Table A3. Cartesian coordinates of the M06-2X/6-31+G(d,p) optimized geometry of ion **1b⁺**. Standard orientation:

Center Number	Atomic Number	Atomic Type	Coordinates (Angstroms)		
			X	Y	Z
1	6	0	-0.521384	0.029902	-0.158358
2	6	0	-1.589601	-0.811694	0.187009
3	6	0	-2.905005	-0.351018	0.148149
4	6	0	-3.130670	0.971939	-0.256026
5	6	0	-2.077746	1.809965	-0.609208
6	6	0	-0.765756	1.344008	-0.564051
7	6	0	-4.057918	-1.238045	0.537987
8	6	0	0.850012	-0.511190	-0.126890
9	8	0	1.050395	-1.751827	-0.660681
10	6	0	1.920636	0.098657	0.410593
11	6	0	1.992857	1.373762	1.186396
12	7	0	3.200583	-0.630275	0.255730
13	6	0	4.241798	0.107044	-0.534858
14	1	0	-1.392120	-1.827760	0.523535
15	1	0	-4.150236	1.345770	-0.296250
16	1	0	-2.278632	2.825941	-0.931985
17	1	0	0.056250	1.985173	-0.867887
18	1	0	-3.721140	-2.246112	0.787301
19	1	0	-4.581369	-0.830307	1.407436
20	1	0	-4.782690	-1.311782	-0.277468
21	1	0	2.411906	2.203306	0.607226

22	1	0	0.991402	1.662393	1.507668
23	1	0	2.603594	1.248097	2.088653
24	1	0	2.986322	-1.525047	-0.205081
25	1	0	5.126227	-0.522680	-0.627142
26	1	0	3.819249	0.328000	-1.514007
27	1	0	4.487573	1.029391	-0.011292
28	1	0	3.579557	-0.859897	1.181449
29	1	0	0.293525	-2.017921	-1.201277

Rotational constants (GHZ): 1.7765132 0.4116427 0.3636817

Table A4. Cartesian coordinates of the M06-2X/6-31+G(d,p) optimized geometry of ion **2b**[+]. Standard orientation:

Center Number	Atomic Number	Atomic Type	Coordinates (Angstroms)		
			X	Y	Z
1	6	0	-1.056960	-0.291959	-0.130468
2	6	0	-1.556745	0.958557	-0.511618
3	6	0	-2.905145	1.250671	-0.330699
4	6	0	-3.758249	0.297079	0.224233
5	6	0	-3.265577	-0.953270	0.596609
6	6	0	-1.918456	-1.252302	0.417259
7	6	0	0.362371	-0.637244	-0.336881
8	8	0	0.642721	-1.851614	-0.897546
9	6	0	1.419789	0.119837	0.000804
10	7	0	2.730890	-0.460100	-0.374381
11	6	0	1.478968	1.415822	0.748248
12	6	0	1.985596	2.593361	-0.094999
13	6	0	3.368648	-1.286020	0.708129
14	1	0	-0.896521	1.688049	-0.971969
15	1	0	-3.292589	2.217329	-0.633927
16	1	0	-4.809376	0.527090	0.362405
17	1	0	-3.928731	-1.693072	1.031725
18	1	0	-1.531130	-2.218706	0.730030
19	1	0	2.115518	1.297054	1.635889

20	1	0	0.476639	1.626117	1.127475
21	1	0	1.992196	3.508893	0.499574
22	1	0	1.349720	2.755969	-0.968999
23	1	0	3.012912	2.447013	-0.450311
24	1	0	3.489455	-0.661158	1.591385
25	1	0	2.698323	-2.117926	0.917677
26	1	0	4.336234	-1.644727	0.357489
27	1	0	3.364661	0.295526	-0.653977
28	1	0	-0.145364	-2.219853	-1.321828
29	1	0	2.584608	-1.061186	-1.195303

Rotational constants (GHZ):   1.3827636   0.4969514   0.3979405

Table A5. Cartesian coordinates of the M06-2X/6-31+G(d,p) optimized geometry of ion **3a**[+]. Standard orientation:

Center Number	Atomic Number	Atomic Type	Coordinates (Angstroms)		
			X	Y	Z
1	6	0	-0.545552	0.097087	-0.001594
2	6	0	-1.595939	-0.828598	0.129315
3	6	0	-2.920785	-0.437874	-0.029921
4	6	0	-3.179119	0.910031	-0.323640
5	6	0	-2.149884	1.839133	-0.455082
6	6	0	-0.827938	1.439744	-0.296215
7	6	0	-4.054681	-1.419208	0.106604
8	6	0	0.824891	-0.386985	0.185443
9	8	0	1.059234	-1.582736	0.411112
10	6	0	2.013441	0.579847	0.182561
11	6	0	2.115576	1.230178	1.567629
12	7	0	3.242616	-0.181734	-0.121084
13	6	0	3.427547	-0.370683	-1.577675
14	1	0	-1.354513	-1.861762	0.359719
15	1	0	-4.208921	1.233996	-0.451645
16	1	0	-2.379384	2.874078	-0.683742
17	1	0	-0.038672	2.175987	-0.404835

18	1	0	-3.687320	-2.421192	0.335056
19	1	0	-4.735874	-1.114918	0.906230
20	1	0	-4.634935	-1.471394	-0.818926
21	1	0	2.941515	1.946002	1.588481
22	1	0	1.196700	1.763702	1.817861
23	1	0	2.286830	0.472260	2.338900
24	3	0	2.829066	-1.999983	0.615490
25	1	0	4.370311	-0.887997	-1.764961
26	1	0	2.609329	-0.979844	-1.973834
27	1	0	3.436442	0.582040	-2.117978
28	1	0	1.859052	1.356098	-0.576757
29	1	0	4.034711	0.350872	0.234093

Rotational constants (GHZ): 1.4907024 0.4057202 0.3631808

Table A6. Cartesian coordinates of the M06-2X/6-31+G(d,p) optimized geometry of ion **4a$^+$**. Standard orientation:

Center Number	Atomic Number	Atomic Type	Coordinates (Angstroms)		
			X	Y	Z
1	6	0	1.078686	-0.192735	0.090673
2	6	0	1.971998	-0.614215	1.090403
3	6	0	3.339858	-0.482979	0.900051
4	6	0	3.826861	0.070656	-0.286266
5	6	0	2.947543	0.492543	-1.284444
6	6	0	1.576726	0.361640	-1.100801
7	6	0	-0.358408	-0.347513	0.341333
8	8	0	-0.772260	-0.870223	1.385299
9	6	0	-1.397592	0.204144	-0.636849
10	7	0	-2.670691	-0.512997	-0.423127
11	6	0	-1.574177	1.717097	-0.381464
12	6	0	-2.071153	2.063101	1.022618
13	6	0	-2.681050	-1.827379	-1.102348
14	1	0	1.574999	-1.040340	2.005406
15	1	0	4.028824	-0.809169	1.671359

16	1	0	4.897122	0.172627	-0.434399
17	1	0	3.331805	0.919235	-2.204260
18	1	0	0.909651	0.691144	-1.890575
19	1	0	-1.052183	0.056723	-1.667571
20	1	0	-2.272730	2.100007	-1.134125
21	1	0	-0.616663	2.213151	-0.565521
22	1	0	-1.370247	1.737227	1.798005
23	1	0	-3.061102	1.634079	1.224842
24	1	0	-2.183623	3.143980	1.126153
25	1	0	-1.918689	-2.473270	-0.657338
26	1	0	-3.656262	-2.299674	-0.972133
27	1	0	-2.472974	-1.737479	-2.174136
28	1	0	-3.417301	0.055848	-0.820149
29	3	0	-2.601157	-0.825821	1.552167

Rotational constants (GHZ):   1.3263148   0.4424122   0.4311162

Table A7. Cartesian coordinates of the M06-2X/6-31+G(d,p) optimized geometry of ion **3b$^+$**. Standard orientation:

Center Number	Atomic Number	Atomic Type	Coordinates (Angstroms)		
			X	Y	Z
1	6	0	-0.484680	0.103232	-0.106716
2	6	0	-1.548725	-0.712947	0.323908
3	6	0	-2.878780	-0.292128	0.227111
4	6	0	-3.131171	0.966818	-0.335138
5	6	0	-2.088419	1.780697	-0.765510
6	6	0	-0.763335	1.354138	-0.657453
7	6	0	-4.009918	-1.139937	0.747312
8	6	0	0.897953	-0.466129	-0.076222
9	8	0	1.033957	-1.657509	-0.624635
10	6	0	1.955964	0.187779	0.465332
11	6	0	2.050508	1.483500	1.200179
12	7	0	3.198695	-0.596887	0.322247
13	6	0	4.242949	0.021853	-0.548693

14	1	0	-1.324109	-1.656698	0.826285
15	1	0	-4.157373	1.312006	-0.425802
16	1	0	-2.306903	2.751357	-1.198829
17	1	0	0.048400	1.980993	-1.014508
18	1	0	-3.674145	-2.146377	1.007079
19	1	0	-4.438671	-0.689564	1.647523
20	1	0	-4.812211	-1.221484	0.009282
21	1	0	2.570290	1.363951	2.159379
22	1	0	2.569601	2.266196	0.634537
23	1	0	1.047105	1.849463	1.424339
24	1	0	2.860533	-1.486432	-0.095346
25	1	0	5.096222	-0.652352	-0.624116
26	1	0	3.797031	0.189887	-1.528062
27	1	0	4.550193	0.970001	-0.109318
28	1	0	3.599912	-0.811258	1.240690
29	3	0	-0.514157	-2.100886	-1.352148

Rotational constants (GHZ): 1.5531459   0.4048271   0.3597366

Table A8. Cartesian coordinates of the M06-2X/6-31+G(d,p) optimized geometry of ion **4b$^+$**. Standard orientation:

Center Number	Atomic Number	Atomic Type	Coordinates (Angstroms)		
			X	Y	Z
1	6	0	1.039779	-0.193871	-0.045456
2	6	0	1.377169	0.914032	0.737756
3	6	0	2.706984	1.320169	0.842468
4	6	0	3.713458	0.620337	0.177491
5	6	0	3.389111	-0.486775	-0.605995
6	6	0	2.059001	-0.894980	-0.713916
7	6	0	-0.352154	-0.739762	-0.098459
8	8	0	-0.475075	-2.016777	0.199546
9	6	0	-1.431412	0.013694	-0.427732
10	7	0	-2.673879	-0.789652	-0.364516
11	6	0	-1.540372	1.413439	-0.945783

12	7	0	-2.371521	2.373370	-0.084662
13	6	0	-3.357518	-0.788833	0.969865
14	1	0	0.596968	1.447545	1.273734
15	1	0	2.959380	2.180621	1.453473
16	1	0	4.746137	0.940965	0.263294
17	1	0	4.165010	-1.017618	-1.148311
18	1	0	1.794410	-1.711643	-1.387373
19	1	0	-1.952890	1.398068	-1.966019
20	1	0	-0.522357	1.798154	-1.050478
21	1	0	-2.323801	3.386476	-0.490306
22	1	0	-2.003588	2.398451	0.945611
23	1	0	-3.430360	2.092967	-0.062024
24	1	0	-3.621320	0.234297	1.228014
25	1	0	-4.247113	-1.417887	0.918751
26	1	0	-2.643601	-1.190482	1.687108
27	1	0	-2.365758	-1.758682	-0.546226
28	3	0	1.098911	-2.640263	0.701006
29	1	0	-3.325234	-0.503576	-1.100480

Rotational constants (GHZ):   1.2694629   0.4785842   0.3882588

Appendix B

Publications related to the thesis:

Nytka M., Borovcová L., Fryčák P., Barták P,, Lemr K. Signal enhancement in desorption nanoelectrospray ionization by custom-made inlet with pressure regulation. J Mass Spectrom. 2020 Oct;55(10):e4642. DOI: 10.1002/jms.4642.

Nytka M., Wan J., Tureček F., Lemr K. Cyclic ion mobility of isomeric new psychoactive substances employing characteristic arrival time distribution profiles and adduct separation. J. Am. Soc. Mass Spectrom. 2024, DOI: 10.1021/jasms.4c00127

RESEARCH ARTICLE

Journal of MASS SPECTROMETRY WILEY

Signal enhancement in desorption nanoelectrospray ionization by custom-made inlet with pressure regulation

Marianna Nytka[1] | Lucie Borovcová[1] | Petr Fryčák[2] | Petr Barták[1] | Karel Lemr[2] 🅾

[1]Department of Analytical Chemistry, Faculty of Science, Palacký University, Olomouc, Czech Republic

[2]Department of Analytical Chemistry, Regional Centre of Advanced Technologies and Materials, Faculty of Science, Palacký University, Olomouc, Czech Republic

Correspondence
Karel Lemr, Department of Analytical Chemistry, Regional Centre of Advanced Technologies and Materials, Faculty of Science, Palacký University, 17. listopadu 12, 771 46, Olomouc, Czech Republic.
Email: karel.lemr@upol.cz

Abstract

The efficiency of desorption/ionization becomes more critical as the sampled surface area decreases. Desorption electrospray and desorption nanoelectrospray belong to ambient ionizations and enable direct surface analysis including mass spectrometric imaging. Lateral resolution in tens of micrometers was demonstrated for desorption nanoelectrospray previously, but sensitivity of the surface scan can be an issue. For desorption electrospray, the drag force in the source is driven by the flow of used gases and vacuum suction. Ion signal intensity can be improved by controlling the nebulizing gas flow rate or auxiliary pumping of a closed compartment in front of the mass spectrometer inlet. Because nanoelectrospray generates charged droplets without the assistance of a nebulizing gas, only vacuum suction drives the gas flow. In this study, the effect of pressure drop between the atmospheric and evacuated region of a mass spectrometer on the ion signal intensity was investigated for desorption nanoelectrospray. A modification of the commercial inlet was designed. An auxiliary pump was directly connected to an inner compartment of the modified mass spectrometer inlet through a needle valve that enabled the regulation of the reduced pressure. Adjustment of the pressure drop significantly increased signal intensity (more than one order of magnitude in some cases). To a lesser extent, the temperature of a heated capillary (an integral part of the inlet) also influenced the signal intensity. The applicability of desorption nanoelectrospray equipped with pressure regulation was demonstrated by the analysis of synthetic cathinones or a pill of paracetamol. Because pressure in the inlet depends on the diameters of orifices and the power of vacuum systems of mass spectrometers, the effect of the pressure regulation can be different for different instruments. Nevertheless, the presented results confirmed the importance of pressure drop-driven transport for desorption nanoelectrospray efficiency and can encourage its new applications.

KEYWORDS

cathinones, desorption nanoelectrospray, mass spectrometry, new psychoactive substances, pressure drop regulation

1 | INTRODUCTION

Desorption nanoelectrospray (nanoDESI) belongs to ambient ionization techniques and was described in 2007.[1] It should not be confused with coincidently abbreviated nanospray desorption electrospray (nano-DESI), which was introduced a few years later and is more related to liquid extraction surface analysis (LESA) than to desorption electrospray (DESI).[2,3] In the very first application of

nanoDESI, chiral analysis of ephedrine in an untreated drop of a commercial pharmaceutical deposited on the analyzed surface was demonstrated using this ion source and the Cooks kinetic method.[1] In comparison with DESI,[4] nanoDESI generates a lower flow rate of spraying liquid and smaller primary charged droplets. Instead of an electrospray tip (tens of micrometers I.D.) it uses a nanoelectrospray tip ($\sim$2 μm I.D.) without the assistance of nebulizing gas. Both techniques are suitable for direct surface analysis, tolerant to sample contamination by salt, and produce ions with similar internal energy. For nanoDESI, the signal-to-noise ratio did not deteriorate substantially for samples containing up to 2.5 mol L^{-1} NaCl.[5] Applicability of nanoDESI was further demonstrated, for example, by chiral analysis of pharmaceuticals in whole blood[6] or analysis of anthocyanins in a drop of red wine.[7] Considering imaging applications, the low flow rate of spraying liquid decreases sample washing off which can be advantageous for lateral resolution and can enable repeat scans of the same surface area. Promising very good resolution of dye squares (60 μm × 60 μm) has been achieved.[8] Although technical development has improved the robustness of nanoDESI[5] and a modification of inlet has allowed its implementation on a Q-TOF mass spectrometer,[8] sensitivity of measurement can still be an issue. Because a very small surface area is sampled, only a tiny amount of analyte is available for desorption and ionization.

The flow rate (pressure) of nebulizing gas is an important experimental parameter in DESI. High gas velocity accelerates primary charged droplets impacting the sample surface. A proper setting of gas flow rate is essential to reach the maximum of ion signal intensity. Above the optimal value, plateau or decrease of ion signal can be observed. At a lower gas flow rate, nebulization may produce larger droplets and be inefficient. A higher flow rate generates smaller droplets at higher velocity confined to a smaller spot. Too high gas flow rate may cause evaporation of droplets before they reach the surface.[9–12] Surface charge imaging revealed that the movement of charged droplets towards the MS inlet is driven by the nebulizing gas flow and the vacuum suction.[13] The vacuum of the mass spectrometer also supported the transport of ions from DESI source through a transport tube up to 3 m long to the MS inlet and enabled non-proximate sampling.[14,15] As remote sampling can benefit from higher gas flow in the transport tube, its effectivity can be improved by additional pumping of a closed compartment situated directly in front of the MS inlet.[16,17] The signal intensity of ions increased rapidly with the maximum at gas flow rate of 25 L min^{-1} which was the highest flow rate applied.[16] Further simulations and experiments have shed light on the ion transport. At atmospheric pressure, laminar flow

effectively transported ions over a few meters with good signal stability.[17] The signal improvement may occur due to better collection efficiency and lower losses of charged droplets/ions in the transfer tube. Remote DESI ionization enabled easier manipulation with larger samples to acquire mass spectrometry image of a whole-body tissue section. Using 500-mm transport tube, ion intensity grew up significantly when the gas flow rate was increased from 0 to 10 L min^{-1}, reached a plateau between 10 and 40 L min^{-1} and then began to decrease.[18] Ion transport simulation for nanoelectrospray confirmed that drag force, electric force, and Brownian force are the dominant forces acting on ions. Drag force is related to gas flow in an ion source, which can be influenced by reduced pressure at the MS inlet.[19] Because nanoDESI uses neither nebulizing gas nor other auxiliary gases (e.g., cone gas), this reduced pressure will drive gas flow in the source and its regulation may influence the intensity of ion signal.

In this study, we designed and investigated a modification of the inlet of a triple quadrupole mass spectrometer that couples nanoDESI with auxiliary pumping. A mixture of new psychoactive substances was used to demonstrate the influence of regulation of pressure drop (pressure difference) between atmospheric and evacuated regions of the mass spectrometer. These compounds represent a group of recently emerging abused drugs and are associated with social and health risks.[20] Higher ion signal intensity can be useful not only for their detection, for example, in seized street samples, but also for other applications of nanoDESI.

2 | EXPERIMENTAL

2.1 | Chemicals and samples

Standards of 3-fluoromethcathinone and other investigated cathinones in the form of hydrochlorides were purchased from Cayman Pharma (Neratovice, Czech Republic) and from Lipomed AG (Arlesheim, Switzerland), respectively (see Figure 1 for structures). LC–MS grade methanol, formic acid (≥98%), hexamethyldisilazane (≥99%), and pyridine (p. a.) were provided by Sigma-Aldrich (Prague, Czech Republic) and by Penta (Czech Republic), respectively. Water was purified using a Milli-Q system (Millipore, Mollsheim, France). Paracetamol (Paralen®, Zentiva–Sanofi Company, Czech Republic) was bought in a drugstore. Standard solutions were prepared in methanol/water 50/50 (v/v) at a concentration of 1 mg ml^{-1} and stored in a fridge. Mixture of methanol/water 75/25 (v/v) acidified by formic acid (2%) was used as the spraying liquid.
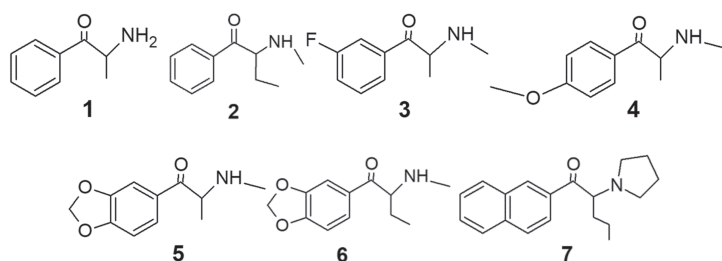

FIGURE 1 Structures of analyzed new psychoactive substances (*m/z* of protonated molecules): (1) cathinone (*m/z* 150); (2) buphedrone (*m/z* 178); (3) 3-FMC (3-fluoromethcathinone; *m/z* 182); (4) methedrone (*m/z* 194); (5) methylone (*m/z* 208); (6) butylone (*m/z* 222); and (7) naphyrone (*m/z* 282)

2.2 | Silanization and sample application

Silanization of microscope slides (Thermo Fisher Scientific, Budapest, Hungary) was carried out in a closed container with hexamethyldisilazane/pyridine 50/50 (v/v) for 2 h at 120°C. Silanized slides were rinsed three times by water in ultrasonic bath for 1 min. Finally, they were left in a laboratory dryer for 10 min at 105°C.

Standard solution of a mixture of new psychoactive substances (1 μg ml^{-1} each) was sprayed using a SunCollect MALDI spotter (SunChrom, Friedrichsdorf, Germany) on silanized microscope slides. Total volume of 56 μl of solution was deposited in five layers on the surface area of 1.89 × 0.6 cm, which corresponds to 0.5 ng mm^{-2} of each substance. Homogenously covered surface was used to evaluate influence of pressure drop regulation on signal intensity of each analyte. Solid samples (traces of new psychoactive substances or paracetamol) were fixed on the microscope slides using a double-sided tape. For experiments in the nanoelectrospray setup, the nanoelectrospray tip was filled by the standard solution of cathinones (1 μg ml^{-1} each) in methanol/water 75/25 (v/v) acidified by formic acid (2%) and the tip was directed towards the inlet of the heated capillary.

2.3 | Instrumentation

Experiments were carried out using a Xevo TQD triple quadrupole mass spectrometer (Waters, Manchester, UK). The commercial inlet of the instrument was replaced by a custom-made inlet (Figure 2). Instead of a cone gas nozzle, an inlet block (f) with a heated capillary (d) and an original sample cone (h) was attached to the mass spectrometer. An auxiliary pump was connected through a port (g). It allowed pumping of the inner compartment of the MS inlet in comparison with designs connecting a pump to a refluence tube[16] or a source chamber[17] in front of the inlet. Pressure drop (difference between atmospheric pressure and pressure in the inlet) was measured by a manometer and regulated by a needle valve, both mounted between a port (g) and the auxiliary pump. The capillary was heated using a
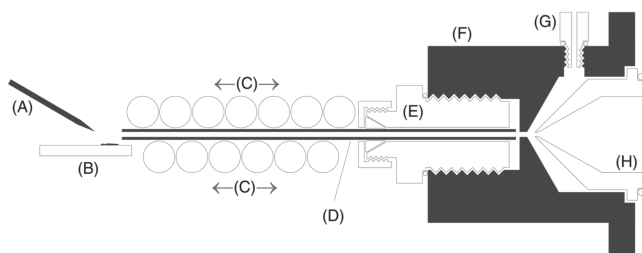

FIGURE 2   Scheme of desorption nanoelectrospray (nanoDESI) source with custom-made MS inlet: (a) nanoelectrospray tip; (b) sample on a support; (c) threads of a heating rope; (d) stainless steel inlet capillary; (e) Swagelok SS-100-1-OR tube fitting, sealing the heated capillary (d) by a ferrule; sealed to the inlet block by an O-ring; (f) inlet block; (g) port hose adapter for auxiliary pump connection, sealed to the inlet block by an O-ring; and (h) sample cone (native part of the mass spectrometer, fitted in its original location and held by the inlet block [f], sealed to the instrument by an O-ring)

heating rope (c) and temperature was controlled by a Regbox heater driver (Jakar Electronics, Karviná, Czech Republic). The interlock for the detection of presence of ESI source and gas flow outlets were blocked. NanoDESI consisted of a nanoelectrospray tip (2 ± 1 μm I.D., PicoTips emitter, New Objective, Woburn, USA) and a sample stage, both manually movable in the x–y–z axes. Proper geometry was set to obtain good spectra quality (nanospray tip–target plate: vertical distance ~2 mm, angle ~30°; nanospray tip–center of sample spot: horizontal distance ~2 mm; microscope slide–heated capillary: vertical distance ~1 mm, angle ~0°; and center of sample spot–heated capillary: horizontal distance ~2 mm). The source parameters were tuned in the positive mode and set as follows: capillary voltage +2.2 kV; TQD source temperature 100°C; temperature of the heated capillary 100°C, 180°C, 200°C, and 220°C; and pressure drop (difference) from 0.08 (closed needle valve) to 0.8 bar. The instrument was operated and data were acquired using Waters MassLynx 4.1 software. Data collected in six replicates (1 min acquisition each) were processed by OriginPro 2020 (OriginLab, Northampton, USA).

3 | RESULTS AND DISCUSSION

The new custom-made mass spectrometer inlet was designed considering three parameters: length of the heated capillary, its temperature, and pressure regulation at the MS inlet. All three parameters can control the desolvation of ions and affect ion transmission and intensity of ion signal. Their influence was evaluated for synthetic cathinones as nanoDESI might be useful for their detection, for example, in seized street samples. Four different lengths of the heated capillary were tested (46, 61, 76, and 99 mm) at 200°C. Although the effect of capillary length was not significant, slightly better ion signal intensities were observed using the shortest one that was selected for the following experiments.

On the contrary, the regulation of pressure drop at the MS inlet significantly influenced the signal intensity. Auxiliary pumping generated a pressure drop at the MS inlet in the range of 0.20–0.80 bar. At reference condition (pressure drop 0.08 bar), the needle valve connecting the auxiliary pump with the MS inlet was closed and the pressure reduction was generated only by the vacuum system of the mass spectrometer. Because pressure drop represents the difference between atmospheric pressure and pressure in the evacuated inlet compartment, its higher value means lower pressure in the inlet and higher vacuum suction. In the tested range, the ion signal intensity of all cathinones grew between 0.08 and 0.20 bar, reached a maximum, and then gradually decreased (Figure 3). The effect is similar to that observed for the extracting gas flow rate in DESI equipped with the transport tube.[18] The signal improvement was compound dependent. Comparing 0.08 and 0.20 bar, the signal intensity increased less than twofold for naphyrone but almost one order for buphedrone and more than one order for cathinone and 3-FMC. Further nanoDESI experiments were performed at pressure drop of 0.40 bar giving slightly lower signal intensities in comparison with 0.20 bar, but the dependencies are flatter around 0.40 bar (Figure 3), and variation of
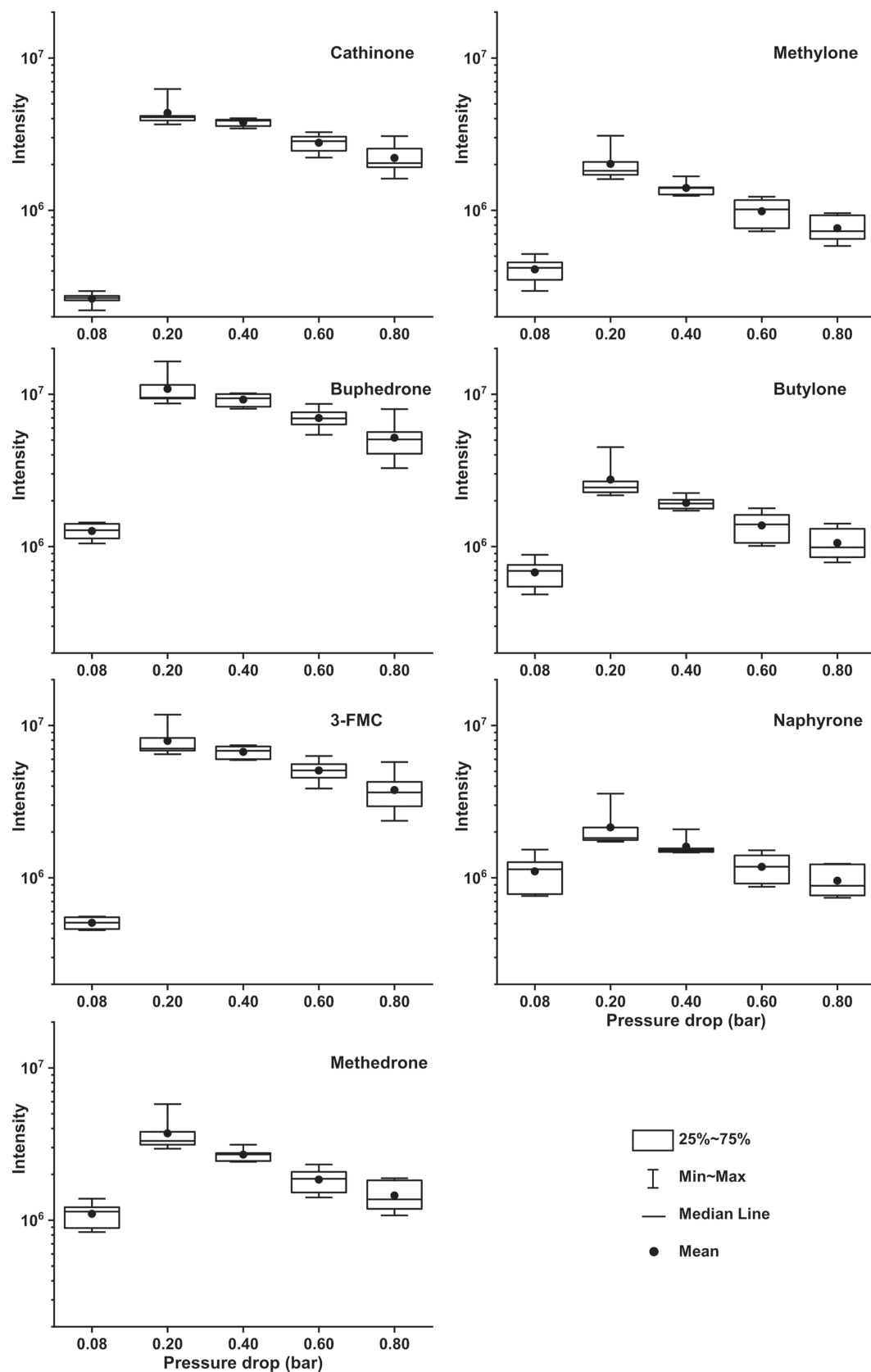
FIGURE 3 Influence of pressure drop on the MH$^+$ ion signal intensity of cathinones ionized by desorption nanoelectrospray (nanoDESI). The temperature of the heated capillary (46 mm) was set at 200°C. Mixture of standards was deposited on a silanized microscope slide

signal intensity is less sensitive to pressure drop changes. Generally, the pressure at MS inlet is determined by the power of the vacuum system of a particular mass spectrometer, and the influence of auxiliary pumping can vary. Its optimum setting can be instrument dependent. Nevertheless, it is evident that vacuum suction is important for nanoDESI efficiency. Because neither nebulizing gas nor auxiliary gas is used, pressure drop regulation is the only available experimental parameter driving drag force in the source. Pressure regulation enabled to increase the drag force occurring due to vacuum suction. The force influenced the transport of charged droplets and ions from the sampling area (atmospheric pressure) to the first evacuated region of the mass spectrometer.

To evaluate the effect of pressure regulation in the nanoelectrospray setup, the nanoelectrospray tip was turned towards the heated capillary inlet. Although such source geometry may not be optimal, a higher pressure drop might help to overcome this drawback. A signal intensity increased substantially between 0.08 and 0.20 bar, and the effect was less compound dependent in comparison with nanoDESI (compare Figures 3 and S1). Vacuum suction enables to collect more charged droplets/ions created by nanoelectrospray and generates a gas flow that can assist in ion evaporation from the charged droplets. As the effect of

pressure drop regulation on signal intensity differs for the analyzed compounds using nanoDESI (Figure 3), we could speculate that the pressure regulation does not influence just the transport of ions but might also affect the process of desorption. Nevertheless, the desorption is dependent on various experimental conditions and properties of analytes (e.g., the composition of spraying liquid, surface activity, and polarity of analytes), and all of them can influence the resulting ion signal intensity in a mass spectrum.

Finally, the temperature of the heated capillary was also considered as an important experimental parameter. Profile of change of signal intensity shown in Figure 4 is typical for five studied analytes (cathinone, methedrone, methylone, butylone, and naphyrone). For buphedrone and 3-FMC, the signal intensities were comparable between 100°C and 200°C (the differences were not statistically significant). For all compounds, a decrease of signal intensity was observed at 220°C. At lower temperature, the droplets/ions can be less effectively desolvated. Higher temperature of the heated capillary can cause too fast solvent evaporation from the nearby sample surface, which can worsen its wetting. Because this wetting forming thin liquid layer is considered to be important for the desorption and ionization in DESI,[11] less effective desorption and ionization may also be observed in nanoDESI. Although the temperature did not show such strong effect as pressure regulation, its proper setting may be beneficial to the quality of mass spectra. The substantial effect of pressure regulation is also evident when mass spectra of the analyzed mixture at 0.08 and 0.40 bar are compared (Figure 5). The signal intensities of all analytes are higher at 0.40 bar. Their increase is significant especially for cathinone (1), buphedrone (2), and 3-FMC (3). No interfering signals were observed for a blank (see Figure S2A).

In proving the effect of pressure regulation in the analysis of "real-world samples," the detection of traces of new psychoactive substances on personal items can represent a relevant example.

Tiny amounts (less than 0.3 mg) of the abused drugs were deposited on a wallet. "Unknown powder" was collected from the surface using double-sided tape on a microscope slide (Figure S3). Desorption and ionization was performed directly from the tape surface. The acquired spectra confirmed the significant influence of reduced pressure regulation (Figure 6). Although the surface for sample deposition was different (tape vs. silanized glass) detection of the abused drugs was significantly improved in this "real sample" analysis too. No interfering signals were observed for a double-sided tape blank (see Figure S2B,C).
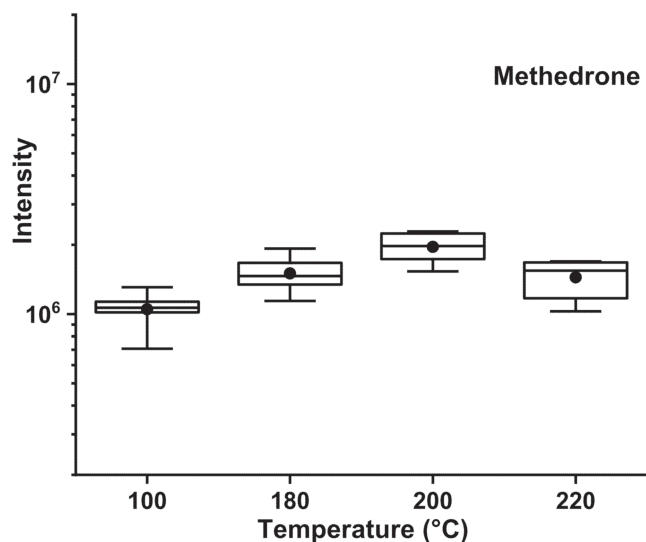

FIGURE 4 Influence of temperature of the heated capillary (46 mm) on the MH$^+$ ion signal intensity of methedrone ionized by desorption nanoelectrospray (nanoDESI). The pressure drop was set at 0.40 bar. Standard was deposited on a silanized microscope slide

FIGURE 5 Desorption nanoelectrospray (nanoDESI) mass spectra of new psychoactive substances without auxiliary pumping (pressure drop of 0.08 bar) and with auxiliary pumping (pressure drop of 0.40 bar). Both spectra are normalized to the highest ion signal intensity of 1.0×10^7. The temperature of the heated capillary was set at 200°C. Mixture of standards was deposited on a silanized microscope slide
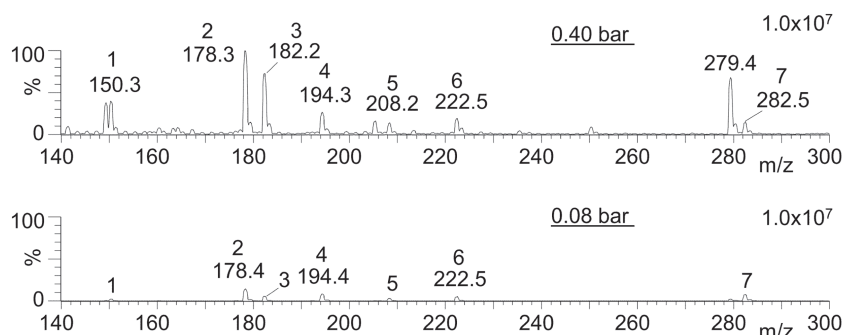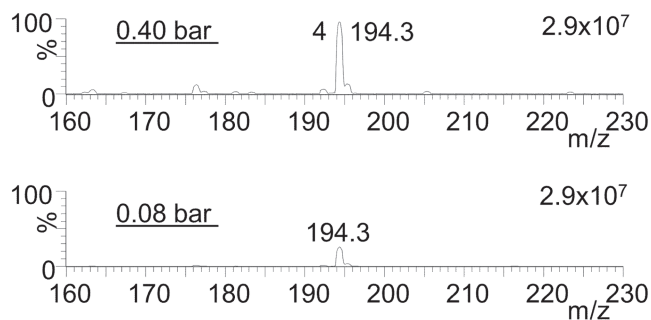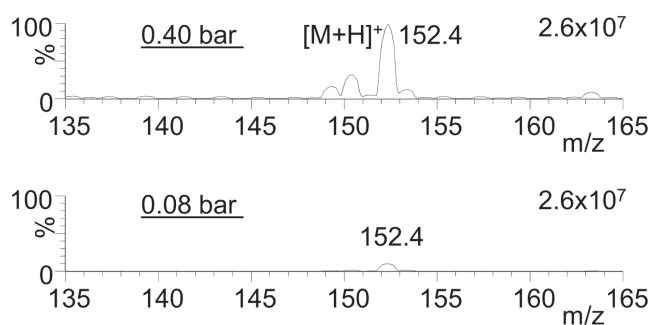
FIGURE 6 Desorption nanoelectrospray (nanoDESI) mass spectra of the trace amount of methedrone on double-sided tape recorded at a pressure drop of 0.08 and 0.40 bar, respectively. A solid sample was collected from the wallet. Both spectra are normalized to the highest ion signal intensity of 2.9×10^7. The temperature of the heated capillary was set at 200°C

FIGURE 7 Desorption nanoelectrospray (nanoDESI) mass spectra of paracetamol traces on double-sided tape recorded at a pressure drop of 0.08 and 0.40 bar, respectively. Both spectra are normalized to the highest ion signal intensity of 2.6×10^7. The temperature of the heated capillary was set at 200°C

Another possible application can be the analysis of pills. A paracetamol pill broken in two pieces was rubbed against double-sided tape on a microscope slide leaving traces of the drug that were directly analyzed (Figure S3). Significant signal intensity improvement was observed (Figure 7). The same results were obtained for the powdered paracetamol proving that different forms of samples can be collected and successfully analyzed. Evidently, the proposed approach can be applied to analyses of different analytes deposited by different ways on either silanized glass or double-sided tape or other surfaces that can be tested in the future.

4 | CONCLUSION

Because nanoDESI with its lateral resolution in tens of micrometers samples small surface area, only a tiny amount of analyte is desorbed and the sensitivity of measurement can be an issue. The yield of ions was significantly improved by properly regulated pressure reduction in the MS inlet. The pressure reduction drives the flow of gas (air) generated by suction to the inlet and, as a consequence, the drag force acting on charged droplets and ions in the source. Regulation of the pressure drop was recognized to have a crucial influence on signal intensity. Both pressure drop and temperature of the heated capillary were tuned to achieve maximum sensitivity. The tested custom-made inlet that permits setting of these experimental parameters supports the applicability of nanoDESI. One order of magnitude higher response was achieved for some of the analyzed new psychoactive substances, which may be critical in the analysis of traces of unknown samples. The new ion source development and described effects of studied experimental parameters can encourage applications of nanoDESI in general. Because various mass spectrometers are equipped with vacuum systems possessing different power, the effect of reduced pressure regulation can be different. Nevertheless, it was confirmed that pressure drop between the atmospheric and evacuated region of a mass spectrometer strongly influences the efficiency of nanoDESI. It should be considered if attaching this ion source to any mass spectrometer.

ORCID

Karel Lemr 🄳 https://orcid.org/0000-0003-3158-0637

REFERENCES

1. Ranc V, Havlíček V, Bednář P, Lemr K. Desorption electrospray: a modern tool for organic surface analysis. _Chem Listy_. 2007;101(6):524-529.
2. Roach PJ, Laskin J, Laskin A. Nanospray desorption electrospray ionization: an ambient method for liquid-extraction surface sampling in mass spectrometry. _Analyst_. 2010;135(9):2233-2236.
3. Ellis SR, Brown SH, In HPM, Blanksby SJ, Mitchell TW. Surface analysis of lipids by mass spectrometry: more than just imaging. _Prog Lipid Res_. 2013;52(4):329-353.
4. Takáts Z, Wiseman JM, Gologan B, Cooks RG. Mass spectrometry sampling under ambient conditions with desorption electrospray ionization. _Science_. 2004;306(5695):471-473.
5. Hartmanová L, Fryčák P, Soural M, Tureček F, Havlíček V, Lemr K. Ion internal energy, salt tolerance and a new technical improvement of desorption nanoelectrospray. _J Mass Spectrom_. 2014;49(8):750-754.
6. Ranc V, Havlíček V, Bednář P, Lemr K. Nano-desorption electrospray and kinetic method in chiral analysis of drugs in whole human blood samples. _Eur J Mass Spectrom_. 2008;14(6):411-417.
7. Hartmanová L, Ranc V, Papoušková B, Bednář P, Havlíček V, Lemr K. Fast profiling of anthocyanins in wine by desorption nano-electrospray ionization mass spectrometry. _J Chromatogr A_. 2010;1217(25):4223-4228.
8. Hartmanová L, Lorencová I, Volný M, et al. Lateral resolution of desorption nanoelectrospray: a nanospray tip without nebulizing gas as a source of primary charged droplets. _Analyst_. 2016;141(7):2150-2154.
9. Venter A, Sojka PE, Cooks RG. Droplet dynamics and ionization mechanisms in desorption electrospray ionization mass spectrometry. _Anal Chem_. 2006;78(24):8549-8555.
10. Costa AB, Cooks RG. Simulation of atmospheric transport and droplet–thin film collisions in desorption electrospray ionization. _Chem Commun_. 2007;(38):3915-3917.

11. Costa AB, Cooks RG. Simulated splashes: elucidating the mechanism of desorption electrospray ionization mass spectrometry. *Chem Phys Lett*. 2008;464(1):1-8.

12. Takáts Z, Wiseman JM, Cooks RG. Ambient mass spectrometry using desorption electrospray ionization (DESI): instrumentation, mechanisms and applications in forensics, chemistry, and biology. *J Mass Spectrom*. 2005;40(10):1261-1275.

13. Gao L, Li G, Cyriac J, Nie Z, Cooks RG. Imaging of surface charge and the mechanism of desorption electrospray ionization mass spectrometry. *J Phys Chem C*. 2010;114(12):5331-5337.

14. Cotte-Rodríguez I, Mulligan CC, Cooks RG. Non-proximate detection of small and large molecules by desorption electrospray ionization and desorption atmospheric pressure chemical ionization mass spectrometry: instrumentation and applications in forensics, chemistry, and biology. *Anal Chem*. 2007;79(18):7069-7077.

15. Cotte-Rodríguez I, Cooks RG. Non-proximate detection of explosives and chemical warfare agent simulants by desorption electrospray ionization mass spectrometry. *Chem Commun*. 2006;(28):2968-2970.

16. He J, Tang F, Luo Z, et al. Air flow assisted ionization for remote sampling of ambient mass spectrometry and its application. *Rapid Commun Mass Spectrom*. 2011;25(7):843-850.

17. Garimella S, Xu W, Huang G, Harper JD, Cooks RG, Ouyang Z. Gas-flow assisted ion transfer for mass spectrometry. *J Mass Spectrom*. 2012;47(2):201-207.

18. Luo Z, He J, Chen Y, et al. Air flow-assisted ionization imaging mass spectrometry method for easy whole-body molecular imaging under ambient conditions. *Anal Chem*. 2013;85(5):2977-2982.

19. Wang W, Bajic S, John B, Emerson DR. Numerical simulation of ion transport in a nano-electrospray ion source at atmospheric pressure. *J Am Soc Mass Spectrom*. 2018;29(3):600-612.

20. United Nations. *World Drug Report 2019*. Vienna: United Nations Publication; 2019.

SUPPORTING INFORMATION

Additional supporting information may be found online in the Supporting Information section at the end of this article.

Cyclic ion mobility of isomeric new psychoactive substances employing characteristic arrival time distribution profiles and adduct separation

SCHOLARONE™
Manuscripts

Cyclic ion mobility of isomeric new psychoactive substances employing characteristic arrival time distribution profiles and adduct separation

Marianna Nytka[1], Jiahao Wan[2], František Tureček[2], Karel Lemr[1,*]

[1]Department of Analytical Chemistry, Faculty of Science, Palacký University, 17. listopadu 12, 77146, Olomouc, Czech Republic

[2]Department of Chemistry, University of Washington, Seattle, 98195-1700, United States

[*]Corresponding author: karel.lemr@upol.cz

ABSTRACT: Analysis of new psychoactive substances (NPS), which is essential for toxicological and forensic reasons, can be made complicated by the presence of isomers. Ion mobility has been used as a standalone technique or coupled to mass spectrometry to detect and identify NPS. However, isomer separation has so far chiefly relied on chromatography. Here we report on the determination of isomeric ratios using cyclic ion mobility-mass spectrometry without any chromatographic separation. Isomers were distinguished by mobility separation of lithium adducts. Alternatively, we used arrival time distribution (ATD) profiles that were characteristic of individual isomers and were acquired for protonated molecules or fragment ions. Both approaches provided comparable results. Calculations were used to determine the structures and collision cross sections of both protonated and lithiated isomers that accurately characterized their ion mobility properties. The applicability of ATD profiles to isomer differentiation was demonstrated using direct infusion and flow injection analysis with electrospray of solutions, as well as desorption electrospray of solid samples. Data processing was performed by applying multiple linear regression to the ATD profiles. Using the proposed ATD profile-based approach, the relationships between the determined and given content of isomers showed good linearity with coefficients of determination typically greater than 0.99. Flow injection analysis using an autosampler allowed us to rapidly determine isomeric ratios in a sample containing two isomeric pairs with a minor isomer of 10% (determined 9.3% of 3-MMC and 11.0% of 3-FMC in a mixture with buphedrone and 4-FMC). The proposed approach is not only useful for NPS, but may be applicable to small isomeric molecules analyzed by ion mobility when complete separation of isomers is not achieved.

INTRODUCTION

New psychoactive substances (NPS) are a growing group of abused drugs. According to 2022 data, more than 1180 NPS have been identified in the last 15 years.[1] Various analytical methods have been employed in NPS analysis, e.g., color and microcrystalline tests, infrared and Raman spectroscopy, nuclear magnetic resonance, mass spectrometry (MS), capillary electrophoresis, chromatography, and others have served to find synthetic cathinones in seized materials.[2] NPS in biological fluids (blood, urine, oral fluid, etc.)[3, 4] and in hair[5, 6] have been analyzed by gas chromatography (GC-MS) and liquid chromatography (LC-MS) with various sample pretreatments. Both techniques are essential for the toxicological screening and confirmation of abused drugs[7]. LC-MS has allowed the monitoring of NPS in pooled urine and urban wastewater (wastewater-based epidemiological studies).[8, 9] The large number of NPS, including many isomers, makes non-target detection challenging. High resolution mass spectrometry is an important tool for solving this analytical task.[9, 10] Mass spectrometry has contributed to the

identification of NPS in consumption products, the study of their metabolism and pharmacokinetics, and the analysis of authentic human samples.[9, 11] In addition to the commonly used MS in NPS' chromatography, gas chromatography-infrared detection[12] and gas chromatography-VUV spectroscopy[13] have been successfully tested. Ambient ionization mass spectrometry has attracted attention, allowing the direct analysis of NPS.[14] Supercritical fluid chromatography (SFC) is a promising alternative to gas and liquid chromatography. A fast chromatographic run (1.6 min) was sufficient to analyze a mixture of 15 NPS and separate isomers.[15] For the detection and quantification of NPS in urine samples, the SFC-MS method was competitive with LC-MS.[16]

As a standalone technique, ion mobility spectrometry (IMS) has been employed to monitor NPS using reduced mobility values.[17-20] Reduced mobility values were also combined with ambient and direct infusion mass spectrometry data to improve NPS confirmation and identification. Rapid screening of 35 NPS was performed by IMS with a [63]Ni ion source and DART-QTOF (direct analysis in real time-

quadrupole-time of flight).[21] Similarly, the screening by [63]Ni-IMS was followed by ESI-QTOF to confirm NPS in 24 seized samples.[22] Drift tube ion mobility spectrometry expanded the detection tools for GC. Retention and drift time values were used for identification. Nine NPS representatives were quantified in oral fluid.[23]

The coupling of ion mobility-mass spectrometry (IM-MS) is a powerful analytical tool, but its application to the analysis of NPS has been limited so far. Compared to [63]Ni-IMS, ESI-IM-MS with a drift tube provided better detection of some cathinones due to their improved ionization. Mass spectrometric data supported identification that was not limited only to the use of drift times. However, the mobility separation of isomers has been a problem for both compared techniques. For example, ESI-IM-MS gave one mobility peak for a mixture of mephedrone (4-MMC), buphedrone, and ethcathinone that remained unresolved.[24] ESI-drift tube IM-MS was used to detect and identify four cathinones and five tryptamines in less than 1 min.[25] Atmospheric pressure chemical ionization drift tube IM-MS achieved lower detection limits than ESI for three cathinones and three synthetic cannabinoids.[26] However, isomeric compounds were not included in these two studies. LC-MS and LC-IM-MS were used to identify the metabolites of two synthetic cannabinoids after their incubation with rat and pooled human hepatocytes. The isomeric metabolites were chromatographically separated and showed different CCS values, but ion mobility separation of isomers was not reported.[27] An LC-IM-MS method has been implemented in clinical routine for the analysis of 71 abused drugs, including NPS, in oral fluids. CCS values supported the identification, but IMS also increased the fragmentation of labile analytes.[28] Ion mobility was integrated into an LC-IM-MS method applicable to the detection and quantification of fentanyl analogs in human urine. Ion mobility separation of metal cation adducts combined with data post-processing by high-resolution demultiplexing was essential for isomer separation. Cations tested included, e.g., alkali and transition metals. No single cation was optimal for all groups of isomers. The use of several metal cations collectively was suggested to separate various isomers sufficiently.[29] Rapid identification of isomeric cathinones differing in ring substitution was performed using ESI-trapped ion mobility-mass spectrometry. The mobilograms of all cathinones revealed the presence of two protomers (O- and N-protonated) whose mobility values allowed the detection of isomers. However, isomeric mixtures were not analyzed.[30] The authors of neither this work nor above cited works have used arrival time distribution (ATD) profiles that might be characteristic of isomers, as we demonstrated earlier for isomeric hyaluronan-derived oligosaccharides.[31, 32]

In the present work, we aimed to investigate cyclic traveling wave ion mobility (cyclic TWIM) of NPS isomers using three isomeric pairs (3-methylmethcathinone and buphedrone; 3-fluoromethcathinone and 4-fluoromethcathinone; 1,3-benzodioxolylbutanamine and methedrone, Figure 1). We evaluated the determination of isomeric ratios in mixtures employing characteristic ATD profiles in comparison with ion mobility separation of sodiated and lithiated molecules. For the analysis of isomeric mixtures, both the use of ATD profiles and the separation of Li^{+} adducts are suitable approaches. We demonstrated that ATD profiles are characteristic of small molecule isomers and

confirmed this observation for both electrospray and desorption electrospray. We simplified the data processing by applying multiple linear regression instead of the previously used fitting.[32] Our results may encourage the wider use of IM-MS in NPS analysis and ATD profiles in the ion mobility of isomers.

EXPERIMENTAL SECTION

Materials and Sample Preparation. Standards of hydrochlorides of 3-methylmethcathinone (3-MMC), 3-fluoromethcathinone (3-FMC), and buphedrone, 4-fluoromethcathinone (4-FMC), 1,3-benzodioxolylbutanamine (BDB), methedrone (see Figure 1 for structures) were purchased from Cayman Pharma (Neratovice, Czech Republic) and Lipomed AG (Arlesheim, Switzerland), respectively. LC-MS grade methanol and water were bought from Fisher Chemical (Fisher Scientific, United Kingdom). Sodium nitrate (p.a.) was provided by Penta (Ing. P.Švec, Czech Republic) and propan-2-ol (LC-MS grade), lithium chloride (≥99.0%, BioXtra), sodium hydroxide (p.a.), formic acid (≥ 98%), N-ethylaniline, acetaminophen, caffeine, sulfaguanidine, and alprenolol by Sigma Aldrich (Prague, Czech Republic).

Stock and working solutions of individual analytes were prepared at the concentrations 1 mg/mL and 100 ng/mL, respectively, in methanol/water (50/50, v/v). Three mixtures of isomers with a total concentration of 100 ng/mL (methanol/water, 50/50, v/v) were used: a) 3-MMC and buphedrone (m/z 178.13); b) 3-FMC and 4-FMC (m/z 182.10); c) BDB and methedrone (m/z 194.13). Isomers were mixed in the ratios: 5 : 95, 10 : 90, 25 : 75, 40 : 60, 50 : 50, 60 : 40, 75 : 25, 90 : 10, 95 : 5. The formation of sodium and lithium adducts was supported by the use of 0.1 mmol/L lithium chloride or sodium nitrate in analyzed mixtures.

Cyclic Ion Mobility-Mass Spectrometry. The experiments were performed on a SELECT SERIES Cyclic IMS Q-TOF[33] (Waters Corp., Wilmslow, UK) equipped with electrospray (ESI) and desorption electrospray (2D-DESI, Prosolia, with a DESI XS sprayer; Waters Corp.) in a positive mode. 0.5 mM sodium formate in propan-2-ol/water (90/10, v/v) was used for the mass calibration (m/z 50-1200). The instrumental parameters were set as follows: 1) default setting - capillary voltage 2 kV, cone voltage 10 V, source temperature 100 °C, desolvation temperature 250 °C, cone gas flow 30 L/h, desolvation gas flow 600 L/h, trap CE 6 V, transfer CE 4 V, stepwave body gradient 20 V, ion guide TW pulse height 0.4 V, trap TW pulse height 4 V, trap entrance 2 V, trap bias 2 V, trap DC -4 V, post trap gradient 3 V, post trap bias 35 V, stepwave RF 200 V, ion guide RF 300 V, driftcell RF 300 V, transfer RF 200 V, helium flow rate 120 mL/min, nitrogen flow rate 40 mL/ min., nitrogen pressure in mobility cell 1.73 mbar; 2) setting for labile compounds (used for BDB and methedrone) - capillary voltage 1 kV, cone voltage 10V, source temperature 100 °C, desolvation temperature 250 °C, cone gas flow 30 L/h, desolvation gas flow 600 L/h, trap CE 2 V, transfer CE 1 V, stepwave body gradient 10 V, ion guide TW pulse height 0.2 V, trap TW pulse height 1 V, trap entrance 1 V, trap bias 1.5 V, trap DC -4 V, post trap gradient 1.5 V, post trap bias 16 V, stepwave RF 100 V, ion guide RF 300 V, driftcell RF 200 V, transfer RF 200 V, transfer RF gain 5 V, TW static height 13 V, wave height 10 V (eject and acquire). Cyclic TWIMS parameters for

ion mobility separation are summarized in the Supporting Information (Table S1 and S2). The precursor ions were isolated in a quadrupole and fragmented in the trap cell with CE 28 V for BDB and methedrone (*m/z* 194.13).

Three sample introduction options were used. Analyzed solutions were directly infused into a normal flow ESI source at a flow rate of 5 µL/min. Flow injection analysis (FIA) was performed on a Waters ACQUITY UPLC I-Class system coupled to an ESI source of SELECT SERIES Cyclic IMS Q-TOF (Waters Corp., Wilmslow, UK) via PEEK tubing (1/16"x0.13 mm). Sample solutions were injected into carrying liquid (methanol/water, 50/50, v/v, 0.1 mL/min). Injection volumes were 5 µL and 10 µL for 3-MMC, buphedrone, 3-FMC, 4-FMC and BDB, methedrone, respectively. For desorption electrospray, samples were deposited onto the Omni Slide Hydrophobic Arrays at 3.5 ng/mm^2 (Prosolia, Waters Corp., Wilmslow, UK). Methanol/water (80/20, v/v) was used as the spray liquid at a flow rate of 2.0 µL/min. The capillary voltage was maintained at 0.75 kV, nebulizing gas pressure 11 psi, source temperature 150 °C, cone voltage 10 V. The DESI geometry was as follows: spray impact angle ~75°, spray nozzle - inlet tube orifice ~4 mm, inlet tube orifice - sample surface ~0.5 mm, spray nozzle – sample surface ~2 mm**.**

Data were acquired, processed and evaluated using Masslynx v.4.2 (Software Change Note 1016, Waters Corp., Wilmslow, UK), a modified version of Driftscope v.2.9 (Waters Corp.), and statistics software OriginPro 2020 (OriginLab, Northampton, USA). Raw arrival times included injection time (ions were transferred into the cyclic mobility cell), drift time (ions were in the cell), and dead time (ions traveled from the cell to the TOF). ATD for specific *m/z* were extracted and smoothed by mean function averaging of 2 points in 1 cycle using MassLynx and exported to the OriginPro. The Composite Spectrum Regression (an application in OriginPro) was used to perform multiple linear regression of ATD profiles. The isomeric ratio was $a_1 : a_2$, where $y = a_0 + a_1x_1 + a_2x_2$. The intensities over the whole range of the ATD profiles of the pure isomers (1 and 2) were used as the input data x_1 and x_2 (independent variables). These profiles were generated as the average of six data acquisitions. The intensities over the entire ATD profile of the isomeric mixture (all six data acquisitions individually) were used as y (dependent variable).

Six data acquisitions were performed for each isomer and each mixture to obtain the relationships between the given and determined isomeric ratios. Model samples containing four analytes and corresponding calibration curve points were analyzed in six replicates by FIA. Outliers in the data, if found, were excluded. Ion structures, charge densities, and relative energies (Figure S1 and S2, Table S4, S5, S6-S13, Supporting Information) were obtained for several tautomers and their conformers by a combination of Born-Oppenheimer molecular dynamics and density functional theory calculations. The structures and charge densities were used to calculate theoretical CCS, as described in the Supporting Information. Experimental values of CCS (Table S14, Supporting Information) were determined using a calibration mixture of N-ethylaniline, acetaminophen, caffeine, sulfaguanidine, and alprenolol according to the procedures described by Bush et al.,[34, 35] and McCullagh et al.[36] Details are provided in the Supporting Information (CCS calibration, Table S3).

RESULTS AND DISCUSSION

Electrospray Mass Spectra. The new psychoactive substances investigated in this study (Figure 1) were easily protonated by electrospray, but isomeric ions [M+H]$^+$ were not well separated by ion mobility, even in multi-pass experiments at higher resolving power. Nevertheless, the arrival time distribution (ATD) profiles were characteristic of the individual isomers (see, e.g., Figure 2). This is in good agreement with our previous observations using the linear and cyclic mobility cell for isomeric oligosaccharides[32] and oligonucleotides,[37] respectively. Due to the low intensity of the sodium adducts (Figure S3, Supporting Information), Na$^+$ and Li$^+$ salts were alternatively added to the analyzed solutions to support adduct formation and to allow their ion mobility analysis.

Isomer Analysis Using Characteristic Arrival Time Distribution vs. Ion Mobility Separation of Lithium Adducts. The first two isomeric pairs were analyzed using direct infusion of solutions into the electrospray. For 3-MMC and buphedrone ([M+H]$^+$, *m/z* 178.13), single pass experiment (the path length L = 98 cm) was insufficient to separate their mixture (Figure 2A). This was consistent with the expected CCS for the keto and enol isomers of protonated 3-MMC (ions **1a$^+$** and **1b$^+$**) and buphedrone (ions **2a$^+$** and **2b$^+$**) that were in the narrow range of 139-141 Å^2 (Figure S1, Supporting Information). The narrow range was also observed for experimental CCS values (Table S14), when the percent difference in collision cross sections determined for isomers by the single pass experiment was 2%. It was estimated that the CCS-based resolving power R_{CCS} of about 104 was required to achieve the two-peak resolution Rp-p = 1.23 (ca. 90% separation, defined for two Gaussian peaks of equal abundance).[38] For buphedrone, the single pass experiment gave $R_{1,CCS} \approx 45$ (both keto- and enol-form contributed to peak width). The resolving power increases with the path length (L) and thus with the number of passes (n) $R_{n,CCS} = R_{1,CCS} \times L^{1/2} = R_{1,CCS} \times n^{1/2}$.[33] Six passes through the cyclic mobility cell should yield $R_{6,CCS} \approx 110$. After the multi-pass experiment with seven passes (L = 686 cm), we were able to separate the major isomeric forms of 3-MMC and buphedrone (experimental $R_{7,CCS} \approx 126$).The signals of both isomers were clearly detected in the mobilograms of their mixtures (Figure 2B). While it can be sufficient for the detection of individual isomers, simple integration of mobility peaks was not possible neither at higher resolving power, as the isomers' ATD profiles became broader and the less abundant enol isomer of 3-MMC still significantly overlapped with buphedrone (Figure 2B). Because ATD profiles are related to extracted ion mobilograms for m/z 178.13, they reflect the migration of protonated molecules and do not include the signal of fragments such as the [MH–H$_2$O]$^+$ ions. Similarly ion mobility peaks of protonated molecules of isomers interfered, e.g., for cathinones and peptides separated by trapped ion mobility[30] and cyclic TWIMS[39], respectively. Broadening of ion mobility signals and more complex ATD profiles of individual isomers at higher resolving power can compromise isomer separation. It can represent a more general issue in ion mobility separation of isomers existing in different conformers or protonation isomers. Such broadening can be suppressed by separating adducts of isomeric molecules with, for example, alkali metal cations. Separation of adducts has been described, e.g., for fentanyl,[29] glycan,[40] and flavonoid[41] isomers. On the contrary,

the broadening can be advantageous if it provides ATD profiles characteristic of individual isomers.
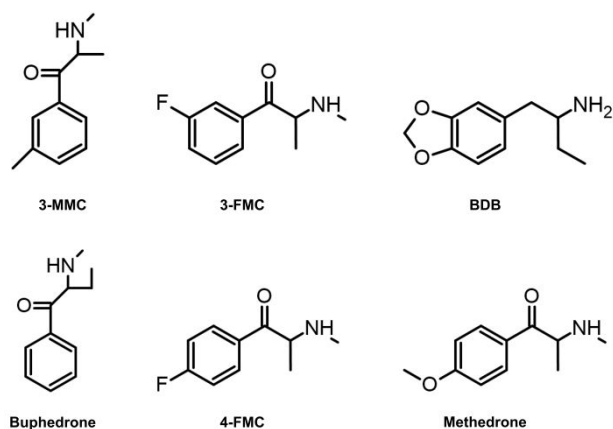

Figure 1. Investigated isomeric pairs: 3-methylmethcathinone (3-MMC) – buphedrone; 3-fluoromethcathinone (3-FMC) – 4-fluoromethcathinone (flephedrone, 4-FMC); 1,3-benzodioxolylbutanamine (BDB) – methedrone.

Since the ATD profiles of protonated 3-MMC and buphedrone differed significantly in the 7 pass experiment (Figure 2B), we performed multiple linear regression (MLR) to determine the isomeric ratio. Compared to our previous fitting procedure using Gaussian functions,[32] the new data processing was easier to implement because MLR is the common part of routinely used software, such as OriginPro.

The relationship between the determined and given content of 3-MMC showed good linearity (Figure 3A), proving the applicability of the proposed procedure using characteristic ATD profiles and MLR in the determination of the isomeric ratio. It is worth noting that even single pass experiment provided the linear relationship but in a limited range (5% to 75% of 3-MMC, Figure S4), since buphedrone was not sufficiently detected at the excess of 3-MMC (3-MMC : buphedrone 95 : 5 and 90 : 10). It is worth noting that we observed good intra-day repeatability of the ATD profiles of the isomers. When necessary, the shift in drift time was compensated by the peak alignment. Inter-day measurements occasionally showed a shift in the drift time and/or in the relative intensities, resulting in a change in the shape of the ATD profiles (Figure S5). It might be due to the variation of experimental parameters such as drift or collision gas pressure for the same instrumental setting. If this is the case, we recommend to acquire a complete data set during one day after the instrument has stabilized for two hours after switching from standby to run mode.
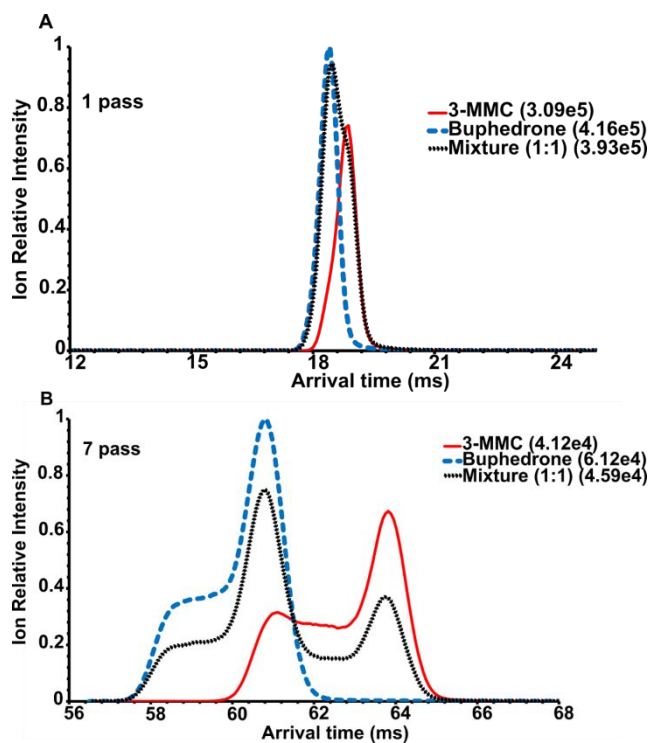

Figure 2. Extracted ATD profiles ([M+H]$^+$, m/z 178.13) of 3-MMC, buphedrone and their mixture (50 : 50): A) 1 pass, B) 7 pass experiment. The highest absolute intensity for each mobilogram is given in brackets.
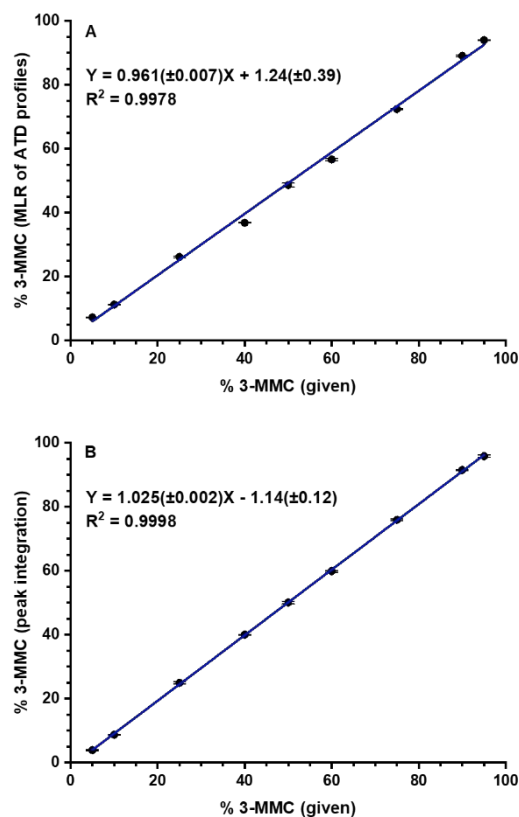

Figure 3. Determination of 3-MMC in the mixture with buphedrone: A) Multiple linear regression (MLR) applied to ATD profiles of protonated molecules, seven pass separation; B) Ion

mobility of lithiated molecules, ten pass separation. Standard deviations of slope and intercept are shown in brackets. Each point was measured in six data acquisitions.

For comparison, we separated sodiated and lithiated molecules in ten passes (compare Figures 4 and S6). Note that the signal intensities of the $[M+Li]^+$ ions were more than one order higher than those of $[M+Na]^+$. Therefore, $[M+Li]^+$ ions were selected for isomeric ratio determination. Sufficient separation (Figure 4) allowed direct integration of the mobility peaks. The measured and given 3-MMC contents showed excellent linearity (Figure 3B). Cationization by these alkali metals affected the formation of ion isomers in the gas phase in that no complex peaks were observed (cf. Figures 2 and 4). This observation was consistent with the calculations of structures and CCS (Figures S1 and S2, Tables S4 and S5, Supporting Information). The differences in CCS for keto (ions $1a^+$ and $2a^+$) and enol (ions $1b^+$ and $2b^+$) isomers of protonated molecules of 3-MMC and buphedrone were 0.4% and 0.6%, respectively. For both 1^+ and 2^+, the enol isomers had higher Gibbs energies than the keto forms (Table S4, Supporting Information) and thus could contribute as only minor components to the signal at m/z 178.13 in mobilograms, as manifested by peaks broadening (Figure 2B). For lithiated isomers (Figure S2, Supporting Information), the keto forms (ions $3a^+$ and $4a^+$) differed by 1.5% in CCS (experimental CCS (Table S14) differed by 1.8% and 1.9% for 1 and 10 passes, respectively). Such a small difference highlighted the significance of multi-pass separation to achieve sufficient resolving power (in analogy to the protonated molecules discussed above). Enol isomers of the lithium ion adducts (ions $3b^+$ and $4b^+$) showed much higher energies than the keto-tautomers (Table S5, Supporting Information), and were unlikely to significantly contribute to the signal at m/z 184.13 in mobilograms. The CCS difference and isomer consistency was reflected by the well separated and symmetrical peaks of Li^+ ion adducts in the ten pass mobilogram (Figure 4). The trends in Figure 3A and B are comparable, although Li^+ adducts' separation gave lower standard deviations of intercept and slope and slightly higher coefficient of determination than multiple linear regression using ATD profiles of protonated molecules. Both approaches represent a useful and comparable alternative to analyzing isomeric mixtures.
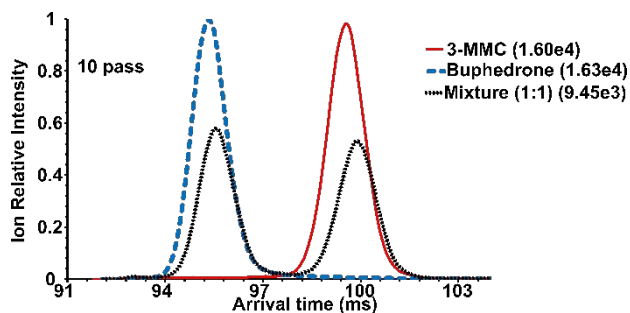

Figure 4. Extracted ATD profiles ($[M+Li]^+$, m/z 184.13) of 3-MMC, buphedrone and their mixture (50 : 50), ten pass experiment. The highest absolute intensity for each mobilogram is given in brackets.

3-FMC and 4-FMC showed symmetrical and highly overlapping ATD profiles of protonated molecules in single pass separation (Figure 5A), which did not allow us to determine the isomeric ratio even after applying multiple

linear regression. In this case, higher resolving power was required, highlighting the advantage of cyclic over linear TWIMS. Ten pass separation provided characteristic ATD profiles of protonated molecules of individual isomers (Figure 5B) and the linear relationship between the determined and given content of 3-FMC in a mixture (Figure 6A). Sodium did not effectively form adducts with FMC isomers (Figure S7A). Lithiated molecules were generated with sufficient intensity and partially resolved in 25 passes (Figure S7B), allowing peak integration. Both approaches, MLR of ATD profiles of protonated molecules and the integration of peaks of Li^+ adducts, were applicable. The relationship between the determined and given content of 3-FMC showed comparable standard deviations of slope and intercept and coefficients of determination (Figures 6A and 6B). Separation of adducts may be more straightforward, but MLR of ATD profiles gave similar results and may be more advantageous when adducts formation or separation is insufficient, as in the case of sodium adducts here.
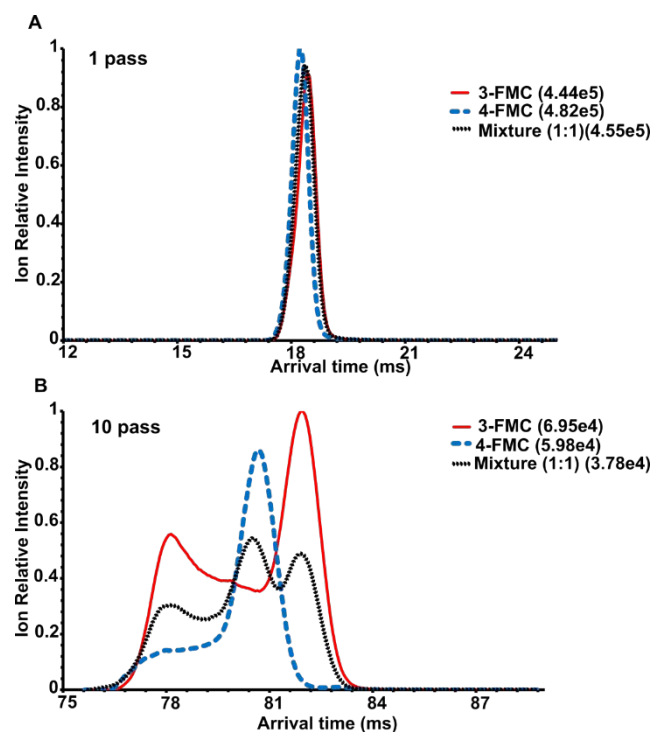

Figure 5. Extracted ATD profiles ($[M+H]^+$, m/z 182.10) of 3-FMC, 4-FMC, and their mixture (50 : 50): A) 1 pass, B) 10 pass experiment. The highest absolute intensity for each mobilogram is given in brackets.
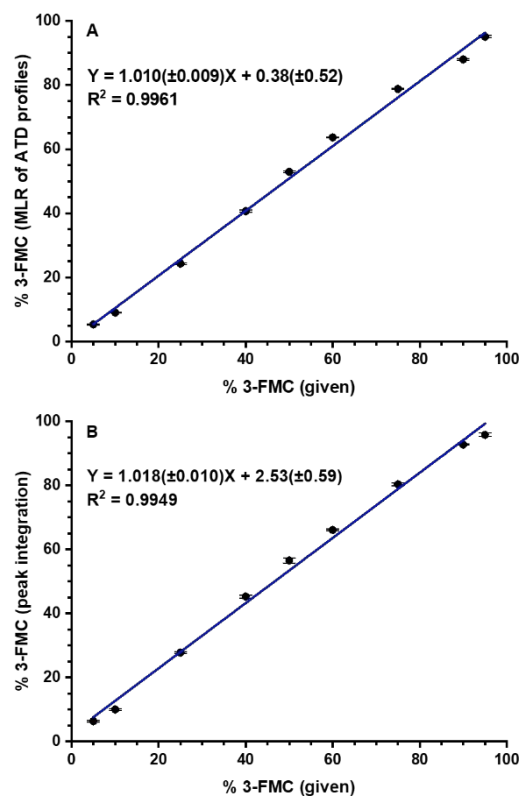
Figure 6. Determination of 3-FMC in the mixture with 4-FMC: A) Multiple linear regression (MLR) applied to ATD profiles of protonated molecules, ten pass separation; B) Ion mobility of lithiated molecules, 25 pass separation. Standard deviations of slope and intercept are shown in brackets. Each point was measured in six data acquisitions.

Flow Injection Analysis of Isomers Using Characteristic ATD Profiles of Fragment Ions. The third pair of isomers showed significant differences in the intensities of the $[M+H]^+$ ions. In the case of BDB, this ion was found to fragment easily. While methedrone is a synthetic cathinone, BDB belongs to the phenylethylamines. The ATD profiles of both BDB and methedrone were symmetrical and completely overlapped (Figure S8). The signal intensities at the maxima of the mobility peaks differed by more than two orders of magnitude (Figure S8A, B), favoring methedrone when we used the same ion source setting (default) as for the previous isomeric pairs. Tuning the ion source and ion optics for BDB increased its signal intensity but decreased the signal intensity of methedrone. The use of three passes instead of one did not sufficiently improve separation and caused a significant decrease in BDB signal intensities (Figure S8C, D). Due to unresolved symmetrical peaks with very different intensities, the use of ATD profiles of protonated molecules for isomer analysis was not possible. We proposed an alternative approach using ATD profiles of fragment ions. Both isomers fragmented to produce ions at m/z 135.04, methedrone also at m/z 135.08 (Figure S9). We activated and fragmented precursor ions $[M+H]^+$ in the trap section (in front of the ion mobility cell) and included both fragment ions (m/z 135.04 and 135.08) in extracted ion mobilograms (Figure 7). ATD profiles were characteristic of individual isomers and partially separated. The experiments were performed using

flow injection analysis as an alternative to direct infusion, allowing for automated injections and faster data acquisition. The coefficient of determination was lower and the standard deviations at the data points were higher (Figure 8) compared to the analyses described above (Figures 3 and 6). This may be due to the more complex experiments requiring the generation and separation of fragment ions. Differentiation of isomers and even analysis of isomeric mixtures was still possible, although accuracy may be limited when one isomer is present in excess. While 5% and 10% BDB mixtures were distinguishable, the isomeric ratios determined at 90% and 95% BDB were not significantly different.
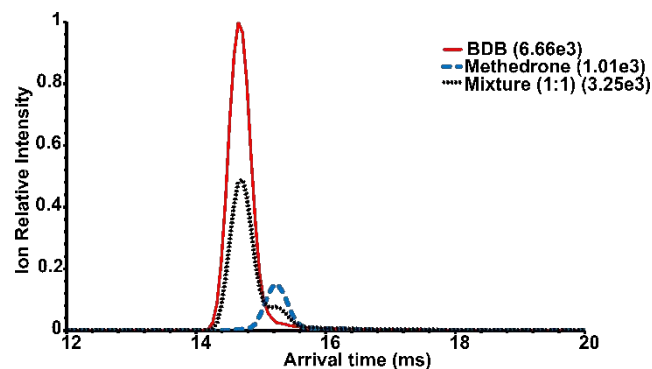

Figure 7. Extracted ATD profiles of fragment ions (m/z 135.04-135.08) of BDB, methedrone, and their mixture (50 : 50) in single pass separation. The highest absolute intensity for each mobilogram is given in brackets.
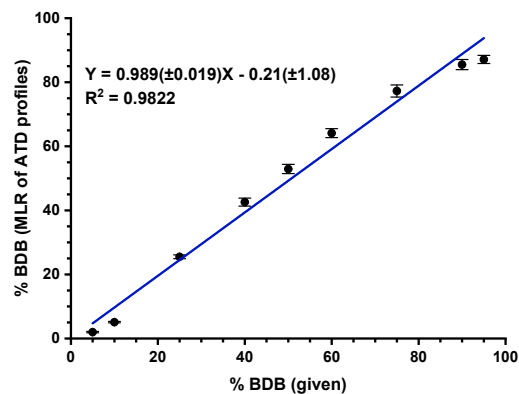

Figure 8. Determination of BDB in the mixture with methedrone. Multiple linear regression (MLR) applied to ATD profiles of fragment ions (m/z 135.04-135.08), single pass separation. Standard deviations of slope and intercept are shown in brackets. Each point was measured in six data acquisitions.

Desorption Electrospray Ionization Generating Characteristic ATD Profiles. In analogy to the experiments described above, all three isomeric pairs ionized by DESI provided ATD profiles characteristic of isomers but with lower intensities (Figure 9). The shapes of the ATD profiles of individual isomers were similar for ESI and DESI (compare Figures 9A-C and 2B, 5B, 7). However, DESI provided different relative ionization yields for some isomers. This resulted in different shapes of ATD profiles of isomeric mixtures when comparing ESI and DESI experiments. While

the shape was very similar for the 3-FMC/4-FMC mixture (Figure 9B, 5B), it was significantly different for the 3-MMC/buphedrone mixture (Figure 9A, 2A). In general, it is not possible to use ATD profiles of individual isomers obtained with one type of ion source to evaluate samples measured with another type of ion source. This is a direct consequence of the different mechanisms of ionization. DESI desorbed and ionized analytes from solid samples deposited on a target in a non-uniform layer (pipetting of solutions and drying on air), which explains the described differences and higher data variability (see error bars in Figure 10) in contrast to ESI. Evaluating data for three studied isomeric pairs, lower accuracy was found for 3-MMC/buphedrone (lower coefficient of determination, higher variability of intercept and slope, Figure 10). Nevertheless, the trend showing the increasing 3-MMC content in a mixture was clearly visible (Figure 10A). Coefficients of determination were higher than 0.99 for other two pairs (Figure 10B, C). DESI extended the applicability of our ATD profile-based approach to the analysis of solid samples.
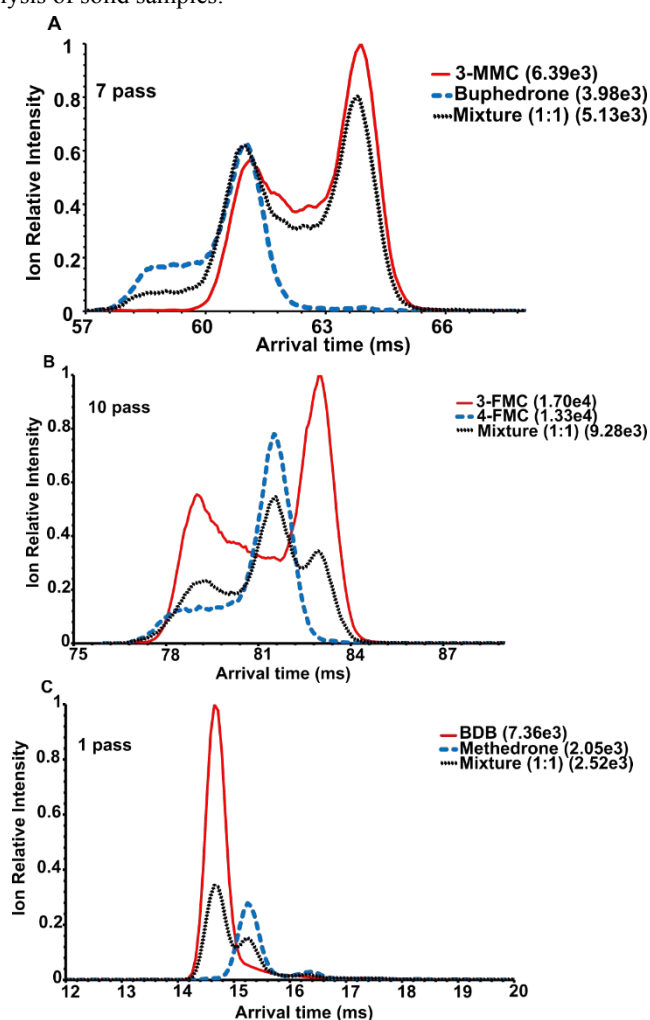

Figure 9. Extracted ATD profiles of individual isomers and their mixtures (50 : 50) desorbed and ionized by DESI: A) 3-MMC and buphedrone ([M+H]+ , m/z 178.13), 7 passes; B) 3-FMC and 4-FMC ([M+H]$^+$, *m/z* 182.10), 10 passes; C) fragment ions (m/z 135.04-135.08) of BDB, methedrone, 1 pass. The highest absolute intensity for each mobilogram is given in brackets.
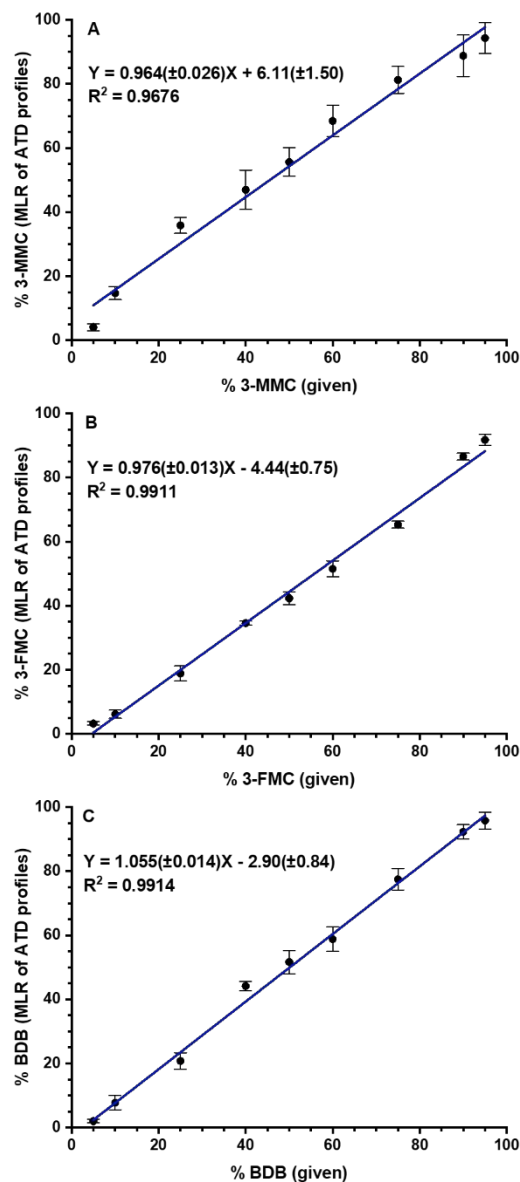

Figure 10. Determination of isomeric ratios using DESI and multiple linear regression (MLR) applied to ATD profiles: A) 3-MMC in the mixture with buphedrone, ([M+H]$^+$, m/z 178.13, 7 passes); B) 3-FMC in the mixture with 4-FMC ([M+H]$^+$, *m/z* 182.10, 10 passes); C) BDB in the mixture with methedrone (fragment ions at m/z 135.04-135.08, 1 pass). Standard deviations of slope and intercept are shown in brackets. Each point was measured in six data acquisitions.

Rapid Determination of Isomeric Ratios in Drugs of Abuse Mixtures. To demonstrate the applicability of ATD profiles in isomeric mixture analysis, we performed a flow injection analysis of four drugs of abuse (two isomeric pairs) in a mixture. Data acquisition for both calibration curves and a sample of abused drugs took less than 3 hours for 96 injections (six replicates of each data point) using an autosampler. Calibration curves were constructed in the minor isomer range of 5% to 45%. With coefficients of determination of 0.9974 and 0.9988, respectively, they showed good linearity and low standard deviations of slopes and intercepts (Figure 11). In a model sample containing both isomeric pairs with 10% of the minor isomer, the contents were found to be 9.3% of 3-MMC

7

(standard deviation 0.37) and 11.0% of 3-FMC (0.42) in the mixture with buphedrone and 4-FMC, respectively. The results have demonstrated the suitability of the proposed method for the determination of isomeric ratios with sufficient accuracy and analytical run time of 1.5 min.
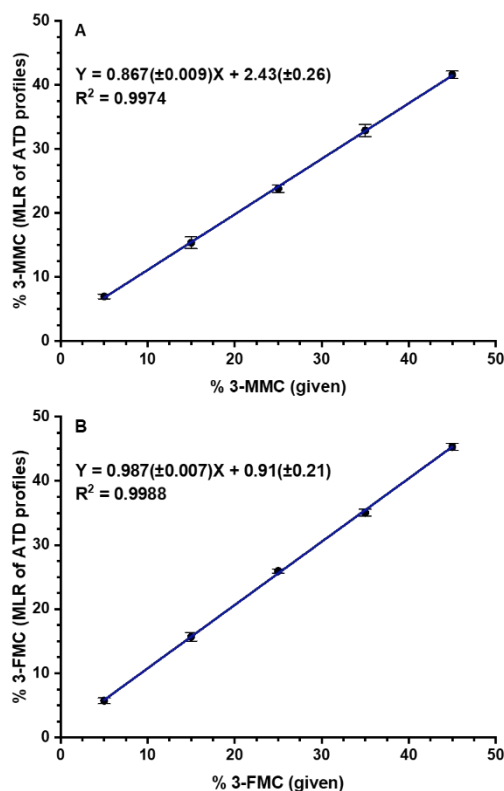

Figure 11. Calibration curves for FIA of two isomeric pairs mixture: A) 3-MMC in the mixture with buphedrone, seven pass separation; B) 3-FMC in the mixture with 4-FMC, ten pass separation. Multiple linear regression (MLR) was applied to ATD profiles of protonated molecules. Standard deviations of slope and intercept are shown in brackets. Each point was measured in six replicates.

CONCLUSIONS

Distinction and quantification of NPS isomers was achieved by two approaches, one relying on the separation of lithium adducts, and the other on multiple linear regression using ATD profiles characteristic of individual isomers and ATD profiles obtained for isomeric mixtures. Direct infusion experiments confirmed both approaches to be comparable. The formation of adducts by electrospray ionization required the addition of Li^+ salt to the sample solution. The higher resolving power of cyclic TWIMS in multi-pass experiments improved the separation of Li^+ ion adducts, whereas the mobility peaks of protonated molecules were broadened and still overlapped due to the presence of tautomers associated with individual ion structures. Similar behavior was observed, e.g., for peptides[39] and oligonucleotides.[37] Previously, ATD profiles were fitted by Gaussian functions and a single ATD function was generated for each isomer. These ATD functions allowed isomeric ratios of oligosaccharides to be determined by ESI-linear TWIMS.[32] Here, the fitting was replaced by multiple linear regression which simplified the analysis.

The isomeric pair of BDB/methedrone showed significant differences in the intensities of $[M+H]^+$ ions and completely overlapping mobility peaks. In this case, the ATD profiles of the fragment ions allowed us to achieve a successful analysis, proving that the proposed approach is not limited to protonated molecules. The analysis was performed by FIA as an alternative to direct infusion. Desorption electrospray was used to analyze solid samples. ATD profiles characteristic of isomers were also observed, although they differed to some extent from those obtained by electrospray. This could be attributed to the different ionization mechanisms, electrospraying of solutions vs. desorption and ionization from solid samples. Finally, the rapid analysis of a mixture containing two isomeric pairs was demonstrated. FIA combined with an autosampler enabled automatic data acquisition which speeded up the analysis.

While the mean mobility values were recently used to identify cathinones while isomeric ratios have not been determined,[30] we confirmed adequate repeatability of the ATD profiles, and included the entire ATD profiles analyzing isomeric mixtures. Although the higher resolving power of cyclic TWIMS may not allow for the complete separation of isomers, it may help to generate more distinct ATD profiles of isomers.

The ATD profile-based approach can also be used to analyze the other groups of isomeric molecules by ion mobility. While the integration of peeks requires a good separation, the described approach is applicable even for overlapping signals.

ASSOCIATED CONTENT

Supporting Information
The Supporting Information is available free of charge on the ACS Publications website.
Instrumental settings of cyclic TWIMS, CCS calibration, M06-2X/6-31+G(d,p) optimized structures of 3-MMC and buphedrone ions with calculated CCS in nitrogen, Relative Gibbs energies of protonated and lithiated molecules of 3-MMC and buphedrone, Experimental CCS of 3-MMC and buphedrone, +ESI-mass spectra of analytes, Determination of 3-MMC in the mixture with buphedrone (single pass separation), Extracted ATD profiles on two different days, Extracted ATD profiles ($[M+Na]^+$) of 3-MMC, buphedrone and their mixture (50:50), Extracted ATD profiles of 3-FMC, 4-FMC, and their mixture (50 : 50) for $[M+Na]^+$ and $[M+Li]^+$, Extracted ATD profiles ($[M+H]^+$) of BDB, methedrone, and their mixture (50 : 50), +ESI mass spectra of methedrone and BDB after single pass separation (PDF)

AUTHOR INFORMATION

Corresponding Author
* **Karel Lemr** − Department of Analytical Chemistry, Faculty of Science, Palacký University, 17. listopadu 12, 779 00 Olomouc, Czech Republic; orcid.org/0000-0003-3158-0637; Phone: +420-585 634 415; Email: karel.lemr@upol.cz.

Author

Marianna Nytka − Department of Analytical Chemistry, Faculty of Science, Palacký University, 17. listopadu 12, 779 00 Olomouc, Czech Republic; orcid.org/0000-0002-9242-8295

Jiahao Wan − Department of Chemistry, Bagley Hall, Box 351700, University of Washington, Seattle, Washington 98195-1700, United States;

František Tureček − Department of Chemistry, Bagley Hall, Box 351700, University of Washington, Seattle, Washington 98195-1700, United States; orcid.org/0000-0001-7321-7858

Complete contact information is available at:

Author Contributions

The manuscript was written through contributions of all authors. All authors have given approval to the final version of the manuscript.

Notes

The authors declare no competing financial interest.

ACKNOWLEDGMENTS

REFERENCES

(1) United Nations Office on Drugs and Crime. *World Drug Report 2023, Executive Summary*; United Nations publication, Vienna, Austria, 2023.

(2) de Campos, E. G.; Krotulski, A. J.; S. De Martinis, B.; Costa, J. L. Identification of synthetic cathinones in seized materials: A review of analytical strategies applied in forensic chemistry. *WIREs Forensic Sci.* **2022**, *4* (5), e1455. DOI: 10.1002/wfs2.1455.

(3) Esteve-Turrillas, F. A.; Armenta, S.; de la Guardia, M. Sample preparation strategies for the determination of psychoactive substances in biological fluids. *J. Chromatogr. A* **2020**, *1633*, 461615. DOI: 10.1016/j.chroma.2020.461615.

(4) Di Trana, A.; Berardinelli, D.; Tini, A.; Zaami, S. The targeted analysis of New Psychoactive Substances in oral fluid through chromatographic-spectrometric methods: review of recent findings. *Eur. Rev. Med. Pharmacol. Sci.* **2022**, *26* (3), 750-754. DOI: 10.26355/eurrev_202202_27982.

(5) Florou, D.; Boumba, V. A. Hair analysis for New Psychoactive Substances (NPS): Still far from becoming the tool to study NPS spread in the community? *Toxicol. Rep.* **2021**, *8*, 1699-1720. DOI: 10.1016/j.toxrep.2021.09.003.

(6) Bolcato, V.; Carelli, C.; Radogna, A.; Freni, F.; Moretti, M.; Morini, L. New Synthetic Cathinones and Phenylethylamine Derivatives Analysis in Hair: A Review. *Molecules* **2021**, *26* (20), 6143. DOI: 10.3390/molecules26206143.

(7) Ferrari Júnior, E.; Leite, B. H. M.; Gomes, E. B.; Vieira, T. M.; Sepulveda, P.; Caldas, E. D. Fatal cases involving new psychoactive substances and trends in analytical techniques. *Front, Toxicol.* **2022**, *4*, 1033733. DOI: 10.3389/ftox.2022.1033733.

(8) Bijlsma, L.; Bade, R.; Been, F.; Celma, A.; Castiglioni, S. Perspectives and challenges associated with the determination of new psychoactive substances in urine and wastewater - A tutorial. *Anal. Chim. Acta* **2021**, *1145*, 132-147. DOI: 10.1016/j.aca.2020.08.058.

(9) Klingberg, J.; Keen, B.; Cawley, A.; Pasin, D.; Fu, S. Developments in high-resolution mass spectrometric analyses of new psychoactive substances. *Arch. Toxicol.* **2022**, *96* (4), 949-967. DOI: 10.1007/s00204-022-03224-2.

(10) Matey, J. M.; Zapata, F.; Menéndez-Quintanal, L. M.; Montalvo, G.; García-Ruiz, C. Identification of new psychoactive substances and their metabolites using non-targeted detection with high-resolution mass spectrometry through diagnosing fragment ions/neutral loss analysis. *Talanta* **2023**, *265*, 124816. DOI: 10.1016/j.talanta.2023.124816.

(11) Fabregat-Safont, D.; Sancho, J. V.; Hernández, F.; Ibáñez, M. The key role of mass spectrometry in comprehensive research on new psychoactive substances. *J. Mass Spectrom.* **2021**, *56* (7), e4673. DOI: 10.1002/jms.4673 (acccessed 2023/08/03).

(12) Shirley Lee, H. Z.; Koh, H. B.; Tan, S.; Goh, B. J.; Lim, R.; Lim, J. L. W.; Angeline Yap, T. W. Identification of closely related new psychoactive substances (NPS) using solid deposition gas-chromatography infra-red detection (GC–IRD) spectroscopy. *Forensic Sci.Int.* **2019**, *299*, 21-33. DOI: 10.1016/j.forsciint.2019.03.025.

(13) Skultety, L.; Frycak, P.; Qiu, C.; Smuts, J.; Shear-Laude, L.; Lemr, K.; Mao, J. X.; Kroll, P.; Schug, K. A.; Szewczak, A.; et al. Resolution of isomeric new designer stimulants using gas chromatography – Vacuum ultraviolet spectroscopy and theoretical computations. *Anal. Chim. Acta* **2017**, *971*, 55-67. DOI: 10.1016/j.aca.2017.03.023.

(14) Boronat Ena, M. d. M.; Cowan, D. A.; Abbate, V. Ambient ionization mass spectrometry applied to new psychoactive substance analysis. *Mass Spectrom. Rev.* **2023**, *42* (1), 3-34. DOI: 10.1002/mas.21695.

(15) Pauk, V.; Žihlová, V.; Borovcová, L.; Havlíček, V.; Schug, K.; Lemr, K. Fast separation of selected cathinones and phenylethylamines by supercritical fluid chromatography. *J. Chromatogr. A* **2015**, *1423*, 169-176. DOI: 10.1016/j.chroma.2015.10.061.

(16) Borovcová, L.; Pauk, V.; Lemr, K. Analysis of new psychoactive substances in human urine by ultra-high performance supercritical fluid and liquid chromatography: Validation and comparison. *J. Sep. Sci.* **2018**, *41* (10), 2288-2295. DOI: 10.1002/jssc.201800006.

(17) Armenta, S.; Garrigues, S.; de la Guardia, M.; Brassier, J.; Alcalà, M.; Blanco, M.; Perez-Alfonso, C.; Galipienso, N. Detection and characterization of emerging psychoactive substances by ion mobility spectrometry. *Drug Test. Anal.* **2015**, *7* (4), 280-289. DOI: 10.1002/dta.1678 (acccessed 2023/08/04).

(18) Metternich, S.; Zoerntlein, S.; Schoenberger, T.; Huhn, C. Ion mobility spectrometry as a fast screening tool for synthetic cannabinoids to uncover drug trafficking in jail via herbal mixtures, paper, food, and cosmetics. *Drug Test. Anal.* **2019**, *11* (6), 833-846. DOI: 10.1002/dta.2565.

(19) Norman, C.; McKirdy, B.; Walker, G.; Dugard, P.; NicDaeid, N.; McKenzie, C. Large-scale evaluation of ion mobility spectrometry for the rapid detection of synthetic cannabinoid receptor agonists in infused papers in prisons. *Drug Test. Anal.* **2021**, *13* (3), 644-663. DOI: 10.1002/dta.2945.

(20) Gallart-Mateu, D.; Bejar-Grimalt, J.; Esteve-Turrillas, F. A.; Armenta, S.; Garrigues, S.; de la Guardia, M. A synergetic approach based on infrared spectroscopy and ion mobility spectrometry for the analysis of seized blotters: Boosting performance. *Microchem. J.* **2022**, *181*, 107810. DOI: 10.1016/j.microc.2022.107810.

(21) Gwak, S.; Almirall, J. R. Rapid screening of 35 new psychoactive substances by ion mobility spectrometry (IMS) and direct analysis in real time (DART) coupled to quadrupole time-of-flight mass spectrometry (QTOF-MS). *Drug Test. Anal.* **2015**, *7* (10), 884-893. DOI: 10.1002/dta.1783.

(22) Yanini, A.; Esteve-Turrillas, F. A.; de la Guardia, M.; Armenta, S. Ion mobility spectrometry and high resolution mass-spectrometry as methodologies for rapid identification of the last generation of new psychoactive substances. *J. Chromatogr. A* **2018**, *1574*, 91-100. DOI: 10.1016/j.chroma.2018.09.006.

(23) Denia, A.; Esteve-Turrillas, F. A.; Armenta, S. Analysis of drugs including illicit and new psychoactive substances in oral fluids by gas chromatography-drift tube ion mobility spectrometry. *Talanta* **2022**, *238*, 122966. DOI: 10.1016/j.talanta.2021.122966.

(24) Joshi, M.; Cetroni, B.; Camacho, A.; Krueger, C.; Midey, A. J. Analysis of synthetic cathinones and associated psychoactive substances by ion mobility spectrometry. *Forensic Sci.Int.* **2014**, *244*, 196-206. DOI: 10.1016/j.forsciint.2014.08.033.

(25) Kanu, A. B.; Brandt, S. D.; Williams, M. D.; Zhang, N.; Hill, H. H. Analysis of Psychoactive Cathinones and Tryptamines by Electrospray Ionization Atmospheric Pressure Ion Mobility Time-of-Flight Mass Spectrometry. *Anal. Chem.* **2013**, *85* (18), 8535-8542. DOI: 10.1021/ac401951a.

(26) Sysoev, A. A.; Poteshin, S. S.; Chernyshev, D. M.; Karpov, A. V.; Tuzkov, Y. B.; Kyzmin, V. V.; Sysoev, A. A. Analysis of New Synthetic Drugs by Ion Mobility Time-of-Flight Mass Spectrometry.

Eur. J. Mass Spectrom. **2014**, *20* (2), 185-192. DOI: 10.1255/ejms.1262 (acccessed 2023/08/19).

(27) Mardal, M.; Dalsgaard, P. W.; Qi, B.; Mollerup, C. B.; Annaert, P.; Linnet, K. Metabolism of the synthetic cannabinoids AMB-CHMICA and 5C-AKB48 in pooled human hepatocytes and rat hepatocytes analyzed by UHPLC-(IMS)-HR-MSE. *J. Chromatogr. B* **2018**, *1083*, 189-197. DOI: 10.1016/j.jchromb.2018.03.016.

(28) Bergstroem, M. A.; Loevgren, H.; Abrahamsson, A.; Eriksson, E. K.; Andersson, M. L.; Komorowska, M.; Axelsson, M. A. B. Rethinking drug analysis in health care: high-throughput analysis of 71 drugs of abuse in oral fluid using ion mobility-high-resolution mass spectrometry. *J. Anal. Toxicol.* **2022**, *46* (7), 765-775. DOI: 10.1093/jat/bkab114.

(29) Aderorho, R.; Chouinard, C. D. Improved separation of fentanyl isomers using metal cation adducts and high-resolution ion mobility-mass spectrometry. *Drug Test. Anal.* **2024**, *16* (4), 369-379. DOI: 10.1002/dta.3550.

(30) Majeed, H. A.; Bos, T. S.; Voeten, R. L. C.; Kranenburg, R. F.; van Asten, A. C.; Somsen, G. W.; Kohler, I. Trapped ion mobility mass spectrometry of new psychoactive substances: Isomer-specific identification of ring-substituted cathinones. *Anal. Chim. Acta* **2023**, *1264*, 341276. DOI: 10.1016/j.aca.2023.341276.

(31) Hermannová, M.; Iordache, A.-M.; Slováková, K.; Havlíček, V.; Pelantová, H.; Lemr, K. Arrival time distributions of product ions reveal isomeric ratio of deprotonated molecules in ion mobility–mass spectrometry of hyaluronan-derived oligosaccharides. *J. Mass Spectrom.* **2015**, *50* (6), 854–863. DOI: 10.1002/jms.3596.

(32) Borovcová, L.; Hermannová, M.; Pauk, V.; Šimek, M.; Havlíček, V.; Lemr, K. Simple area determination of strongly overlapping ion mobility peaks. *Anal. Chim. Acta* **2017**, *981*, 71-79. DOI: 10.1016/j.aca.2017.05.003.

(33) Giles, K.; Ujma, J.; Wildgoose, J.; Pringle, S.; Richardson, K.; Langridge, D.; Green, M. A Cyclic Ion Mobility-Mass Spectrometry System. *Anal. Chem.* **2019**, *91* (13), 8564-8573. DOI: 10.1021/acs.analchem.9b01838.

(34) Bush, M. F.; Campuzano, I. D. G.; Robinson, C. V. Ion Mobility Mass Spectrometry of Peptide Ions: Effects of Drift Gas and Calibration Strategies. *Anal. Chem.* **2012**, *84* (16), 7124-7130. DOI: 10.1021/ac3014498.

(35) Bush, M. F.; Hall, Z.; Giles, K.; Hoyes, J.; Robinson, C. V.; Ruotolo, B. T. Collision Cross Sections of Proteins and Their Complexes: A Calibration Framework and Database for Gas-Phase Structural Biology. *Anal. Chem.* **2010**, *82* (22), 9557-9565. DOI: 10.1021/ac1022953.

(36) McCullagh, M.; Goscinny, S.; Palmer, M.; Ujma, J. Investigations into pesticide charge site isomers using conventional IM and cIM systems. *Talanta* **2021**, *234*, 122604. DOI: 10.1016/j.talanta.2021.122604.

(37) Wan, J.; Nytka, M.; Qian, H.; Lemr, K.; Tureček, F. Do d(GCGAAGC) Cations Retain the Hairpin Structure in the Gas Phase? A Cyclic Ion Mobility Mass Spectrometry and Density Functional Theory Computational Study. *J. Am. Soc. Mass. Spectrom.* **2023**, *34* (10), 2323-2340. DOI: 10.1021/jasms.3c00228.

(38) Dodds, J. N.; May, J. C.; McLean, J. A. Correlating Resolving Power, Resolution, and Collision Cross Section: Unifying Cross-Platform Assessment of Separation Efficiency in Ion Mobility Spectrometry. *Anal. Chem.* **2017**, *89* (22), 12176-12184. DOI: 10.1021/acs.analchem.7b02827.

(39) Kováč, A.; Majerová, P.; Nytka, M.; Cechová, M. Z.; Bednář, P.; Hájek, R.; Cooper-Shepherd, D. A.; Muck, A.; Lemr, K. Separation of Isomeric Tau Phosphopeptides from Alzheimer's Disease Brain by Cyclic Ion Mobility Mass Spectrometry. *J. Am. Soc. Mass. Spectrom.* **2023**. DOI: 10.1021/jasms.2c00289.

(40) Zheng, X.; Zhang, X.; Schocker, N. S.; Renslow, R. S.; Orton, D. J.; Khamsi, J.; Ashmus, R. A.; Almeida, I. C.; Tang, K.; Costello, C. E.; et al. Enhancing glycan isomer separations with metal ions and positive and negative polarity ion mobility spectrometry-mass spectrometry analyses. *Anal. Bioanal. Chem.* **2017**, *409* (2), 467-476. DOI: 10.1007/s00216-016-9866-4.

(41) de Bruin, C. R.; Hennebelle, M.; Vincken, J. P.; de Bruijn, W. J. C. Separation of flavonoid isomers by cyclic ion mobility mass spectrometry. *Anal. Chim. Acta* **2023**, *1244*, 340774. DOI: 10.1016/j.aca.2022.340774.

For Table of Contents Only
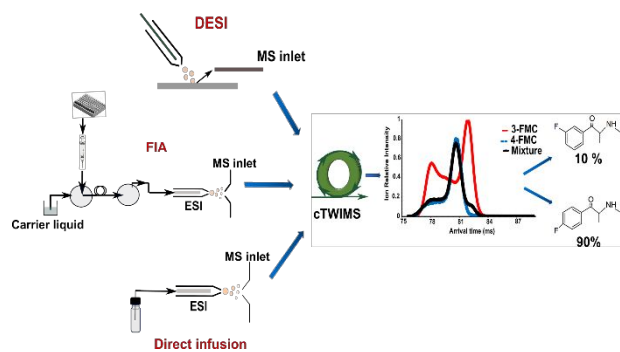
PALACKÝ UNIVERSITY IN OLOMOUC

Faculty of Science

Department of Analytical Chemistry

SUMMARY OF DOCTORAL THESIS

COMBINATION OF IONIZATION TECHNIQUES AND ION MOBILITY-MASS SPECTROMETRY IN THE ANALYSIS OF NEW PSYCHOACTIVE SUBSTANCES

Autor: Marianna Nytka, M.Sc.
Field of study: Analytical Chemistry
Supervisor: Prof. RNDr. Karel Lemr, Ph.D.

Olomouc 2024

SUMMARY

This dissertation thesis is devoted to the application of different ionization techniques and ion mobility-mass spectrometry in the analysis of new psychoactive substances. The main goal of this work is to investigate ionization and ion mobility, developing a new modification of desorption nanoelectrospray and a new approach to cyclic ion mobility of new psychoactive substances (NPS). The knowledge was used to develop new methods for identifying and distinguishing abused drugs.

The theoretical part is focused on ambient ionization mass spectrometry, particularly spray-based liquid extraction techniques, and on ion mobility-mass spectrometry (IM-MS). It also covered the application of ambient ionization in analyses of new psychoactive substances and coupling ambient ionization to IM-MS.

The first part of the research covers enhancing ionization efficiency of desorption nanoelectrospray by implementing pressure regulation at the inlet of the mass spectrometer. The influence of the transfer capillary length, pressure drop, and the heating capillary temperature was tested by analyzing NPS. It was confirmed that the pressure regulation between the mass spectrometer's atmospheric and evacuated region and the heated capillary temperature is crucial to maximize sensitivity. The applicability of the modified inlet was tested by analyzing the trace amount of synthetic cathinone on a wallet surface and paracetamol tablets.

The second part of the research focuses on analyzing isomeric mixtures of NPS by cyclic ion mobility-mass spectrometry. Two approaches to determine their isomeric ratios were proposed. The separation of lithium adducts in multipass experiments was compared with the simple procedure based on multiple linear regression applied to characteristic arrival time distribution (ATD) profiles of isomers and their mixture. Direct infusion and flow injection analysis with electrospray, and desorption electrospray for solid samples were employed. Both approaches, lithiated molecules separation and ATD profiles of protonated molecules or ion fragments, provided comparable results. While adducts need to be sufficiently separated, the ATD profile approach can be used for overlapping signals.

SOUHRN

Hlavním cílem této práce je výzkum ionizace a iontové mobility, který zahrnoval především vývoj citlivější modifikace desorpčního nanoelektrospreje a nový přístup k cyklické iontové mobilitě nových psychoaktivních látek (NPS). Poznatky byly využity k vývoji nových postupů pro identifikaci a rozlišení zneužívaných drog.

Teoretická část je zaměřena na hmotnostní spektrometrii s ionizací ambientními technikami, zejména technikou kapalinové extrakce na bázi sprejování, a na hmotnostní spektrometrii ve spojení s iontovou mobilitou (IM-MS). Dále pojednává o ambientních technikách využitých při analýze nových psychoaktivních látek a jejich spojení s IM-MS.

První část výzkumu zahrnuje zvýšení intenzity signálu pro desorpční ionizaci nanoelektrosprejem zavedením regulace tlaku na vstupu hmotnostního spektrometru. Na analýze NPS byl testován vliv délky vstupní vyhřívané kapiláry, snížení tlaku a teploty vyhřívané kapiláry. Bylo potvrzeno, že pro dosažení maximální citlivosti je rozhodující regulace tlaku mezi atmosférickou a vakuovou částí hmotnostního spektrometru a teplota vyhřívané kapiláry. Použitelnost upraveného vstupu do hmotnostních spektrometru byla testována na detekci stopového množství syntetického katinonu na povrchu peněženky a na analýze tablet neopioidní analgetika a antipyretika.

Druhá část výzkumu byla zaměřena na analýzu izomerních směsí NPS pomocí cyklické iontové mobility-hmotnostní spektrometrie. Byly navrženy dva přístupy ke stanovení jejich izomerních poměrů. Separace aduktů lithia ve víceprůchodových experimentech byla porovnána s jednoduchým postupem založeným na mnohonásobné lineární regresi aplikované na profily charakteristické distribuce doby příchodu (ATD) izomerů a jejich směsi. Byla použita přímá infuze a průtoková injekční analýza s elektrosprejem a rovněž desorpční elektrosprej pro pevné vzorky. Oba přístupy, separace lithiovaných molekul a ATD profily protonovaných molekul nebo iontových fragmentů, poskytly srovnatelné výsledky. Zatímco adukty je třeba dostatečně separovat, pro překrývající se signály lze využít ATD profily charakteristické pro jednotlivé izomery

Table of Contents

1 INTRODUCTION

The production of new psychoactive substances often consists of the variation of functional group position or, more generally, the production of isomers. It increases the requirements for analyses when developing rapid, selective, sensitive methods, which are essential to detect and separate an increasing number of NPS Ambient ionization coupled with ion mobility-mass spectrometry (IM-MS) represents a promising tool for solving this analytical task. This coupling provides a fast (millisecond timescale) gas-phase separation with minimal sample pretreatment. So far, the application of this method is limited in the analysis of NPS.

This doctoral thesis focuses on enhancing ion transport in desorption nanoelectrospray by pressure regulation at the mass spectrometry inlet. A mixture of new psychoactive substances was used to evaluate the influence of pressure regulation, the temperature of the heated capillary, and its length. The applicability of desorption nanoelectrospray was proven by analyzing traces of abused drugs or a non-opioid analgesic and antipyretic agent.

Cyclic ion mobility-mass spectrometry was used to discriminate NPS isomers and determine their ratios. The high resolving power of multipass experiments could not resolve isomeric protonated molecules. Nevertheless, the characteristic ATD profiles were obtained by direct infusion or flow injection analysis with electrospray and desorption electrospray ionization. Characteristic ATD profiles of protonated molecules provided comparable results to the separation of lithium adducts, which opens new possibilities for the differentiation of isomers of small organic molecules.

2 THEORETICAL PART

2.1 Ambient Ionization Mass Spectrometry

Since 2004, when Cooks et al. [1] presented desorption electrospray ionization-mass spectrometry (DESI-MS), and 2005, when Laramee and Cody [2] presented direct analysis in real time (DART), the rise of ambient techniques began. In ambient ionization mass spectrometry (AIMS), samples are ionized under ambient conditions with minimal or no sample preparation [3]. AIMS sources have compatibility with multiple mass spectrometers and allow rapid, in-situ [4] and in vivo analysis [5]. Most AIMS sources can be classified based on their desorption process into three groups [6]: a) liquid extraction – mainly utilizes the ESI mechanism; b) plasma desorption (thermal) – based on the same principles as atmospheric pressure chemical ionization (APCI), where the ions are produced using a corona discharge; c) Laser ablation/desorption (laser-based) techniques - the analyte's desorption is performed by irradiation with high power lasers.

The liquid extraction techniques can be divided by the sample processing into three groups: spray desorption, substrate spray (e.g., paper spray (PS), probe electrospray ionization (PESI), etc.), and liquid microjunction (e.g., liquid microjunction-surface sampling probe (LMJ-SSP), liquid extraction surface analysis (LESA), nano-DESI) [6].

The next subchapter will be dedicated only to spray desorption techniques.

2.1.2 Spray-Based Ambient Ionization Mass Spectrometry

Part of this section was published in a first-author publication [7] and adapted and reprinted with permission from the journal:

Nytka, M, Borovcová, L, Fryčák, P, Barták, P, Lemr, K. Signal enhancement in desorption nanoelectrospray ionization by custom-made inlet with pressure regulation. J Mass Spectrom. 2020;55:e4642.https://doi.org/10.1002/jms.4642 Copyright 2020 John Wiley & Sons, Ltd.
 License number 5730170914154.

Author's Contribution. Marianna Nytka – investigation, formal analysis, visualization, and writing the original draft.

Spray-based ambient techniques use the charged droplets produced from the solvent spray to desorb or extract analyte from the sample surface. During this process, desorbed analytes undergo an electrospray-like ionization mechanism by ion evaporation or charge residues [8,9]. Desorbed analytes are ionized and sent to a mass spectrometer for analysis [6].

The most used spray-based AIMS technique is desorption electrospray ionization-mass spectrometry (DESI-MS). In DESI, the desorption and ionization is accomplished by a droplet pick–up mechanism [10] . The surface is sprayed with the charged solvent droplets generated with the assistance of the nebulizing gas, providing the thin wet film on the sample's surface. This process is followed by solid-liquid microextraction and production of the secondary droplets drawn towards the mass spectrometer inlet by an electric field potential. Nitrogen is typically used as a nebulizing gas. DESI-MS requires minimal sample preparation and no matrix deposition compared with MALDI [8]. Reproducibility in DESI experiments depends on the geometry, the pressure of the nebulizing gas, the composition and flow rate of the spraying liquid, and the surface's properties from which the analyte is desorbed [10,12]. DESI has a myriad of qualitative and quantitative applications, such as the detection of inks [13,14], polymers [15–17], explosives, chemical warfare [18,19], cancer biomarkers [20–22], and proteins [23].

Another modification of the DESI source, desorption nanoelectrospray (nanoDESI, Fig. 5), was reported in 2007 by Ranc et al. [24]. It should not be confused with coincidently abbreviated nanospray desorption electrospray (nano-DESI), which was introduced a few years later and is more related to liquid extraction surface analysis (LESA) than to desorption electrospray (DESI). Nano-DESI uses two capillaries without the assistance of the nebulizing gas to create a liquid microjunction, the principle of the technique differs from DESI and nanoDESI. [25,26].

Compared with DESI, nanoDESI generates a lower flow rate of spraying liquid and smaller primary charged droplets. Instead of an electrospray tip (tens of micrometers ID), it uses a nanoelectrospray tip (~2 μm ID) without the assistance of nebulizing gas. Both techniques are suitable for direct surface analysis, are tolerant to sample contamination by salt, and produce ions with similar internal energy. In the first application of nanoDESI, the chiral analysis of ephedrine in an untreated drop of the commercial pharmaceutical deposited on the surface was demonstrated using this ion source and the Cooks kinetic

method. This method is based on forming trimeric clusters of the analyte with a chiral selector (usually optically pure reference substance) and a metal ion. Two fragmentation pathways can occur, one with the loss of the selector and the second with the loss of the analyte. The ratio of fragment intensities depends on the relative stability of the complexes formed by the different enantiomers [24]. The applicability of nanoDESI was shown further, for example, by chiral analysis of pharmaceuticals in whole blood [29] or analysis of anthocyanins in a drop of red wine [30]. Although technical development has improved the robustness of nanoDESI [28] and a modification of the inlet has allowed its implementation on a Q-TOF mass spectrometer [27], the sensitivity of the measurements can still be an issue. Due to the small surface area sampled, only a tiny amount of analyte is available for desorption and ionization.

2.2. Ion Mobility – Mass Spectrometry

Ion mobility (IM) is a powerful tool for separating ions in drift gas ("buffer gas") under the electric field. The electric field accelerates ions through the inert gas, producing collisions of ions with the buffer gas. Those collisions produce friction force. If collisions are frequent enough, electric force and friction force cancel each other, and the stationary state can be achieved, providing a constant average speed (drift velocity, V_d). Therefore, drift velocity is proportional to the electric field (E), and ion mobility (K) ($v_d = KE$). The mobility, K, can be determined by the time (t_d) that ions spend inside a mobility cell of fixed length (L) ($K = \frac{V_d}{E} = \frac{L}{t_d \cdot E}$) [50,51].

The mobility K depends on the mass and charge of the ions and their shape. Therefore, small ions have higher drift velocities than larger, less mobile ions.

The mobility of an ion is related to its collision cross-section (CCS). IM measurements determine the integral of the collision cross-section on the collision energy distribution [50]. Momentum transfer collision integral (Ω or CCS) describes the collisions of ions with the buffer gas and ion conformations in a mobility cell and can be calculated

by the fundamental low-field mobility equation (Mason-Schamp): $\Omega = \frac{\frac{3}{16}\left(\frac{2\cdot\pi}{\mu \cdot k_b \cdot T}\right)^{1/2} \cdot z \cdot e}{N_0 \cdot K_0}$,

where e is charge of the electron; $z \cdot e$ - ion charge; N_0 - buffer gas density; μ - reduced mass; k_b – Boltzann's constant; T- absolute temperature in drift region.

There are three ways to characterize ions in ion mobility spectrometry (IMS): drift time (t_d), reduced mobility (K_0), and CCS (Ω). The drift time depends on the instrument

and its conditions. Consequently, most databases for IM-MS measurements contain CCS values [53]. The CCS values for different IMS platforms may differ up to 2% [54]. Ion mobility-mass spectrometry (IM-MS) is used to separate conformational isomers or complex mixtures of isobars or isomers. IM-MS separates the charge states of ions (e.g., proteins) or filters the spectra by extracting the targeted analytes' signals [50].

Several IMS platforms are available on the market, as seen in. Those ion mobility spectrometers can be divided into three categories: a) time-dispersive (drift tube IMS (DTIMS), traveling wave IMS (TWIMS)), b) space or spatially dispersive (high-field asymmetric IMS (FAIMS), differential mobility analyzer (DMA), c) ion trapping and selective release (trapped IMS (TIMS)) [55].

TWIMS was first introduced by Waters Corp. in 2006 [57]. Similarly to DTIMS, there is no specific buffer gas flow in the drift region. IM cell consists of stacked ring electrodes on which the oscillation electric field is applied, which propels ions like on waves with the assistance of RF confinement to focus ion packets. TWIMS instruments need to use CCS calibration [58–60]. Cyclic TWIM consists of a closed-looped separator with a 98 cm path length that allows multipass separation. Ions arrive at the entrance/exit multifunction array of pin electrodes (T-Wave array). As this T-Wave array can be programmable, it can accelerate ions sidewise by a traveling wave to the cyclic separator region. Aside from the cyclic drift cell, the instrument has two chambers, pre-array store (before cyclic ion mobility (cIM) but after the trap region and post-array (after the cIM) but before the transfer region). Pre-array store and post-array are located in the same chamber as the cyclic ion mobility. They are used to transport the ions on and from the T-Wave array. Also, they can store the ions from the mobility experiments ("slices of ions") from the T-wave array [63]. This technology gives a unique possibility to perform IMS^n experiments. Ions are separated in multipass experiments. Higher resolving power (R) (up to ~750) can be achieved by increasing the number of passes (time that ions spend inside the mobility cell), which correlates with path length ($R \sim R_1 \cdot$ (number of passes)$^{0.5} \propto R \sim L^{0.5}$) [63]. The part of the ions can be isolated according to the arrival time and ejected to the pre-array store. The remaining part of ions, which are still in the mobility cell, can be removed by being ejected to TOF without triggering the data acquisition. Upon the reinjection from the pre-array store to the T-Wave array, potential can be applied to increase kinetic energy and, as a consequence, to induce the collision activation of ions. Therefore, the fragments can enter the T-Wave array for separation. These steps can be repeated, leading to IMS^n experiments [63–65].

3 AIMS OF THE DISSERTATION THESIS

The thesis aimed to investigate ionization by developing the new modification of desorption nanoelectrospray ionization and to find new approach to cyclic ion mobility of new psychoactive substances. Different ionization techniques (ESI, nano-DESI, and DESI) and cyclic traveling wave ion mobility were used.

This dissertation thesis can be divided into the following tasks:

1. To develop the modification of desorption nanoelectrospray to improve ion transmission to increase the applicability of the ionization source;

2. To develop a simple procedure of isomeric ratio determination using characteristic ATD profiles of individual isomers.

The results could be found in articles published in [7] and [67].

4 EXPERIMENTAL PART

4.1 Signal Enhancement of Desorption Nanoelectrospray Ionization by Pressure Regulation at the Mass Spectrometer Inlet

This work was published in a first-author publication [7] and adapted and reprinted with permission from the journal:

Nytka, M, Borovcová, L, Fryčák, P, Barták, P, Lemr, K. Signal enhancement in desorption nanoelectrospray ionization by custom-made inlet with pressure regulation. J Mass Spectrom. 2020;55:e4642.https://doi.org/10.1002/jms.4642 Copyright 2020 John Wiley & Sons, Ltd.
Licence number 5730170914154.

Author's Contribution. Marianna Nytka – investigation, formal analysis, visualization, and writing the original draft.

Samples´ preparation

Stock solutions were prepared with a concentration of 1 mg/mL in methanol/ water (1:1, v/v) and stored in a fridge. The working solution of a mixture was prepared by diluting the stock solutions to a final concentration of 1 µg/mL. NanoDESI analysis was performed using a mixture of methanol/water (75/25, v/v) as a spraying solvent.

Microscope slide treatment and sample deposition

The silanization procedure was performed and optimized at the Department of Analytical Chemistry, Palacký University Olomouc. It is based on immersing the microscope slides into the hexamethyldisilazane/ pyridine (50/50, v/v) in a closed vessel for 2 h at 120 °C with subsequent washing with water and ultrasonication for 1 min in water. The mixture of analytes was deposited (total volume 56 µl in five layers) onto silanized slides by SunCollect MALDI spotter (SunChrom, Friedrichsdorf, Germany) to generate homogeneous layers. The final concentration of each analyte on the surface was 0.5 ng/mm^2 (surface area of 1.89 x 0.6 cm).

Instruments

Analysis of NPS was performed on Xevo T.Q.D. triple quadrupole mass spectrometer (Waters, Manchester, UK) with modified custom-made inlet (Fig. 1).
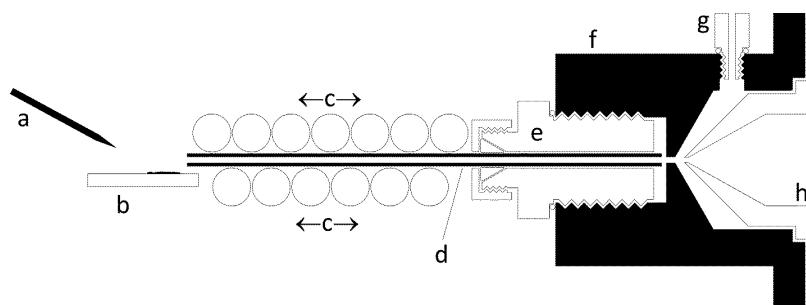
Figure 1 Scheme of custom-made MS inlet: a - nanoelectrospray tip; b - sample on support; c - threads of a heating rope; d - stainless steel inlet capillary; e - Swagelok SS-100-1-OR tube fitting, sealing the heated capillary (d) by a ferrule; sealed to the inlet block by an O-ring; f - inlet block; g - reduced pressure port hose adapter, sealed to the inlet block by an O-ring; h - sample cone (native part of the mass spectrometer, fitted in its original location and held by the inlet block (f), sealed to the instrument by an O-ring). Reprinted and adapted from [7]. Copyright 2020 John Wiley & Sons, Ltd

Data were collected in positive ionization mode six times (1 min acquisition each). The nanoDESI consists of an inlet block, heated capillary, and original sample cone. The inlet block is equipped with a port for an auxiliary pump connection. It allowed pumping of the inner compartment of the MS inlet in comparison with designs connecting a pump to a refluence tube [68] or a source chamber [69] in front of the inlet. Pressure drop (difference between atmospheric pressure and pressure in the inlet) was measured by a manometer and regulated by a needle valve, both mounted between a port (g) and the auxiliary pump. The capillary was heated by a heating rope connected to the Regbox heater driver (Jakar Electronics, Karvina, Czech Republic). As in the DESI source [1], the gas flow outlet and the interlock for the ESI source were blocked. Desorption nanoelectrospray consisted of a nanoelectrospray tip (2 ± 1 μm I.D., PicoTips emitter, New Objective, Woburn, USA) and a sample stage, both manually movable in the x – y – z axes.

Proper geometry was set to obtain the best spectra quality: nanospray tip - target plate: vertical distance ~ 2 mm; angle ~ 30°; nanospray tip - the center of sample spot: horizontal distance ~ 2 mm; microscope slide - heated capillary: vertical distance ~ 1 mm, angle ~ 0°; center of sample spot - heated capillary: horizontal distance ~ 2 mm.

Source parameters were tuned in positive ionization mode and set as follows: capillary voltage 2.2 kV, TQD source temperature 100 °C, temperature of the heated capillary 100°C, 180 °C, 200 °C, 220 °C, pressure drop from 0.08 (closed needle valve) to 0.8 bar. MassLynx 4.1 software (Waters Corp., Wilmslow, UK) was used for instrument

operation and data acquisition. Data were collected in six replicates (1 min acquisition each) and processed by OriginPro 2020 (OriginLab, Northampton, USA).

4.2 Cyclic Ion Mobility-Mass Spectrometry of New Psychoactive Substances

This work was published as a first-author publication [67] and with the permission adapted and reprinted from:

Nytka M., Wan J., Tureček F., Lemr K. Cyclic ion mobility of isomeric new psychoactive substances employing characteristic arrival time distribution profiles and adduct separation. J. Am. Soc. Mass Spectrom. 2024; https://doi.org/10.1021/jasms.4c00127

ACS open access

Author's Contribution. Marianna Nytka – investigation, formal analysis, visualization, and writing the original draft.

Samples' preparation

Stock and working solutions of individual analytes were prepared at concentrations of 1 mg/mL and 100 ng/mL, respectively, in methanol/water (1/1, v/v). Isomeric mixtures with a total concentration of 100 ng/mL (methanol/ water, 1/1 v/v) were analyzed: a) 3-MMC and buphedrone (*m/z* 178.13); b) 3-FMC and 4-FMC (*m/z* 182.11); c) BDB and methedrone (*m/z* 194.13). They were prepared in isomeric ratios: 5%, 10%, 25%, 40%, 50%, 60%, 75%, 90%, 95%. Six data acquisitions were performed for each solution. The model samples for FIA-cIM-MS analysis were prepared in the range from 5% to 45% in six replicates, one data acquisition for each replica was performed.

CCS calibrants (small molecules mixture) were prepared with the working concentration of 2 µg each/mL (acetonitrile/water (1/1) with 0.1 % of formic acid).

Instrument

Cyclic ion mobility- mass spectrometry

The analyses were conducted on SELECT SERIES Cyclic IMS Q-TOF (Waters Corp., Wilmslow, UK). Samples were directly infused into a normal flow ESI source at the flow rate of 5 µL/min and measured in positive ionization mode. 0.5 mmol/L sodium formate in propan-2-ol/water (90/10, v/v) was used for mass calibration (*m/z* 50-1200). The instrument was operated under two sets of settings: 1) default setting - capillary voltage 2

kV, cone voltage 10 V, source temperature 100 °C, desolvation temperature 250 °C, cone gas flow 30 L/h, desolvation gas flow 600 L/h, trap CE 6 V, transfer CE 4 V, stepwave body gradient 20 V, ion guide TW pulse height 0.4 V, trap TW pulse height 4 V, trap entrance 2 V, trap bias 2 V, trap DC -4 V, post trap gradient 3 V, post trap bias 35 V, stepwave RF 200 V, ion guide RF 300 V, driftcell RF 300 V, transfer RF 200 V, helium flow rate 120 mL/min, nitrogen flow rate 40 mL/ min., nitrogen pressure in mobility cell 1.73 mbar; TW static height 15 V, wave height 15 V (eject and acquire); 2) setting for labile compounds (used for BDB and methedrone) - capillary voltage 1 kV, cone 10V, source temperature 100 °C, desolvation temperature 250 °C, cone gas flow 30 L/h, desolvation gas flow 600 L/h, trap CE 2 V, transfer CE 1 V, stepwave body gradient 10 V, ion guide TW pulse height 0.2 V, trap TW pulse height 1 V, trap entrance 1 V, trap bias 1.5 V, trap DC -4 V, post trap gradient 1.5 V, post trap bias 16 V, stepwave RF 100 V, ion guide RF 300 V, driftcell RF 200 V, transfer RF 200 V, transfer RF gain 5 V, TW static height 13 V, wave height 10 V (eject and acquire). The precursor ion was selected in quadrupole resolution with highmass 15, lowmass 4.9 for protonated ions, and highmass 10, lowmass 2 for the adduct ions.

Flow injection analysis

FIA-cIM-MS analyses were performed on the Waters ACQUITY UPLC I-Class system fitted with the PEEK tubing (1/16"x0.13 mm) to bypass the column. It was coupled with the SELECTED SERIES Cyclic IMS (Waters Corp., Wilmslow, UK) and operated in positive ionization mode. The instrument settings and the ion mobility were the same as for direct infusion. The precursor ion was isolated in quadrupole and then fragmented in the trap cell with CE 28 V for BDB and methedrone (*m/z* 194.11). Methanol/water (1/1, v/v) was selected as a carrying liquid with a flow rate of 0.1 mL/min. Injection volume was 5.0 μL for 3-MMC and buphedrone *(m/z* 178.13); 3-FMC and 4-FMC (*m/z* 182.11) pairs. Samples were measured in six replicates, and one data acquisition was made for each replicate. The injection volume for BDB and methedrone was 10.0 μL.

Desorption electrospray

The mixtures of isomeric pairs with the same ratios as for the ESI-cIM-MS experiments (see the Chemicals and samples´ preparation) were deposited onto the Omni Slide Hydrophobic Arrays (Prosolia, Waters Corporation, Wilmslow, UK). The amount on the spot was 3.54 ng/mm^2 and was calculated by the mass of the analyte on the spot divided by the area of the spot. Analysis was performed on Select Series Cyclic IMS

equipped with a 2D-DESI ionization source (Prosolia, Waters Corporation, Wilmslow, UK). The original sprayer was replaced with a DESI XS sprayer (Waters Corporation, Wilmslow, UK). Methanol/water (80/20, v/v) was used as a spraying solvent at 2.0 µL/min. The capillary voltage was held at 0.75 kV; the nebulizing pressure was 0.076 MPa; source temperature was set to 150 °C; the cone voltage to 10 V.

DESI sprayer geometry was set as follows: the spray impact angle was 75°; spray nozzle to the inlet tube orifice was 4 mm; distance between the inlet tube orifice and the surface ~0.5 mm; spray nozzle to the surface distance was 2 mm.

Born-Oppenheimer molecular dynamics (BOMD) trajectory calculations

Prediction of structures' geometries and theoretical calculations of CCS values was performed by Prof. Tureček's team at the University of Washington in Seattle, U.S.A. (Details see in [67])

Briefly, ion structures were obtained by applying Born-Oppenheimer molecular dynamics (BOMD) trajectory calculations of several initial conformers, tautomers, and protonation isomers. That was followed by gradient geometry optimization with density functional theory. Collision cross sections (CCS) in nitrogen were calculated using the modified ion trajectory method (MobCal$_{MPI}$) [70–72] using the MK charge densities. The reported CCS and standard deviations are obtained from averaging data from ten trajectory runs.

Table 1 Relative energies of protonated molecules [67]. ACS open access

Ion	Relative Gibbs Energy[a,b]		
	B3LYP[c]	M06-2X	M06-2X[d]
	6-31 +G(d,p)	6-31 +G(d,p)	def2qzvpp
(3-MMC-keto+H)$^+$ (**1a$^+$**)	0.0	0.0	0.0
(Buphedrone-keto+H)$^+$ (**2a$^+$**)	16	15	14
(3-MMC-enol+H)$^+$ (**1b$^+$**)	45	33	31
(Buphedrone-enol+H)$^+$ (**2b$^+$**)	62	50	47

[a]In kJ mol^{-1}. [b]Including zero-point energies, enthalpies, and entropies and referring to 310 K. [c]Fully optimized with GD3-BJ empirical dispersion corrections. [d]Single-point energy calculations on M06-2X/6-31+G(d,p) optimized geometries.

Table 2 Relative energies of [M+Li]$^+$ ions [67]. ACS open access

Ion	Relative Gibbs Energy[a,b]		
	B3LYP[c]	M06-2X	M06-2X[d]
	6-31 +G(d,p)	6-31 +G(d,p)	def2qzvpp
(3-MMC-keto+Li)$^+$ (**3a$^+$**)	0.0	0.0	0.0

(Buphedrone-keto+Li)$^+$ (**4a**$^+$)	17	15	16
(3-MMC-enol+Li)$^+$ (**3b**$^+$)	82	78	75
(Buphedrone-enol+Li)$^+$ (**4b**$^+$)	101	95	93

[a]In kJ mol^{-1}. [b]Including zero-point energies, enthalpies, and entropies and referring to 310 K. [c]Fully optimized with GD3-BJ empirical dispersion corrections. [d]Single-point energy calculations on M06-2X/6-31+G(d,p) optimized geometries.

Data were acquired and processed using Masslynx v.4.2 (Software Change Note 1016, Waters Corp., Wilmslow, UK), a modified version of Driftscope v.2.9 (Waters Corp., Wilmslow, UK), and processed in OriginPro 2020 (OriginLab, Northampton, USA).

Cyclic-TWIM C.C.S. calibration for multipass separation

The mixture of small molecules (Table 1) was directly infused into the ESI source using default settings. The flow rate was set to 5µL/min. Each *m/z* of the calibrant was isolated in quadrupole and sent to one pass (98 cm) and two passes (196cm) separation in the cTWIM cell. The data was peak detected with Drifscope 2.9 software. CCS calibration was performed according to the procedure of McCullagh et al. [73]. Arrival time is the value that includes injection time (time needed for ions to arrive on the T-Wave array), drift time (time that ions spend inside the mobility cell), and dead time (time the ions exit the mobility cell to reach the detector).

We used the calibrant's arrival times at the peak's apex. The arrival time in bin number was converted to a millisecond scale. This was performed by multiplying the bin number by the number of TOF pushes per bin and the V mode pusher period for a specific mass range (*m/z* 50-1200, 0.066). The result of multiplication was added ADC start delay (includes the injection time and separation time). The calibration drift times (cycle time) were calculated by subtracting the arrival time for 1 pass (t_{a1p}) from two passes arrival time

The time ion exiting the cyclic cell to reach the detector (dead time) (t_0) was calculated by subtracting the cycle time from 1 pass data. For the analytes, CCS values were calculated using respective drift times.

Excel file provided by Waters Corp. (e.g. the one from © Johanna Hofmann, Kevin Pagel, Fritz-Haber-Institute of the Max-Planck-Institute, Berlin) was used to evaluate CCS values. A calibration curve was constructed by plotting ln(CCS', Å^2) vs. ln(t_d'). Calibration curves were constructed for protonated molecules(ln(CCS') = 0.3501 × ln(t_d) + 5.8621, R^2 = 0.9952 and lithiated molecules (ln(CCS') = 0.3617 × ln(t_d) + 5.842, R^2 = 0.9953).

Table 3 Ions Used for CCS Calibration [67]. ACS open access

Name of the Compound	m/z	z	MW (Da)	$^{DT}CCS_{N2}$ (Å²)	Ref.	Separation Time* (ms)
N-ethylaniline	122.12	1	121.18	124.50	[76]	6
Acetaminophen	152.07	1	151.17	130.40	[76]	8
Caffeine	195.10	1	194.19	136.90	[77]	10
Suflaguanidine	215.06	1	214.05	148.40	[78]	10
Alprenolol	250.20	1	249.34	157.50	[76]	12

* 2 pass separation experiments

5 RESULTS AND DISCUSSION

5.1 Signal Enhancement of Desorption Nanoelectrospray Ionization by Pressure Regulation at the Mass Spectrometer Inlet

This work was published in a first-author publication [7] and adapted and reprinted with permission from the journal:

Nytka, M, Borovcová, L, Fryčák, P, Barták, P, Lemr, K. Signal enhancement in desorption nanoelectrospray ionization by custom-made inlet with pressure regulation. J Mass Spectrom. 2020;55:e4642. https://doi.org/10.1002/jms.4642 Copyright 2020 John Wiley & Sons, Ltd. Licence number 5730170914154.

Author's Contribution. Marianna Nytka –investigation, formal analysis, visualization, and writing the original draft.

The new custom-made mass spectrometer inlet was designed and constructed considering three parameters: length of the heated capillary, its temperature, and pressure regulation at the MS inlet (the first vacuum stage). All three parameters can control the desolvation of ions, affect ion transmission, and increase the intensity of the ion signal. Their influence was evaluated for synthetic cathinones as nanoDESI might be useful for their detection, e.g., in seized street samples. Four different lengths of the heated capillary

were tested (46, 61, 76, and 99 mm) at 200 °C. Although the effect of the capillary length was insignificant, slightly better ion signal intensities were observed using the shortest one selected for the following experiments.

5.1.1 Influence of the Pressure Drop

The regulation of pressure drop at the MS inlet significantly influenced the signal intensity. Auxiliary pumping generated a pressure drop at the MS inlet in the 0.20–0.80 bar range. At reference condition (the lowest pressure drop 0.08 bar, which means the highest pressure in the inlet), the needle valve connecting the auxiliary pump with the MS inlet was closed, and the pressure reduction was generated only by the vacuum system of the mass spectrometer. Since pressure drop represents the difference between atmospheric pressure and pressure in the evacuated inlet compartment, its higher value means lower pressure in the inlet and, thus, higher vacuum suction. In the tested range, the ion signal intensity of all NPS grew between 0.08 and 0.20 bar, reached a maximum increasing the signal intensity less than two-fold for naphyrone but almost one order for buphedrone and more than one order for cathinone and 3-FMC.

Further, nanoDESI experiments were performed at a pressure drop of 0.40 bar, giving slightly lower signal intensities than 0.20 bar. Nevertheless, the dependencies are flatter at around 0.40 bar (Fig. 2), and variation of signal intensity is less sensitive to pressure drop changes.
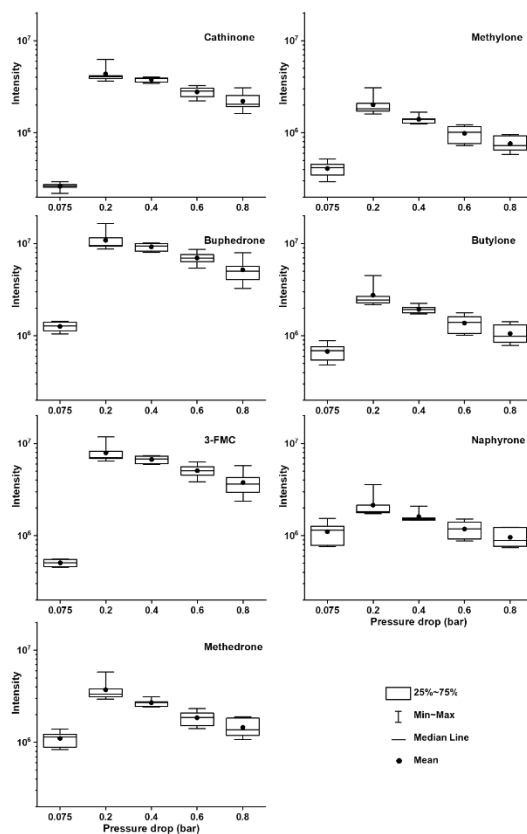
Figure 2. Influence of pressure drop on the $[M+H]^+$ ion signal intensity of cathinones ionized by desorption nanoelectrospray (nanoDESI). The temperature of the heated capillary (46 mm) was set to 200 °C. A mixture of the standards was deposited on a silanized microscope slide [7]. Copyright © 2020 John Wiley & Sons, Ltd

5.1.2 Influence of the Temperature of the Heated Capillary

Finally, the heated capillary's temperature was also considered as an important experimental parameter. Four temperatures of heated capillary were tested: 100 °C, 180 °C, 200 °C, 220 °C. For buphedrone and 3-FMC, the signal intensities were comparable between 100 °C and 200 °C (the differences were not statistically significant). A decrease in signal intensity was observed at 220 °C for all compounds. Although the temperature did not show such a strong effect as pressure regulation, its proper setting may be beneficial to the quality of mass spectra. The substantial effect of pressure regulation is also evident when the mass spectra of the analyzed mixture at 0.08 and 0.40 bar are compared (Fig3).
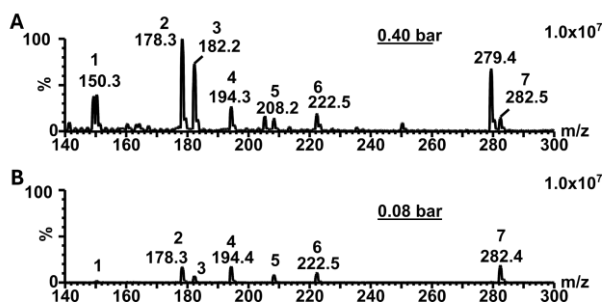
Figure 3. Desorption nanoelectrospray (nanoDESI) mass spectra of NPS (A) with the auxiliary pumping pressure drop 0.40 bar and (B) without the auxiliary pumping (B) pressure drop 0.08 bar. Both spectra are normalized to the highest ion signal intensity of 1.0×10^7 . The temperature of the heated capillary was set to 200 °C. The mixture of standards was deposited on a silanized microscope slide. Numbers indicated at each mass spectra correspond to $[M+H]^+$ of (1) cathinone, *m/z* 150 ;(2) buphedrone, *m/z* 178; (3) 3-FMC *m/z* 182; (4) methedrone, *m/z* 194; (5) methylone *m/z* 208; (6) butylone *m/z* 222; (7) naphyrone, *m/z* 282 [7]. Copyright 2020 John Wiley & Sons, Ltd

The signal intensities of all analytes are higher at 0.40 bar. Their increase is significant, especially for cathinone (1), buphedrone (2), and 3-FMC (3). No interfering signals were observed for a blank .

5.1.3 Analysis of Model Samples

The effect of pressure regulation was proven in the analysis of "real-world samples," where detecting traces of NPS on personal items can represent a relevant example. Tiny amounts (less than 0.3 mg) of the abused drugs were deposited on the wallet. "Unknown powder" was then collected from the surface using double-sided tape on a microscope slide and subjected to analysis by nanoDESI.

Desorption and ionization were performed directly from the tape surface. The acquired spectra confirmed the significant influence of reduced pressure regulation (Fig. 4). Although the surface for sample deposition was different (tape vs. silanized glass), detection of the abused drugs was also significantly improved in this "real sample" analysis.
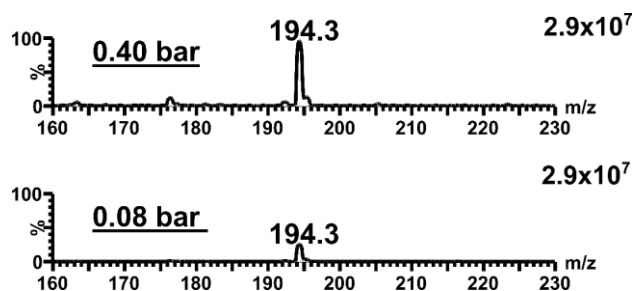
Figure 4. Desorption nanoelectrospray (nanoDESI) mass spectra of the trace amount of methedrone on double-sided tape recorded at a pressure drop of 0.40 (A) and 0.08 bar (B), respectively. A solid sample was collected from the wallet. Both spectra are normalized to the highest ion signal intensity of 2.9×10^7. The temperature of the heated capillary was set at 200 °C [7]. Copyright 2020 John Wiley & Sons, Ltd

Another possible application can be the analysis of pills. Significant signal intensity improvement was observed when applying pressure drop of 0.40 bar (Fig.5). The same results were obtained for the powdered paracetamol, proving that different forms of samples can be collected and successfully analyzed. Evidently, the proposed approach can be applied to analyses of different analytes deposited in different ways on silanized glass, double-sided tape, or other surfaces that can be tested in the future.

Figure 5. Desorption nanoelectrospray (nanoDESI) mass spectra of paracetamol traces on double-sided tape recorded at a pressure drop of (A) 0.40 bar and (B) 0.08 bar. Both spectra are normalized to the highest ion signal intensity of 2.6×10^7. The temperature of the heated capillary was set at 200 °C [7]. Copyright 2020 John Wiley & Sons, Ltd

5.1.4 Conclusion

Because nanoDESI with its lateral resolution in tens of micrometers samples small surface area, only a tiny amount of analyte is desorbed, and the measurement sensitivity

can be an issue. The yield of ions was significantly improved by properly regulated pressure reduction in the MS inlet. The pressure reduction drives the flow of gas (air) generated by suction to the inlet and, consequently, the drag force acting on charged droplets and ions in the source. Regulation of the pressure drop was recognized to have a crucial influence on signal intensity. Both the pressure drop and temperature of the heated capillary were tuned to achieve maximum sensitivity. The change in signal intensity for some of the compounds was more than one order of magnitude higher. The tested custom-made inlet permits the setting of these experimental parameters and supports the applicability of nanoDESI. One order of magnitude higher response was achieved for some of the analyzed new psychoactive substances, which may be critical in the analysis of traces of unknown samples. The development of a new ion source and the described effects of studied experimental parameters can encourage applications of nanoDESI in general. The impact of the reduced pressure regulation can differ for different mass spectrometers due to the different power of vacuum systems. Nevertheless, it was confirmed that pressure drop between the atmospheric and evacuated region of a mass spectrometer strongly influences the efficiency of nanoDESI. It should be considered if this ion source is attached to any other mass spectrometer.

5.2 Cyclic Ion Mobility-Mass Spectrometry of New Psychoactive Substances

This work was published as a first-author publication [67] and with the permission adapted and reprinted from:

Nytka M., Wan J., Tureček F., Lemr K. Cyclic ion mobility of isomeric new psychoactive substances employing characteristic arrival time distribution profiles and adduct separation. J. Am. Soc. Mass Spectrom. 2024; https://doi.org/10.1021/jasms.4c00127

ACS open access

Author's Contribution. Marianna Nytka – investigation, formal analysis, visualization, and writing the original draft.

New psychoactive substances were easily protonated by electrospray but were not well separated by ion mobility even at higher resolving power. Nevertheless, the arrival time distribution (ATD) profiles were characteristic of the individual isomers (see, e.g.,

Fig. 6). This agrees with the previous observations using the linear and cyclic mobility cell for isomeric oligosaccharides [79] and oligonucleotides [80]. Mass spectra of standards were inspected on the presence of sodium and potassium adducts. Only sodium adducts were present at low intensity Therefore, due to the low adduct formation Na^+, Li^+, K^+, $Ag^{+,}$ and Cs^+ salts were alternatively added to the analyzed solutions to support adduct formation and to allow their ion mobility analysis. The results showed sufficient intensities for high-resolution cTWIM experiments for solely Na^+ and Li^+ adduct ions.

5.2.1 Protonated Molecules vs Li-Adducts

The pairs 3-MMC and buphedrone or 3-FMC and 4-FMC were directly infused into the electrospray. Both pairs underwent the single pass (98 cm) separation. It enabled the recognition of the individual isomers for 3-MMC and buphedrone ([M+H]$^+$, *m/z* 178.13), but it was insufficient for the mixture (Fig. 6A).
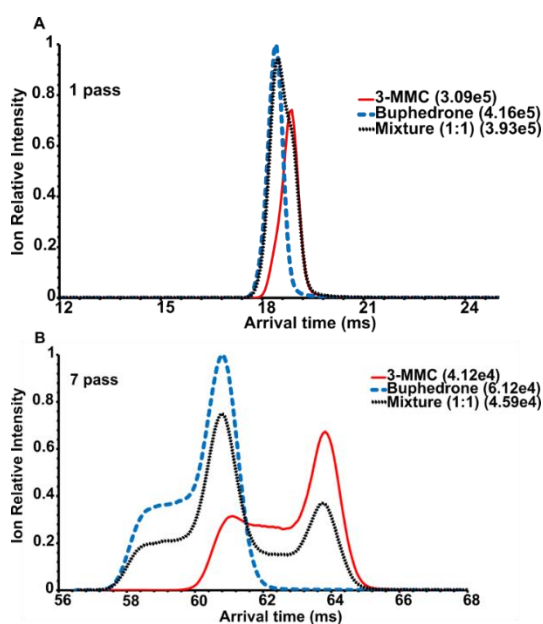

Figure 6. Extracted ATD profiles ([M+H]$^+$, *m/z* 178.13) of 3-MMC, buphedrone and their mixture (50 : 50): (A) 1 pass, (B) 7 pass experiment. The highest absolute intensity for each mobilogram is given in brackets [67]. ACS open access

Seven pass (686 cm) separation experiments for 3-MMC and buphedrone showed that we could recognize the major forms in a mixture, but complete separation was not achieved (Fig. 6B). This was consistent with the expected CCS for the keto and enol isomers of protonated 3-MMS and buphedrone that were in the narrow range of 139-141 Å^2. The narrow range was also observed for experimental CCS values.

The experimental CCS values were averaged from six data acquisitions. The cycle time and dead time were calculated from one pass and seven pass data of analytes. CCS values in 1 pass fwere 145 Å^2, and 142.1 Å^2 for 3-MMC and buphedrone, respectively. CCS values in 7 pass experiments were 142.0 Å^2 (enol-form) and 144.8 Å^2 (keto-form) for 3-MMC, and for buphedrone they were 140.2 Å^2 (enol-form) and 141.9 Å^2 (keto-form). The difference between the experimental and calculated CCS was < 3% for 3-MMC and <1% for buphedrone. These results are consistent with measurements under the same conditions taken four years ago in 2020. The standards underwent the five pass separation. The experimental C.C.S. for 3-MMC were 141.8 Å^2 and 144.8 Å^2, and for buphedrone were 139.5 Å^2 and 141.8 Å^2. These results show good reproducibility of CCS determination over multiple years.

The previously reported $^{DT}CCS_{N2}$ value for buphedrone was 141.2 Å^2 [81]. That correlates well with the cTWIM measurements and the calculated CCS for the keto form. There are no current research articles that would show CCS values for 3-MMC. Only one report of the CCS values of 3-MMC with linear TWIM measurements was found in the diploma thesis of Ondruchová Jana. In her work, the CCS were 144.9 Å^2 and 142.7 Å^2 for 3-MMC and buphedrone, respectively [82]. Those values correspond to the dominant keto form. CCS values from linear TWIM for 3-MMC correlate well with the cTWIM results. The higher error between theoretical and calculated CCS values for multipass experiments could be explained by the inconsistencies of CCS of calibrants presented in databases, sometimes ranging up to 10 Å^2 for different compounds.

It was estimated that the CCS-based resolving power R_{CCS} of about 104 was required to achieve the two-peak resolution $R_{p-p} = 1.23$ (ca. 90 % separation, defined for two Gaussian peaks of equal abundance) [83]. For buphedrone, the single pass experiment gave $R_{1,\,CCS} \approx 45$ (both keto- and enol-form contributed to peak width). After the multi-pass experiment with seven passes (L = 686 cm), we were able to separate the major isomeric forms of 3-MMC and buphedrone (experimental $R_{7,CCS} \approx 126$). The signals of both isomers were clearly detected in the mobilograms of their mixtures (Fig. 6B). While it can be sufficient for the detection of individual isomers, simple integration of mobility peaks was not possible even at higher resolving power, as the isomers' ATD profiles became broader. The less abundant enol isomer of 3-MMC still significantly overlapped with buphedrone (Fig. 6B).

The higher number of passes (higher resolving power) did not improve the separation. It just broadened the ATD profiles of isomers. Peak broadening at higher

resolving power can compromise the separation of isomers. This is more significant for more complex ATD profiles of the individual isomers. It can be a general issue when separating isomers existing in different conformer (protomer) states. However, the broadening effect can be suppressed by separating adducts of isomeric molecules with alkali metal cations. Separation of adducts has been described, e.g., for fentanyl [84], glycan [85], and flavonoid [86] isomers. On the other hand, if the broadening effect is characteristic of individual isomers, it can be advantageous. Both approaches are demonstrated in the following examples.

Multiple linear regression (MLR) was performed on ATD profiles of protonated 3-MMC and buphedrone to determine the isomeric ratio. The isomeric ratio was a_1:a_2, where $y = a_0 + a_{1x1} + a_{2x2}$.

Averaged intensities of the overall extracted ATD profiles of the individual isomers (six data acquisitions) and the intensity of the ATD profile of the mixture (six data acquisitions individually) represented the input data, independent (x_1,x_2) and dependent (y) variables, respectively. Compared to the previous fitting procedure using Gaussian functions [79], the new data processing was more accessible to implement because MLR is the common part of routinely used software, such as OriginPro. The relationship between the determined and given content of 3-MMC showed good linearity .
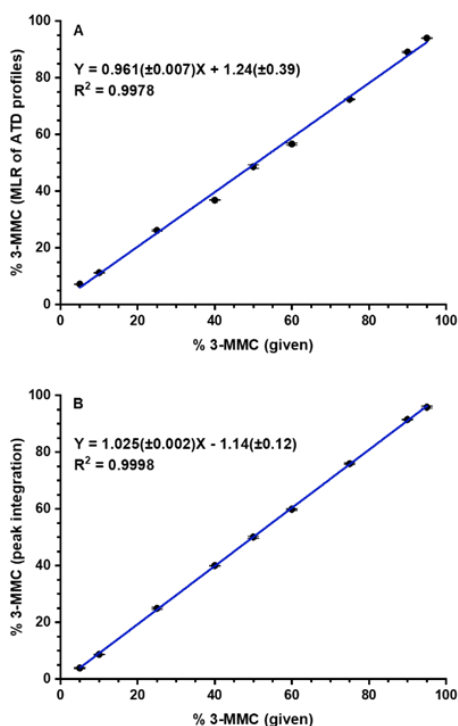
Figure 7. Determination of 3-MMC in the mixture with buphedrone: (A) Multiple linear regression (MLR) applied to ATD profiles of protonated molecules, seven pass separation; (B) Ion mobility of lithiated molecules, ten pass separation. Standard deviations of slope and intercept are shown in brackets. Each point was measured in six data acquisitions [67]. ACS open access

This proves that the proposed procedure is useful in defining the isomeric ratio using the ATD profiles and MLR Notably, the linear calibration curve was obtained in single-pass experiments but in a limited range (5%-75% of 3-MMC) due to insufficient detection of buphedrone in excess of 3-MMC in a mixture (95:5 and 90:10). The higher resolving power helped to overcome this issue (Fg. 7A).

For MLR application, we evaluated stability of ATD profiles. Good intra-day repeatability of mobilograms of the isomers was observed. Inter-day measurements showed the shift in arrival time and/or relative intensities of the conformers (protomers), which led to a change in the shape of the mobilograms.

This shift might be due to the drift or collision gas pressure variation for the same instrumental setting. To minimize such variation, we recommend waiting two hours to stabilize the gas pressure after switching from standby to run mode. If necessary, the shift in the arrival time was compensated by peak alignment.

Sodium and lithium adducts of 3-MMC and buphedrone were separated in 10 pass experiments (980 cm). Lithium adducts showed more than one order higher signal intensity than sodium adducts (see Fig.8). Therefore, $[M+Li]^+$ ions were selected for isomeric ratio determination. Baseline separation allowed direct integration of the peaks (Fig. 32) and provided good linearity for the dependence between the determined and given 3-MMC content (Fig. 8B). The adduct ion formation can affect the conformation of ions in the gas phase due to the coordination at different positions [87,88] The conformers for $[M+Li]^+$ (Fig. 8B) were not observed compared to protonated molecules. This result was consistent with the calculations of structures and CCS. The differences in theoretical CCS for keto (ions **1a**$^+$ and **2a**$^+$) and enol (ions **1b**$^+$ and **2b**$^+$) isomers of protonated molecules of 3-MMC and buphedrone were 0.4 % and 0.6 %, respectively. For both **1**$^+$ and **2**$^+$, the enol isomers had higher Gibbs energies than the keto forms (Table 1) and thus could contribute as minor components to the signal at *m/z* 178.13 in mobilograms, as manifested by peaks broadening (Fig. 6B). For lithiated isomers, the keto forms (ions **3a**$^+$ and **4a**$^+$) differed by 1.5 % in CCS Enol isomers of the Li$^+$ adducts (ions **3b**$^+$ and **4b**$^+$) showed much higher

energies than the keto-tautomers and were unlikely to significantly contribute to the signal at *m/z* 184.13 in mobilograms. This was consistent with the well separated symmetrical peaks of Li⁺ adducts in ATD. (Fig. 8B). The experimental CCS values for $[M+Li]^+$ of 3-MMC were 154.0 Å^2 (1 pass separation) and 153.3 Å^2 (10 pass), and for buphedrone 151.2 Å^2 (1 pass) and 150.4 Å^2 (10 pass). Those results fit well with the theoretically calculated ones (see Fig. 8; difference < 2 %). The relationships in Fig. 7 showed that the separation of lithium adducts gave lower standard deviations of intercept and slope and a slightly higher coefficient of determination than the MLR approach. Nevertheless, both approaches are comparable and useful for the determination of isomeric ratios in mixtures.
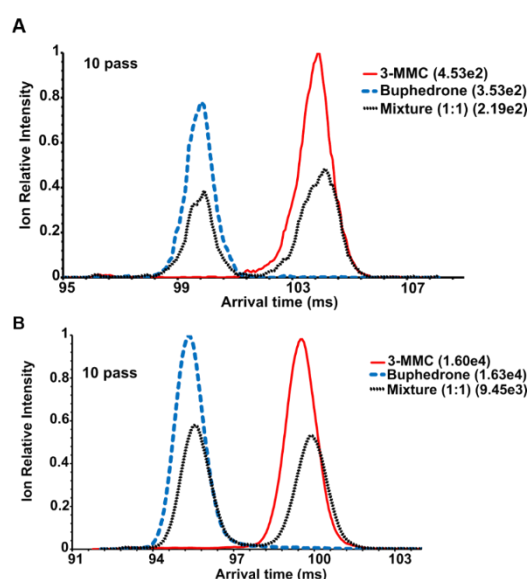

Figure 8. Extracted ATD profiles of 3-MMC, buphedrone and their mixture (50 : 50), ten pass experiment of A) $[M+Na]^+$, *m/z* 200.10 and B) $[M+Li]^+$, *m/z* 184.13. The highest absolute intensity for each mobilogram is given in brackets [67]. ACS open access.

Protonated molecules of 3-FMC and 4-FMC produced symmetrical and highly overlapping mobility peaks that hindered the determination of the isomeric ratio by multiple linear regression in single pass separation (Fig. 9A). Ten pass (980 cm) separation provided partial separation of the isomers in a mixture and produced the characteristic mobilogram profiles for individual isomers, as shown in Fig. 9B.
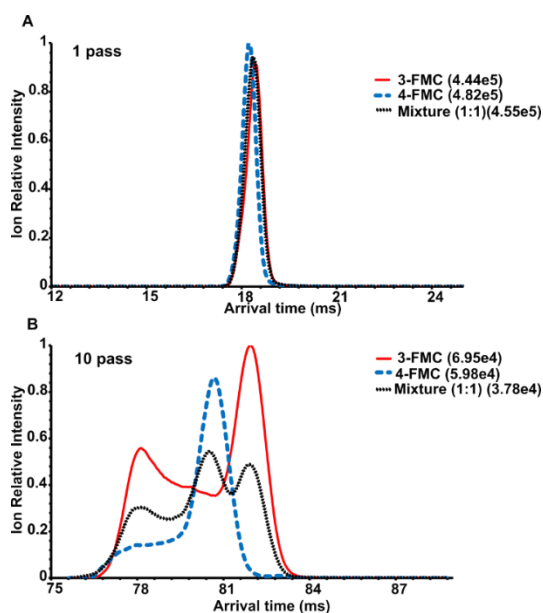
Figure 9. Extracted ATD profiles ([M+H]$^+$, *m/z* 182.10) of 3-FMC, 4-FMC, and their mixture (50 : 50): (A) 1 pass, (B) 10 pass experiment. The highest absolute intensity for each mobilogram is given in the brackets [67]. ACS open access.

The high resolving power enabled MLR to produce the linear dependence of determined and given 3-FMC content in a mixture (Y = 1.010 ($\pm$0.009)X + 0.38($\pm$0.52), R^2=0.9961). These results highlight the advantage of cyclic TWIMS over the linear cell.

It was observed that 3-FMC and 4-FMC did not efficiently form the sodium adducts (Fig. 10A). [M+Li]$^+$ were generated with sufficient intensity, enabling partial separation in 25 pass experiments (2450 cm) shown in Fig. 10B. It allowed the peak integration (Y = 1.018($\pm$0.10)X + 2.53($\pm$0.59), R^2 = 0.9849). The relationship between the determined and given content of 3-FMC in a mixture of protonated and lithiated molecules produced comparable standard deviations of slope, intercept, and coefficient of determination. MLR of ATD profiles gave similar results to the separation of adducts and may be more advantageous when adduct formation or separation is insufficient, as in the case of sodium adducts.
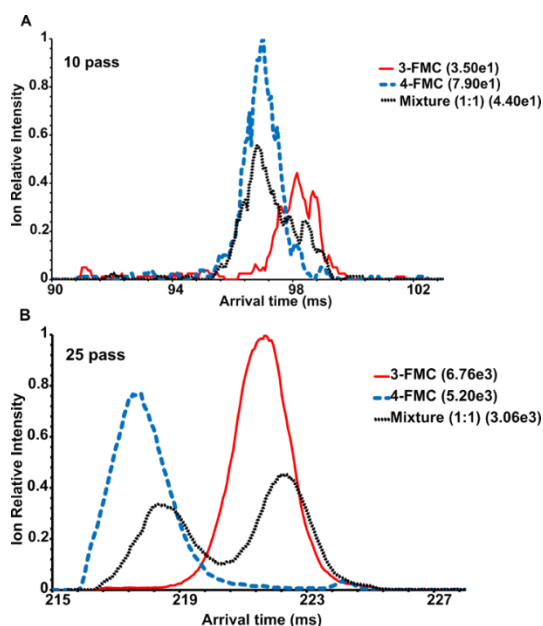
Figure 10. Extracted ATD profiles of 3-FMC, 4-FMC, and their mixture (50 : 50): (A) [M+Na]⁺, *m/z* 204.08; 10 passes; (B) [M+Li]⁺, *m/z* 188.11; 25 passes. The highest absolute intensity for each mobilogram is given in brackets [67]. ACS open access.

5.2.2 Flow Injection Analysis of Isomers using Ion Mobility-Mass Spectrometry of Fragment Ions

BDB and methedrone showed a significant difference in the intensities of protonated molecules. BDB and methedrone belong to phenylamines and synthetic cathinones, respectively. Both isomers produce symmetrical and completely overlapped ATD profiles. Signal intensities at the peak maxima in a single pass and three pass separation showed the two order difference using the default instrument settings. Settings for labile analytes were used to decrease the fragmentation of protonated BDB and increase its intensity. Nevertheless, the three pass experiment did not improve the separation of the isomers and led to a decrease in the intensity of BDB. Even at these conditions, both isomers produced symmetric and overlapped peaks with a significant difference in intensity, which hindered the use of the ATD profiles.

Furthermore, we proposed another approach using the ATD profiles of the fragments. The experiments were performed by flow injection analysis, allowing faster data acquisition. The precursor ion *m/z* 194.11 ([M+H]⁺) was isolated in the quadrupole and fragmented in the trap cell (before the cIM cell). BDB and methedrone produced product ions at *m/z* 135.04, and methedrone also fragmented to *m/z* 135.08.
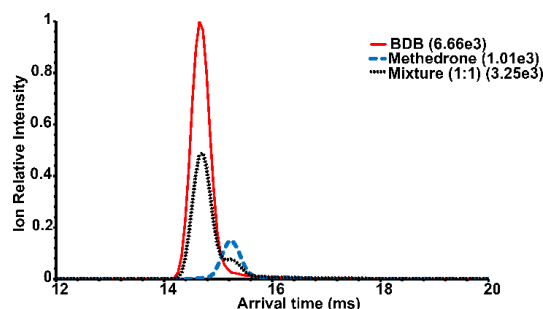
Figure 11. Extracted ATD profiles of fragment ions (*m/z* 135.04-135.08) of BDB, methedrone, and their mixture (50:50) in single pass separation. The highest absolute intensity for each mobilogram is given in brackets [67]. ACS open access.

Both fragments (*m/z* 135.04 and *m/z* 135.08) were included in the extracted ATD profiles (Fig. 11). The mobilograms were characteristic for each isomer and partially separated, which allowed the use of the MLR approach. The linear dependence between the determined and given BDB content in the mixture produced a lower coefficient of determination and higher standard deviations for slope and intercept compared to the other two isomeric pairs (Y=0.989($\pm$0.019)X-0.21($\pm$1.08), R^2 = 0.9822). This might be due to the more complex experiment requiring the generation and separation of the fragmented ions. The determined contents for 90% and 95% of BDB in a mixture were not significantly different. Nevertheless, the determination of isomeric ratios and separation of isomers were still possible, although with lower accuracy in a higher content of BDB.

5.2.3 Desorption Electrospray Ionization of Isomers

Similarly to the direct infusion and flow injection analysis, all three pairs were ionized by DESI, providing the characteristic ATD profiles with lower intensities (Fig. 12). The shapes of the ATD profiles are similar to the ESI source for 3-FMC and 4-FMC (Fig. 9B and 12B). In contrast, due to the different ionization mechanisms, the ATD profiles for 3-MMC and buphedrone are significantly different (Fig. 6B and 12A). Therefore, it is impossible to use ATD profiles of individual isomers produced by ESI to evaluate the samples measured by the DESI source.
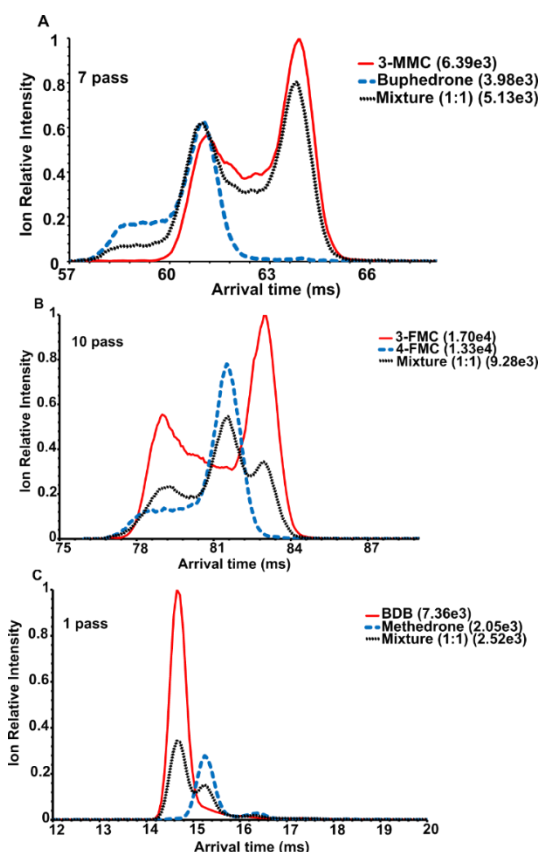
Figure 12. Extracted ATD profiles of individual isomers and their mixtures (50 : 50) desorbed and ionized by DESI: (A) 3-MMC and buphedrone ([M+H]$^+$, *m/z* 178.13), 7 passes; (B) 3-FMC and 4-FMC ([M+H]$^+$, *m/z* 182.10), 10 passes; (C) fragment ions *(m/z 135.04-135.08)* of BDB, methedrone, 1 pass. The highest absolute intensity for each mobilogram is given in brackets [67]. ACS open access.

The analytes were pipetted onto the hydrophobic spot and left to dry on air. It formed the heterogeneous layer that explained higher data variability (error bars Fig. 13) compared to ESI. Linear dependence between the determined and given content of 3-MMC in a mixture (Fig. 13A) showed a lower coefficient of determination and higher standard deviations for slope and intercept in contrast to the other two pairs. Despite that, the increase in the 3-MMC content was visible. For other two pairs, higher coefficients of determination, lower standard devitions of slopes and intercepts as well as narrower error bars were achieved. DESI-cIM-MS proved the applicability of the ATD profile-based method on solid samples.
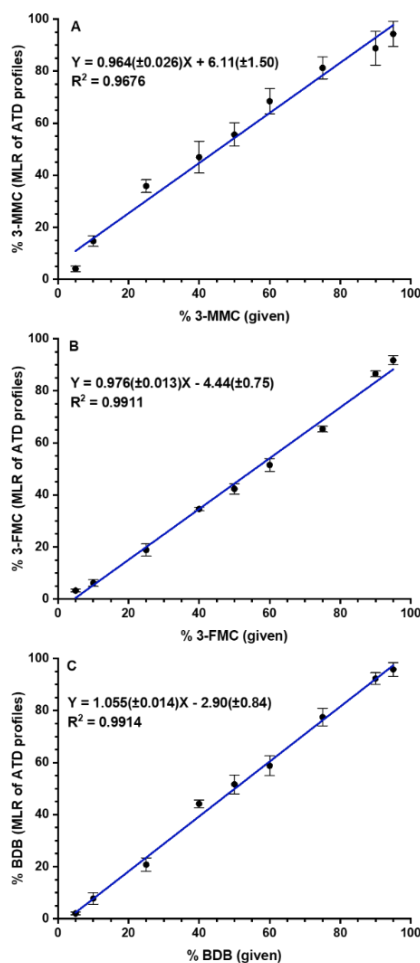
Figure 13. Determination of isomeric ratios using DESI and multiple linear regression (MLR) applied to ATD profiles: (A) 3-MMC in the mixture with buphedrone, ($[M+H]^+$, *m/z* 178.13, 7 passes); (B) 3-FMC in the mixture with 4-FMC ($[M+H]^+$, *m/z* 182.10, 10 passes); (C) BDB in the mixture with methedrone (fragment ions at *m/z* 135.04-135.08, 1 pass). Standard deviations of slope and intercept are shown in brackets. Each point was measured in six data acquisitions [67]. ACS open access.

5.2.4 Analysis of the Model Samples

Flow injection analysis was used to analyze two isomeric pairs of synthetic cathinones (four analytes) in a mixture. Calibration was prepared in a range of 5% to 45%. Six replicates of calibration and sample solutions were injected (5 µL) into the flow of methanol-water (50:50, v/v). FIA with autosampler allowed rapid and automatic data, decreasing the acquisition time to 3 hours for 96 injections with the time of the analysis 1.5 min when compared to direct infusion (more than one week). Linear correlation for 3-MMC/buphedrone and 3-FMC/4-FMC showed good linearity with the coefficient of

determination 0.9974 (Y=0.867(±0.09)X + 2.43(±0.26)) and 0.9988 (Y=0.987(±0.007)X + 0.91(±0.21)), respectively. In model samples containing two pairs of isomers in a mixture with 10% of 3-MMC and 3-FMC, the determined content of 3-MMC was 9.3% with a standard deviation of 0.37, and for 3-FMC, it was 11.0 %, and 0.42. The obtained results showed a good accuracy of this method.

5.2.5 Conclusion

Two approaches based on the separation of lithium adducts and on multiple linear regression using the characteristic ATD profiles of individual isomers and ATD profiles from the isomeric mixtures were shown to be efficient in distinguishing and quantifying NPS isomers. The formation of lithium adducts by adding its salt to the sample solution showed the best results for these applications. The higher resolving power of cyclic TWIMS in multipass experiments improved the separation of Li-ion adducts, whereas the mobility peaks of protonated molecules were broadened and still overlapped due to the presence of tautomers associated with individual ion structures. In the previous report, ATD profiles were fitted by Gaussian functions, and a single ATD function was generated for each isomer. These ATD functions allowed determining isomeric ratios of oligosaccharides by ESI linear TWIMS [79]. Here, the fitting was replaced by multiple linear regression, which noticeably simplified the analysis. Direct infusion experiments confirmed that both approaches, the separation of lithiated molecules and the use of ATD profiles characteristic to isomers, are comparable.

The isomeric pair of BDB/methedrone showed significant differences in the intensities of $[M+H]^+$ ions and completely overlapping mobility peaks. In this case, the ATD profiles of the fragment ions allowed us to achieve a successful analysis, proving that the proposed approach is not limited to only protonated molecules. These analyses were performed by FIA as an alternative to direct infusion. Obviously, this approach is feasible for liquid samples. In the case of solid samples, desorption electrospray was utilized. DESI-cIM-MS provided characteristic ATD profiles of isomers, although they differed to some extent from those obtained by electrospray. This could be attributed to the different ionization mechanisms, electrospraying of solutions vs. desorption, and ionization from solid samples. Finally, the rapid analysis of a mixture containing two isomeric pairs was demonstrated. FIA combined with an autosampler enabled automatic data acquisition, speeding up the analysis.

The mean mobility values were recently used to identify cathinones, while isomeric ratios have not been determined [89]. We confirmed the excellent repeatability of the ATD profiles and included the entire ATD profiles analyzing isomeric mixtures. Although the higher resolving power of cyclic TWIMS may not allow for the complete separation of isomers, it may help to generate more distinct ATD profiles of isomers.

The ATD profile-based approach can generally be used to analyze isomeric molecules by ion mobility. While the integration of peaks requires a good separation, the described approach is applicable even for overlapping signals.

6 CONCLUSION AND OUTLOOK

Coupling different ionization techniques with IM-MS has excellent potential for detecting and separating isomers in mixtures. Nevertheless, some AIMS have never been hyphened with ion mobility; some are only at the beginning of this fruitful collaboration.

NanoDESI, with the improved custom-made inlet, showed great applicability in detecting the NPS on the silanized glass surface. The increased ionization efficiency of nanoDESI should encourage new applications. Nevertheless, a few modifications can still be made, starting with automating spraying solvent delivery by possibly connecting it to a nanoLC pump, which will allow high-resolution MS imaging measurements as well as coupling it with cTWIM.

Ion mobility faces a new revolution with the production of high-resolving power IMS systems (cyclic TWIM, SLIM, TIMS), which has opened the possibility for new applications. cTWIM can reveal the hidden conformers/protomers, which cannot be seen in linear TWIM or lower resolving power instruments.

A new, simple approach for isomeric ratio determination in mixtures was performed by multiple linear regression of characteristic ATD profiles that overlapped in a mixture for protonated ions (generally for any overlapped ions). This method also showed excellent results by using the characteristic ATDs of fragment ions. Coupling the DESI source with cTWIMS demostrated the application of our approach on solid samples. Therefore, it might also be used in the future for quantitative imaging experiments. The different profiles of ATDs produced by ESI and DESI experiments could lead to more fundamental experiments based on the effect of desorption in DESI on ATD profiles in cTWIM and how different parameters of ion optics can influence the results.

REFERENCES

[1]   Z. Takáts, J.M. Wiseman, B. Gologan, R.G. Cooks, Mass Spectrometry Sampling Under Ambient Conditions with Desorption Electrospray Ionization, Science (1979) 306 (2004) 471–473. https://doi.org/10.1126/science.1104404.

[2]   R.B. Cody, J.A. Laramée, H.D. Durst, Versatile new ion source for the analysis of materials in open air under ambient conditions, Anal Chem 77 (2005) 2297–2302. https://doi.org/10.1021/ac050162j.

[3]   C.L. Feider, A. Krieger, R.J. Dehoog, L.S. Eberlin, Ambient Ionization Mass Spectrometry: Recent Developments and Applications, Anal Chem 91 (2019) 4266–4290. https://doi.org/10.1021/acs.analchem.9b00807.

[4]   KI. Kocurek, R.L. Griffiths, H.J. Cooper, Ambient ionisation mass spectrometry for in situ analysis of intact proteins, Journal of Mass Spectrometry 53 (2018) 565–578. https://doi.org/10.1002/jms.4087.

[5]   J. Balog, S. Kumar, J. Alexander, O. Golf, J. Huang, T. Wiggins, N. Abbassi-Ghadi, A. Enyedi, S. Kacska, J. Kinross, G.B. Hanna, J.K. Nicholson, Z. Takats, In Vivo Endoscopic Tissue Identification by Rapid Evaporative Ionization Mass Spectrometry (REIMS), Angewandte Chemie 127 (2015) 11211–11214. https://doi.org/10.1002/ange.201502770.

[6]   A.R. Venter, K.A. Douglass, J.T. Shelley, G. Hasman, E. Honarvar, Mechanisms of real-time, proximal sample processing during ambient ionization mass spectrometry, Anal Chem 86 (2014) 233–249. https://doi.org/10.1021/ac4038569.

[7]   M. Nytka, L. Borovcová, P. Fryčák, P. Barták, K. Lemr, Signal enhancement in desorption nanoelectrospray ionization by custom-made inlet with pressure regulation, Journal of Mass Spectrometry 55 (2020). https://doi.org/10.1002/jms.4642.

[8]   Z. Takáts, J.M. Wiseman, R.G. Cooks, Ambient mass spectrometry using desorption electrospray ionization (DESI): Instrumentation, mechanisms and applications in forensics, chemistry, and biology, Journal of Mass Spectrometry 40 (2005) 1261–1275. https://doi.org/10.1002/jms.922.

[9]   J.B. Fenn, Ion Formation from Charged Droplets: Roles of Geometry, Energy, and Time, J Am Soc Mass Spectrom 4 (1993) 524–535.

[10]   A. Venter, P.E. Sojka, R.G. Cooks, Droplet dynamics and ionization mechanisms in desorption electrospray ionization mass spectrometry, Anal Chem 78 (2006) 8549–8555. https://doi.org/10.1021/ac0615807.

[11]   R. Javanshad, R. Panth, T.L. Maser, A.R. Venter, Helium assisted desorption and spray ionization, Int J Mass Spectrom 479 (2022). https://doi.org/10.1016/j.ijms.2022.116891.

[12] M. Volný, A. Venter, S.A. Smith, M. Pazzi, R.G. Cooks, Surface effects and electrochemical cell capacitance in desorption electrospray ionization, Analyst 133 (2008) 525–531. https://doi.org/10.1039/b717693g.

[13] D.R. Ifa, L.M. Gumaelius, L.S. Eberlin, N.E. Manicke, R.G. Cooks, Forensic analysis of inks by imaging desorption electrospray ionization (DESI) mass spectrometry, Analyst 132 (2007) 461–467. https://doi.org/10.1039/b700236j.

[14] A. Khatami, S.S. Prova, A.K. Bagga, M. Yan Chi Ting, G. Brar, D.R. Ifa, Detection and imaging of thermochromic ink compounds in erasable pens using desorption electrospray ionization mass spectrometry, Rapid Communications in Mass Spectrometry 31 (2017) 983–990. https://doi.org/10.1002/rcm.7867.

[15] M. Friia, V. Legros, J. Tortajada, W. Buchmann, Desorption electrospray ionization - Orbitrap mass spectrometry of synthetic polymers and copolymers, Journal of Mass Spectrometry 47 (2012) 1023–1033. https://doi.org/10.1002/jms.3057.

[16] J.A. Amalian, T. Mondal, E. Konishcheva, G. Cavallo, B.E. Petit, J.F. Lutz, L. Charles, Desorption Electrospray Ionization (DESI) of Digital Polymers: Direct Tandem Mass Spectrometry Decoding and Imaging from Materials Surfaces, Adv Mater Technol 6 (2021). https://doi.org/10.1002/admt.202001088.

[17] M.F. Mirabelli, A. Chramow, E.C. Cabral, D.R. Ifa, Analysis of sexual assault evidence by desorption electrospray ionization mass spectrometry, Journal of Mass Spectrometry 48 (2013) 774–778. https://doi.org/10.1002/jms.3205.

[18] I. Cotte-Rodríguez, R.G. Cooks, Non-proximate detection of explosives and chemical warfare agent simulants by desorption electrospray ionization mass spectrometry, Chemical Communications (2006) 2968–2970. https://doi.org/10.1039/b606020j.

[19] F. Bianchi, A. Gregori, G. Braun, C. Crescenzi, M. Careri, Micro-solid-phase extraction coupled to desorption electrospray ionization-high-resolution mass spectrometry for the analysis of explosives in soil, Anal Bioanal Chem 407 (2015) 931–938. https://doi.org/10.1007/s00216-014-8208-7.

[20] A.M. Porcari, J. Zhang, K.Y. Garza, R.M. Rodrigues-Peres, J.Q. Lin, J.H. Young, R. Tibshirani, C. Nagi, G.R. Paiva, S.A. Carter, L.O. Sarian, M.N. Eberlin, L.S. Eberlin, Multicenter Study Using Desorption-Electrospray-Ionization-Mass-Spectrometry Imaging for Breast-Cancer Diagnosis, Anal Chem 90 (2018) 11324–11332. https://doi.org/10.1021/acs.analchem.8b01961.

[21] S. Banerjee, R.N. Zare, RJ Tibshirani, CA Kunder, R. Nolley, R. Fan, J.D. Brooks, G.A. Sonn, Diagnosis of prostate cancer by desorption electrospray ionization mass spectrometric imaging of small metabolites and lipids, Proc Natl Acad Sci U S A 114 (2017) 3334–3339. https://doi.org/10.1073/pnas.1700677114.

[22] K. Margulis, A.S. Chiou, S.Z. Aasi, R.J. Tibshirani, J.Y. Tang, R.N. Zare, Distinguishing malignant from benign microscopic skin lesions using desorption electrospray ionization mass spectrometry imaging, Proc Natl Acad Sci U S A 115 (2018) 6347–6352. https://doi.org/10.1073/pnas.1803733115.

[23] K.A. Douglass, A.R. Venter, Protein analysis by desorption electrospray ionization mass spectrometry and related methods, Journal of Mass Spectrometry 48 (2013) 553–560. https://doi.org/10.1002/jms.3206.

[24] Ranc Václav, Havlicek Vladimír, Bednar Petr, Lemr Karel, Desorption electrospray: A modern tool for organic surface analysis., Chem. Listy 101 (2007) 524–529.

[25] P.J. Roach, J. Laskin, A. Laskin, Nanospray desorption electrospray ionization: An ambient method for liquid-extraction surface sampling in mass spectrometry, Analyst 135 (2010) 2233–2236. https://doi.org/10.1039/c0an00312c.

[26] S.R. Ellis, S.H. Brown, M. In Het Panhuis, S.J. Blanksby, T.W. Mitchell, Surface analysis of lipids by mass spectrometry: More than just imaging, Prog Lipid Res 52 (2013) 329–353. https://doi.org/10.1016/j.plipres.2013.04.005.

[27] L. Hartmanová, I. Lorencová, M. Volný, P. Fryčák, V. Havlíček, H. Chmelíčková, T. Ingr, K. Lemr, Lateral resolution of desorption nanoelectrospray: A nanospray tip without nebulizing gas as a source of primary charged droplets, Analyst 141 (2016) 2150–2154. https://doi.org/10.1039/c5an02665b.

[28] L. Hartmanová, P. Fryčák, M. Soural, F. Tureček, V. Havlíček, K. Lemr, Ion internal energy, salt tolerance and a new technical improvement of desorption nanoelectrospray, Journal of Mass Spectrometry 49 (2014) 750–754. https://doi.org/10.1002/jms.3383.

[29] V. Ranc, V. Havlíček, P. Bednar, K. Lemr, Nano-Desorption Electrospray and Kinetic Method in Chiral Analysis of Drugs in Whole Human Blood Samples, European Journal of Mass Spectrometry 14 (2008) 411–417. https://doi.org/10.1255/ejms.978.

[30] L. Hartmanova, V. Ranc, B. Papouskova, P. Bednar, V. Havlicek, K. Lemr, Fast profiling of anthocyanins in wine by desorption nano-electrospray ionization mass spectrometry, J Chromatogr A 1217 (2010) 4223–4228. https://doi.org/10.1016/j.chroma.2010.03.018.

[31] United Nations Office on Drugs and Crime, The Synthetic Drug Phenomenon, World Drug Report 2023, 2023. https://doi.org/https://doi.org/10.18356/9789210028233c022.

[32] E. Cuypers, A.J. Bonneure, J. Tytgat, The use of presumptive color tests for new psychoactive substances, Drug Test Anal 8 (2016) 137–141. https://doi.org/10.1002/dta.1847.

[33] H. Muhamadali, A. Watt, Y. Xu, M. Chisanga, A. Subaihi, C. Jones, D.I. Ellis, O.B. Sutcliffe, R. Goodacre, Rapid detection and quantification of novel psychoactive substances (NPS) using Raman spectroscopy and surface-enhanced Raman scattering, Front Chem 7 (2019). https://doi.org/10.3389/fchem.2019.00412.

[34]   E. G. de Campos, A.J. Krotulski, B. S. De Martinis, J.L. Costa, Identification of synthetic cathinones in seized materials: A review of analytical strategies applied in forensic chemistry, WIREs Forensic Science 4 (2022). https://doi.org/10.1002/wfs2.1455.

[35]   V. Bolcato, C. Carelli, A. Radogna, F. Freni, M. Moretti, L. Morini, New synthetic cathinones and phenylethylamine derivatives analysis in hair: A review, Molecules 26 (2021). https://doi.org/10.3390/molecules26206143.

[36]   D. Florou, V.A. Boumba, Hair analysis for New Psychoactive Substances (NPS): Still far from becoming the tool to study NPS spread in the community?, Toxicol Rep 8 (2021) 1699–1720. https://doi.org/10.1016/j.toxrep.2021.09.003.

[37]   F.A. Esteve-Turrillas, S. Armenta, M. de la Guardia, Sample preparation strategies for the determination of psychoactive substances in biological fluids, J Chromatogr A 1633 (2020). https://doi.org/10.1016/j.chroma.2020.461615.

[38]   N. Talaty, C.C. Mulligan, D.R. Justes, A.U. Jackson, R.J. Noll, R.G. Cooks, Fabric analysis by ambient mass spectrometry for explosives and drugs, Analyst 133 (2008) 1532–1540. https://doi.org/10.1039/b807934j.

[39]   N. Stojanovska, M. Tahtouh, T. Kelly, A. Beavis, S. Fu, Presumptive analysis of 4-methylmethcathinone (mephedrone) using Desorption Electrospray Ionisation - Mass Spectrometry (DESI-MS), Australian Journal of Forensic Sciences 46 (2014) 411–423. https://doi.org/10.1080/00450618.2013.879206.

[40]   N. Stojanovska, T. Kelly, M. Tahtouh, A. Beavis, S. Fu, Analysis of amphetamine-type substances and piperazine analogues using desorption electrospray ionisation mass spectrometry, Rapid Communications in Mass Spectrometry 28 (2014) 731–740. https://doi.org/10.1002/rcm.6832.

[41]   JFA Filho, NA dos Santos, K.B. Borges, V. Lacerda, F.S. Pelição, W. Romão, Fiber spray ionization mass spectrometry in forensic chemistry: A screening of drugs of abuse and direct determination of cocaine in urine, Rapid Communications in Mass Spectrometry 34 (2020). https://doi.org/10.1002/rcm.8747.

[42]   A.H. Grange, G.W. Sovocool, Detection of illicit drugs on surfaces using direct analysis in real time (DART) time-of-flight mass spectrometry, Rapid Communications in Mass Spectrometry 25 (2011) 1271–1281. https://doi.org/10.1002/rcm.5009.

[43]   R.A. Musah, M.A. Domin, M.A. Walling, J.R.E. Shepard, Rapid identification of synthetic cannabinoids in herbal samples via direct analysis in real time mass spectrometry, Rapid Communications in Mass Spectrometry 26 (2012) 1109–1114. https://doi.org/10.1002/rcm.6205.

[44]   M.A. Marino, B. Voyer, R.B. Cody, A.J. Dane, M. Veltri, L. Huang, Rapid Identification of Synthetic Cannabinoids in Herbal Incenses with DART-MS and NMR, J Forensic Sci 61 (2016) 82–91. https://doi.org/10.1111/1556-4029.12932.

[45] L. Habala, J. Valentová, I. Pechová, M. Fuknová, F. Devínsky, DART - LTQ ORBITRAP as an expedient tool for the identification of synthetic cannabinoids, Leg Med 20 (2016) 27–31. https://doi.org/10.1016/j.legalmed.2016.03.006.

[46] J. Ji, J. Wang, Y. Zhang, Rapid screening of 23 synthetic cannabinoids in blood by direct analysis in real time - Tandem mass spectrometry, Int J Mass Spectrom 469 (2021). https://doi.org/10.1016/j.ijms.2021.116667.

[47] C.N. McEwen, R.G. McKay, B.S. Larsen, Analysis of solids, liquids, and biological tissues using solids probe introduction at atmospheric pressure on commercial LC/MS instruments, Anal Chem 77 (2005) 7826–7831. https://doi.org/10.1021/ac051470k.

[48] E. Jagerdeo, A. Wriston, Rapid analysis of forensic-related samples using two ambient ionization techniques coupled to high-resolution mass spectrometers, Rapid Communications in Mass Spectrometry 31 (2017) 782–790. https://doi.org/10.1002/rcm.7844.

[49] T.H. Kuo, E.P. Dutkiewicz, J. Pei, C.C. Hsu, Ambient Ionization Mass Spectrometry Today and Tomorrow: Embracing Challenges and Opportunities, Anal Chem 92 (2020) 2353–2363. https://doi.org/10.1021/acs.analchem.9b05454.

[50] A.E. Ashcroft, F. Sobott, V. Gabelica, New Developments in Mass Spectrometry No. 11 Ion Mobility-Mass Spectrometry: Fundamentals and Applications Edited 1.1 What is Ion Mobility Spectrometry? 1.1.1 Spectrometry Ion Mobility-Mass Spectrometry: an Overview, 2022. www.rsc.org.

[51] L.A. Viehland, E.A. Mason, Gaseous Ion Mobility in Electric Fields of Arbitrary Strength*, Ann Phys (N Y) 91 (1975) 499–533.

[52] W.F. Siems, L.A. Viehland, H.H. Hill, Improved momentum-transfer theory for ion mobility. 1. Derivation of the fundamental equation, Anal Chem 84 (2012) 9782–9791. https://doi.org/10.1021/ac301779s.

[53] V. Gabelica, E. Marklund, Fundamentals of ion mobility spectrometry, Curr Opin Chem Biol 42 (2018) 51–59. https://doi.org/10.1016/j.cbpa.2017.10.022.

[54] V. Gabelica, A.A. Shvartsburg, C. Afonso, P. Barran, J.L.P. Benesch, C. Bleiholder, M.T. Bowers, A. Bilbao, M.F. Bush, J.L. Campbell, I.D.G. Campuzano, T. Causon, B.H. Clowers, C.S. Creaser, E. De Pauw, J. Far, F. Fernandez-Lima, J.C. Fjeldsted, K. Giles, M. Groessl, C.J. Hogan, S. Hann, H.I. Kim, R.T. Kurulugama, J.C. May, J.A. McLean, K. Pagel, K. Richardson, M.E. Ridgeway, F. Rosu, F. Sobott, K. Thalassinos, S.J. Valentine, T. Wyttenbach, Recommendations for reporting ion mobility Mass Spectrometry measurements, Mass Spectrom Rev 38 (2019) 291–320. https://doi.org/10.1002/mas.21585.

[55] J.C. May, J.A. McLean, Ion mobility-mass spectrometry: Time-dispersive instrumentation, Anal Chem 87 (2015) 1422–1436. https://doi.org/10.1021/ac504720m.

[56] J.N. Dodds, E.S. Baker, Ion Mobility Spectrometry: Fundamental Concepts, Instrumentation, Applications, and the Road Ahead, J Am Soc Mass Spectrom 30 (2019) 2185–2195. https://doi.org/10.1007/s13361-019-02288-2.

[57] SD. Pringle, K. Giles, J.L. Wildgoose, J.P. Williams, S.E. Slade, K. Thalassinos, R.H. Bateman, M.T. Bowers, J.H. Scrivens, An investigation of the mobility separation of some peptide and protein ions using a new hybrid quadrupole/travelling wave IMS/oa-ToF instrument, Int J Mass Spectrom 261 (2007) 1–12. https://doi.org/10.1016/j.ijms.2006.07.021.

[58] A.A. Shvartsburg, R.D. Smith, Fundamentals of traveling wave ion mobility spectrometry, Anal Chem 80 (2008) 9689–9699. https://doi.org/10.1021/ac8016295.

[59] K. Giles, J.P. Williams, I. Campuzano, Enhancements in travelling wave ion mobility resolution, in: Rapid Communications in Mass Spectrometry, 2011: pp. 1559–1566. https://doi.org/10.1002/rcm.5013.

[60] A.T. Kirk, C.R. Raddatz, S. Zimmermann, Separation of isotopologues in ultra-high-resolution ion mobility spectrometry, Anal Chem 89 (2017) 1509–1515. https://doi.org/10.1021/acs.analchem.6b03300.

[61] Y.M. Ibrahim, A.M. Hamid, L. Deng, S.V.B. Garimella, I.K. Webb, E.S. Baker, R.D. Smith, New frontiers for mass spectrometry based upon structures for lossless ion manipulations, Analyst 142 (2017) 1010–1021. https://doi.org/10.1039/c7an00031f.

[62] L. Deng, I.K. Webb, S.V.B. Garimella, A.M. Hamid, X. Zheng, R. V. Norheim, S.A. Prost, G.A. Anderson, J.A. Sandoval, E.S. Baker, Y.M. Ibrahim, R.D. Smith, Serpentine Ultralong Path with Extended Routing (SUPER) High Resolution Traveling Wave Ion Mobility-MS using Structures for Lossless Ion Manipulations, Anal Chem 89 (2017) 4628–4634. https://doi.org/10.1021/acs.analchem.7b00185.

[63] K. Giles, J. Ujma, J. Wildgoose, S. Pringle, K. Richardson, D. Langridge, M. Green, A Cyclic Ion Mobility-Mass Spectrometry System, Anal Chem 91 (2019) 8564–8573. https://doi.org/10.1021/acs.analchem.9b01838.

[64] S. Ollivier, L. Tarquis, M. Fanuel, A. Li, J. Durand, E. Laville, G. Potocki-Veronese, D. Ropartz, H. Rogniaux, Anomeric Retention of Carbohydrates in Multistage Cyclic Ion Mobility (IMS n): De Novo Structural Elucidation of Enzymatically Produced Mannosides, Anal Chem 93 (2021). https://doi.org/10.1021/acs.analchem.1c00673.

[65] C. Eldrid, A. Ben-Younis, J. Ujma, H. Britt, T. Cragnolini, S. Kalfas, D. Cooper-Shepherd, N. Tomczyk, K. Giles, M. Morris, R. Akter, D. Raleigh, K. Thalassinos, Cyclic Ion Mobility-Collision Activation Experiments Elucidate Protein Behavior in the Gas Phase, J Am Soc Mass Spectrom 32 (2021) 1545–1552. https://doi.org/10.1021/jasms.1c00018.

[66] A. Kováč, P. Majerová, M. Nytka, M.Z. Cechová, P. Bednář, R. Hájek, D.A. Cooper-Shepherd, A. Muck, K. Lemr, Separation of Isomeric Tau Phosphopeptides from

Alzheimer's Disease Brain by Cyclic Ion Mobility Mass Spectrometry, J Am Soc Mass Spectrom (2023). https://doi.org/10.1021/jasms.2c00289.

[67] M. Nytka, J. Wan, F. Tureček, K. Lemr, Cyclic ion mobility of isomeric new psychoactive substances employing characteristic arrival time distribution profiles and adduct separation, J Am Soc Mass Spectrom (2024).

[68] J. He, F. Tang, Z. Luo, Y. Chen, J. Xu, R. Zhang, X. Wang, Z. Abliz, Air flow assisted ionization for remote sampling of ambient mass spectrometry and its application, Rapid Communications in Mass Spectrometry 25 (2011) 843–850. https://doi.org/10.1002/rcm.4920.

[69] S. Garimella, W. Xu, G. Huang, J.D. Harper, R.G. Cooks, Z. Ouyang, Gas-flow assisted ion transfer for mass spectrometry, Journal of Mass Spectrometry 47 (2012) 201–207. https://doi.org/10.1002/jms.2955.

[70] C. Ieritano, W.S. Hopkins, Assessing collision cross section calculations using MobCal-MPI with a variety of commonly used computational methods, Mater Today Commun 27 (2021). https://doi.org/10.1016/j.mtcomm.2021.102226.

[71] C. Ieritano, J. Crouse, J.L. Campbell, W.S. Hopkins, A parallelized molecular collision cross section package with optimized accuracy and efficiency, Analyst 144 (2019) 1660–1670. https://doi.org/10.1039/c8an02150c.

[72] A. Haack, C. Ieritano, W.S. Hopkins, MobCal-MPI 2.0: an accurate and parallelized package for calculating field-dependent collision cross sections and ion mobilities, Analyst 148 (2023) 3257–3273. https://doi.org/10.1039/d3an00545c.

[73] M. McCullagh, S. Goscinny, M. Palmer, J. Ujma, Investigations into pesticide charge site isomers using conventional IM and cIM systems, Talanta 234 (2021). https://doi.org/10.1016/j.talanta.2021.122604.

[74] M.F. Bush, Z. Hall, K. Giles, J. Hoyes, C. V. Robinson, B.T. Ruotolo, Collision cross sections of proteins and their complexes: A calibration framework and database for gas-phase structural biology, Anal Chem 82 (2010) 9557–9565. https://doi.org/10.1021/ac1022953.

[75] B.T. Ruotolo, J.L.P. Benesch, A.M. Sandercock, S.J. Hyung, C. V. Robinson, Ion mobility-mass spectrometry analysis of large protein complexes, Nat Protoc 3 (2008) 1139–1152. https://doi.org/10.1038/nprot.2008.78.

[76] I. Campuzano, M.F. Bush, C. V. Robinson, C. Beaumont, K. Richardson, H. Kim, H.I. Kim, Structural characterization of drug-like compounds by ion mobility mass spectrometry: Comparison of theoretical and experimentally derived nitrogen collision cross sections, Anal Chem 84 (2012) 1026–1033. https://doi.org/10.1021/ac202625t.

[77] K.M. Hines, D.H. Ross, K.L. Davidson, M.F. Bush, L. Xu, Large-Scale Structural Characterization of Drug and Drug-Like Compounds by High-Throughput Ion Mobility-

Mass Spectrometry, Anal Chem 89 (2017) 9023–9030. https://doi.org/10.1021/acs.analchem.7b01709.

[78] J.A. Picache, B.S. Rose, A. Balinski, K.L. Leaptrot, SD. Sherrod, J.C. May, J.A. McLean, Collision cross section compendium to annotate and predict multi-omic compound identities, Chem Sci 10 (2019) 983–993. https://doi.org/10.1039/c8sc04396e.

[79] L. Borovcová, M. Hermannová, V. Pauk, M. Šimek, V. Havlíček, K. Lemr, Simple area determination of strongly overlapping ion mobility peaks, Anal Chim Acta 981 (2017) 71–79. https://doi.org/10.1016/j.aca.2017.05.003.

[80] J. Wan, M. Nytka, H. Qian, K. Lemr, F. Tureček, Do d(GCGAAGC) Cations Retain the Hairpin Structure in the Gas Phase? A Cyclic Ion Mobility Mass Spectrometry and Density Functional Theory Computational Study, J Am Soc Mass Spectrom 34 (2023) 2323–2340. https://doi.org/10.1021/jasms.3c00228.

[81] R. Lian, F. Zhang, Y. Zhang, Z. Wu, H. Ye, C. Ni, X. Lv, Y. Guo, Ion mobility derived collision cross section as an additional measure to support the rapid analysis of abused drugs and toxic compounds using electrospray ion mobility time-of-flight mass spectrometry, Analytical Methods 10 (2018) 749–756. https://doi.org/10.1039/c7ay02808c.

[82] Ondruchová Jana, Účinný Srážkovy Průřez Při Identifikaci Drog Spojením Iontové Mobility s Hmotnostní Spectrometrií, Univerzita Palackého v Olomouci, 2016.

[83] J.N. Dodds, J.C. May, J.A. McLean, Correlating Resolving Power, Resolution, and Collision Cross Section: Unifying Cross-Platform Assessment of Separation Efficiency in Ion Mobility Spectrometry, Anal Chem 89 (2017) 12176–12184. https://doi.org/10.1021/acs.analchem.7b02827.

[84] R. Aderorho, C.D. Chouinard, Improved separation of fentanyl isomers using metal cation adducts and high-resolution ion mobility-mass spectrometry, Drug Test Anal 16 (2024) 369–379. https://doi.org/10.1002/dta.3550.

[85] X. Zheng, X. Zhang, N.S. Schocker, R.S. Renslow, D.J. Orton, J. Khamsi, R.A. Ashmus, I.C. Almeida, K. Tang, C.E. Costello, R.D. Smith, K. Michael, E.S. Baker, Enhancing glycan isomer separations with metal ions and positive and negative polarity ion mobility spectrometry-mass spectrometry analyses, Anal Bioanal Chem 409 (2017) 467–476. https://doi.org/10.1007/s00216-016-9866-4.

[86] CR de Bruin, M. Hennebelle, J.P. Vincken, W.J.C. de Bruijn, Separation of flavonoid isomers by cyclic ion mobility mass spectrometry, Anal Chim Acta 1244 (2023). https://doi.org/10.1016/j.aca.2022.340774.

[87] A.L. Rister, T.L. Martin, E.D. Dodds, Application of Group I Metal Adduction to the Separation of Steroids by Traveling Wave Ion Mobility Spectrometry, J Am Soc Mass Spectrom 30 (2019) 248–255. https://doi.org/10.1007/s13361-018-2085-9.

[88] D. Hadavi, E. de Lange, J. Jordens, Y. Mengerink, F. Cuyckens, M. Honing, Adduct ion formation as a tool for the molecular structure assessment of ten isomers in traveling wave and trapped ion mobility spectrometry, in: Rapid Communications in Mass Spectrometry, John Wiley and Sons Ltd, 2019: pp. 49–59. https://doi.org/10.1002/rcm.8419.

[89] H.A. Majeed, T.S. Bos, R.L.C. Voeten, R.F. Kranenburg, A.C. van Asten, G.W. Somsen, I. Kohler, Trapped ion mobility mass spectrometry of new psychoactive substances: Isomer-specific identification of ring-substituted cathinones, Anal Chim Acta 1264 (2023). https://doi.org/10.1016/j.aca.2023.341276.

CURRICULUM VITAE

Name:	Marianna Nytka
Year and place of birth:	1994, Uzhhorod, Ukraine
E-mail:	mariannanytka@gmail.com, marianna.nytka@upol.cz

Education

2011-2015	B.Sc. studies, Analytical Chemistry, Chemistry Faculty, Uzhhorod National University, Ukraine. Thesis: Studies of superionic materials and heat-resistant alloys as active substances of ISE.
2015-2017	M.Sc. study, Analytical Chemistry, Chemical Faculty, Uzhhorod National University, Ukraine. Thesis: Comparative characteristics of solid-state and plastificated potentiometric sensors
2017-now	Ph.D study, Analytical Chemistry, Faculty of Science, Palacky University in Olomouc, Czech Republic. Topic: Combination of ionization techniques and ion mobility-mass spectrometry in the analysis of new psychoactive substances

Internship

2019	Research stay, Department of Chemistry and Biochemistry, University of Texas at Arlington, TX, USA, 6 months (supervisor: prof. Kevin Schug).

Awards

2017-2021	Fisher Scholarship for foreigner students
2021	1st place in the section "Chemistry-Doctoral students"-Dean's Award.

Projects

2018	IGA UP: Efficient processing of samples with complex matrices, team member
2019	IGA UP: Innovative methods of analyzing samples with complex matrices, team member
2019	Support of Academic mobility at Palacky University Olomouc CZ.02.2.69/0.0/0.0/16_027/0008482 (mobility n.36)
2020	IGA_PrF_2020_030: Modern trends in the analysis of samples with complex matrices, team member
2020-2022	OA ITI – ARTECA Advanced physico-chemical methods in research and protection of cultural and art heritage CZ.0.2.1.01/0.0/0.0/17_048/0007378, team member
2020-2022	TAČR TL04000476: The effect of disinfectants on historical surfaces among visiting historical institutions during emergency epidemiological measures (SPP 663103131), team member

2021	IGA_PrF_2021_021: New trends in the analysis of complex samples, team member
2022	IGA_PrF_2022_023: Modern methods of processing complex samples, team member
2023-now	GAČR (23-07254S): "Shape of mobility peaks as a tool for discrimination of isomers by ion mobility-mass spectrometry"; team member
2023	IGA_PrF_2023_027: Application of instrumental methods in the analysis of substances in complex matrices, team member
2024	IGA_PrF_2024_026: Modern methods of analysis for complex samples

Pedagogical activities

2020	Teaching of Laboratory Documentation in English language (ACH/LADA), 1 semester
2021	Teaching of Laboratory Documentation in English language (ACH/LADA), 1 semester
2022	Teaching of Laboratory Documentation in English language (ACH/LADA), 1 semester
2023	Teaching of Practicals in Analytical Chemistry (Czech language), 1 semester
2023	Teaching of English for Chemists 2 (ACH/CHA2), 4 hours, taken and correction of exam

| 2023 | Teaching of Technical English, 4 hours |
| 2024 | Teaching of Practicals in Analytical Chemistry (Czech language), 1 semester |

International/Czech conferences and summer schools

The 43rd International Symposium on Capillary Chromatography & The 16th GCxGC Symposium – May 12th- 17th, 2019 Fort Worth, Texas USA. Poster, "Mass spectrometry of new psychoactive substances using desorption nanoelectrospray with improved custom-made inlet" Nytka M., Borovcova L., Barták P., Fryčák P., Lemr K.

Prague Meeting on Historical Perspectives of Mass Spectrometry, October 13-14, 2021 Prague, Czech Republic. Poster "Multipass Separation of Synthetic Cathinones by Cyclic Ion Mobility: Collision Cross Section Determination" Nytka M., Palmer M., Muck A., Lemr K.

Advances in Chromatography and Electrophoresis& Chiranal 2022- June 13th-16th ,2022 Olomouc, Czech Republic. Oral presentation "Cyclic ion mobility-mass spectrometry of isomeric cathinones" Nytka M., Palmer M., Muck A., Lemr K.

"Advanced Mass Spectrometry Applied To Cultural Heritage "Bordeaux Summer School and The 10th International MaSC MeetingMass Spectrometry and Chromatography in Cultural Heritage", Bordeaux, France, September 26-30, 2022

Czech Mass Spectrometry Conference 2023, Brno, June 19 – 21, 2023. Oral presentation: "Multiple linear regression of mobilograms of isomeric new synthetic drugs analyzed by cyclic ion mobility", Nytka M., Lemr K

SELECT SERIES on Tour: In-Person Meeting, Bellinzona, Switzerland, May 15th 2024. Oral presentation: "Cyclic Ion Mobility of Peptides – from Alzheimer's Disease Brain to Photochemical Crosslinking", Nytka M.

72nd ASMS Conference on Mass Spectrometry and Allied Topics, Anaheim Convention Center, Anaheim, California, USA, June 2-6, 2024. Poster: "Flow injection analysis of new psychoactive substances using cyclic ion mobility mass spectrometry", Nytka M., Tureček F., Lemr K.

Advances in Chromatography and Electrophoresis & Chiranal 2024- June 17th-20th ,2024 Olomouc, Czech Republic. Poster: "Desorption Electrospray Ionization Coupled to Cyclic Ion Mobility in Analysis of New Psychoactive Substances". Nytka M., Wan J., Tureček F., Lemr K.

Publications

Nytka M, Borovcová L, Fryčák P, Barták P, Lemr K. Signal enhancement in desorption nanoelectrospray ionization by custom-made inlet with pressure regulation. J Mass Spectrom. 2020 Oct;55(10):e4642. doi: 10.1002/jms.4642.

Liu.Y,Liu Y, Nytka M, Huang S.R, Lemr K, Turecek F. Probing d- and l-Adrenaline Binding to β2-Adrenoreceptor Peptide Motifs by Gas-Phase Photodissociation Cross-Linking and Ion Mobility Mass Spectrometry. J. Am. Soc. for Mass Spectrom. 2021, 32 (4), 1041-1052 doi: 10.1021/jasms.1c00019

Kováč A., Majerová P., Nytka M., Zajacová Cechová M., Bednář P., Hájek R., Cooper-Shepherd Dale A., Muck A., and Lemr K. Separation of Isomeric Tau Phosphopeptides from Alzheimer's Disease Brain by Cyclic Ion Mobility Mass Spectrometry. , J. Am. Soc. Mass Spectrom. 2023, 34, 3, 394–400. doi: 10.1021/jasms.2c00289

Wan J., Nytka M., Qian H., Lemr K and Tureček F. Do d(GCGAAGC) Cations Retain the Hairpin Structure in the Gas Phase? A Cyclic Ion Mobility Mass Spectrometry and Density Functional Theory Computational Study. J. Am. Soc. Mass Spectrom. 2023, 34 (10), 2323-2340. doi: 10.1021/jasms.3c00228

Wan J., Nytka M., Qian H., Vu K., Lemr K., Tureček F. Nitrile Imines as Peptide and Oligonucleotide Photo-Cross-Linkers in Gas Phase Ions. J. Am. Soc. Mass Spectrom. 2024, 35, 2. doi: 10.1021/jasms.3c00379.

Nytka M., Wan J., Tureček F., Lemr K. Cyclic ion mobility of isomeric new psychoactive substances employing characteristic arrival time distribution profiles and adduct separation. J. Am. Soc. Mass Spectrom. 2024, DOI: 10.1021/jasms.4c00127

Other activities:

Member of Czech Society of Mass Spectrometry (2023-now)

Consultation of bachelor thesis: Matěj Rousek.

Consultation of master thesis: Dominik Halman

Reviewer of 1 publication for Monastshefte für Chemie (Impact Factor: 1.8).

Contract research for TEVA Czech Industries.